UNIVERSITY OF SOUTHAMPTON

FACULTY OF ENGINEERING, SCIENCE & MATHEMATICS

OPTOELECTRONICS RESEARCH CENTRE

PULSE-PUMPING OF CASCADED RAMAN FIBRE AMPLIFIERS

by

Carl Farrell

Thesis for the degree of Doctor of Philosophy

Oct 2010

University of Southampton

ABSTRACT

FACULTY OF ENGINEERING, SCIENCE & MATHEMATICS

OPTOELECTRONICS RESEARCH CENTRE

Doctor of Philosophy

PULSE-PUMPING OF CASCADED RAMAN FIBRE AMPLIFIERS

by Carl Farrell

In this thesis, I investigate cascaded Raman fibre amplifiers (RFAs) pumped with shaped optical pulses delivered from a Yb doped fibre MOPA source. RFAs offer the potential to generate gain at any arbitrary wavelength with an appropriate pump source, limited only by the fibre's transparency range. The use of a counter-propagating signal and pump creates a continuous gain, despite the instantaneous nature of stimulated Raman scattering (SRS). A high power Yb doped fibre source emitting around the 1050 to 1100 nm region offers a flexible pump source that can in principle be used to generate gain for any signal from ~1100 to 2000 nm in a silica-based fibre via cascaded SRS. This opens up opportunities for an ultra-broadband amplifier with unmatched spectral width. Furthermore, by using a pump source that is in a MOPA configuration there is a high degree of control over the output characteristics which offers the potential of near-instantaneous electronic control of ultra-broadband Raman gain spectra.

In the simplest configuration, cascaded Raman wavelength shifting across a wide range of wavelengths using single-level pump pulses (i.e., approximate super-Gaussian pulses) is investigated. Using a silica-based highly nonlinear fibre (HNLF), cascaded Raman wavelength shifting up to seven Stokes orders is demonstrated and counter-propagating gain measurements are made across all seven Stokes orders. From a pump wavelength of 1064 nm, the peak gain of the 7^{th} Stokes order was ~1575 nm which demonstrated the potential for gain covering more than 500 nm. I believe this is the first time such a measurement has been undertaken. Other fibre types were also studied for comparison. Furthermore, the noise performance and gain saturation properties of cascaded RFAs were investigated, as well.

In a more advanced configuration, the Raman gain spectra produced from pumping the HNLF with step-shaped pump pulses are investigated. Such pulses consist of multiple levels with different, controllable, instantaneous powers. By adjusting the power of each step appropriately I show that different parts of the pulse transfer their energy to different Stokes orders, leading to a controllable gain spectrum covering multiple Stokes orders at the same time. I further study how the gain spectrum can be controlled by manipulating the individual duty cycle of each section of the step-shaped pump pulses as well as using multiple pump wavelengths in a time-division multiplexed pumping scheme. Single and dual wavelength pumping of various fibres with step-shaped pulses was experimentally demonstrated. Raman gain spectra spanning two and three Stokes orders and covering over 100 nm were realised. Computer simulations are also carried out for pumping with more than two pump wavelengths and for gain spectra targeting gain simultaneously up to seven Stokes orders and covering up to ~500 nm. This shows that the use of step-shaped pulses and multiple pump wavelengths allow for further increase and control of the useable bandwidth.

List of Contents

List of Figures

List of Tables

List of Abbreviations

AOM	Acousto-Optic Modulator
ASE	Amplified Spontaneous Emission
ASS	Amplified Spontaneous Scattering
AWG	Arbitrary Waveform generator
CP	Cladding Pumped
CW or cw	Continuous Wave
DCF	Double-Clad Fibre
DCFL	Double-Clad Fibre Laser
DM	Direct Modulation
DOP	Degree of Polarisation
DSF	Dispersion-Shifted Fibre
EDFA	Erbium Doped Fibre Amplifier
EM	Electromagnetic
EOM	Electro-Optic Modulator
ESA	Excited-State Absorption
FOM	Figure-of-Merit
FP	Fabry-Perot
FBG	Fibre Bragg Grating
FRIP	Fibre Refractive Index Profile
FWHM	Full-Width Half-Maxima
FWM	Four-Wave Mixing
GVD	Group Velocity Dispersion
HNLF	Highly Nonlinear Fibre
LD	Laser Diode
LMA	Large-Mode-Area
LP	Linearly Polarised
MCVD	Modified Chemical Vapour Deposition
MOPA	Master-Oscillator Power-Amplifier
NF	Noise Figure
OSA	Optical Spectrum Analyser
PM	Polarisation Maintaining

RBS	Rayleigh backscattering
RE	Rare-earth
RFA	Raman Fibre Amplifier
RFL	Raman Fibre Laser
RIN	Relative Intensity Noise
RIP	Refractive Index Profile
SBS	Stimulated Brillouin Scattering
SC	Supercontinuum
SFG	Sum-Frequency Generation
SHG	Second Harmonic Generation
SNR	Signal-to-Noise Ratio
SOP	State of Polarisation
SPM	Self-Phase Modulation
SRS	Stimulated Raman Scattering
TDM	Time-Division Multiplexed
TE	Transverse Electric
TFB	Tapered Fibre Bundle
TIR	Total Internal Reflection
TLS	Tunable Laser Source
TM	Transverse Magnetic
WDM	Wavelength-Division Multiplexed
XPM	Cross-Phase Modulation
YDF	Ytterbium-Doped Fibre
YDFA	Ytterbium-Doped Fibre Amplifier
ZDW	Zero-Dispersion Wavelength

Academic Thesis: Declaration of Authorship

I, Carl Farrell declare that this thesis entitled Pulse-pumping of cascaded Raman fibre amplifiers and the work presented in it are my own and has been generated by me as the result of my own original research.

I confirm that:

1. This work was done wholly or mainly while in candidature for a research degree at this University;

2. Where any part of this thesis has previously been submitted for a degree or any other qualification at this University or any other institution, this has been clearly stated;

3. Where I have consulted the published work of others, this is always clearly attributed;

4. Where I have quoted from the work of others, the source is always given. With the exception of such quotations, this thesis is entirely my own work;

5. I have acknowledged all main sources of help;

6. Where the thesis is based on work done by myself jointly with others, I have made clear exactly what was done by others and what I have contributed myself;

7. Either none of this work has been published before submission, or parts of this work have been published as:

- C. Farrell, C. Codemard, and J. Nilsson, "Spectral gain control using shaped pump pulses in a counter-pumped cascaded fiber Raman amplifier," Opt. Express **18**(23), 24126-24139 (2010).
- C. Farrell, C. Codemard, and J. Nilsson, "A counter-propagating cascaded Raman fiber amplifier pulsed pumped with a 1.06 μm source," *Frontier in Optics*, (16-20 Sept 2007, San Jose, CA, 2007), paper FWB2.
- C. Farrell, C. Codemard, and J. Nilsson, "A Raman fibre amplifier generating simultaneous gain across multiple Stokes orders by using step shaped optical pulses," *3rd EPS/QEOD Europhoton Conference*, (31 Aug - 05 Sep 2008, Paris, France, 2008), paper THoC5.
- J. Nilsson, S. Yoo, P. Dupriez, C. Farrell, M. S. Z. Abidin, J. Ji, J.-N. Maran, C. Codemard, Y. Jeong, J. K. Sahu, D. J. Richardson, and D. N. Payne, "Fiber MOPAs with high control and high power," *AOE*, (30 Oct - 2 Nov 2008, Shanghai, 2008), paper SaB2.

Signed: Carl Farrell

Date: 15/10/10

Acknowledgements

First of all, I would like to thank my supervisor Professor Johan Nilsson for all his help, guidance and sharing his insights into the workings of fibre amplifiers.

I would also like to thank Dr. Christophe Codemard and Dr. Pascal Dupriez for all their help throughout my PhD, including providing me with invaluable training in the laboratory at the beginning of this work.

I am grateful to all fellow members of the high power fibre laser (HPFL) group, past and present for their help in various situations.

I am also grateful to Simon Butler, Timothy McIntyre and Chris Nash for their technical advice and providing various mechanical bits and pieces for the construction of my experimental set-up.

I acknowledge Masashi Onishi, Masaaki Hirano and Takashi Sasaki of Sumitomo Electric Industries, Ltd for providing the highly nonlinear fibre used in many of the experiments.

I also acknowledge the support of an EPRSC studentship.

Chapter 1 - Introduction

1.1 Topic overview

The use of optical fibres as host media for lasers and amplifiers has proved very successful, culminating in one of the most versatile light sources to date, and has provided several key advantages over other types of laser and amplifier designs such as gas and crystal based systems. A standard optical fibre is made from high-purity silica glass and will guide light via the process of total internal reflection (TIR) at the interface between the core and a lower refractive index cladding. One of the benefits of these optical fibres is that they can exhibit extremely low intrinsic losses. This combined with the fact that the optical fibre operates as a waveguide (i.e., diffraction is eliminated) means that they are capable of guiding light over fibre lengths of up to ten's of kilometres. Furthermore by control of the refractive index profile the propagation characteristics (i.e., dispersion and modal content) throughout the fibre can be tailored to suit ones needs. Dispersion properties of fibres are important for most applications but the ability to control the modal content through the refractive index profile is one of the most attractive features of optical fibres and is one of the main reasons behind the success of fibre-based lasers and amplifiers.

To create a fibre-based laser or amplifier one needs to provide a mechanism for optical gain in the optical fibre itself. Currently the two most recognised methods will use rare-earth (RE) doped fibres where the fibre is doped with fluorescent RE ions or Raman generating fibres where the fibre utilises the nonlinear process of stimulated Raman scattering (SRS). Both methods employ optical pumping and operate by converting photons from an external pump source into photons of a new desired wavelength within the fibre itself. This conversion of photons (usually to a longer wavelength) can be stimulated by other photons at the desired wavelength, which leads to an optical amplification process. Such optical gain makes fibre amplifiers and lasers possible. While the basic operating principles are similar the underlying physics behind both processes is very different. This leads to each method having advantages and disadvantages that the other does not possess and can make one method more suitable for certain applications.

RE doped fibre devices use the atomic transitions of RE ions to convert the wavelength of photons. Therefore the energy level structure i.e., the absorption and emission spectra of these ions are crucial to their usefulness. The RE ions are excited by absorbing photons from an external optical pump source (usually a semiconductor diode laser) and then new photons are emitted at wavelengths that are characteristic to the RE ions in the fibre. Amplification at these emitted wavelengths can be achieved via the process of stimulated emission of radiation. Although they have to be optically pumped, RE doped fibre devices have provided many advantages over other laser types such as the generation of new wavelengths, good thermal management and much improved beam quality, as well as the possibility of a rugged, compact, alignment-free, all-fibre set-up. Furthermore the tight beam confinement and low background loss can make RE doped fibre devices highly efficient with low lasing thresholds [1]. Also with non-standard optical fibre geometries like double-clad fibres (DCFs) and micro-structured fibres the range of applications has been further expanded. For example DCF technology has enabled high power operation with up to 10 kilowatts of continuous wave (CW) output power available in a nearly singlemode output beam and tens of kilowatts of CW output power in a multimode output beam [2].

All in all RE doped fibres have proved very attractive and useful gain media for amplifiers and lasers but the reliance of the spectral output on the energy level structure of the RE ions is a clear drawback. Although having covered a wide range of the spectrum from 400 nm to 3000 nm with different host glasses there are still important wavelengths that cannot be generated directly from RE doped fibres. In RE doped silica fibres, which are preferred because of their efficiency and power scalability the wavelength coverage is further reduced to only a few sections of the 900 – 2100 nm wavelength range.

One way round this limited wavelength coverage is to use the nonlinear effect of SRS in optical fibres. In SRS, intense pump light from an external source interacts with the glass fibre through inelastic scattering, producing light that is shifted to a lower frequency (i.e., longer wavelength) by an amount dictated by the fibre's composition and molecular structure. This longer wavelength is usually referred to as the Stokes wavelength and amplification can be realized when this transfer of photons from the pump wavelength to the Stokes wavelength becomes stimulated. Once again the advantage created by the optical fibre's geometry plays a major role in the operation of Raman fibre devices with the possibility of long interaction lengths and tight,

singlemode confinement. But the key feature of SRS is that the shift in wavelength is a characteristic of the fibre itself and therefore its spectral location can be changed by simply changing the wavelength of the pump source. In principle, SRS in optical fibres offers the potential to generate gain at arbitrary wavelengths with an appropriate pump source, limited only by the fibre's transparency range. However, although any optical fibre can produce amplification through SRS, the practicality and usefulness of some fibres can still be limited by the high thresholds and high powers necessary to initiate SRS. Raman fibre devices are typically core pumped since the tight confinement of a small core area assists in lowering the power threshold for Raman generation, although it still remains relatively high. However, the CW power from a commercially available fibre-delivered singlemode laser diode (LD), suitable for core-pumping, is currently limited to around 1 W, depending on the output wavelength (see for instance [3]). Furthermore, diodes cannot generate high peak powers in the pulsed regime. Therefore, this limits the range of applications to those using CW pumping and long lengths of fibre (greater than 10 km) to create significant gain, such as in distributed amplifiers in optical fibre communication systems. Nevertheless, Raman generation in fibres can be further enhanced, even with CW diode-pumping, by the addition of certain co-dopants such as germanium (Ge) into silica-based fibres or by optimizing the design of the fibre geometry itself or both. Such fibres possess an increased functionality (e.g., lower power thresholds) and a wider range of potential uses such as high power operation.

While it is fair to say that RE doped fibre devices have had the most impact on the amplifier and laser industry, Raman fibre devices always remain of great interest due to their wavelength versatility. In recent years Raman fibre devices have seen a renewed attraction due to the availability of singlemode fibre pump sources with high average and peak powers. These high power singlemode fibre pump sources are based on RE doped DCFs, which can convert the output from a high power multimoded LD into a high power singlemode output that is fibre delivered. Much higher powers can now be coupled directly into an optical fibre for Raman generation via free-space optics or by fusion splicing the fibres together. Furthermore as these high power singlemode fibre sources continue to be developed with ever increasing amounts of control and sophistication they are proving ideal pump sources for many applications including a whole host of nonlinear processes. This is opening up new and exciting opportunities in existing areas of research such as SRS in optical fibres.

1.2 History of rare-earth and Raman fibre-based amplifiers and lasers

The first laser emitting at optical wavelengths was demonstrated back in 1960 by T. H. Maiman at the Hughes Research laboratory [4]. Laser action was achieved by pumping a ruby crystal with a high power flash lamp, resulting in optical radiation at 694 nm. Also during this period, E. Snitzer started to recognize the potential advantages of an optical fibre cavity and began publishing work on RE doped fibre devices, constructing what is considered to be the first RE doped fibre laser using neodymium (Nd) ions just 3 years later in 1963 [5-7]. While the first RE laser by Snitzer was a great achievement, the active sample was very "lossy", multimoded, and a flash lamp was used for side pumping the sample. This meant long lengths could not be used and a lot of power from the broadband flash-lamp was not absorbed, making the laser inefficient. As a result, the progress of RE doped fibre devices was hindered over the next couple of decades until the mid 1980s.

Around the same time as the first RE doped fibre devices, the first observation of SRS was reported. After the initial discovery of spontaneous Raman scattering in liquids by C. V. Raman and K. S. Krishnan in 1928 [8], it took the advent of the laser before SRS was observed. In 1962 E. J. Woodbury and W. K. Ng were operating a ruby laser when they observed optical emission at a wavelength of 767 nm [9]. The wavelength did not coincide with any of the emission lines reported for the fluorescence spectrum of ruby and it only occurred when they operated the laser in pulsed mode. Although they did not know it straight away, they later confirmed with other colleagues that this was in fact SRS and it originated in the nitrobenzene liquid of the Kerr cell that they were using to pulse the ruby laser [10]. Further research on SRS was restricted at this time as it required pump powers in excess of 10 kW – a massive amount at the time. This was until 1970 when E. P. Ippen, working at Bell Labs, made a breakthrough in lowering the power threshold needed for SRS. Once again this was achieved by confining the pump laser radiation in a waveguide using a liquid core fibre [11]. Shortly afterwards in, 1971, Ippen along with co-workers R. H. Stolen and A. R. Tynes observed SRS in an all glass optical fibre for the first time [12]. They recognized the potential of using SRS in glass fibres to construct broadband amplifiers and tunable lasers due to its broad Raman gain bandwidth. But they also highlighted the need for better quality fibres with low background loss so long lengths of fibres could be used to further lower the power threshold for Raman generation.

Throughout the 1970s and 80s, a considerable amount of research was carried out on SRS and other nonlinear effects in fibres (see [13, 14] and references in them). This coincided with an intense period of research into developing low-loss optical fibres for use in optical fibre communication systems [15]. The fabrication of low loss optical fibres would automatically benefit Raman generation and aid the research process but the incorporation of RE ions into optical fibres with low loss was still proving problematic. As optical fibre communication systems started to mature and expand throughout the 1980s, interest in optical amplifiers started to grow. Initial systems used electro-optic repeaters to boost the power of attenuated signals. This added a lot of cost and complexity to the system which was not desired [16]. Raman fibre amplifiers (RFAs) were seen as potential candidates and were already being investigated in research labs for use in optical fibre communications systems [17-19]. However they were always going to be hindered by the high threshold powers and the lack of reliable, high power, compact lasers that could be used as pump sources in communication systems. Eventually the race to provide an optical amplifier in optical fibre communication systems would be won by a RE doped fibre amplifier.

In 1985 a team at the University of Southampton reported an improvement in fabrication of RE doped fibres by using a novel extension of the modified chemical vapour deposition (MCVD) process [20, 21]. They used a technique called solution doping for incorporating the RE ions into the fibre preform which resulted in low loss RE doped fibres. One year later, in 1986, the same team working at the University of Southampton reported an erbium (Er) doped fibre amplifier (EDFA) at 1.54 μm with 26 dB of gain [22]. This wavelength just happened to coincide with the low loss 3rd window of optical fibre communication systems which, coupled with its intrinsic fibre compatibility, made the EDFA one of the most significant discoveries of recent years. During this time there had also been a significant improvement in LD technology which in reality is the only practical pump source for pumping RE doped fibres. With laser sources, longitudinal pumping can be employed instead of side pumping with "bulky" flash-lamps. Furthermore LD pump sources can be selected to pump only the most favourable energy levels to give compact low loss fibre devices with high efficiencies, just as required for optical fibre communication systems. In the early 1990s the EDFA was commercialized. This still remains the most important RE doped fibre application but there has also been a lot of focus on other aspects of RE doped fibres and in particular, high power operation.

High power fibre lasers became a possibility when J. Kafka of Spectra Physics suggested LD pumping of DCFs in the late 1980s [23]. The DCF structure, previously proposed by Maurer [24], when pumped by LDs, increased the power that could be coupled into the fibre while maintaining a singlemode output at the laser wavelength. Building on the progress made in the optical communications industry and adopting a lot of their technologies, high-power singlemode operation of RE doped fibres became available at power levels beyond what is possible with conventional solid state rod lasers or semiconductor lasers. By the end of the 1990s, the singlemode output power from a double-clad fibre laser (DCFL) had already increased to 110 W [25]. Such high powers had already rejuvenated interest in RFAs for optical fibre communications systems. During the early 1990s interest in RFAs had subsided somewhat due to the EDFA. However some researchers from the General Physics Institute (Moscow) and AT&T Bell Labs were still active and began to look at the possibility of using RFAs for the 2nd window of optical fibre communication systems operating at 1.31 μm. A practical pump source still eluded them but they still made significant progress using a cascaded Raman fibre laser (RFL). Experiments had already been demonstrated showing that 1 μm radiation could be efficiently converted to anywhere in the 1.1 – 1.7 μm spectral region via a cascade of SRS [26]. By using an Nd:YAG laser emitting 1.064 μm radiation, the 3rd Stokes wavelength of 1.24 μm was obtained via cascaded SRS in a high Ge doped fibre which had been shown to exhibit a higher Raman cross-section than pure silica fibres. In 1994 E. M. Dianov *et al.* were able to demonstrate an RFA in the region of 1.31 μm using this cascaded RFL as their pump source [27]. Further advances were made when S. G. Grubb *et al.* demonstrated an RFA at 1.31 μm in the same year but they used a high power Nd doped DCFL as the pump source for the cascaded RFL and fibre Bragg gratings (FBG) as reflectors to form the cavity [28]. This breakthrough provided a practical all-fibre pump source. In 1995 S. G. Grubb *et al.*, also demonstrated a cascaded Raman fibre laser (RFL) at 1.48 μm, again constructed using FBGs as mirrors and pumped by a high power ytterbium (Yb) doped DCFL [29]. This provided high enough pump powers so that researchers could demonstrate some of the advantages that the RFA had over the EDFA, which resulted in a significant increase in the number of publications at major conferences [30]. With further advances on LD pump sources in the 14XX nm range [31], RFAs are now being used to complement EDFAs in optical fibre communication systems.

In the last decade there has been a major drive behind optical fibre technology for non-telecommunication applications. With the DCF architecture, singlemode output powers have increased to a level that makes them prime candidates in many laser applications. Several RE ions have been investigated for their use in high power fibre lasers with Yb, Nd, Er, holmium (Ho) and thulium (Tm) the most prominent. In terms of raw power and efficiency, Yb doped fibres offer the best results with output powers up to 135 W available within what is considered to be a standard core diameter, typically 6 to 9 microns [32]. Furthermore by using so called large-mode-area (LMA) Yb doped fibres, singlemode (or nearly singlemode) output powers beyond the kilowatt level have been demonstrated in the laboratory [33] and are now commercially available [34]. With such high powers available in a singlemode beam and further advances on low-loss, high Raman gain fibres, the output power from RFAs and RFLs has also increased opening up new potential applications such as harmonic generation to visible wavelengths for bio-medical applications and laser guide star programs [35]. The current record for a RFL was set in 2009 and stands at 153 W at 1120 nm [36]. Furthermore an output power of 81 W for a 1480 nm RFL has also been recently realised [37], which is a 23 dB improvement on the maximum output power currently commercially available from singlemode LDs at that wavelength [38].

In recent years more and more emphasis is being placed on using DCFs in the power amplifier stage of a master-oscillator power-amplifier (MOPA) configuration. The MOPA configuration consists of a low power source (i.e., master oscillator) and a chain of power amplifiers. Control over the temporal, spatial and spectral properties can be much simpler at low powers and can be achieved with high precision. The output from the master oscillator, or seed laser as it is more commonly known, can then be amplified in a chain of amplifiers to high power levels while maintaining the desired characteristics of the seed laser. Such control at high power levels can be extremely difficult in standard laser configurations with just an oscillator. Reaching power levels from a few watts to beyond the kilowatt level with a high degree of control make the MOPA source unique and has opened up exciting opportunities in existing areas of research as well as potential new ones. They can be used as standalone devices or as sophisticated pump sources. Beam combination of several RE doped fibre MOPA sources with single frequency, single polarization and singlemode outputs is seen as the route forward to generating output powers of tens of kilowatts or higher. Nonlinear conversion processes like SRS, harmonic generation, supercontinuum generation and

parametric processes are also using the fibre MOPA configuration in various forms as optimized pump sources to increase efficiencies and power levels at exotic wavelengths. And with the ever increasing advances in fibre design and fabrication, the future for fibre-based light sources looks bright and very interesting with plenty of opportunities for further development and interesting new concepts.

1.3 Motivations

The motivation behind this thesis is to investigate ways of further exploiting the wavelength coverage available through SRS by taking advantage of recent advances in high power RE doped fibre sources. Optical amplification based on SRS in optical fibres offers the potential to generate gain at any arbitrary wavelength with an appropriate pump source. This has proved a very effective and successful way of providing gain at those wavelengths not directly available with rare-earth doped fibres. So far however most of this success has been achieved using CW pump sources (see [39] and references in it) for developing Raman fibre lasers. Pulse-pumping was employed during the early days of SRS research, but more out of necessity than choice. Such pump sources lacked any real control over the pulse parameters so therefore an investigation into pulsed cascaded Raman devices pumped by a MOPA source could open up new ideas or improve current experimental set-ups.

In recent years there has been renewed interest in the pulse-pumping of Raman amplifiers. This has been mainly in the telecommunications area through time-division multiplexed (TDM) pumping schemes [40-42], but also in other areas due to advances in diode-seeded high power fibre MOPA systems [43]. The idea behind TDM pumping is to multiplex several pump wavelengths together with each one producing its own individual Raman gain spectrum. The result of this is several overlapping Raman gain spectrums which can be tailored to produce a flat ultra-broadband Raman gain spectrum. However due to pump-to-pump Raman interactions that occur with CW pumping, the shorter wavelength pumps quickly transfer their energy to the longer wavelength pumps resulting in higher power demands on the shorter wavelength pumps in order to achieve a flat Raman gain spectrum [44]. To overcome this problem and avoid these interactions it was proposed to separate the pump wavelengths in time (i.e., pulse-pumping) so they are never simultaneously present at the same location

within the fibre and to use a counter-propagating signal since the gain in the co-propagating direction would be temporally modulated [40, 45] due to the near instantaneous nature of SRS. This work is primarily concerned with generating gain from multiple pump sources over a single Raman conversion step. Furthermore, it targets only the 1.5 μm spectral region of the spectrum and uses long amplification lengths (tens of kilometres) to enable the use of low-power pump sources. There is also a lot of emphasis placed on the noise performance of such amplifiers. Pumping schemes based on cascaded SRS have also been employed in the telecommunication area as a way of improving the noise performance [46, 47]. With cascaded SRS, when most of the pump power is converted to the Stokes wavelength; this can then act as a pump source for further SRS, generating gain at wavelengths further away from the initial pump wavelength. But again this work only targets the 1.5 μm spectral region and only considers gain across one Stokes order.

Another option is to use pulse-pumping of a cascaded RFA with shorter fibres of a few kilometres in length more accustomed to a discrete or lumped amplifier, with well controlled pulses (peak power, duty cycle, etc) from a MOPA source. The MOPA configuration allows for excellent control of the pulse parameters which is not easily available from Q-switched or mode-locked lasers. Moreover, a diode-seeded high power Yb doped fibre source emitting around the 1050 to 1100 nm region offers a flexible pump source that can in principle be used to generate gain for any signal from ~1100 to 2000 nm in a silica-based fibre via cascaded SRS. For a given fibre, the number of conversion steps in the cascade and thus the spectral location of the Raman gain will depend primarily on the instantaneous pump power, which opens up the potential for a controllable gain spectrum through control of the pulse parameters. For a given average power that is set by the final power-amplifier stage of the MOPA, the peak power of a pulse can be varied by varying the duty cycle. A high duty cycle would lower the peak power and the number of conversion steps resulting in gain at shorter wavelengths closer to the pump. On the other hand, a low duty cycle would increase the peak power and the number of conversion steps and therefore push the gain out to longer wavelengths. It would also be possible to fix the duty cycle and vary the peak power by adjusting the average output power from the MOPA source. Furthermore, control over the shape of the pump pulses would allow an additional opportunity to control the resulting gain spectrum. Pulses with a square or rectangular profile would allow for a full conversion of energy from the pump to a Stokes order without gain at any

intermediate orders, thus increasing the conversion efficiency compared from that obtained with a Gaussian pulse for instance. Also pulses with varying peak power could be used to generate gain at multiple Stokes orders simultaneously, leading to a controllable ultra-broadband Raman gain spectrum. Again the actual shape of the pulse would determine the conversion efficiency to each Stokes order. It should also be possible to multiplex several pump wavelengths like previously done in TDM pumping schemes to fill in any gaps on the gain spectrum between neighbouring Stokes orders. The shift in wavelength between the pump at 1050 nm and the 1st Stokes order in a pure silica fibre is approximately 50 nm. Therefore pump wavelengths between 1050 and 1100 nm could potentially fill in any gaps between neighbouring Stokes orders. LDs are readily available covering the spectral region from 1050 to 1090 nm (see for instance [48]), assisted by temperature tuning of the wavelength in some cases. Furthermore the broad-gain bandwidth of Yb doped fibres would permit amplification of these wavelengths to high powers.

Another feature of this work is the use of a silica-based highly nonlinear fibre (HNLF) for the RFA which was fabricated by Sumitomo Electric Industries [49]. One drawback to SRS is the high pump power required to generate it in standard optical fibres like SMF-28 [50], especially in the case of cascaded SRS. Although this is relatively easily overcome with today's high power fibre laser sources, the pump power required for Raman generation can be reduced by the use of optical fibres with a high Raman fibre gain coefficient, thus providing more flexibility for the targeted RFA. In addition, the SMF-28 fibre, which is based on a step index refractive index profile, exhibits a zero dispersion wavelength (ZDW) value typically around the 1310 nm spectral region. A ZDW located within the window of operation of a targeted RFA would cause the Raman cascade to breakdown due to other competing nonlinear processes [51]. HNLFs exhibiting a high Raman fibre gain coefficient, low attenuation and tailored chromatic dispersion profiles are attractive media for discrete RFAs [52]. Furthermore silica-based HNLFs also have the added advantage that they can potentially be spliced to the pump source or other components like fibre-pig-tailed isolators and wavelength-division multiplexing (WDM) fibre couplers. By combining a pulsed Yb MOPA source and a silica-based HNLF it should be possible to realise an ultra-broadband Raman amplifier with a controllable gain spectrum that has not been demonstrated before.

Finally although the work carried out in this thesis uses a Yb MOPA pump source and a silica-based Raman generating fibre, this work could be extended to operate in other wavelength regions by the use of other RE MOPA pump sources and different types of optical fibres such as those using chalcogenide glasses.

1.4 Thesis outline

This first chapter provides an introduction into the area of research undertaken throughout this PhD project which is basically, pulse-pumping of a cascaded Raman fibre amplifier (RFA) with a RE doped fibre source. This begins with a brief topic overview highlighting the main areas of importance to this thesis, namely, optical fibres, RE doped fibre sources and Raman generation in optical fibres. This is followed by an historical review before finishing off by presenting the motivations behind the work carried out throughout this project.

The second chapter is an expansion of the topic overview, thus providing the relevant background theory to this work. This chapter begins by reviewing the principles and properties of optical fibres highlighting their usefulness as host media for amplifiers and lasers. Next the relevant Raman theory is covered, focussing on the Raman Effect in optical fibres and its role in the construction of broadband amplifiers. Finally the last section in this chapter will cover RE doped fibres and in particular Yb doped fibres, focussing on their suitability as pump sources for Raman generation in optical fibres.

The third chapter marks the beginning of the practical section, focussing on the experimental results achieved throughout the project. The first part of this chapter describes the construction of the Yb doped MOPA source and the issues that arose during the build before moving on to the characterisation of the cascaded RFA. The performance of all amplifiers can be analysed in terms of several key characteristics. These are gain, efficiency, noise and saturation properties. The first targeted cascaded RFA operates in a counter-propagating configuration, uses a single pump source with a fixed output wavelength. This RFA only targets gain across a single Stokes order at any one time (i.e., single-channel amplification) but has the flexibility of controlling the pulse parameters to increase the conversion efficiency and shift the Raman gain to any desired Stokes order within the transparency window of the Raman fibre. Throughout

the rest of this chapter we report on the gain measurements taken under different operating conditions for such an amplifier.

Chapter 4 concludes the characterisation of the single-channel cascaded RFA by reporting measurements taken on the temporal gain variations, noise performance and saturation properties. The principal source of noise in optical amplifiers is amplified spontaneous emission (ASE). In the case of Raman amplifiers, this is sometimes also known as amplified spontaneous scattering. Many other sources of noise are possible but their importance can be considered application driven. Therefore a proof of principle study on any optical amplifier should include measurements of the ASE noise power to assess potential implications on the performance. Furthermore saturation effects also place an upper limit on the maximum achievable gain/power possible in any amplifier. Again many types of saturation effects exist depending on the type of amplifier. For an RFA, the most important saturation effects are due to pump depletion caused by cascaded Raman conversion and gain saturation caused by an increase in the input signal power. We investigate these effects for the single-channel pulse-pumped cascaded RFA and again present experimental results.

In chapter 5 the focus shifts to pulse-shaping and an investigation into the Raman gain spectrum produced from pumping a Raman fibre with step shaped optical pulses delivered from the Yb doped fibre MOPA source. Such pulses contain sections with different instantaneous powers which can be controlled by adjusting the height of each step. By adjusting the height of each step appropriately we show that the instantaneous powers can be tailored so that different parts of the pump pulses transfer their energy to different Stokes orders leading to a controllable ultra-broadband gain spectrum covering multiple Stokes orders.

Chapter 6 builds on the results achieved in chapter 5 by using two pump wavelengths and multi-level pump pulses for pumping the cascaded RFA. This extends the useable bandwidth of the Raman gain spectrum by filling in the gaps between neighbouring Stokes orders. Comparisons are also made between the resulting Raman gain spectra that are produced from different optical fibres. Furthermore, the simulated gain spectra produced from using multiple pump wavelengths and multi-level pump pulses are also presented.

Finally, chapter 7 concludes this thesis with a summary of the main results achieved throughout this thesis before finishing with comments for the possibilities for future work.

1.5 References

[1] P. Urquhart, "Review of Rare-Earth Doped Fiber Lasers and Amplifiers," IEE Proc.-J Optoelectronics **135**(6), 385-402 (1988).

[2] E. Stiles, "New developments in IPG fiber laser technology," *Proceedings of 5th International Workshop on Fiber Lasers*, (Dresden, Germany, 2009).

[3] Information available at: http://www.Bookham.com.

[4] T. H. Maiman, "Stimulated optical radiation in ruby masers," Nature **187**, 493 (1960).

[5] E. Snitzer, "Optical Maser Action in Nd^{+3} in a Barium Crown Glass," Phys. Rev. Lett. **7**, 444 (1961).

[6] E. Snitzer, "Proposed Fiber Cavities for Optical Masers," J. Appl. Phys. **32**(1), 36-39 (1961).

[7] E. Snitzer, "Neodymium glass laser," *Proceedings of the Third International Conference on Solid State Lasers*, (Paris, France, 1963), 999-1019.

[8] C. V. Raman and K. S. Krishnan, "A new type of secondary radiation," Nature **121**, 501-502 (1928).

[9] E. J. Woodbury and W. K. Ng, "Ruby laser operation in the near IR," Proc. IRE **50**, 2367 (1962).

[10] G. Eckhardt, R. W. Hellwarth, F. J. McClung, S. E. Schwarz, D. Weiner, and E. J. Woodbury, "Stimulated Raman scattering from organic liquids," Phys. Rev. Lett. **9**(11), 455-457 (1962).

[11] E. P. Ippen, "Low-power quasi-cw Raman oscillator," Appl. Phys. Lett. **16**(8), 303-305 (1970).

[12] R. H. Stolen, E. P. Ippen, and A. R. Tynes, "Raman oscillation in glass optical waveguide," Appl. Phys. Lett. **20**(2), 62-64 (1972).

[13] R. H. Stolen, "Nonlinearity in fiber transmission," Proc. of the IEEE **68**(10), 1232-1236 (1980).

[14] W. J. Tomlinson and R. H. Stolen, "Nonlinear phenomena in optical fibers," IEEE Communications Magazine **26**(4), 36-44 (1988).

[15] F. P. Kapron, D. B. Keck, and R. D. Maurer, "Radiation losses in glass optical waveguides," Appl. Phys. Lett. **17**(10), 423-425 (1970).

[16] J. Hecht "The evolution of Optical amplifiers," Optics and Photonics News, August, 2002.

[17] E. Desurvire, M. Papuchon, J. P. Pocholle, J. Raffy, and D. B. Ostrowsky, "High-gain optical amplification of laser diode signal by Raman scattering in single-mode fibres," Electron. Lett. **19**(19), 751-753 (1983).

[18] J. Hegarty, N. A. Olsson, and L. Goldner, "CW pumped Raman preamplifier in a 45 km-long fibre transmission system operating at 1.5 μm and 1 Gbit/s," Electron. Lett. **21**(7), 290-292 (1985).

[19] N. Edagawa, K. Mochizuki, and Y. Iwamoto, "Simultaneous amplification of wavelength-division-multiplexed signals by a highly efficient fibre Raman amplifier pumped by high-power semiconductor lasers," Electron. Lett. **23**(5), 196-197 (1987).

[20] R. J. Mears, L. Reekie, S. B. Poole, and D. N. Payne, "Neodymium-Doped Silica Single-Mode Fiber Lasers," Electron. Lett. **21**(17), 738-740 (1985).

[21] S. B. Poole, D. N. Payne, and M. E. Fermann, "Fabrication of low-loss optical fibres containing rare-earth ions," Electron. Lett. **21**, 737 (1985).

[22] R. J. Mears, L. Reekie, I. M. Jauncey, and D. N. Payne, "High-gain rare-earth-doped fiber amplifier at 1.54 μm," *Optical Fiber Communication Conference* (Reno, Nevada, 1987), paper W12.

[23] J. Kafka, "Laser diode pumped fiber laser with pump cavity," US patent 4,829,529 (1989).

[24] R. D. Maurer, "Optical waveguide light source," US patent 3,808,549 (1974).

[25] V. Dominic, S. MacCormack, R. Waarts, S. Sanders, S. Bicknese, R. Dohle, E. Wolak, P. S. Yeh, and E. Zucker, "110 W fiber laser," *Proc. Conf. Lasers Electro. Optics*, (Baltimore, MD, USA, 1999), paper CPD11.

[26] C. Lin, L. G. Cohen, R. H. Stolen, G. W. Tasker, and W. G. French, "Near-infrared sources in 1-1.3 μm region by efficient stimulated Raman emission in glass fibers," Opt. Commun. **20**(3), 426-428 (1977).

[27] E. M. Dianov, A. A. Abramov, M. M. Bubnov, A. M. Prokhorov, A. V. Shipulin, G. G. Devjatykh, A. N. Guryanov, and V. F. Khopin, "30 dB gain Raman amplifier at 1.3 μm in low-loss high GeO_2-doped silica fibres," Electron. Lett. **31**(13), 1057-1058 (1995).

[28] S. Grubb, T. Erdogan, V. Mizrahi, T. Strasser, W. Y. Cheung, W. A. Reed, P. J. Lemaire, A. E. Miller, S. G. Kosinski, G. Nykolak, and P. C. Becker, "1.3 μm

cascaded Raman amplifier in germanosilicate fibers," *Proc. Optical Amplifiers and their Applications*, (Breckenridge, Colorado, 1994), paper PD3-1.

[29] S. Grubb, T. Strasser, W. Y. Cheung, W. A. Reed, V. Mizrachi, T. Erdogan, P. J. Lemaire, A. M. Vengsarkar, and D. J. Digiovanni, "High power, 1.48 μm cascaded Raman laser in germanosilicate fibers," *Proc. Optical Amplifiers and their Applications*, (Davos, Switzerland, 1995), Paper SaA4.

[30] J. Bromage, "Raman amplification for fiber communications systems," J. Lightwave Technol. **22**(1), 79-93 (2004).

[31] N. Tsukiji, J. Yoshida, T. Kimura, S. Koyanagi, and T. Fukushima, "Recent progress of high power 14XX nm pump lasers," *Proc. ITcom Active and Passive Optical Components for WDM Communications*, (Denver, CO, USA, 2001), 349-360.

[32] N. S. Platonov, D. V. Gapontsev, V. P. Gapontsev, and V. Shumilin, "135 W CW fiber laser with perfect single mode output," *Proc. Conf. Lasers Electro-Optics*, (Long Beach, CA, USA, 2002), paper CPDC3.

[33] Y. Jeong, J. K. Sahu, D. N. Payne, and J. Nilsson, "Ytterbium-doped large-core fiber laser with 1.36 kW continuous-wave output power," Opt. Express **12**, 6088 (2004).

[34] Information available at: http://www.ipgphotonics.com.

[35] J. T. Murray, W. T. Roberts, W. L. Austin, R. C. Powell, and D. Bonaccini, "Fiber Raman laser for sodium guide star," Proc. SPIE **3353**, 330-339 (1998).

[36] Y. Feng, L. R. Taylor, and D. B. Calia, "150 W highly-efficient Raman fiber laser," Opt. Express **17**(26), 23678-23683 (2009).

[37] J. W. Nicholson, M. F. Yan, P. Wisk, J. Fleming, F. DiMarcello, E. Monberg, T. Taunay, C. Headley, and D. J. DiGiovanni, "Raman fiber laser with 81 W output power at 1480 nm," Opt. Lett. **35**(18), 3069-3071 (2010).

[38] Information available at: http://www.furukawa.co.jp/fitel/eng/active/pumping.html.

[39] J. L. Archambault and S. G. Grubb, "Fiber gratings in lasers and amplifiers," J. Lightwave Technol. **15**(8), 1378-1390 (1997).

[40] L. F. Mollenauer, A. R. Grant, and P. V. Mamyshev, "Time-division multiplexing of pump wavelengths to achieve ultrabroadband, flat, backward-pumped Raman gain," Opt. Lett. **27**(8), 592 (2002).

[41] C. R. S. Fludger, V. Handerek, N. Jolley, and R. J. Mears, "Novel ultra-broadband high performance distributed Raman amplifier employing pump modulation," *Optical Fiber Communications Conference*, (Anaheim, CA, USA, 2002), paper WB4.

[42] P. J. Winzer, J. Bromage, L. E. Nelson, M. D. Mermelstein, C. Horn, and C. H. Headley, "Repetition rate requirements for time-division multiplexed Raman pumping," J. Lightwave Technol. **22**(2), 401-408 (2004).

[43] P. Dupriez, C. Farrell, M. Ibsen, J. K. Sahu, J. Kim, C. Codemard, Y. Jeong, D. J. Richardson, and J. Nilsson, "1 W average power at 589 nm from a frequency doubled pulsed Raman fiber MOPA system," Proc. SPIE **6102,** (2006).

[44] P. M. Krummrich, R. E. Neuhauser, and C. Glingener, "Bandwidth limitations of broadband distributed Raman fiber amplifiers for WDM systems," *Optical Fiber Communications Conference*, (Anaheim, CA, USA, 2001), paper MI3.

[45] C. R. S. Fludger, V. Handerek, and R. J. Mears, "Pump to signal RIN transfer in Raman fiber amplifiers," J. Lightwave Technol. **19**(8), 1140-1148 (2001).

[46] V. Dominic, A. Mathur, and M. Ziari, "Second-order distributed Raman amplification with a high-power 1370 nm laser diode," *Proc. Optical Amplifiers and their Applications*, (Stresa, Italy, 2001), paper OMC6.

[47] S. B. Papernyi, V. B. Ivanov, Y. Koyano, and H. Yamamoto, "Sixth-order cascaded Raman amplification," *Optical Fiber Communication Conference*, (Anaheim, CA, USA, 2005), paper OThF4.

[48] Information available at: http://www.qphotonics.com.

[49] Information available at: http://www.sumitomo.com/.

[50] Information available at: http://www.corning.com/opticalfiber/.

[51] C. Lin, V. T. Nguyen, and W. G. French, "Wideband near-I.R. continuum (0.7-2.1 μm) generated in low-loss optical fibres," Electron. Lett. **14**(25), 822-823 (1978).

[52] T. Okuno, M. Hirano, T. Nakanishi, and M. Onishi, "Highly-nonlinear optical fibers and their applications," Sumitomo Electric Industries (SEI) Technical review **62**, 34-40 (2006).

Chapter 2 – Background

This chapter provides an overview of theory and information required to understand the experimental and theoretical work reported in later chapters. First of all, section 2.1 reviews the principles and properties of optical fibres highlighting their usefulness as host media for amplifiers and lasers. Then, in section 2.2, the relevant Raman theory is covered, focussing on the Raman Effect in optical fibres and its role in the construction of broadband amplifiers. Finally, section 2.3 covers RE doped fibres and in particular Yb doped fibres, focussing on their suitability as pump sources for Raman generation in optical fibres.

2.1 Optical fibre characteristics

An optical fibre is a dielectric optical waveguide that confines and guides electromagnetic (EM) radiation in the form of light along its length. A conventional optical fibre is a single solid structure, cylindrical in form, which consists of a core region in the centre surrounded by a cladding region with a lower refractive index. Light is confined and guided within the core via the process of total internal reflection (TIR) due to the difference in the core and cladding refractive indices. The critical angle, θ_c, at which TIR occurs is defined as, $\theta_c = \sin^{-1}\left(\frac{n_2}{n_1}\right)$, where n_1 is the core refractive index, n_2 is the cladding refractive index and θ_c is measured with respect to the normal at the core/cladding interface. Surrounding the cladding will be a protective layer usually referred to as a buffer coating to further protect the fibre from any external influences. Figure 2.1 shows a schematic of a conventional optical fibre. Typically with a conventional optical fibre the buffer coating layer will have a diameter of 250 μm, the cladding diameter will be 125 μm and the core will have a diameter of 6-10 μm for singlemode operation or anything up to 62.5 μm for multimode operation.

A key feature of the optical fibre is that there is a high degree of control available over how light propagates along its length. Important aspects such as waveguide modes, attenuation, dispersion and nonlinear effects in optical fibres all have

a dependency on the optical fibre's structure, geometry and the materials used to create it. By careful coordination of the core diameter and the core/cladding refractive indices, the propagation characteristics can be controlled and manipulated to meet the requirements for certain applications. Furthermore, changing the design of the refractive index profile (RIP) away from the conventional step-index profile (see figure 2.1) can also be used as a means for further manipulation.

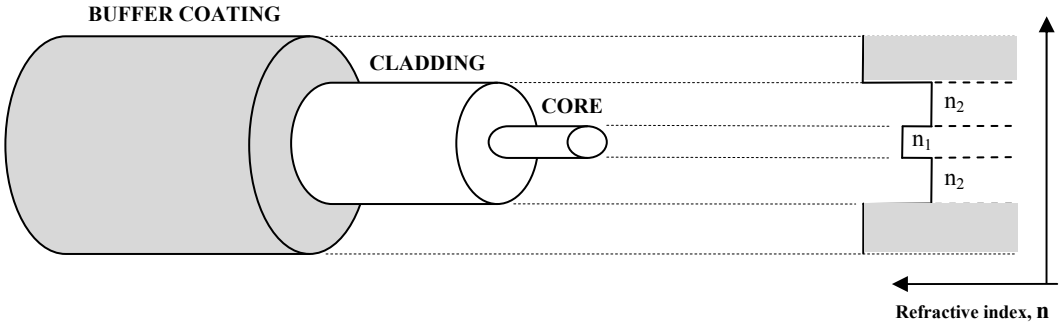

Figure 2.1 Schematic of a conventional optical fibre with corresponding refractive index profile where $n_1 > n_2$.

2.1.1 Optical fibre modes

A simple picture of how light waves propagates in optical fibre waveguides may well suggest that light incident on the core/cladding interface at all angles greater than the critical angle will be bound and guided along an optical fibres length. In fact only certain incident angles result in confinement, meaning that there are only certain paths a light wave can follow down an optical fibre. These allowed angles of incidence or pathways give rise to the origin of fibre modes. A full treatment requires the use of electromagnetic theory and the subsequently derived Maxwell's equations. The EM light field that is guided along an optical fibre can be represented by a superposition of these modes. The number of modes allowed to propagate in an optical fibre can range from one mode to many thousands of modes. Propagation modes can even be completely absent at some wavelengths, while a fibre that does not support any mode at any wavelength would hardly be considered to be an optical fibre.

Each of these bound modes consists of a simple EM field distribution that forms a standing wave pattern in the transverse direction and that propagates along the fibre length with a distinct propagation constant [1]. The allowed EM field distributions of an optical fibre are determined by the solutions obtained from solving the wave

equation that is derived from the Maxwell equations (see for instance [2]). For a linear, homogeneous, isotropic dielectric material having no currents and free charges the following wave equations can be derived for the electric and magnetic fields, **E** and **H** [2]:

$$\nabla^2 \mathbf{E} = n^2 k_0^2 \mathbf{E} \tag{2.1}$$

$$\nabla^2 \mathbf{H} = n^2 k_0^2 \mathbf{H} \tag{2.2}$$

where k_0 is the free-space wave vector which is given by $k_0 = \frac{\omega}{c} = \frac{2\pi}{\lambda}$ and n is the materials refractive index. Equations 2.1 and 2.2 apply to an optical fibre with a step-index refractive index profile (i.e., homogeneous) where $n = n_1$ across the core and $n = n_2$ across the cladding (see figure 2.1). For an optical fibre whose refractive index varies continuously across the core and cladding cross section, equation 2.1 would contain an extra term which would increase the complexity. However, since the point here is only to give an introduction into the concept of fibre modes the simplest fibre design of a step-index profile will be used.

The approach is to look separately for solutions in the core and the cladding and finally match the fields at the core/cladding interface using Maxwell's equations. In this case with constant-index regions, these boundary conditions correspond to the missing terms in the limit of discontinuous variations. In a cylindrical coordinate system (see figure 2.2) corresponding to an optical fibre structure the wave equation becomes:

$$\frac{\partial^2 U}{\partial r^2} + \frac{1}{r}\frac{\partial U}{\partial r} + \frac{1}{r^2}\frac{\partial^2 U}{\partial \phi^2} + \frac{\partial^2 U}{\partial z^2} + n^2 k_0^2 U = 0 \tag{2.3}$$

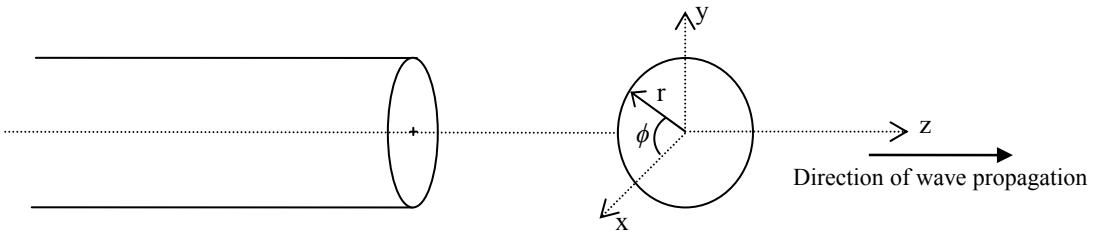

Figure 2.2 Cylindrical co-ordinate system.

where $U = U(r,\phi,z)$ represents the field **E** or **H,** and r and ϕ are cylindrical coordinates. We are interesting in solutions that take the form of waves travelling in the z direction with a propagation constant β, so that the z-dependence of U is of the form, $e^{-j\beta z}$. In addition, each field component must not change when the coordinate ϕ is increased by 2π. We therefore assume that the dependence on ϕ is harmonic and takes the form, $e^{-jl\phi}$, where l is an integer that can be positive or negative. Substituting $U(r,\phi,z) = u(r)e^{-jl\phi}e^{-j\beta z}$ into equation (2.3) produces the following ordinary differential equation:

$$\frac{d^2u}{dr^2} + \frac{1}{r}\frac{du}{dr} + \left(\left(n^2k_0^2 - \beta^2\right) - \frac{l^2}{r^2}\right)u = 0 \qquad (2.4)$$

where, $u(r)$ is the transverse field distribution which depends only on the radial position, r. Equation (2.4) defines the transverse field distribution and represents a Bessel differential equation which appears in all kinds of problems with cylindrical symmetry. The solutions of Bessel's equations take on different forms depending on the sign of $\left(n^2k_0^2 - \beta^2\right)$. In the core region where the values of the propagation constants (β) are less than the wavenumber (nk_0), the solutions take on an oscillatory form (i.e., sine or cosine function). In the cladding region where values of the propagation constants (β) are greater than the wavenumber (nk_0), the solutions take on a decaying form which decay exponentially with respect to the fibre radius, r. Equation (2.4) can therefore be written separately for the core and cladding regions:

$$\frac{d^2u}{dr^2} + \frac{1}{r}\frac{du}{dr} + \left(\zeta^2 - \frac{l^2}{r^2}\right)u = 0, \qquad r < a \text{ (core)} \qquad (2.5)$$

$$\frac{d^2u}{dr^2} + \frac{1}{r}\frac{du}{dr} - \left(\gamma^2 + \frac{l^2}{r^2}\right)u = 0, \qquad r > a \text{ (cladding)} \qquad (2.6)$$

where, $r = a$ is the distance to the core/cladding interface. ζ and γ are termed the mode parameters for the core and cladding, respectively, and are defined as follows:

$$\zeta^2 = n_1^2k_0^2 - \beta^2, \qquad \beta < n_1k_0 \qquad (2.7)$$

$$\gamma^2 = \beta^2 - n_2^2 k_0^2, \qquad \beta > n_1 k_0 \tag{2.8}$$

Moreover the solutions to equations (2.5) and (2.6) can be characterised as follows:

$$u(r) \propto \begin{cases} J_l(\varsigma r), & r < a \quad (core) \\ K_l(\gamma r), & r > a \quad (cladding) \end{cases} \tag{2.9}$$

where, $J_l(x)$ is the Bessel function of the first kind and order l and represents the mode field in the core, and $K_l(x)$ is the modified Bessel function of the second kind and order l which represents the mode field in the cladding. Figure 2.3 gives two examples of the radial distribution $u(r)$. The mode parameters ζ and γ determine the rate of change of $u(r)$ in the core and cladding, respectively. For instance, a large value of ζ means a faster oscillation of the radial distribution in the core. Also a large value of γ means a faster decay and smaller penetration of the wave into the cladding.

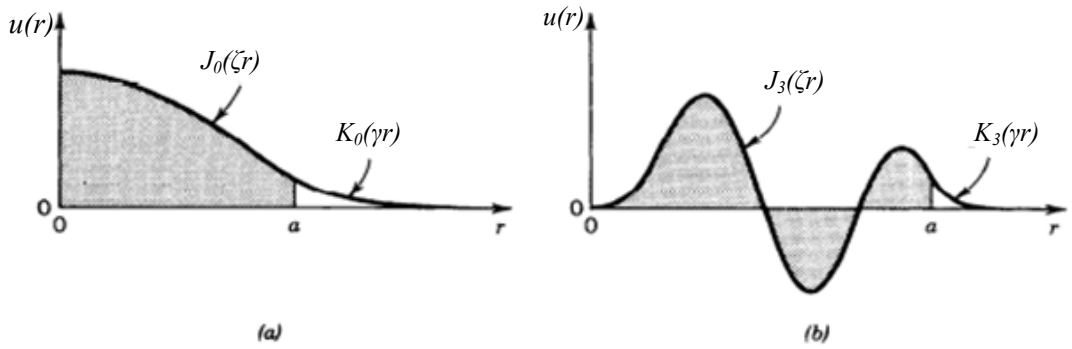

Figure 2.3 Two examples of the radial distributions given by equation (2.9) for (a) l=0 and (b) l=3. The core/cladding interface is located at r=a (figure extracted from [2]).

As can be seen from equations (2.7) and (2.8) the sum of the squares of ζ and γ is a constant so that as ζ increases, γ decreases and the field penetrates further into the cladding. As ζ exceeds the constant, $\left(n_1^2 - n_2^2\right)k_0^2$, ζ becomes imaginary and the wave ceases to be bound to the core and the mode is said to be cut off. It is convenient to normalize ζ and γ by defining:

$$U = \varsigma a, \qquad W = \gamma a, \tag{2.10}$$

The sum of the squares of U and W define a very important parameter which is usually referred to as the normalised frequency, V, but is also known as the V parameter or the V number:

$$V = \left(U^2 + W^2\right)^{1/2} = ka(n_1^2 - n_2^2)^{1/2} = \frac{2\pi}{\lambda} a(NA) \qquad (2.11)$$

where, NA is the numerical aperture of the fibre and the relationships $NA = \left(n_1^2 - n_2^2\right)^{1/2}$ and $k = \frac{2\pi}{\lambda}$ are used. The normalised frequency, V, determines how many modes a fibre can support and combines in a very useful manner the dependency of the modal content on three important design variables for an optical fibre: namely the core radius a, the NA and the operating wavelength λ [3].

As mentioned earlier the exact solutions for the mode propagation constants and their corresponding mode field distributions *u(r)* can be obtained by looking separately for solutions in the core and the cladding and matching the fields at the core/cladding interface using Maxwell's equations and the relevant boundary conditions. The exact modes of a fibre are designated either transverse electric (TE), transverse magnetic (TM) or hybrid (HE or EH) where both the electric and magnetic field have a longitudinal component. Solving the exact mode fields and propagation constants of an optical fibre is both lengthy and complex. However it has been shown that this process can be simplified in the case of most practical fibres which satisfy the weakly-guiding approximation. Under this approximation the relative index difference, Δ, between the core and the cladding is considered very small (i.e., Δ<<1) and therefore $n_1 \approx n_2$. In this case it has been shown that the longitudinal components of both the electric and magnetic fields are small compared to the transverse components [4]. Hence approximate solutions for the full set of HE, EH, TE and TM modes may be given by two linearly polarised components. These linearly polarised (LP) modes are not exact modes of the fibre except for the fundamental (lowest order) mode. However, when Δ<<1 is satisfied, then some modes occur which will have almost identical propagation constants. Such modes can be treated as degenerate. Specific superpositions of degenerate modes characterised by a common propagation constant correspond to particular LP modes regardless of their HE, EH, TE and TM field configurations. LP modes are characterized by two subscripts, l and m, which are termed the azimuthal

mode number and the radial mode number, respectively. There are in general 2*l* field maxima around the circumference of the fibre core and *m* field maxima along a radius vector (see figure 2.3) [3].

Figure 2.4 shows a schematic of the first three guided modes of a fibre (i.e., LP_{01}, LP_{11} and LP_{21}) and a higher order mode, LP_{42}. Except for azimuthally invariant modes (LP_{0m}), these modes are degenerate, in that they split into two modes that are rotated by a quarter angular period with respect to each other. These are known as sine and cosine modes.

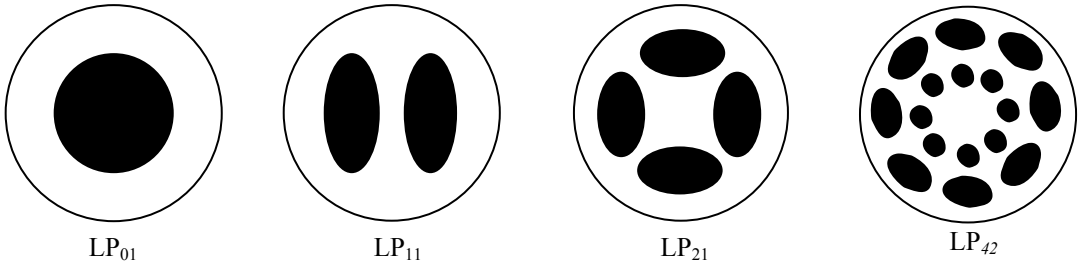

Figure 2.4 Schematic showing the distinctive mode patterns of four individual linearly polarised modes.

The point at which modes cease to be guided or cut off is an important design parameter that can be found in terms of the normalised frequency. As outline earlier, a mode will be cut off when the mode parameter, $\gamma = 0$. Therefore from equation (2.11), the cut-off frequency, V_c can be defined as, $V_c = U_c = \frac{2\pi}{\lambda} a(NA)$, where U_c is the value of U at the cut-off point, corresponding to the m^{th} root of the $J_{l-1}(U)$ Bessel function for LP_{lm} modes. The most important cut-off condition is the point at which the fibre supports only the fundamental mode (i.e., the LP_{01} mode). This condition occurs when the LP_{11} is cut-off and is identified by the first point at which $J_0(V_c) = 0$, resulting in a value of $V_c \approx 2.405$. The cut-off frequency for all other LP modes can be found in the same way. For most applications the description of fibre modes in terms of LP modes is not only sufficient but more practical. Note also that although exceptions exist, in most fibres the LP-modes are polarisation-degenerate, so that each guided LP-mode comprises two polarisation-modes.

2.1.2 Attenuation

Attenuation is another important fibre parameter that indicates how transparent a particular fibre is and serves as a measure of the loss in power of light as it propagates along a fibre. Attenuation values will vary depending on the fibre materials and the wavelength of operation. The most popular material of choice for fabricating optical fibres is high-purity silica (SiO_2) glass. Dopants such as germanium (Ge), phosphorus (P), aluminium (Al), fluorine (F) and boron (B) are then incorporated into the silica glass to modify the refractive indices. Ge, P and Al are used to raise the refractive index, whereas F and B are used to decrease the refractive index. In a typical singlemode transmission fibre such as SMF-28 the core is doped with Ge so that it makes up ~3 mol%, giving a relative index difference, Δ of ~0.33%, so an absolute index difference of ~0.05. Figure 2.5 shows a typical attenuation profile for such a fibre [3]. The attenuation profile can be readily characterised by three dominating loss mechanisms, as highlighted in figure 2.5. As light propagates along a fibre, it experiences Rayleigh scattering which results in light being scattered randomly in all directions. Most of this light will be reflected backwards or out of the core, thus resulting in a loss of power for the forward propagating light. These losses arise from microscopic variations in the material density, from compositional fluctuations, and from structural inhomogeneities or defects occurring during the fibre manufacture. They give rise to refractive index variations which act as scattering points and cause a Rayleigh-type scattering of the light to occur. Since Rayleigh scattering follows a characteristic λ^{-4} dependence, it decreases dramatically with increasing wavelength [3]. Rayleigh scattering is an intrinsic effect and represents the theoretical limit on the lowest possible attenuation values in fibres. It is also worth noting that the variations in the material density and the compositional fluctuations are dependent on the amount of dopants that are added to the core. Therefore a higher level of dopant, such as Ge, into the core will result in higher scattering losses. It can be seen from figure 2.5 that the minimum loss is located around the 1.55 μm region which is the main optical communication window.

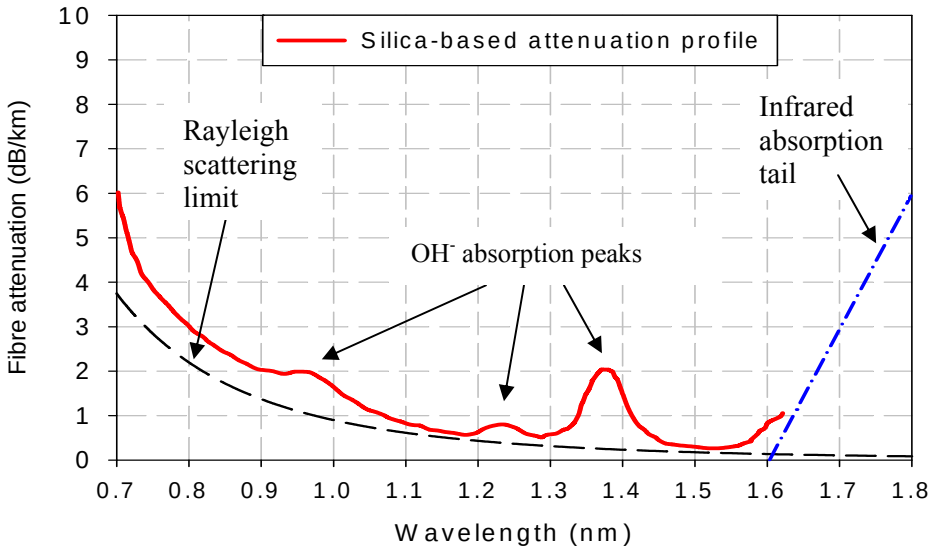

Figure 2.5 A typical attenuation versus wavelength plot for a silica-based optical fibre.

In modern day fibres with low levels of Ge in the core this attenuation value is typically ~0.2 dB/km and is very close to the Rayleigh limit. This represents a length of 15 km before half the power is lost. Even lower attenuation values of 0.1484 dB/km have been achieved with a pure silica core fibre [5]. Moreover, an attenuation value of ~1 dB/km is possible in the wavelength region of 1-1.1 µm which constitutes another useful operating window as it coincides with readily available high power sources in the 1.06-1.1 µm wavelength band. The scattering loss increases rapidly for shorter wavelengths owing to the λ^{-4} dependence but silica fibres remain useful for many applications even at UV wavelengths. At this point band-edge absorption becomes the dominant loss, growing very quickly to unacceptable values.

Although the Rayleigh scattering continues to decrease for wavelengths longer than 1550 nm, the long wavelength side of the spectrum is bounded by another intrinsic absorption effect called multiphonon absorption. This interaction between light and molecular vibrations within the glass results in the light being absorbed and lost. In a silica-based fibre with low Ge-doping, this will typically start to affect the attenuation profile around the region of 1.6-1.8 µm depending on the actual level of doping.

Finally there are also extrinsic absorption losses due to impurities in fibre. The main one of concern as highlighted in figure 2.5 is due to water (as the hydroxyl or OH- ion) dissolved into the fibre during fabrication. This can result in several peaks which exhibit a higher loss than that imposed by the Rayleigh scattering limit. The main peak is located at ~1.38 µm with two smaller peaks at ~1.25 µm and ~0.95 µm. The actual

attenuation levels of these peaks will vary from fibre to fibre depending on the fabrication process. In fact, so called "dry fibres" can be fabricated with no water peaks present (see for example, Allwave® fibre [6]).

However, even with these water peaks the silica-based optical fibre still offers potential for operation over a wide bandwidth (1-1.7 μm) with low losses over distances up to several km's and therefore presents possibilities for a number of applications, including that of a broadband discrete Raman amplifier.

2.1.3 Dispersion

There are several sources of dispersion in optical fibres. First of all one must consider the material dispersion (or bulk dispersion) which is an intrinsic property of the fibre's composite materials due to the refractive index, $n(\lambda)$, being a function of wavelength. As a consequence different spectral components propagate at different speeds given by, $v = c/n(\lambda)$. The variation of $n(\lambda)$ in the transparent region of an optical fibre can be well approximated by using the Sellmeier equation [7]:

$$n^2(\lambda) = 1 + \sum_{i=1}^{3} \frac{B_i \lambda^2}{\lambda^2 - \lambda_i^2} \tag{2.12}$$

Here, λ_i and B_i are the experimentally determined Sellmeier coefficients. The material dispersion is then given by the material dispersion parameter, D_M:

$$D_M = -\frac{\lambda}{c}\frac{d^2 n}{d\lambda^2} \tag{2.13}$$

It tells us how the group velocity changes with wavelength, and thus how a spectrally finite pulse broadens in time. It is often expressed in units of ps nm^{-1} km^{-1}. The wavelength dependence of $n(\lambda)$ and D_M is shown in figure 2.6 for the material compositions of pure Si, pure Ge and a sample of Ge-doped Si [7, 8]. The effect of doping Si with Ge, is a linear increase in the refractive index with Ge dopant concentration (mol%). This translates into a shift in the material dispersion profile (see figure 2.6(b)) which is highlighted by noting the location of the zero-dispersion

wavelength (ZDW), λ_D. The ZDW is the point at which D_M becomes equal to zero. It separates a region of negative dispersion on the short wavelength side and a region of positive dispersion on the longer wavelength side. For pure Si and pure Ge, this occurs at a wavelength of 1.27 µm and 1.74 µm, respectively. The value of λ_D for Ge-doped SiO_2 would lie between these two values depending on the actual Ge dopant concentration. Similar graphs can be plotted for other dopants such as P, Al, F and B as long as the Sellmeier coefficients are known.

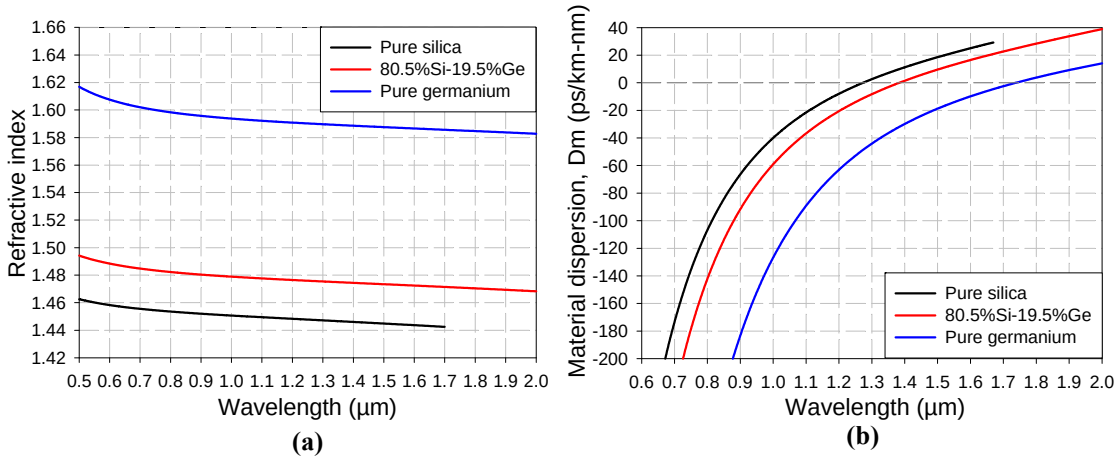

Figure 2.6 Dependence of refractive index and material dispersion with wavelength: (a) refractive index of pure silica, germanium doped silica and pure germanium as a function of wavelength; (b) material dispersion of pure silica, germanium doped silica and pure germanium as a function of wavelength.

In addition to the intrinsic material dispersion, there also exists a type of dispersion called waveguide dispersion. As the name suggests, it is a consequence of the mere confinement of light to the core of a fibre waveguide. It was shown earlier how light propagates in fibres with only certain field distributions known as modes characterised by a distinct propagation constant (or phase velocity). The group velocity of the modes is given by $v_g = \left(\frac{d\beta}{d\omega}\right)^{-1}$ and depends on wavelength even if material dispersion is negligible. This dependence results from the dependence of the field distribution in the fibre on the ratio between the core radius and the wavelength. If this ratio is altered by changing the wavelength, the relative amount of optical power in the core and cladding is modified. Since the phase velocities in the core and cladding are different, the phase as well as the group velocity of the mode is altered. The waveguide dispersion is given by the waveguide dispersion parameter, D_W [2]:

$$D_W = -\left(\frac{1}{2\pi c}\right) V^2 \frac{d^2\beta}{dV^2} \tag{2.14}$$

Since the propagation constant β for a given fibre is dependent on the normalised frequency V, the waveguide dispersion parameter D_W is also a function of V. It was shown earlier that for a given wavelength the normalised frequency is dependent on the fibre design parameters (see equation 2.11). Therefore the waveguide dispersion is also dependent on the fibre design parameters and provides a useful way to modify the total dispersion profile of a fibre. For a singlemode fibre the total dispersion, D_T (or chromatic dispersion) is given by the combination of D_M and D_W.

In the most common fibre designs the D_M and D_W parameters are of opposite sign at wavelengths longer than the ZDW and can therefore be made to cancel each other at some longer wavelengths. Figure 2.7 shows a plot of the dispersion parameters D_M, D_W and D_T for a step-index fibre and shows the effect of reducing the core size while increasing the index difference, Δn to maintain a constant normalised frequency parameter, V [9].

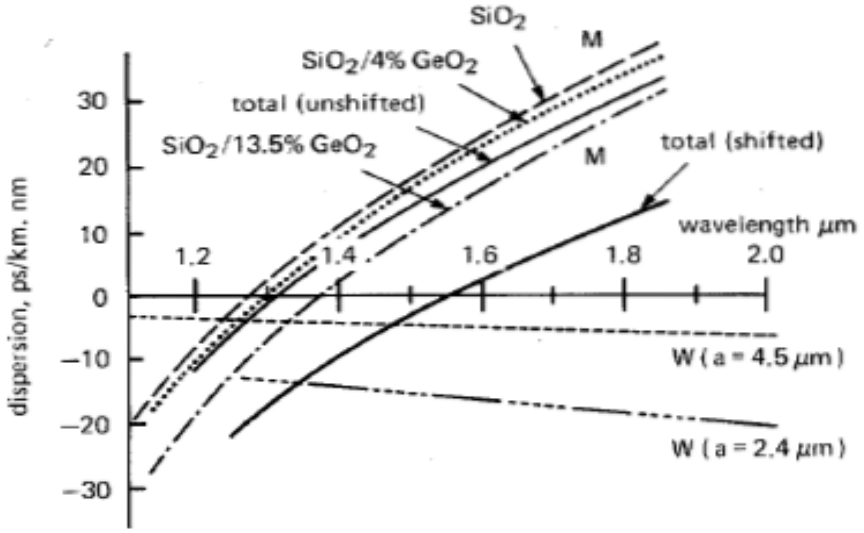

Figure 2.7 Material (M), waveguide (W) and total dispersion for two step-index fibres with different core sizes and germanium concentrations (figure extracted from [9]).

The total dispersion (unshifted) curve corresponds to that of a standard singlemode step-index fibre at 1.55 μm (i.e., a_1=2.2 μm and Δn_1=0.012). The effect of a smaller core size and a higher Δn on the waveguiding contribution to the total dispersion (shifted) can then be seen in figure 2.7 and results in a large shift of the ZDW point. The core radius in this case was reduced to 1.2 μm while the index difference was increased so that the

fibre was still singlemode at 1.55 μm. Further control over the waveguide dispersion has also been shown by modifying the refractive index profiles away from the conventional step-index profile (see for instance [2]).

In multimode fibres there also exists an additional type of dispersion which is due to the differences in group velocities of the individual modes. This difference would introduce a time delay between the individual modes since they propagate at different speeds inside the fibre. Also, although the contribution of material dispersion to the total dispersion is the same, the waveguide dispersion contribution for each mode is different. However, modal dispersion can be eliminated or reduced by allowing just the fundamental mode, or a few modes, to propagate. Graded-index structures can also reduce the modal dispersion significantly.

The importance of dispersion and the effect it has on light propagating in a fibre is dependent on the operating conditions. Important factors could be the operating wavelength, the modal content of the fibre and whether the light propagating in the fibre is CW or pulsed, and if the light is pulsed, what is its pulse width. Dispersion can play an important role in the propagation of pulses inside a fibre since it can induce pulse broadening as a result of different wavelengths within the pulse travelling at different speeds. Dispersion-induced pulse broadening can be detrimental in optical fibre communication systems where short pulses propagate along ten's of kilometres of fibre [3]. However it is very much dependent on the duration of the pulses. At this point it is worth-while introducing the length parameter related to dispersion which can give an indication of the role it will play. In the case of transform-limited pulses, the dispersion length, L_D becomes:

$$L_D = \frac{T_0^2}{|\beta_2|} \tag{2.15}$$

where T_0 is the pulse duration (half width at the 1/e intensity point) and β_2 is the group-velocity dispersion (GVD) parameter, related to the dispersion parameter by $D_T = -\frac{2\pi c}{\lambda^2}\beta_2$. When the fibre length L is such that $L<<L_D$ then dispersion-induced pulse broadening can be neglected. If we take a standard fibre such as SMF-28 with a value of $D_T = -32\ ps/km \cdot nm$ at a wavelength of λ=1.064 μm, this corresponds to a value of $|\beta_2| \approx 20\ ps^2/km$. Therefore, a 100 ps transform-limited pulse has a dispersion

length of approximately 500 km in such a fibre. Therefore it is safe to say that for transform-limited pulses with nanosecond durations or longer, the dispersion-induced broadening can be neglected for fibre lengths of several kilometres. Nevertheless, even when dispersion-induced broadening can be neglected, dispersion can still play a crucial role when considering nonlinear effects in fibres, including the Raman amplifiers that I have studied.

2.1.4 Nonlinear effect in fibres

Nonlinear effects arise in optical fibres as a consequence of intense EM fields modifying the optical response of the fibres material, compared to lower EM intensities. Optical fibres can support a vast number of nonlinear effects which can transform the spatial, temporal and spectral structure of the initial EM field and the way it propagates along the fibre. Consequently nonlinear effects are not welcome for many applications. However they have also produced a wide range of desirable effects and interesting phenomena in fibres bringing about a whole host of new and potential applications. A good example is that nonlinear effects can turn fibres into wavelength converters allowing the generation of light at new wavelengths.

The origin of nonlinear effects arises from several effects such as the motion of bound electrons and the oscillation of nuclei under the influence of an applied EM field. In general, at low intensities, when an electric field **E** propagates through a material, a polarisation density **P** (or dipole moment per unit volume) is induced which depends linearly on the electric field **E** so that:

$$\mathbf{P} = \varepsilon_0 \chi^{(1)} \mathbf{E} \tag{2.16}$$

where ε_0 is the vacuum permittivity and $\chi^{(1)}$ is the linear susceptibility. The effects of the linear susceptibility such as dispersion, spontaneous Rayleigh scattering and absorption are included through the refractive index n and the attenuation coefficient α. As the applied field becomes more intense this relationship is no longer satisfied and the induced polarisation now depends nonlinearly on the applied electric field. In this case the polarisation is now expressed as a power series expansion [10]:

$$\mathbf{P} = \varepsilon_0(\chi^{(1)} \cdot \mathbf{E} + \chi^{(2)} \cdot \mathbf{EE} + \chi^{(3)} \cdot \mathbf{EEE} + \cdots) \tag{2.17}$$

where $\chi^{(2)}$ and $\chi^{(3)}$ are the second- and third-order nonlinear susceptibilities, from which arise a whole host of nonlinear effects. The second order susceptibility is responsible for such nonlinear effects as second harmonic generation (SHG) and sum-frequency generation (SFG). However, second order nonlinear effects are not generally seen in optical fibres as they require structures that lack inversion symmetry and silica is in fact a symmetric structure.

As a result, the lowest order nonlinear effects in fibres are a consequence of the third-order nonlinear susceptibility $\chi^{(3)}$. This is responsible for such effects as four-wave mixing (FWM), the intensity-dependent refractive index and stimulated inelastic scattering processes amongst others. A good review of nonlinear effects in fibres is given by Agrawal [10]. One thing that becomes clear is that all these nonlinear effects exhibit a threshold-like behaviour. However this is not only dependent on the intensity in the fibre, but also has a dependency on other parameters such as pulse width, dispersion profiles and the material properties. Consequently, multiple nonlinear effects may occur inside a fibre, which are interrelated or simply one nonlinear effect may dominate. The focus of this thesis is mainly on the nonlinear effect of SRS and the regime in which it dominates. Stimulated Raman scattering falls into the category of stimulated inelastic scattering processes and arises from induced changes in the motion of nuclei under the influence of an applied EM field.

2.1.4.1 Raman scattering

As touched on in the introductory section, Raman scattering is the inelastic scattering of light by matter. In the case of pure-silica fibres, this is through interactions with the vibrational modes (also called optical phonons) of the silica molecules. The incident light is scattered with a change in frequency that is determined by the frequency of the molecular vibration. Normally the incident light will lose energy in exciting the vibration, according to the well known relation $E = h\nu = h\frac{c}{\lambda}$ and consequently be scattered at a longer wavelength. However, if the molecule is already in an excited vibrational state, the incident light interacts through a relaxation in which case it will gain energy and be scattered at a shorter wavelength. Light scattered at a

longer wavelength is referred to as Stokes light whereas light scattered at a shorter wavelength is referred to as anti-Stokes light. Typically the probability of anti-Stokes scattering is much smaller than Stokes scattering by a Boltzmann factor of $\exp\left(-\frac{\hbar\omega}{K_B T}\right)$ due to the fact that the molecule is less likely to be in an excited state. Therefore anti-Stokes scattering cannot generate gain and plays no role in the context of RFAs and so will not be considered again.

Furthermore, at low intensity levels only a small fraction of the incident light, approximately 1 part in 10^6, is scattered into the Stokes wave and is spontaneous in its nature [11]. However under the excitation of intense pump light that is guided along an optical fibre, the Stokes wave can continue to propagate with the pump light. The spontaneously scattered Stokes light then beats with the pump in a way that enhances the probability of Raman scattering. The probability is proportional to the intensity of the pump as well as the Stokes wave. Under these conditions it is possible for a large portion of the initial pump light to be transferred to the Stokes wave. Alternatively, signal light at the Stokes wavelength can be coupled into the fibre along with the pump light, resulting in the signal being amplified through the stimulated conversion process. The signal is amplified in accordance with a gain parameter called the Raman-gain coefficient, which is denoted by g_R. The value of g_R varies depending on the frequency difference between the pump and signal. In pure silica fibres it extends over a large frequency range of approximately 40 THz with a broad peak situated near 13.2 THz. At a pump wavelength of 1 μm, this translates to a shift of 46 nm with a peak value, $g_R = 1\times10^{-13}\, m/W$. This set-up forms the basis of a Raman fibre amplifier (RFA) and the main topic of this thesis, i.e., pulse-pumping of a cascaded RFA. Since this is the case, we shall dedicate the next section to the properties of RFA's. To conclude this section we shall look briefly at the nonlinear effects that can impede Raman generation and stop the SRS process from occurring.

An RFA involves the interaction of light offset at different wavelengths which can have important consequences when pulses are used. Due to dispersion, pulses at different wavelengths propagate at different speeds within the fibre. This feature leads to a walk-off effect, whereby a faster moving pulse walks through (or away from) the slower moving pulse and the interaction between the two pulses gradually comes to an

end over some length of fibre. This length parameter is usually typified by the walk-off length, L_W which is defined by [12]:

$$L_W = \frac{T_0}{v_g^{-1}(\lambda_1) - v_g^{-1}(\lambda_2)} \tag{2.18}$$

For a pulse duration T_0 >10 ns (@1064 nm), propagating along a length of SMF-28 fibre, L_W exceeds 1 km for the pump and Stokes wavelengths and obviously increases with pulse duration. To extract the maximum achievable gain from the RFA this walk-off effect has to be avoided. This mode of operation where GVD effects become insignificant corresponds to the so-called quasi-CW regime [10]. In this regime the CW theory is approximately valid and can in fact be used in many instances to analyse the properties of Raman fibre devices. Moreover it also represents a possible regime in which SRS can be employed as the dominant nonlinear effect leading to Raman fibre devices that can be operated in a controlled manner where only the fundamental properties of SRS in fibres need to be considered. In fact in this quasi-CW regime (T_0 >~10 ns) the dominating nonlinear effects are SRS, stimulated Brillouin scattering (SBS) and FWM.

2.1.4.2 Brillouin scattering

Brillouin scattering is similar to Raman scattering in that it is also a form of inelastic light scattering. The difference is that Brillouin scattering involves the interaction of light with acoustic waves (also called acoustic phonons). Once again at low intensity levels only a small fraction of the incident power is scattered to the Stokes wave and is spontaneous in its nature. However like SRS, the Brillouin scattering process can become stimulated through the use of intense pump light and therefore more efficient. In this case, intense pump light propagating along the fibre beats with the Stokes wave, which reinforces the acoustic wave through the electrostriction process. Electrostriction is the change in the fibre's material density induced by the presence of an intense electric field. The Stokes light interferes with the pump light to produce a periodic density wave that propagates at the speed of sound in the medium corresponding to the difference frequency of the pump and Stokes waves. Since the refractive index changes with material density, this density wave manifests into a

moving fibre Bragg grating (FBG). In a singlemode optical fibre, these moving FBG's scatter the pump light backwards. Moreover, since the FBG is moving the scattered light is downshifted in frequency corresponding to a Doppler shift associated with the moving grating. The frequency of the scattered light therefore matches the frequency of the initial spontaneous Stokes light. This is the process behind SBS in fibres. In contrast to SRS, the peak value for the Brillouin gain coefficient, g_B occurs at a frequency shift of 10 – 100 GHz and exhibits an extremely narrow bandwidth of $\Delta\nu_B$~10 – 100 MHz. At a pump wavelength of 1 μm this translates to a shift of only 33 pm with a peak value of $g_B \approx 5\times10^{-11} m/W$. This is in fact nearly three orders of magnitude larger than the peak Raman gain coefficient.

Therefore SBS can in fact occur in optical fibres at input power levels much lower than those required for SRS. It therefore represents an obstacle to overcome when constructing RFAs. However since the bandwidth of Brillouin gain is very narrow, the full Brillouin gain is only reached with a pump source with a narrow spectral width. It has been shown that the SBS gain reduces by a factor of $1+\Delta\nu_P/\Delta\nu_B$, where $\Delta\nu_P$ is the spectral linewidth of the pump source [13]. Consequently the SBS threshold increases significantly when $\Delta\nu_P >> \Delta\nu_B$ [10]. To compare the threshold power levels between SBS and SRS it is worthwhile to consider the equations derived to estimate the critical power for these stimulated inelastic scattering processes to occur. The critical power is defined as the amount of input pump power required for half the pump power to be transferred to the Stokes wave for a given fibre. The critical powers, P^{Cr} are given by the following two equations [14]:

$$P_{SRS}^{Cr} \approx 16\frac{A_{eff}}{g_R L_{eff}} \tag{2.19}$$

$$P_{SBS}^{Cr} \approx 21\frac{A_{eff}}{g_B L_{eff}}\left(1+\frac{\Delta\nu_P}{\Delta\nu_B}\right) \tag{2.20}$$

where A_{eff} and L_{eff} are the effective area and effective length of the fibre, respectively. Therefore, for SRS to occur before SBS the critical powers levels must be so that $P_{SRS}^{Cr} < P_{SBS}^{Cr}$. Figure 2.8 shows the critical power levels for SRS and SBS versus pump source linewidth. For the purposes of the calculation the fibre has a length of 1 km, an effective area equal to 10 μm^2 and a background loss of 1 dB/km at a wavelength of

1 μm. It basically shows that for a linewidth greater than 4 GHz, the SRS threshold is lower than that of SBS. The conclusion is that an RFA can be constructed by using a broad bandwidth pump source so that $P_{SRS}^{Cr} < P_{SBS}^{Cr}$.

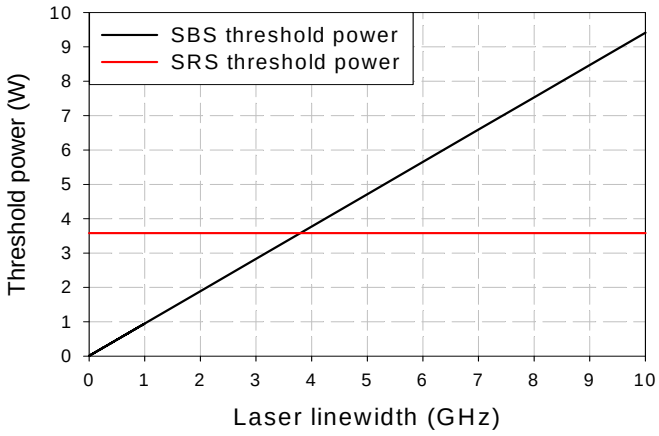

Figure 2.8 Plot showing SRS and SBS critical power levels versus laser linewidth of the pump source.

However, it must be noted that in the case of an RFA, a narrow linewidth signal could also generate SBS. If an amplified narrow linewidth signal is desired then other ways to suppress SBS must be explored. This could for example involve broadening the Brillouin gain bandwidth, $\Delta\nu_B$ (see for instance [15, 16]).

In my experiments the pump and signal linewidths were sufficiently large for avoiding SBS.

2.1.4.3 Four-wave mixing

Another nonlinear effect that can compete with SRS in the quasi-CW regime is FWM. As the name suggests this process involves interaction among four optical waves through the nonlinear response of bound electrons. Optical waves at three frequencies ω_1, ω_2 and ω_3 interact in the optical fibre to generate a fourth optical wave at a frequency ω_4. Energy conservation restricts the frequency at which the optical waves may be generated such that $\omega_4 = \omega_1 + \omega_2 - \omega_3$. Furthermore the efficiency of the power transfer to the newly generated frequency depends on momentum conservation in a process referred to as phase matching. The phase-matching requirement in an optical fibre is given by [10]:

$$\Delta\beta = \beta_1 + \beta_2 - \beta_3 - \beta_4 = (\tilde{n}_1\omega_1 + \tilde{n}_2\omega_2 - \tilde{n}_3\omega_3 - \tilde{n}_4\omega_4)/c = 0 \qquad (2.21)$$

where $\tilde{n}_1$, $\tilde{n}_2$, $\tilde{n}_3$ and $\tilde{n}_4$ are the effective indices of the four optical waves. Therefore the efficiency of FWM in optical fibres depends on dispersion properties of the optical fibre. In the partially degenerate case of $\omega_1 = \omega_2$, two optical waves of the same frequency produce two sidebands located symmetrically at frequencies ω_3 and ω_4 so that $2\omega_1=\omega_3+\omega_4$. Generally the low-frequency sideband at ω_3 and the high frequency sideband at ω_4 are also referred to as the Stokes and anti-Stokes bands. This represents a case whereby a single intense pump wave propagating along the fibre can initiate the FWM process. If the phase matching condition is met, the Stokes and anti-Stokes waves are generated from noise or from a weak input signal wave at ω_3 or ω_4, which is then amplified.

In the presence of the strong intensities that are needed for FWM, the phase-matching requirement is modified by self-phase modulation (SPM) and cross-phase modulation (XPM). The total phase mismatch is then given by:

$$\kappa = \Delta\beta + 2\gamma P_p \qquad (2.22)$$

where P_p is the incident pump power and γ is the averaged nonlinear parameter. The corresponding FWM gain is given by:

$$g = \sqrt{(\gamma P_p)^2 - \left(\frac{k}{2}\right)^2} \qquad (2.23)$$

There are several methods to achieve phase-matching such as using the different phase velocities of the waveguide modes in multimode and birefringent fibres or by employing a pump wavelength close to the ZDW of the fibre [17]. The maximum gain occurs at $k=0$ (perfect phase-matching) and is given by:

$$g^{\max} = \gamma P_P = g_{FWM}\left(\frac{P_P}{A_{eff}}\right) \qquad (2.24)$$

where the relation $\gamma = n_2\omega_P/cA_{eff}$ is used and therefore $g_{FWM} = 2\pi n_2/\lambda_p$. Here n_2 is the nonlinear contribution to the refractive index. Typically the FWM gain coefficient is

larger than the Raman gain coefficient by about a factor of 2, although this value depends on polarisation. Achieving phase-matching using the region around the zero-dispersion point represents the main problem in RFAs. Thus a ZDW located within the bandwidth of operation of the RFA could be detrimental as the FWM process would take over from SRS.

In conclusion, although the SBS and FWM processes can potentially have higher gain coefficients and lower power thresholds, this only occurs under certain conditions. In the absence of a ZDW wavelength lying within the operating bandwidth of the proposed Raman amplifier and a narrow linewidth source, the SRS process dominates for the quasi-CW (T_0 >~10 ns) regime. I investigated fibres both with and without ZDW in the wavelength region used in experiments.

2.2 Properties of a Raman fibre amplifier (RFA)

An RFA involves a pump wave which couples power to a signal wave via the process of SRS along a length of optical fibre. In its simplest form this process is described by the following two coupled equations:

$$\frac{dP_S}{dz} = -\alpha_S P_S + C_R P_P P_S \tag{2.25}$$

$$\frac{dP_P}{dz} = -\alpha_P P_P - \frac{\lambda_S}{\lambda_P} C_R P_P P_S \tag{2.26}$$

where P_S and P_P represent the signal and pump power levels and the factor λ_S / λ_P accounts for the vibrational loss. The first term on the RHS of the coupled equations represents the background loss experienced by the signal and pump, where α_S and α_P are the linear attenuation coefficients at their respective wavelengths. The terms containing a product $P_P P_S$, describe the coupling of power between the pump and signal. The SRS process provides gain for the signal (at a longer wavelength) and occurs at the expense of the pump (at a shorter wavelength) which consequently undergoes nonlinear depletion. The last term of equation (2.25) therefore represents the signal growth whereas the last term of equation (2.26) represents depletion of the pump. The strength

of this coupling between the pump and signal is determined by the Raman fibre gain coefficient, C_R [18].

For situations where the pump depletion term can be neglected, there exists an analytic solution to the coupled equations which proves very useful. This is valid when the signal input power is small or the fibre is short, and provides the small-signal gain of the amplifier. Through some integration and substitution between the coupled equations the small signal net gain is given by:

$$G^{net} = \frac{P_S(L)}{P_S(0)} = \exp(-\alpha_S L)\exp(C_R L_{eff} P_P) \tag{2.27}$$

where L_{eff} is the effective interaction length for SRS and is reduced from the actual amplifier length L due to attenuation of the pump.

$$L_{eff} = \frac{(1-\exp(-\alpha_P L))}{\alpha_P} \tag{2.28}$$

From equation (2.27) it is also useful from a practical point of view to define the on-off Raman gain. This is defined as the increase in signal power at the output of the amplifier when the pump power is turned on and therefore takes the signal background loss out of the equation so that:

$$G^{on-off} = \frac{P_S(L)\ with\ pump\ on}{P_S(L)\ with\ pump\ off} = \frac{P_S(L)}{P_S(0)\exp(-\alpha_S L)} = \exp(C_R L_{eff} P_P) \tag{2.29}$$

From equations (2.27) and (2.29) it is clear that the Raman gain depends on the input pump power, the effective length and the Raman fibre gain coefficient. Therefore an RFA would clearly benefit from all these parameters boasting high values. Furthermore they can be traded against each other, so that a high value on one of these parameters can relax the requirement for a high value on the others. For instance the available pump power may be limited in some way or the fibre length may be fixed.

2.2.1 Raman fibre gain coefficient

The Raman fibre gain coefficient is an important parameter when characterising Raman amplifiers as it plays an important role in the rate at which power is transferred from the pump wave to the signal wave. The Raman fibre gain coefficient C_R, is expressed as follows:

$$C_R = \frac{g_R}{A_{eff} K} \tag{2.30}$$

where g_R is the Raman gain coefficient, A_{eff} is the effective area of the fibre and K is the polarisation factor.

The Raman gain coefficient is related to the spontaneous Raman cross-section of the fibre and thus determines the strength of the Raman scattering process and the spectral structure of the Raman gain spectrum. The Raman gain coefficient is related to the spontaneous cross section by the relation [19]:

$$g_R(\nu) = \sigma(\nu) \frac{\lambda_{Stokes}^3}{c^2 h n^2 (\eta(T) + 1)} \tag{2.31}$$

where $\sigma(\nu)$ is the spontaneous Raman cross-section at a given frequency ν, taking into account the temperature of the scattering medium. $\eta(T)$ is the Bose-Einstein population factor which is also dependent on temperature, while the other symbols take on their usual meanings.

Figure 2.9 shows the Raman gain spectrum for fused silica (SiO_2) at a pump wavelength of 1 μm [10]. The spectral features correspond to the frequencies of several vibrational modes in the silica glass matrix. Due to the amorphous nature of silica and the resulting site to site variations within the glass matrix, the vibrational frequencies spread out into bands that overlap thus producing the broad spectrum shown in figure 2.9. The dominant Raman gain peaks in the vicinity of 13 THz corresponds to a Si–O–Si bond bending vibration [20]. It also has a wide bandwidth of approximately 8 THz (FWHM) making it very useful for constructing broadband fibre amplifiers.

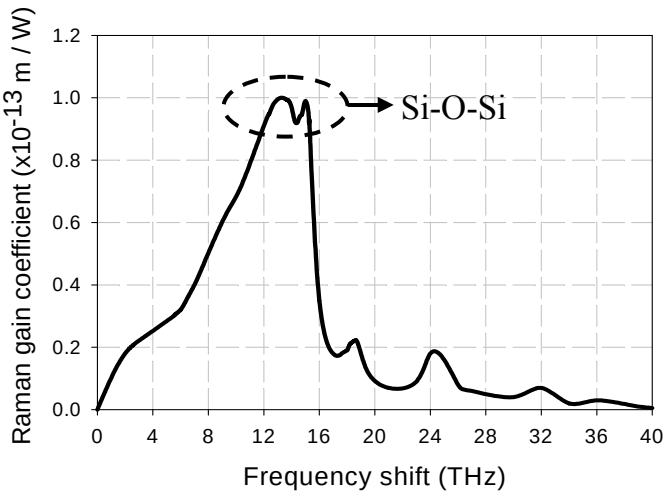

Figure 2.9 Raman gain spectrum for fused silica at a pump wavelength λ_P=1 μm.

The Raman gain coefficient also depends on the fibres composition and since dopants are added to the core to raise the refractive indices, this will have an effect on the Raman gain spectrum. Figure 2.10 (a) shows the Raman spectra of germanium and phosphorous which are two dopants that are commonly added to silica. The y-axis represents the Raman gain coefficient whereby the value of g_R for pure silica has been normalised to one [21]. It shows how phosphorous exhibits a large Stokes shift at 1330 cm^{-1} (~39 THz) which is useful for frequency shifts over a large spectral range. Moreover it shows how the peak of the Ge Stokes shift directly overlaps the Si Stokes shift with a much higher intensity. In fact Ge has a scattering cross-section 9.2 times higher than silica which translates to a gain coefficient that is ~7.7 times higher as shown on the graph. Figure 2.10 (b) also shows that just like the refractive index, the Raman cross section also increases linearly with the Ge doping concentration [22]. The inclusion of Ge results in the double peak feature of Si (see figure 2.9) disappearing into a slightly narrower single peak that is shifted by a small amount from 13.2 to 13 THz. Therefore Ge doped Si fibres can be used to increase the Raman gain coefficient from that of pure Si. However it should be noted that increasing the Ge concentration also increases the NA through the core refractive index and the fibres attenuation. An increase in the NA results in a higher V-number (see equation (2.11)) which can make the fibre multimoded over a certain wavelength range. Alternatively, the core size can be reduced to keep the fibre singlemode at a fixed V-number. This reduces the effective area, which can further increase the Raman gain efficiency.

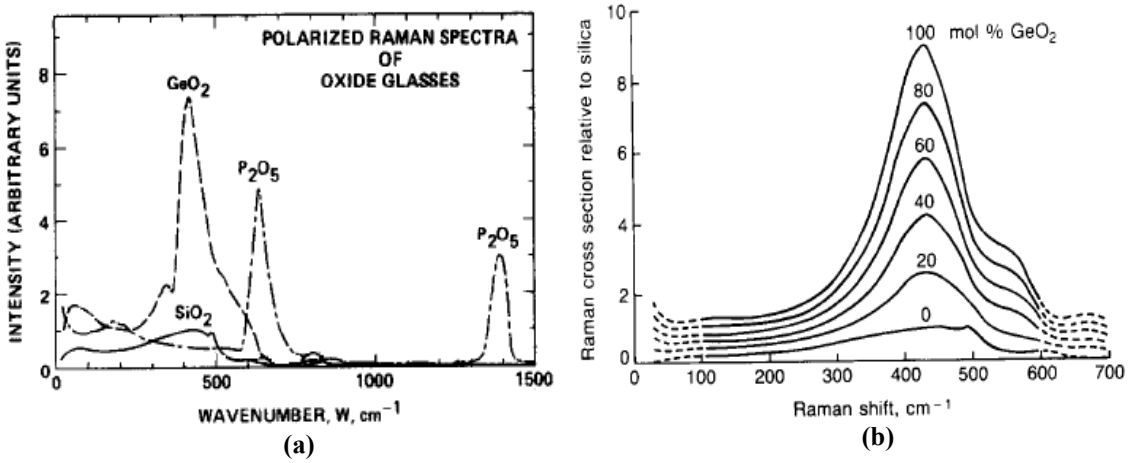

Figure 2.10 Raman gain spectra of various glass formers. (a) The relative Raman spectra of SiO_2, GeO_2 and P_2O_5 with SiO_2 normalised to one (figure extracted from [21]). (b) Zero Kelvin Raman cross-section of germanosilicate glass relative to pure silica (figure extracted from [22]).

The effective area is another important parameter relating the spatial profile of the pump and Stokes wave to the SRS transfer process. This is necessary to determine the intensity inside the fibre since the core area does not match that of the mode field. The effective area is determined from the mode field distribution and the overlap between the pump and Stokes waves and takes the following form:

$$A_{eff} = \frac{\int_A |u_P|^2 dA \int_A |u_S|^2 dA}{\int_A |u_P|^2 |u_S|^2 dA} \tag{2.32}$$

where u_P and u_S represent the mode field distributions over the fibre cross section A and p and s are indices which represent the pump and Stokes wave. This expression can be simplified if one assumes that the mode field distributions are the same for both the pump and Stokes so that $u_P = u_S$. Furthermore if the fibre is singlemode and we approximate the mode field distribution by a Gaussian function, the effective area is further simplified to $A_{eff} \approx \pi w^2$ where w is the mode field radius.

Raman gain is polarisation-dependent and so the polarisation state of the pump and signal waves must be taken into account. The parameter K is used to do this. The maximum value of g_R can only be achieved when the pump and signal waves are co-polarised so that K=1 and typically requires polarisation maintaining (PM) fibres. If the pump and signal are orthogonally polarised it has been shown that the gain coefficient is approximately an order of magnitude smaller [23]. To avoid this situation arising, the

gain can be made polarisation independent by employing either a pump or signal that has an unpolarised state. In this case it has been shown that the parameter K takes on a value of 2 [23].

Although both g_R and A_{eff} can be calculated from knowledge of the fibre refractive index profile (FRIP), it is often more practical to actually measure C_R using equation 2.29 where:

$$C_R = \frac{g_R}{A_{eff} K} = \frac{G^{on-off}(dB)}{4.343 \cdot L_{eff} \cdot P_p} \tag{2.33}$$

This actually gives a more accurate value and takes into account the fact that the Ge concentration typically varies across the cross section of the fibres core and therefore so does g_R. For instance a FRIP different to that of a standard step-index is typically used to modify the dispersion profile (see earlier section on dispersion) or to reduce the optical losses in high Ge-doped fibres [24].

While the Raman fibre gain coefficient is important in determining the rate at which power is transferred from the pump to the signal, other important properties are the bidirectional nature of the Raman gain process and the response time at which it occurs. When the interaction between pump photons and optical phonons takes place during the Raman scattering process, energy and momentum must be conserved (see figure 2.11), so that the following criteria is met [25]:

$$\omega = \omega' \pm \Omega \;\; ; \quad \mathbf{k} = \mathbf{k}' \pm \mathbf{K} \tag{2.34}$$

where ω, $\mathbf{k}$ refer to the incident pump photon, ω', $\mathbf{k}'$ refer to the scattered photon and Ω, $\mathbf{K}$ refer to the phonon created or destroyed in the scattering process.

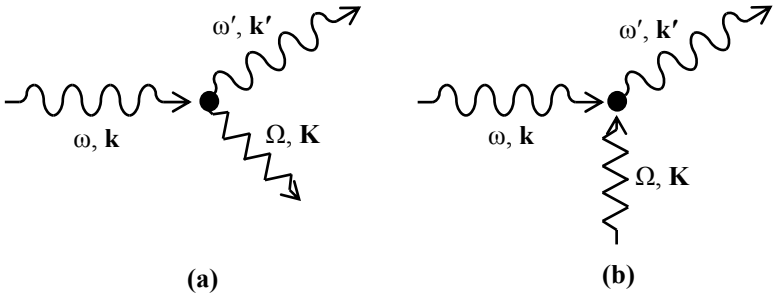

Figure 2.11 Raman scattering of a photon with emission or absorption of a phonon, (a) Stokes emission and (b) Anti-Stokes emission.

The optical phonons that participate in the Raman interaction exist with a broad range of wavevectors and thus phase matching can be easily achieved for all propagation directions between the pump and signal photons. Therefore, Raman gain for a signal wave in an optical fibre is available in both the forward and backward directions relative to the pump wave. This means the pump and signal waves in a RFA can be co-propagating or counter-propagating inside the Raman generating fibre. At any given point in the fibre, the co- and counter-propagating Raman gain are essentially the same, but over the length of a fibre differences in saturation characteristics and evolution of the polarisation of the Stokes wave can lead to significant differences.

In addition the response time of the Raman scattering process is very fast, typically below ~100 fs for silica and germanium fibres [26, 27]. However, when using pump pulses with durations in the ns regime (i.e., throughout this thesis) or longer, the SRS process can be considered instantaneous. This too leads to different characteristics for a Raman amplified signal depending on its relative direction to the pump wave.

2.2.2 Cascaded Raman generation

In the pump depletion regime, power is transferred rapidly from the pump to the Stokes wave so that most of the pump power is in the Stokes wave. If the power in the first-order Stokes becomes large enough it can itself act as a pump for a second-order Stokes wave and so on. At the same time, the Stokes waves (and the pump waves) induce nonlinear absorption (through SRS) at the shorter wavelengths. If the initial pump power launched into the fibre is large enough, higher-order Stokes waves can be generated in what is called cascaded Raman generation.

In this case, a set of coupled-wave equations has to be solved to fully take into account pump depletion due to the generation of higher-order Stokes waves. For pulse-pumping the Raman cascade, the time dependence can also be taken into account. The coupled-wave equations are then given in the following general form [28]:

$$\frac{\partial P_i}{\partial z}+\frac{1}{v_{g,i}}\frac{\partial P_i}{\partial t}=P_i\left[-\alpha_i+\sum_{j=1}^{i-1}\frac{g_R(\nu_j-\nu_i)}{A_{eff}K}P_j-\sum_{j=i+1}^{n}\frac{\nu_i}{\nu_j}\frac{g_R(\nu_i-\nu_j)}{A_{eff}K}P_j\right] \qquad (2.35)$$

where the index i represents the ith signal wave at a frequency ν_i. The index j represents all other signals in descending frequency order such that the terms $j=0$ and $j=n$

represent the pump frequency and final Stokes frequency, respectively. Furthermore, v_g is the group velocity of the pulse. If pulses are not used the time derivative disappears and the equation simply reduces to that of CW pumping. For the simulations carried out in this thesis, the CW pumping version of this equation was employed. Other effects can also be added to equation (2.35) if needed, such as spontaneous Raman scattering and the back capturing of Rayleigh scattering. Also the propagation direction of the pump and signal must also be taken into account. It must be noted that equation (2.35) is only valid for pulses in the quasi-CW regime where effects like GVD, SPM and XPM do not affect the system.

2.2.3 Raman fibre amplifier configurations

Raman fibre amplifiers can be split loosely into two categories based on fibre length and net gain. These are the distributed RFA and the discrete (or lumped) RFA. The primary goal of the distributed RFA is to counteract the passive attenuation loss experienced by a signal propagating along a transmission fibre in long haul optical fibre communications systems. The gain is distributed along the length of the fibre where typical fibre lengths are greater than 50 kilometres and only a net gain close to zero is desired. On the other hand, the fibre lengths involved with discrete RFAs are typically much shorter. The Raman gain is provided at discrete sections of a system set-up, in which case the fibre of a discrete amplifier configuration can be wound onto a drum and packaged into a box with a small foot print. Discrete RFAs can be used for lossless dispersion compensation [29] as well as providing large net gains. For large net gains, it is beneficial to use a fibre with a high Raman fibre gain coefficient. It is also worth pointing out that the shortest fibre length will be restricted by the available pump power and how much of that pump power can be coupled into the core of the fibre.

For both types of RFA, many different configurations exist for the amplifier set-up. Figure 2.12 shows a typical set-up for a RFA. The Raman gain fibre can be either a standard transmission fibre or a high Raman gain efficiency fibre. The pump and signal are combined through some coupling mechanism that could be by use of WDM couplers for an all-fibre device or by using dichroic mirrors and lenses for free-space coupling. There are also many pumping schemes. If the pump and signal are coupled into the fibre at the same end and co-propagate in the fibre, it is called co-pumping. If the pump and signal are coupled into the fibre at opposite ends so that they are counter-

propagating, it is called counter-pumping. There is also a case where the fibre is pumped from both ends, which is called bidirectional pumping.

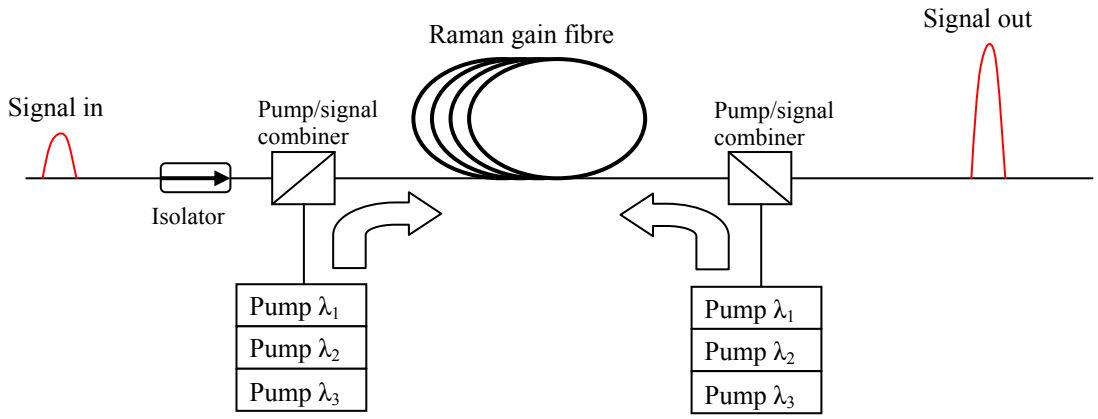

Figure 2.12 Schematic of a typical set-up for a RFA configuration.

Also the pump source may consist of a single wavelength or a pump block consisting of multiple pump wavelengths, each generating gain at different Stokes wavelengths and combining to give ultra-broadband amplification. Furthermore, the pump source may be CW or pulsed which leads to some significant differences in the signal amplification for different pumping directions.

Figure 2.13 shows the evolution of the signal power that is amplified through SRS along a 100 km length of SMF-28 fibre with three different pumping configurations reproduced from the commercial software package VPIphotonics^{TM} [30]. The output from the all the pump sources is CW with a wavelength of 1459.55 nm. It is clear that there are differences between the different pumping schemes. In the co-pumping scheme, a pump power of 867 mW was employed and the gain occurs at the beginning of the fibre and the signal strength is strong throughout the fibre. However, if the signal power becomes too high it can induce nonlinear effects which distort the signals properties and ultimately results in signal errors at the output. In the counter-pumping scheme, a pump power of 380 mW was employed and the gain occurs at the output end of the fibre after the signal experiences significant attenuation, for fibres as long as this one. If the signal power level drops too low it can pick up a substantial noise penalty. On the other hand counter-pumping has been shown to limit the impact of another source of noise due to the pump-to-signal relative intensity noise (RIN) transfer [31]. RIN transfer gives an indication of how a minute change in the pump light

intensity normalised by the overall pump light intensity affects the signal noise and is a noise contribution common to Raman devices due to the fast gain dynamics of SRS. It can be problematic in co-pumped RFAs [31]. The bidirectional pumping scheme employs a co-propagating and a counter-propagating pump power of 193 mW (i.e., a total pump power of 386 mW). It shows a more evenly distributed signal power level which reduces the impact of both the noise penalty from a low power signal and the nonlinear penalty from a high power signal.

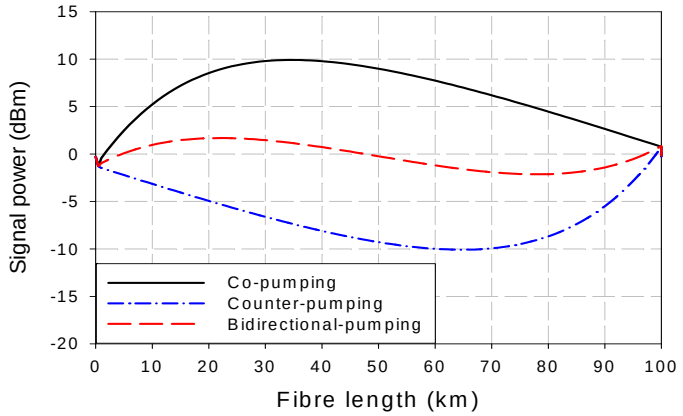

Figure 2.13 The signal power evolution along a 100 km fibre with co-pumping, counter-pumping and bidirectional pumping schemes.

The high RIN transfer of a co-propagating pump can impact the performance although new pump sources have recently been developed with low RIN values [32]. Furthermore, the impact of a noise penalty induced by a low signal power can be reduced by using a high order Raman pumping scheme in a counter-pumped configuration. In this pumping scheme the main pump is separated by two or more Stokes orders from the signal, with pumps also located at intermediate orders. The highest order pump (i.e., furthest from the signal) carries the highest power, while the intermediate pump orders carry lower powers that are unable to generate the required signal amplification through SRS on their own. The highest order pump with the highest power amplifies the next lowest order pump which then amplifies the next lowest order pump and so on, until the first-order pump is reached which then amplifies the signal. This has been shown to push the gain further inside the fibre resulting in less deviation for the signal from its input power level [33]. Figure 2.14 highlights this by comparing 1st-order and 3rd-order pumping for a counter-pumped RFA, again reproduced from the

commercial software package VPIphotonics^{TM} [30]. In this example the transmission fibre is a 120 km length of SMF-28. In the case of the first-order counter-pumped RFA, a pump wavelength of 1455 nm was used with a CW pump power of 850 mW. For the third-order counter-pumped RFA, the third-, second- and first-order pumps were located at 1276 nm, 1356 nm and 1455 nm, with powers of 3.315 W, 1 mW and 10 mW, respectively. This technique of reducing the variation of signal power along the fibres length is more important for distributed RFAs.

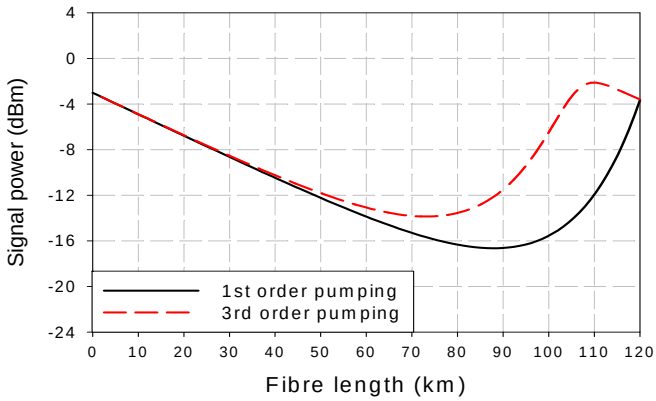

Figure 2.14 Comparison of the signal power evolution along a 120 km fibre for a 1st-order and 3rd-order counter-pumped RFA.

The use of multiple pump sources at different wavelengths with overlapping Raman gain spectra can be used to extend the Raman gain over a 100 nm bandwidth in the 1.5 μm band [34, 35]. Figure 2.15 shows how the individual gain spectra contribute to the overall gain spectrum. The shape of the individual gain spectra is the same for all pump wavelengths and the magnitude of the gain is proportional to the power of the individual pump sources. The overall gain spectrum is simply a superposition of all the individual gain spectra. If the magnitude of gain were to be calculated based on the individual pump powers launched at the fibre input, then the overall gain spectrum would be that of the curve given by the red dashed line in figure 2.15. However in practise, there are interactions between the individual pump waves, whereby the shorter-wavelength pump gives energy to the long-wavelength pump via SRS. This process of pump-to-pump Raman interactions results in a tilt in the overall gain spectrum (see the black curve in figure 2.15). One way round this problem is to modify the pump power distribution among the individual pump sources so that the shortest wavelength pump has more power [34].

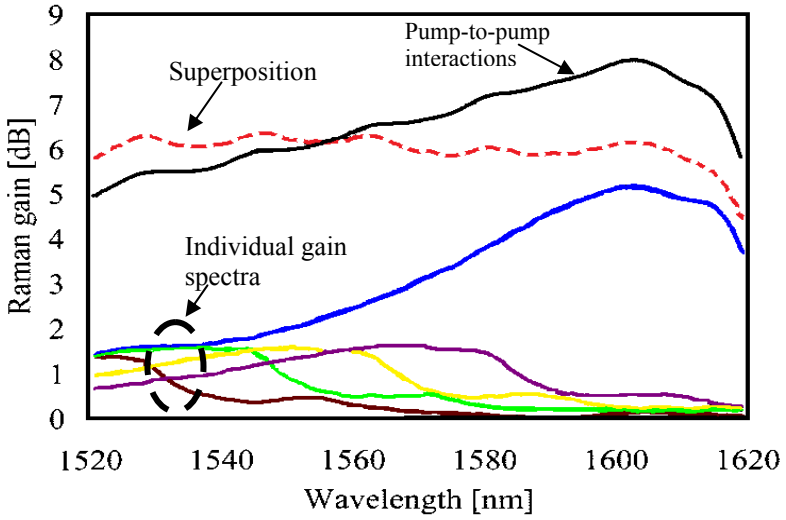

Figure 2.15 Raman gain spectrum produced from multiple pump wavelengths including the individual gain spectra and their overall gain spectrum using superposition and including pump-to-pump Raman interactions (figure extracted from [35]).

Another solution, as outlined in the introduction section is to adopt a time-division multiplexed (TDM) pumping scheme [36]. Pump-to-pump Raman interactions can be avoided by separating the different pump wavelengths in time (i.e., in the case of pulse-pumping) so that they do not spatially overlap inside the fibre. Pulse-pumping leads to different gain characteristics for a co-propagating signal and a counter-propagating signal. This is important in both a distributed and a discrete RFA. A signal only experiences gain when and where it overlaps with a pump pulse and no gain in between. Due to the instantaneous nature of SRS, the Raman gain will have a temporal profile that follows that of the pump profile. When a CW signal co-propagates with the pump pulses, it is amplified according to the temporal Raman gain profile and therefore the pump profile. The CW signal will therefore become temporally modulated and will exit the fibre as a pulsed signal. If the signal is pulsed then it must be launched into the fibre at the same time as the pump pulse through some time synchronisation method. In a co-propagating set-up it is the peak power of the pump pulse that determines the magnitude of the Raman gain.

In a counter-propagating set-up, the signal which is travelling in the opposite direction to the pump will have passed through many pump pulses upon exiting the fibre and so will experience an averaging effect. In this case, although it is the peak power that determines the rate of conversion from the pump to the co-propagating Stokes wave (which dominates over the counter-propagating one due to a higher gain), it is the average power that determines the average Raman gain in the counter-

propagating direction. The average pump power, P_P^{av} is related to the peak pump power, P_P^{pk} by the duty cycle, d so that $P_P^{av} = P_P^{pk} d$. The duty cycle is given by $d = T_{PW} / T_R$, where T_{PW} is the pulse width and T_R is the pulse period, equal to the inverse of the pulse repetition frequency (PRF). Using equation (2.29), the expected co- and counter-propagating on-off gains are then given by:

$$G_{co}^{on-off} = \exp(C_R L_{eff} P_P^{pk}) \tag{2.36}$$

$$G_{counter}^{on-off} = \exp(C_R L_{eff} P_P^{av}) = \exp(C_R L_{eff} P_P^{pk} d) \tag{2.37}$$

Thus, in a logarithmic (decibel) scale, the average gain in the counter-propagating direction is given by $G_{counter}^{on-off}(dB) = G_{co}^{on-off}(dB) \times d$. Since equation (2.19) implies that SRS limits the Raman gain to roughly 16 Np = 69.5 dB (in the co-propagating direction in this case), a low duty cycle would make it difficult to achieve a high counter-propagating gain.

Furthermore, for a pulse-pumped counter-propagating system there has to be many pulses in the fibre so that sufficient averaging can take place. If this is not the case then severe fluctuations from the average gain value can occur resulting in high temporal gain variations similar to that of a co-propagating set-up. In the worst case scenario a pulse train with a low repetition rate could completely fill the entire fibre with a single pulse at one moment, but then leave the fibre completely empty of pump light at a later time. This means the signal will effectively experience CW pumping and then no pumping at all, yielding maximum gain and then no gain for some amount of time. This would result in a large variation in gain for the signal thus making it temporally modulated just like the co-propagating case. However, a high repetition rate, even with a lower duty cycle, can avoid large temporal gain variations while still allowing several pump wavelengths to be multiplexed together to achieve the desired broadband Raman gain spectrum. In practice the interval between the pump pulses (i.e., inverse of the repetition rate) should be much smaller than the transit time of a pump pulse through the fibre. Obviously for a given duty cycle there will be some upper limit for the repetition rate before walk-off effects come in to play and the quasi-CW assumption is no longer valid. Reducing the effect of temporal gain variations on a

counter-propagating signal is important if the temporal profile of the input signal (whether CW or pulsed) is to be maintained at the output of the amplifier.

Another decisive factor when employing pulse pumping of the RFA is the shape of the pump pulses which determines the efficiency of the pump-to-Stokes transfer and the maximum achievable gain in cases when the pump becomes depleted. This can be easily seen by visualising the transfer of energy from various pump pulse shapes. Figure 2.16 illustrates the effect by showing the shape of the original pump pulse, the depleted pump pulse and the generated Stokes pulse for a 1st-order Gaussian pulse, a 3rd-order super-Gaussian pulse and a rectangular pulse. The rate of conversion is determined by the peak power of the pulse and since the power varies across the profile of the Gaussian pulse, different sections of the pulse transfer at different rates. When the centre of the pulse has transferred to the 1st-order Stokes wave, the wings of the Gaussian pulse remain with the pump wave [37]. Any attempt to transfer this remaining power to the 1st-Stokes order by further increasing the pump power results in the generation of a 2nd-order Stokes wave. In the process the 2nd-order Stokes wave starts to deplete any 1st-order Stokes wave that it overlaps with, co-propagating as well as counter-propagating. With a rectangular pulse the peak power is constant across the profile of the pulse and therefore all sections of the pulse experience the same rate of conversion.

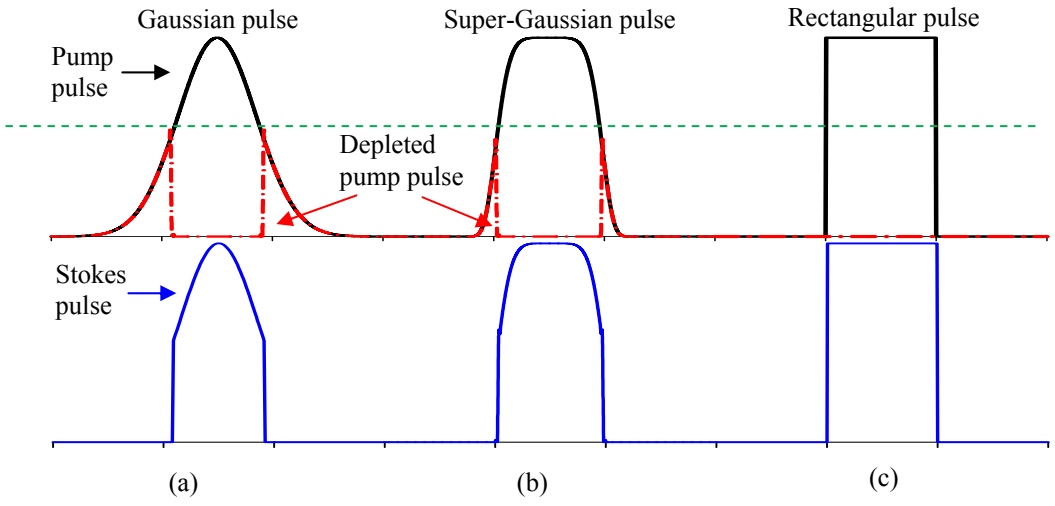

Figure 2.16 Illustration showing the depletion of pump pulses in the SRS process. (a) shows a Gaussian pulse, (b) shows a 3rd-order super-Gaussian pulse and (c) shows a rectangular pulse. The black line indicates the initial pump pulse, the red line indicates the depleted pump pulse and the blue line indicates the Stokes pulse.

In this case it is theoretically possible to transfer the maximum possible energy from the pump to the 1st-order Stokes wave. This leads to the highest 1st-Stokes gain. There will always be the loss associated with the generation of vibrational modes. For peak powers sufficient to generate cascaded SRS, the Gaussian pulse results in the simultaneous excitation of multiple Stokes orders, according to the instantaneous power of the pump pulse. However, with a rectangular shaped pulse the pulse energy can be efficiently transferred to any given Stokes order (see for instance [38]).

In practise a perfect rectangular pulse is difficult to produce and one is more likely to use something similar to a high-order super-Gaussian pulse which has sharper leading and trailing edges compared to a Gaussian pulse. The result is less power being left in the wings of the pulse (see figure 2.16) and therefore a more efficient transfer of power compared to the Gaussian pulse.

2.3 RE doped fibre devices for pump sources

Double-clad RE-doped fibres acting as brightness converters make ideal pump sources for Raman generation, especially for core-pumped Raman devices. The work carried out in this thesis is primarily concerned with using Yb doped DCF pump sources. In this section Yb doped fibres, DCFs and the different laser and amplifier configurations will be reviewed.

2.3.1 Properties of ytterbium doped silica fibres

Ytterbium is a RE ion that is widely used as a dopant for providing gain in silica-based fibres. An attractive feature of the Yb ion is its relatively simple energy level structure, which consists of two manifolds; the ground manifold $^2F_{7/2}$ with four sublevels and the excited manifold $^2F_{5/2}$ with three sublevels (see figure 2.17 (a)) [39]. This helps to avoid unwanted effects that are present in other RE ions such as excited-state absorption (ESA) which ultimately lead to an increasing amount of nonradiative transitions and therefore lower efficiencies. Consequently higher concentrations of Yb ions can be incorporated into the silica fibre which is required for high power operation. Figure 2.17 (b) shows the absorption and emission cross-sections of Yb in an

aluminosilicate glass which dictates the strength of absorption and emission at a particular wavelength. It should be noted that the spectra would vary slightly for other glass hosts such as germanosilicate and phosphosilicate.

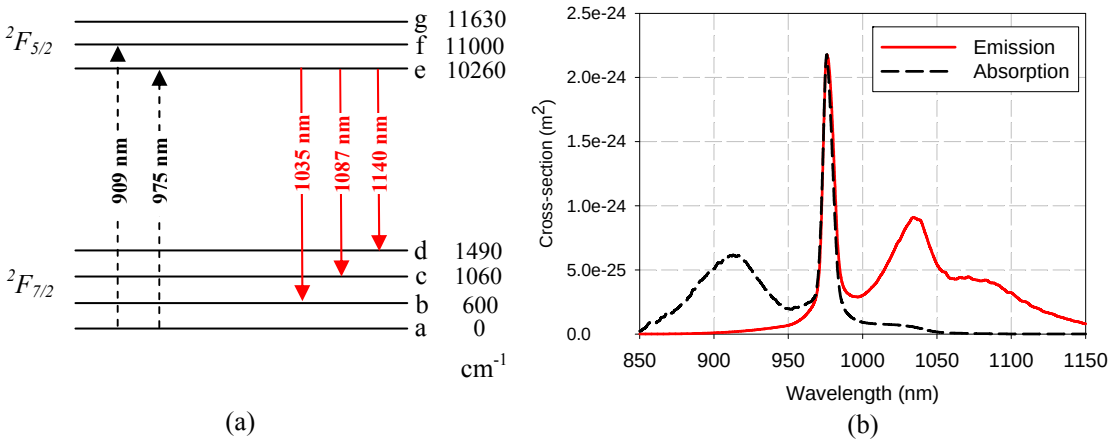

Figure 2.17 (a) Energy level structure of Yb. (b) Absorption and emission cross-sections of Yb ions for a aluminosilicate glass.

As typical for RE ions in a glass fibre, Yb can absorb and emit light over 10's of nanometres. The absorption spectrum extends over a wide range but exhibits two main peaks at ~915 nm and 975 nm which match the output wavelengths of commercially available laser diodes. It also allows the use of high-power diode pump sources. These typically have linewidths of a few nanometres, which can be too wide for efficient pumping, but not in this case. Even so optimum pumping on the 975 nm peak requires active cooling since a slight shift in the wavelength of the pump can result in a significant change in absorption and potential problems. This is less of a problem for a 915 nm pump source. The emission cross-section shows potential for generating gain across a wide spectral region although typical Yb DCFs tend to operate in the range from 1050 to 1120 nm. This makes tuneable lasing and broadband amplification a possibility which is useful for many applications. This close proximity between the absorption and emission wavelengths also provides a low quantum defect which is advantageous as little energy is wasted as heat. The amplification and gain is attained when the populations of the energy levels involved (upper and lower laser level) is inverted. The excited state lifetime of Yb ions in silica based fibres is typically around 0.8 to 1.5 ms [40]. Such a relatively long, "meta-stable", lifetime helps in obtaining a population inversion of the system and thus providing the amplification through

stimulated emission. Again the exact value will vary from fibre to fibre and depends on the host's composition.

2.3.2 Double-clad fibre technology

Rare-earth-doped DCF is the key component behind Raman fibre devices reaching power levels beyond 1 W. Since Raman fibre devices are optically pumped they are heavily dependent on the availability and specifications of the optical pump sources. For the core pumped Raman fibre devices that I study, Yb-doped DCF is used to provide a high-power singlemode pump source for the Raman fibre. Figure 2.18 shows a schematic of a DCF. Here the core is surrounded by two claddings instead of the usual one. The laser gain is still provided in the core but pump light is now launched into the larger inner cladding and confined by the presence of the outer cladding. The refractive indices of the fibre are made such that the core can be singlemode at the laser wavelength while the inner cladding is highly multimoded at the pump wavelength. This relaxes the requirement of beam quality on high power pump diodes which are inherently highly multimoded and allows for a significant increase in the output power of a singlemode beam.

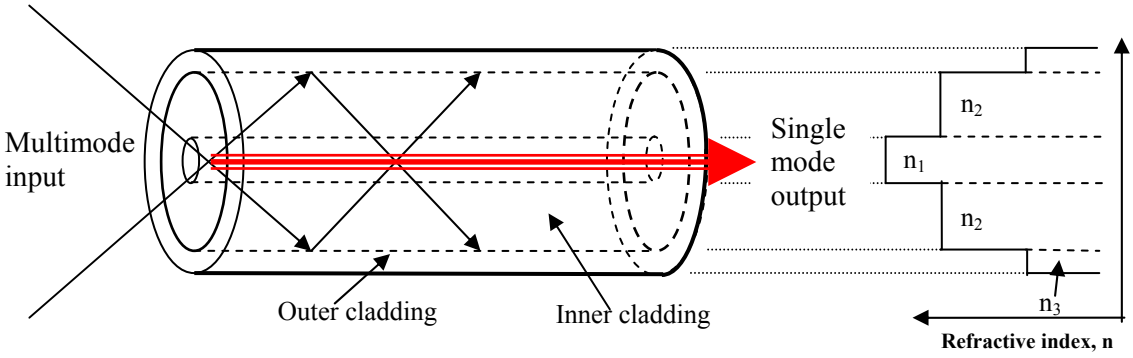

Figure 2.18 Schematic of a double-clad fibre with its corresponding refractive index profile where $n_1 > n_2 > n_3$.

One real problem with this design is obtaining significant absorption of the pump light in the core by the RE ions. Pump absorption in DCFs is relatively low since the pump light propagates predominantly outside the core where the RE ions are typically situated. In fact it is possible for some pump modes, known as skew modes, to be launched into the inner cladding and never overlap with the core and excite the RE ions. This affects the efficiency and ultimately leads to a significant increase in the

absorption length and thus the device length. To counteract this one can use the technique of bending the fibre or change the geometry of the fibre (i.e., inner cladding) to induce mode mixing and improve the absorption. Figure 2.19 gives some examples of fibre designs where the absorption has been shown to increase from that of a standard circular DCF (see for instance [41]). These include designs where the core is offset from the middle and the inner cladding is made rectangular or D-shaped, amongst others.

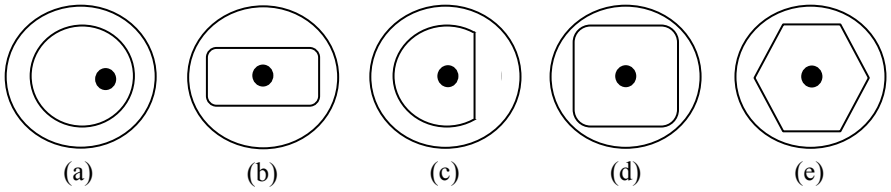

Figure 2.19 Alternative inner cladding shapes to break the circular symmetry: (a) off-set core, (b) rectangular cladding, (c) D-shaped cladding, (d) square cladding and (e) hexagonal cladding.

On the whole, depending on the fraction of the fibre cross-section that is doped (typically given by the inner-cladding to core area ratio), the pump absorption of DCFs is relatively low. As a consequence, relatively long fibres of typically 10 m or more are needed to absorb the pump.

Another important design consideration is that of the pump injection arrangement. Several methods have been employed at some stage throughout this thesis. These are pumping via free-space optics, pumping via a tapered fibre bundle (TFB) [42] and pumping via the use of the GTWave^{TM} [43] fibre format.

The free-space coupling scheme launches light directly into the inner cladding at one or both ends of the DCF via coupling optics such as lenses and dichroic mirrors. Due to its simplicity and flexibility this end-pumping technique is often considered first when characterising DCFs. This is especially true in a research environment when pushing DCFs to their limits in terms of power and also testing new fibre designs such as microstructured DCFs. However the use of free-space optics requires precise and stable alignment. Furthermore it means that one or both ends of the DCF become unavailable for splicing which is often undesired since spliced so-called all-fibre devices are free from misalignment issues and can be made compact and extremely robust. This has led to other pump coupling techniques being developed. The TFB combines multiple pump sources without the use of free-space optics to couple the pump light into the inner cladding. Figure 2.20 show a schematic of a 6+1:1 TFB with

six pump port and one signal port for signal feed-through. Typically 7 or 19 fibres are bundled together in a close-packed formation, heated to melting temperature and then drawn down into a taper. A single passive fibre is then spliced to the taper as the output. The tapered region is coated with low-index polymer. If all the fibres are multimode pump fibres then it is simply a pump combiner (i.e., without signal feed-through).

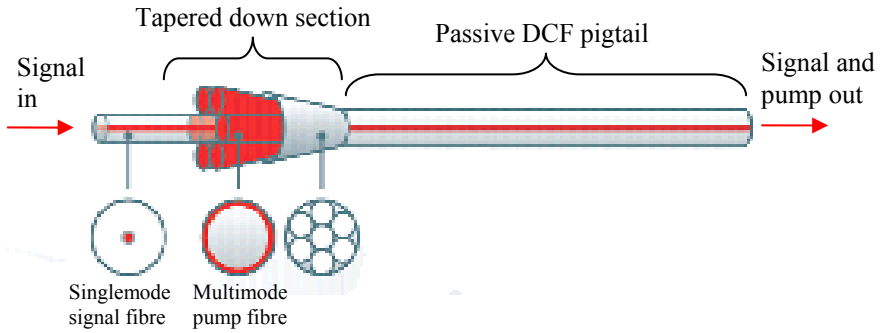

Figure 2.20 Schematic of a 7x1 tapered fibre bundle with 6 pump fibres and a signal feed-through (figure extracted from [6]).

However if a signal fibre is used for the centre fibre then a passive DCF can be spliced to the taper which provides a means for combining and separating multimode pump and singlemode signal fibres. The TFB then has 6 multimode fibres for coupling pump light into the inner cladding of the DCF. A RE-doped DCF is spliced onto the output pigtail. Therefore a signal source and several pump sources can be spliced to the gain fibre via the TFB without impeding each other and without the need for constant monitoring of alignment.

Another double-clad pumping scheme employed in this thesis is the GTWave fibre which is shown in figure 2.21. Like the TFB, the GTWave also allows the combining and separating of the pump and signal in an all-fibre format. The GTWave consists of 2 or 3 fibres, one signal fibre with a RE-doped core and then one or two multimode pump fibres. These fibres are closely packed together so that the pump fibres are touching the signal fibre and then coated with a low index polymer to ensure waveguiding. Once the GTWave is coated the fibres are broken out at each end and matching fibre pigtails (which are separated) are spliced onto the ends. Any pump light launched into the pump fibres then couples between all three fibres in the GTWave section where it is absorbed by the doped core of the signal fibre. The GTWave is different to the TFB and free-space pumping schemes in that the pump injection into the

RE-doped fibre (or strand) is distributed along the length of GTWave. This is in contrast to the two method discussed previously where the pump light is coupled into the ends of the DCF.

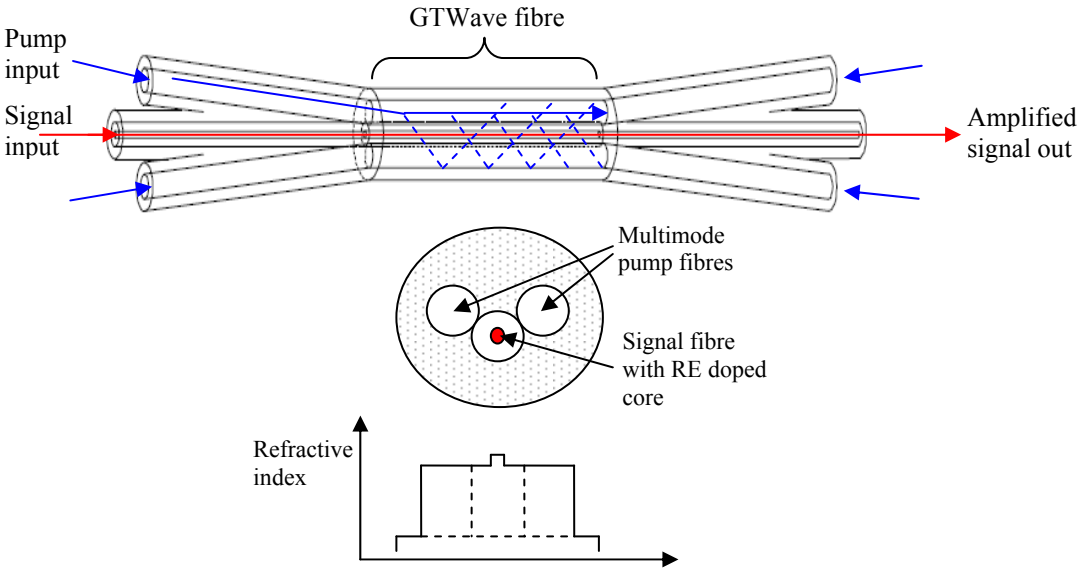

Figure 2.21 Schematic of the GTWave fibre set-up along with a diagram of the GTWave cross-section and corresponding refractive index profile. Courtesy of SPI laser.

These all-fibre pumping schemes, which have only recently been developed to a high standard, mean that other all-fibre and fibre pigtailed components such as FBGs, isolators and WDM couplers can also be spliced into the signal path for the construction of more complex high power devices with increased functionality. A basic configuration of a RE doped fibre laser is shown in figure 2.22 which utilises free-space coupling optics. The cavity is formed by a flat cleave at the output end and an external reflector at the opposite end. The pump and laser wavelengths are combined and separated by use of a dichroic mirror. The laser can be operated in CW mode or in pulsed mode by inserting a modulator into the cavity, usually on the side of the external cavity mirror. If the external cavity mirror is replaced with a seed laser and the RE-doped fibre is angle-cleaved at both ends, the RE-doped fibre can be operated as an amplifier for a seed source. However free-space pumping is only really practical for single fibre devices and is less appropriate for cascading several RE doped fibres in a chain whereby the power level is increased to high power by a series of amplifiers.

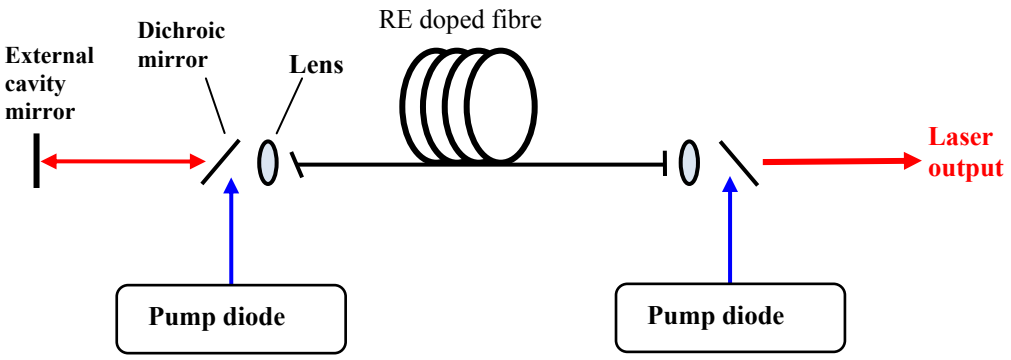

Figure 2.22 Schematic of a basic diode-pumped RE doped fibre laser.

Therefore the use of a free-spaced MOPA configuration is not really viable. One of the main reasons for this is that if one of the amplifiers at the beginning of the MOPA chain becomes misaligned the higher power amplifiers further up the chain would be operating without a seed signal present. This un-seeded state usually leads to self-pulsations within the amplifier and catastrophic damage, resulting in the MOPA having to be re-worked. However the all-fibre pumping format eliminates this problem and makes the MOPA configuration very desirable (see figure 2.23). Determining the characteristics of the seed source at low-power levels means that well developed, high-grade, telecommunication technologies can be used to give a high degree of control. This highly controlled seed source is then amplified to high power-levels through a chain of fibre amplifiers while maintaining the initial characteristics of the seed source. The fibre MOPA source is therefore free from some of the restrictions that are imposed on single fibre oscillators such as that shown in figure 2.22.

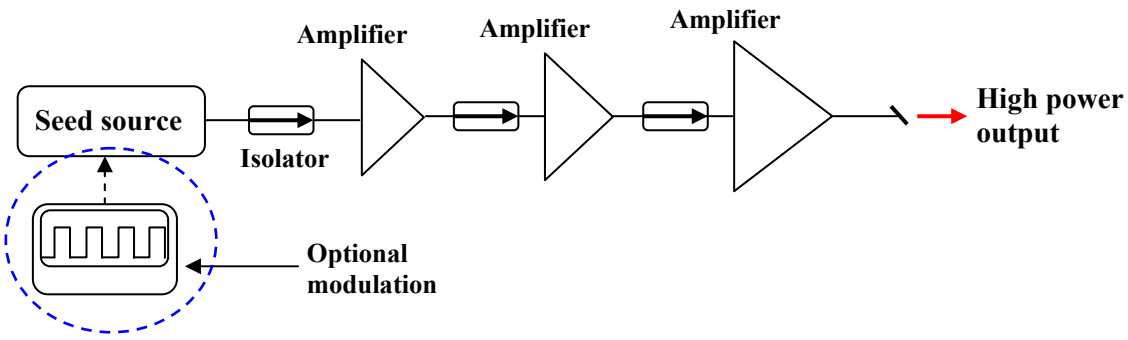

Figure 2.23 Schematic showing a fibre MOPA configuration which includes a seed source and a chain of three fibre amplifiers.

An example could be the restrictions imposed on the pulse parameters by a Q-switched fibre laser source. For instance repetition rates are limited by the amount of

time it takes to replenish the upper laser level population and the pulse build-up time is proportional to the cavity length [44]. Consequently high repetition rates with high duty cycles are difficult to obtain and the use of such a source for certain applications (e.g., counter-pumped RFA) is limited. Furthermore the power of such devices is limited, especially in an all-fibre format where fibre-pigtailed acousto-optic modulators (AOMs) are restricted to around 5 W of average power (see for instance [45]). However as already mentioned, with the MOPA configuration the pulse parameters can be set at low powers by modulating the output of a fibre-delivered semiconductor diode laser. In this instance the laser diode can be either directly modulated or can have its CW output modulated by a fibre-pigtailed AOM or electro-optic modulator (EOM). Both cases offer much better scope for varying the pulse parameters and can produce higher repetition rates and higher duty cycles and over a wider range.

The fibre MOPA source can still be limited at the high power end of the chain by the power-handling capacity of the pump-combining technique and other components such as isolators which are typically used between the amplifier stages to suppress feedback. Fibre-pigtailed isolators made with standard singlemode fibres have been developed to withstand up to 30 W input power with reasonably low insertion losses [46]. Also, in the pursuit of ultrahigh power-levels (beyond 100 W) the design parameters of DCFs have ultimately had to increase in size taking it away from the standard dimensions such as a 125 μm cladding diameter. The size of the inner cladding along with its respective NA is being pushed to its limits in order to accommodate the ever-rising amounts of pump power while maintaining good pump launch efficiency, reasonable absorption and a singlemode output for the signal. Thermal management also becomes more pronounced, especially in all-fibre systems due to the generation of potentially fatal hot-spots at splice points such as in the taper section on the TFB.

However core-pumped RFAs do not require ultra-high power levels. Even though the RE doped DCF has increased singlemode power levels comfortably above the 1 W level the core pumped RFA still suffers from similar issues as RE-doped fibres, such as separation of the pump and signal beams. When using free-space coupling optics with a dichroic mirror in a lab bench set-up, this is primarily due to the high thermal load produced at the fibre input when coupling a large amount of power into such a small core area. Eventually the rising temperature causes thermal fluctuations in the alignment and the launch efficiency drops considerably with possible end facet damage. An “all-fibre” set-up would be preferable also for the RFA, but component

availability and capabilities are issues. Thus the maximum launched power for an amplifier configuration is limited by components such as isolators and WDM couplers to combine and separate the pump and signal. A WDM coupler fabricated with standard fibre can typically handle power levels of 10 W with active cooling (see for instance [47]), although the manufacturers usually specify a much lower power-handling capability. Furthermore, recently WDM couplers handling power levels up to 180 W were used to produce a 150 W RFL [48], although no information was given about the WDM couplers. However, such fused-fibre couplers do not have the bandwidth required for ultra-broad amplification, and more advanced high-power ultra-broad couplers have yet to be developed. Even so, in the case of producing 10 W's of power for a core pumped RFA, one can be bold enough to say that the TFB and GTWave technologies are developed enough to withstand these power levels while still using standard dimension fibres. Thus, "all-fibre" pump MOPAs have been used for the RFAs I have investigated, and the stability and reliability they offer have been pre-requisites for this work.

2.4 References

[1] G. Keiser, *Optical Fiber Communications* (McGraw-Hill, New York, 1983).

[2] B. E. A. Saleh and M. C. Teich, *Fundamental of Photonics* (John Wiley & Sons Inc., New York, 1991).

[3] J. M. Senior, *Optical Fiber Communications: Principles and Practice, 2nd Ed.* (Prentise Hall, New York, 1992).

[4] D. Gloge, "Weakly guiding fibers," Appl. Opt. **10**(10), 2252-2258 (1971).

[5] K. Nagayama, M. Kakui, M. Matsui, T. Saitoh, and Y. Chigusa, "Ultra-low-loss (0.1484 dB/km) pure silica core fibre and extension of transmission distance," Electron. Lett. **38**(20), 1168-1169 (2002).

[6] Information available at: http://www.ofsoptics.com.

[7] J. W. Fleming, "Material dispersion in lightguide glasses," Electron. Lett. **14**(11), 326-328 (1978).

[8] J. W. Fleming, "Dispersion in GeO_2-SiO_2 glasses," Appl. Opt. **23**(24), 4486-4493 (1984).

[9] B. J. Ainslie and C. R. Day, "A review of single-mode fibers with modified dispersion characteristics," J. Lightwave Technol. **4**(8), 967-979 (1986).

[10] G. P. Agrawal, *Nonlinear Fiber Optics, 3rd Ed.* (Academic Press Inc, San Diego CA, 2001).

[11] R. W. Boyd, *Nonlinear optics, 2nd Ed.* (Academic Press Inc, San Diego CA, 2003).

[12] R. H. Stolen and A. M. Johnson, "The effect of pulse walkoff on stimulated Raman scattering in fibers," IEEE J. Quantum Electron. **22**(11), 2154-2160 (1986).

[13] E. Lichtman, A. A. Friesem, R. G. Waarts, and H. H. Yaffe, "Stimulated Brillouin scattering excited by two pump waves in single-mode fibers," J. Opt. Soc. Am. B **4**(9), 1397-1403 (1987).

[14] R. G. Smith, "Optical power handling capacity of low loss optical fibers as determined by stimulated Raman and Brillouin scattering," Appl. Opt. **11**(11), 2489-2494 (1972).

[15] J. M. Cahavez Boggio, J. D. Marconi, and H. L. Fragnito, "Experimental and numerical investigation of the SBS-threshold increase in an optical fiber by applying strain distributions," J. Lightwave Technol. **23**(11), 3808-3814 (2005).

[16] M. J. Li, X. Chen, J. Wang, S. Gray, A. Liu, J. A. Demeritt, A. Boh Ruffin, A. M. Crowley, D. T. Walton, and L. A. Zenteno, "Al/Ge co-doped large mode area fiber with high SBS threshold," Opt. Express **15**(13), 8290-8299 (2007).

[17] R. H. Stolen and J. E. Bjorkholm, "Parametric amplification and frequency conversion in optical fibers," IEEE J. Quantum Electron. **18**(7), 1062-1072 (1982).

[18] J. Bromage, "Raman amplification for fiber communications systems," J. Lightwave Technol. **22**(1), 79-93 (2004).

[19] R. H. Stolen and E. P. Ippen, "Raman gain in glass optical waveguides," Appl. Phys. Lett. **22**(6), 276-278 (1973).

[20] N. Shibata, M. Horigudhi, and T. Edahiro, "Raman spectra of binary high-silica glasses and fibers containing GeO_2, P_2O_5 and B_2O_3," J. Non-Cryst. Sol. **45**, 115-126 (1981).

[21] F. L. Galeener, J. C. Mikkelsen, R. H. Geils, and W. J. Mosby, "The relative Raman cross sections of vitreous SiO_2, GeO_2, B_2O_2 and P_2O_5 " Appl. Phys. Lett. **32**(1), 34-36 (1978).

[22] S. T. Davey, D. L. Williams, B. J. Ainslie, W. J. M. Rothwell, and B. Wakefield, "Optical gain spectrum of GeO_2-SiO_2 Raman fibre amplifiers," IEE Proceedings-J Optoelectronics **136**(6), 301-306 (1989).

[23] R. H. Stolen, "Polarization effects in fiber Raman and Brillouin lasers," IEEE J. Quantum Electron. **15**(10), 1157-1160 (1979).

[24] M. M. Bubnov, S. L. Semjonov, M. E. Likhachev, E. M. Dianov, V. F. Khopin, M. Y. Salganskii, A. N. Guryanov, J. C. Fajardo, D. V. Kuksenkov, J. Koh, and P. Mazumder, "On the origin of excess loss in highly GeO_2-Doped single-mode MCVD fibers " IEEE Photon. Technol. Lett. **16**(8), 1870-1872 (2004).

[25] C. Kittel, *Introduction to Solid State Physics, 8th Ed.* (John Wiley & Sons, Inc., 2005).

[26] R. H. Stolen, J. P. Gordon, W. J. Tomlinson, and H. A. Haus, "Raman response function of silica-core fibers," J. Opt. Soc. Am. B **6**(6), 1159-1166 (1989).

[27] K. Rottwitt and J. H. Povlsen, "Analyzing the fundamental properties of Raman amplification in optical fibers," J. Lightwave Technol. **23**(11), 3597-3605 (2005).

[28] V. E. Perlin and G. Herbert, "Optimal design of flat-gain wide-band fiber Raman amplifiers," J. Lightwave Technol. **20**(2), 250-254 (2002).

[29] Y. Emori, Y. Akasaka, and S. Namiki, "Broadband lossless DCF using Raman amplification pumped by multichannel WDM laser diodes," Electron. Lett. **34**(22), 2145-2146 (1998).

[30] Information available at: http://www.vpiphotonics.com/.

[31] C. R. S. Fludger, V. Handerek, and R. J. Mears, "Pump to signal RIN transfer in Raman fiber amplifiers," J. Lightwave Technol. **19**(8), 1140-1148 (2001).

[32] Y. Ohki, N. Hayamizu, S. Irino, H. Shimizu, J. Yoshida, and N. Tsukiji, "Pump laser module for co-propagating Raman amplifier," Furukawa review **24**, 6-12 (2003).

[33] J.-C. Bouteiller, K. Brar, J. Bromage, S. Radic, and C. Headley, "Dual-order Raman pump," IEEE Photon. Technol. Lett. **15**(2), 212-214 (2003).

[34] H. Kidorf, K. Rottwitt, M. Nissov, M. Ma, and E. Rabarijaona, "Pump interactions in a 100-nm bandwidth Raman amplifier," IEEE Photon. Technol. Lett. **11**(5), 530-532 (1999).

[35] S. Namiki and Y. Emori, "Ultrabroad-band Raman amplifiers pumped and gain-equalized by wavelength-division-multiplexed high-power laser diodes," IEEE J. Sel. Top. Quantum. Electron. **7**(1), 3-16 (2001).

[36] L. F. Mollenauer, A. R. Grant, and P. V. Mamyshev, "Time-division multiplexing of pump wavelengths to achieve ultrabroadband, flat, backward-pumped Raman gain," Opt. Lett. **27**(8), 592 (2002).

[37] C. Lin and R. H. Stolen, "New Nanosecond Continuum for Excited-State Spectroscopy," Applied Physics Letters **28**(4), 216-218 (1976).

[38] K. K. Chen, S. U. Alam, P. Horak, C. A. Codemard, A. Malinowski, and D. J. Richardson, "Excitation of individual Raman Stokes lines in the visible regime using rectangular-shaped nanosecond optical pulses at 530 nm," Opt. Lett. **35**(14), 2433-2435 (2010).

[39] H. M. Pask, R. J. Carman, D. C. Hanna, A. C. Tropper, C. J. Mackechnie, P. R. Barber, and J. M. Dawes, "Ytterbium-doped silica fiber lasers: Versatile sources for the 1-1.2 μm region," IEEE J. Sel. Top. Quantum. Electron. **1**(1), 2-13 (1995).

[40] R. Paschotta, J. Nilsson, A. C. Tropper, and D. C. Hanna, "Ytterbium-doped fiber amplifiers," IEEE J. Quantum Electron. **33**(7), 1049-1056 (1997).

[41] A. Liu and K. Ueda, "The absorption characteristics of circular, offset, and rectangular double-clad fibers," Opt. Commun. **132**, 511-518 (1996).

[42] D. J. DiGiovanni, "Tapered fiber bundles for coupling light into and out of cladding-pumped fiber devices," US patent 5,864,644 (1999).

[43] A. B. Grudinin, "Multi-fibre arrangements for high power fibre lasers and amplifiers," US 6,826,335 (2004).

[44] M. J. F. Digonnet, *Rare-earth-doped fiber lasers and amplifiers, 2nd Ed.* (Marcel Dekker, New york, 2001).

[45] Information available at: http://www.goochandhousego.com.

[46] Information available at: http://www.eotech.com.

[47] J. C. Jasapara, M. J. Andrejco, A. D. Yablon, J. W. Nicholson, C. Headley, and D. DiGiovanni, "Picosecond pulse amplification in a core-pumped large-mode-area erbium fiber," Opt. Lett. **32**(16), 2429-2431 (2007).

[48] Y. Feng, L. R. Taylor, and D. B. Calia, "150 W highly-efficient Raman fiber laser," Opt. Express **17**(26), 23678-23683 (2009).

Chapter 3 – Raman gain over an ultra-wide range of wavelengths

In this chapter, optical amplification based on pulse-pumped cascaded SRS is investigated as a means of providing amplification over an ultra-wide range of wavelengths. Pulse pumping opens up further opportunities for controlling the Raman gain spectrum that are not available with CW pumping. It is then necessary to know how the amplifier performs in terms of gain, under different operating conditions such as different pump duty cycles and different fibre compositions. This first targeted cascaded RFA operates in a counter-propagating configuration and uses a single pump source with a fixed output wavelength. This RFA only targets gain across a single Stokes order at any one time (i.e., single-channel amplification), and represents the simplest configuration of the ones I have studied. Still, it has the flexibility of controlling the pulse parameters to increase the conversion efficiency and shift the Raman gain to any desired Stokes order within the transparency window of the Raman fibre.

There are three main aspects to the experimental set-up which will be looked at in the next section. First of all, there is the pump source which is based on a MOPA configuration. Then there is the Raman gain measurement technique which requires a seed source over a wide range of wavelengths in order to measure the full span of the ultra-broadband gain spectrum. Last of all, there is the choice of fibres for Raman generation which are characterised in terms of the Raman fibre gain coefficient and dispersion.

3.1 Experimental set-up

3.1.1 Pump source: Yb-doped fibre MOPA

The pump source used for the experiments in this chapter is a Yb-doped fibre amplifier cascade seeded by a directly modulated semiconductor LD. Direct modulation (DM) of the semiconductor seed laser not only provides the flexibility in varying the pulse parameters but also solves one of the primary problems in building the pump source for the cascaded RFA. This is the issue of SBS. There are many ways to increase

the SBS threshold independently of the SRS threshold but the simplest and most practical solution here is to use a seed laser with a broad linewidth since the RFA does not require a narrow-linewidth pump source. Standard semiconductor LDs employing a Fabry-Perot (FP) resonator are usually specified with effective linewidths of the order of a few nanometres which would be enough to increase SBS threshold above that of SRS. However within this effective linewidth there are actually several longitudinal modes which results in multiple peaks that exhibit a much narrower linewidth (see figure 3.1).

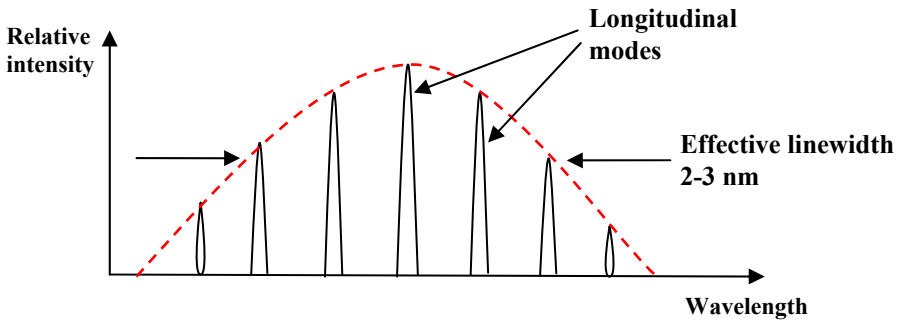

Figure 3.1 Simplified schematic showing the basic spectral structure of a laser diode output.

The individual longitudinal modes can initiate SBS at a much lower power level than that required for SRS, in particular since the power distribution between the longitudinal modes can vary stochastically. This can be a problem when producing pulses by using external devices such as AOMs and EOMs to modulate the CW output of a FP laser diode. In fact when this set-up was attempted, SBS occurred in the Yb-doped amplifiers making the pump source for the RFA unstable. However with DM, the LD is internally modulated by controlling the injection current to the device. Under these conditions it has been shown that the longitudinal modes exhibit broader linewidths as a result of frequency-chirp-induced spectral broadening (see for instance [1]). In this case no SBS was observed and so this was the method used for producing pulses from the seed source.

A schematic of the MOPA source is shown in figure 3.2. As mentioned in the previous chapters the MOPA configuration allows for excellent control of the output by using a highly controlled low-power seed source that is amplified to high power in a chain of amplifiers while still maintaining the desired characteristics of the seed laser. In the case of the MOPA source used here, it is control of the temporal characteristics

through DM of the seed laser that is utilised. This temporal control that is available with the MOPA configuration provides a pump source that opens up new opportunities for controlling the nonlinear process of SRS in optical fibres. The seed source uses a semiconductor LD manufactured by Lumics GmbH [2]. The LD was encased in a standard 14 pin butterfly package and operated with an output wavelength of 1064.4 nm. It was capable of giving an average output power of up to 330 mW. The LD was mounted on a commercial pulsed seed LD driver board, manufactured by Analog Modules, Inc [3], which was capable of producing pulse durations from 20 ns up to CW with rise times of the order of 10 ns. The driver was controlled by electrical pulses from a Tektronix AWG610 arbitrary waveform generator (AWG) which provides the desired pulse parameters and shape. At this stage the peak power of the pulses was kept constant at 330 mW so that the average power varied according to the duty cycle. The seed laser was protected by a 1064 nm fibre-pigtailed isolator which had an insertion loss of ~1.5 dB. After the isolator a 1x2 fused tap coupler with a 99/1 coupling ratio at 1064 nm was spliced into the set-up. This is an important component as the seed laser characteristics can be monitored through the 1% port on an oscilloscope without taking too much power out of the main path.

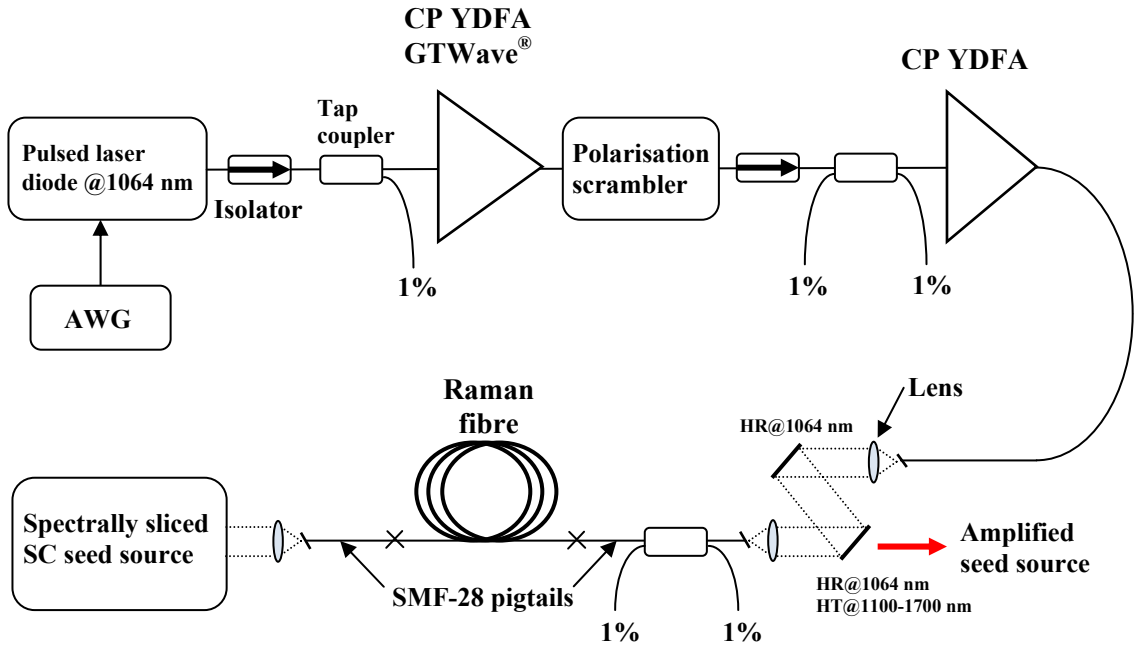

Figure 3.2 Schematic of the MOPA pump source. AWG: Arbitrary waveform generator; CP: Cladding pumped; YDFA: Ytterbium-doped fibre amplifier; HR: High reflectivity; HT: High transmission.

This also helps for making sure the seed laser is working, ensuring that the amplifiers are not turned on without a seed present. The seed is then launched into the first Yb-doped amplifier which was a 6 m long GTWave cladding-pumped amplifier. The signal fibre pigtails have 6/125 μm core/cladding diameters and an NA of the core of 0.14. The GTWave bundle also comprised two multimode pump pigtails with 105/125 μm core/cladding diameters and an NA of 0.22. The amplifier was counter-pumped with a 915 nm source so that the seed signal power was increased to ~400 mW before the next isolator. This resulted in the maximum power allowed at the input of the isolator following the loss incurred in the polarisation scrambler. The polarisation scrambler is necessary since Raman gain is polarisation-dependent and the optical output from a laser diode is strongly polarised. Even though non-PM fibres are used throughout the MOPA chain the output can still exhibit a high degree of polarisation (DOP). However, because non-PM fibres are used, the polarisation can drift and change over time which affects the Raman gain measurements, leading to variations and a lack of repeatability. By using the polarisation scrambler the light is depolarised so that the DOP is close to zero over a time average. This was verified by implementing a polarisation controller in the MOPA chain after the polarisation scrambler. With the polarisation scrambler turned OFF, the polarisation controller could significantly change the Raman gain for a given pump power meaning there were strong polarisation effects. However when the polarisation scrambler was turned ON, the polarisation controller had no affect on the Raman gain measurement. However the depolarisation is not complete, in that the state of polarisation changes much slower than the Raman response time, the amount of walk-off between pump and signal, and the flight-time through the fibre.

Next the (partly) depolarised light was launched into the second amplifier. The amplifier was a 5 m long cladding pumped YDF with a 10/126.5 μm core/cladding diameter and a core-NA of 0.08 (Coractive LAS-Yb-10-02), ensuring that the core was singlemode. A TFB was used to combine the pump and signal in a co-pumping configuration. A difference in the core diameter and NA of the TFB signal fibre and YDF led to ~3 dB splice loss but there was still enough seed power to saturate the final amplifier of the MOPA chain.

The MOPA source could potentially reach an average power level of tens of watts, although the maximum used for the experiments in this chapter was approximately 8 W. As mentioned in the background section, this was due to the

amount of power that could be free-spaced coupled into a small-core fibre for Raman generation. Free-space coupling was employed so that a dichroic mirror could be used to separate the Raman pump (at 1064 nm) and an ultra-broad range of Raman signal wavelengths (see figure 3.2). Figure 3.3 shows the transmission properties of the dichroic mirror used in the experimental set-up. It was required to have high reflectivity (> 99%) at the pump wavelength of 1064 nm and high transmission at the Stokes wavelengths ranging from 1120-1700 nm. Another important aspect of the free-space coupling section is that the fibre ends are clamped in water-cooled mounts. Typical launch efficiencies for this type of set-up are ~80% but without adequate heat sinking this value is only achievable at power levels below 3 W and furthermore requires constant monitoring and adjustments between 2 and 3 W. However with the fibre ends clamped in water-cooled mounts, good launch efficiency is possible up to ~7-8 W before it starts to drift out of alignment and requires constant monitoring and adjustments. Also it is necessary to only have about 1 mm of the fibre end extruding out of the water-cooled mount. This improves heat removal from the fibre tip and restricts movement. The resulting MOPA was adequate for the experiments of this chapter.

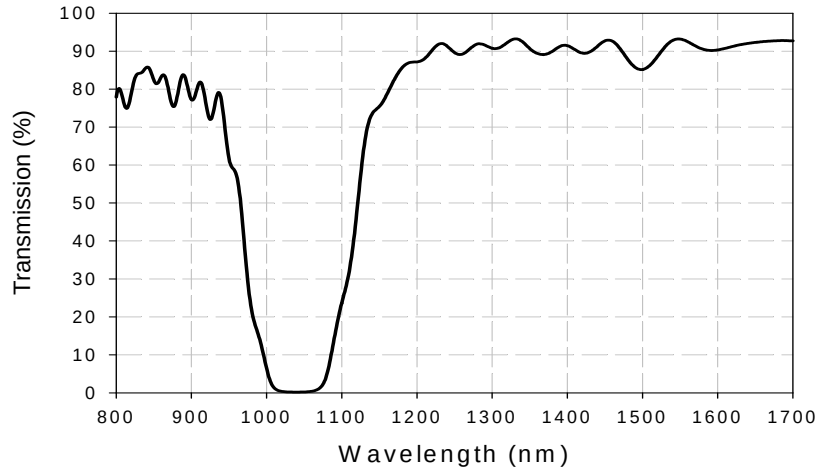

Figure 3.3 Transmission properties of the dichroic mirror at an incidence angle of 45^{o} used to separate the pump and signal of the RFA.

3.1.2 Supercontinuum source

With the MOPA pump source built, the seed source for the cascaded RFA was constructed. The target was to generate and measure Raman gain across a wavelength range from the pump wavelength to the edge of the transparency window of the Raman

generating fibre. This required a flexible seed source from 1064 nm to 1700 nm. Therefore a supercontinuum (SC) light source was chosen, as shown schematically in figure 3.4. The SC source uses a MOPA configuration seeded by a tuneable laser source (TLS) in the 1.5 μm region which is directly modulated by a pulse generator. The TLS emits 4 ns long pulses with a repetition rate of 100 kHz. Given that a TLS normally emits a single line with sub-MHz linewidth, SBS is a concern. However several factors influence the pulse characteristics and linewidth. First of all by using 4 ns pulse durations, SBS can be avoided so that the necessary peak powers are attainable [4]. The reason is that at such pulse durations, even the linewidth of an initially transform-limited pulse, when broadened by SPM is sufficient to suppress SBS. Furthermore, in my case, the seed pulses are not transform-limited since direct modulation chirps the pulse. The pulses are then amplified by two cascaded Er-based fibre amplifiers. The first is a core-pumped EDFA and the second is a cladding-pumped erbium:-ytterbium co-doped fibre amplifier (EYDFA). The MOPA produced pulses with peak powers of the order of 375 W corresponding to an average power of 150 mW.

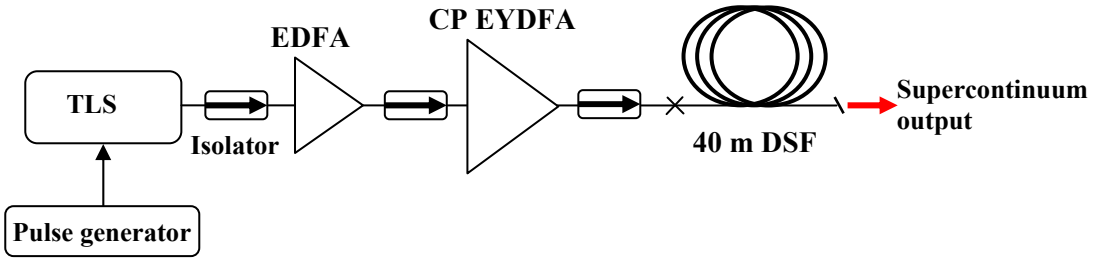

Figure 3.4 Schematic of the supercontinuum source which was used to seed the ultra-broadband Raman amplifier.

The pulses were then launched in to a 40 m long piece of Pirelli Freelight™ DSF for SC generation. This DSF had a ZDW of 1532 nm and was pumped with a wavelength of 1542 nm from the MOPA source, resulting in the optical spectrum shown in figure 3.5. The SC spectrum comfortably spans from 1064 to 1700 nm. In fact the full spectrum extends beyond 1750 nm but this is the limit of the wavelength detection range of the optical spectrum analyser (OSA) used for the measurement. However, coverage to 1700 nm was sufficient for my experiments.

For spectral gain measurements, this SC output was then launched into a monochromator which could slice up the full spectrum into 2 nm wide segments using a "bulk" diffraction grating. The centre wavelength of each segment was dictated by the

angle of the diffraction grating. Thus, the SC source followed by a monochromator provided a temporally modulated spectrally narrow input seed signal to the RFA which was tunable over the full range of wavelengths shown in figure 3.5. The launched seed power to the RFA varied by around 5 dB depending on wavelength, from ~2 μW to ~6 μW.

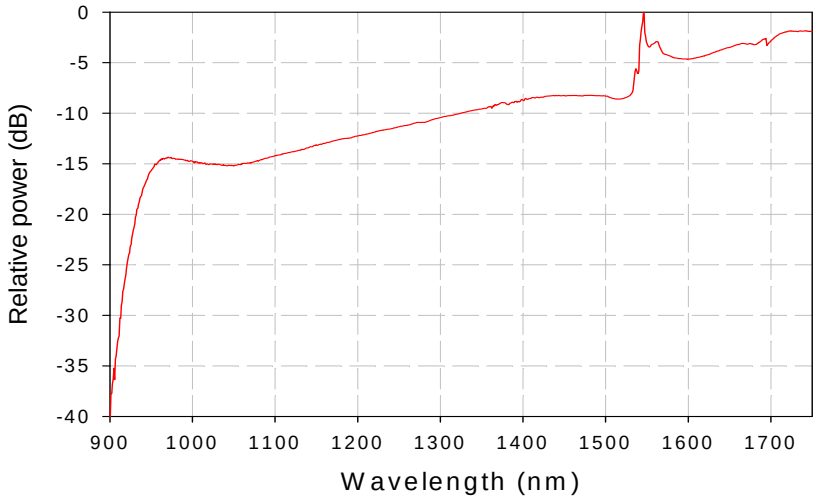

Figure 3.5 A plot showing the optical spectrum of the supercontinuum output used to measure ultra-broadband Raman gain.

3.1.3 Raman gain fibre

For the majority of the experimental work, three optical fibres were used for the purpose of cascaded Raman generation. Each fibre can be characterised by their Raman fibre gain coefficients, which differ as a consequence of different Ge dopant concentrations and different effective areas. The FRIPs of the three fibres are shown in figure 3.6. The SMF-28 and Freelight™ DSF FRIPs were measured experimentally whereas the Sumitomo HNLF FRIP is an approximation. The first fibre is SMF-28 fabricated by Corning™ which uses a standard step-index profile and is primarily used for optical communication systems. The second fibre is Freelight™ fabricated by Pirelli (now Prysmian cables & systems) and is a DSF also used primarily for optical communication systems. The third is a HNLF fabricated by Sumitomo Electric Industries, Ltd designed specifically for enhancing the nonlinear response with an increased Ge content and a smaller core diameter. The variation between the core/cladding refractive indices and core diameters is clear to see from the FRIPs. From the FRIPs it was determined that the SMF-28 had the lowest Ge content of ~3.5% (mol)

and as expected the Sumitomo HNLF had the highest Ge content of ~26% (mol). Furthermore it is possible to calculate the Raman gain coefficient from the Ge dopant concentration and estimate the Raman fibre gain coefficient. With a 26% (mol) concentration of Ge and using reference [5] the Raman gain coefficient for the HNLF is calculated to be ~2.87x10^{-13} m/W. This is in comparison to pure-silica which has a Raman gain coefficient of ~1x10^{-13} m/W at a wavelength of 1 μm.

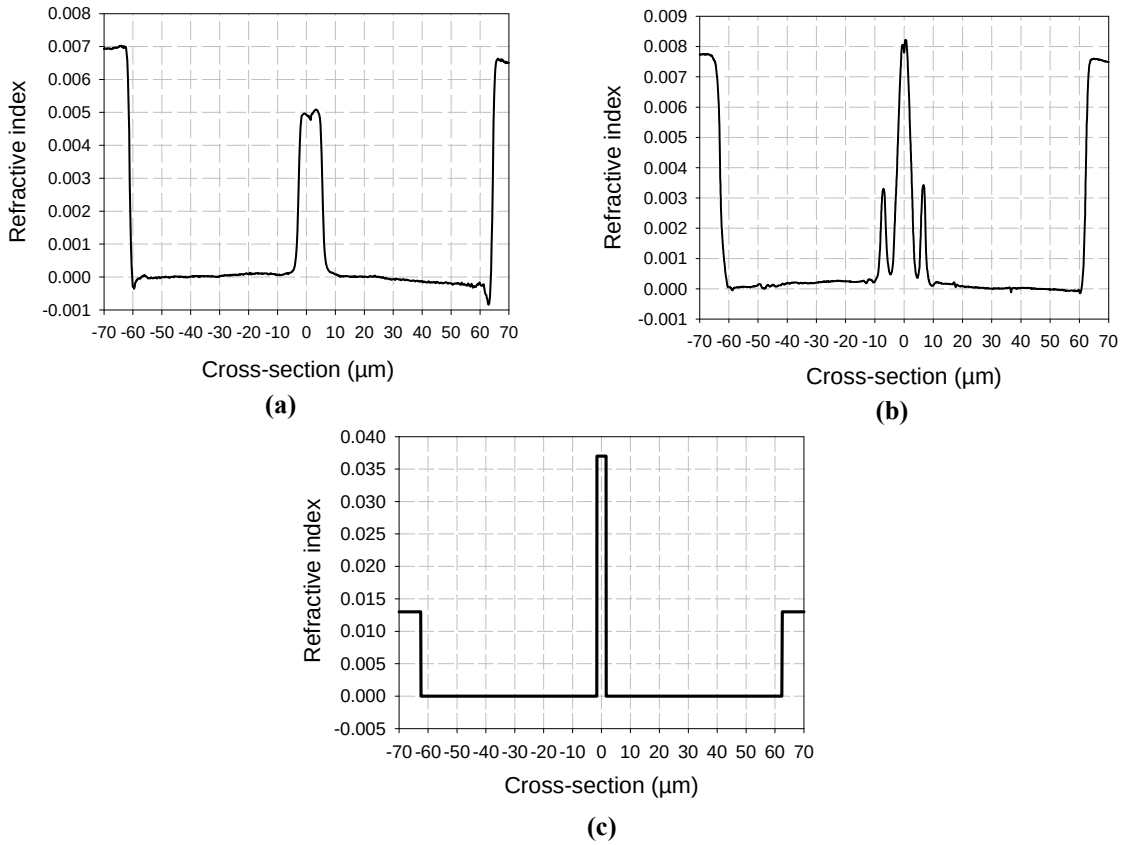

Figure 3.6 Refractive index profiles of three fibres used for cascaded Raman generation: (a) Corning™ SMF-28, (b) Pirelli Freelight™ DSF and (c) Sumitomo HNLF (approximate).

If we estimate the effective area to be 10 μm^2, then the Raman fibre gain coefficient C_R for unpolarised light is ~0.0144 m^{-1}W^{-1}. However, as mentioned in the background section it is often more accurate to measure values of C_R experimentally. Using equation 2.33 from the background section the Raman fibre gain coefficient was measured for all three fibres using the set-up shown in figure 3.2, except that the pump source was CW instead of pulsed. Then for a given pump power, the Raman gain was measured while tuning the seed source over the appropriate range of wavelengths. Figure 3.7 shows the Raman fibre gain coefficient spectra that were obtained for the three fibres. As expected there were significant differences between the peak values.

The peak Raman fibre gain coefficient value for the SMF-28, Freelight™ DSF and HNLF was 0.776 $km^{-1}W^{-1}$, 1.668 $km^{-1}W^{-1}$ and 14.26 $km^{-1}W^{-1}$, respectively. The measured value for the HNLF is very close to the estimated value. It can also be seen how the gain spectrum changes to a single peak that shifts to a slightly shorter wavelength as the Ge concentration increases, as mentioned in chapter 2. These Raman fibre gain coefficient spectra can be used to calculate the pump power required for a given fibre and for simulation purposes.

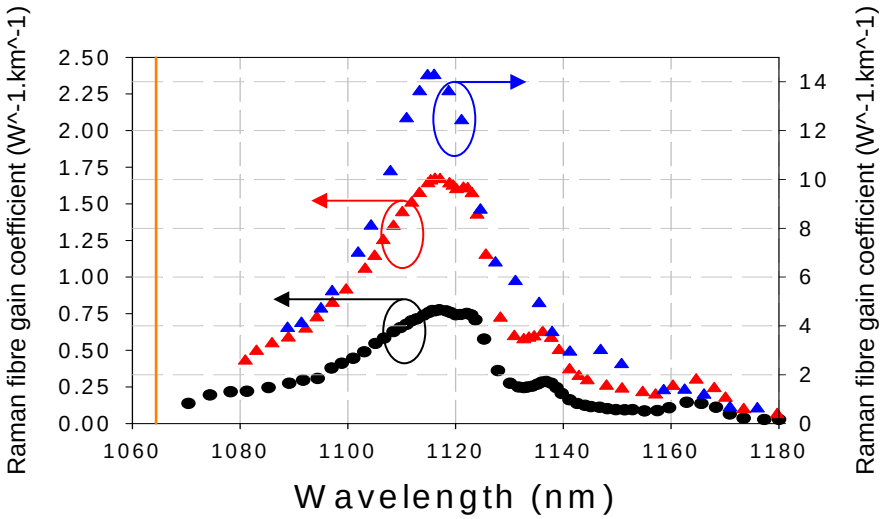

Figure 3.7 Raman fibre gain coefficient spectra for three different fibres. (a) Black curve: Corning™ SMF-28, (b) Red curve: Pirelli Freelight™ DSF and (c) Blue curve: Sumitomo HNLF.

An additional way to grade these fibres in terms of their potential use in discrete RFAs is the figure of merit (*FOM*) which is given by $FOM = C_R/\alpha_P$. Since an increase in the Raman fibre gain coefficient can often lead to an increase in fibre attenuation, the FOM takes this into account. Using the Raman fibre gain coefficient values from figure 3.7, the FOM values for the SMF-28, Freelight™ DSF and HNLF are 1.034 $dB^{-1}W^{-1}$, 2.075 $dB^{-1}W^{-1}$ and 8.590 $dB^{-1}W^{-1}$, respectively. The HNLF has an FOM that is over four times higher than the Freelight™ DSF and over eight times higher than the SMF-28 fibre.

Another important aspect of these fibres is the dispersion profile. It is possible to measure dispersion using a pulse delay measurement (see for instance [6]). This technique measures differences in the time delay between pulses of different wavelengths propagating through the fibre. Once again the SC source and the monochromator were used to scan through the wavelength range from 1060 to 1700 nm and a detector and oscilloscope were used to measure the time delay for pulses of

different wavelengths. Figure 3.8 shows the pulse delay measurements for the SMF-28, Freelight™ DSF and HNLF along with their respective dispersion curves, which were determined by differentiating the time delay with respect to wavelength. From the dispersion curves it can seen that the SMF-28 has a ZDW of ~1312 nm, the Freelight™ DSF has had its ZDW shifted out to ~1484 nm and the Sumitomo HNLF does not have a ZDW and therefore only exhibits negative (i.e., normal) dispersion in the investigated wavelength range.

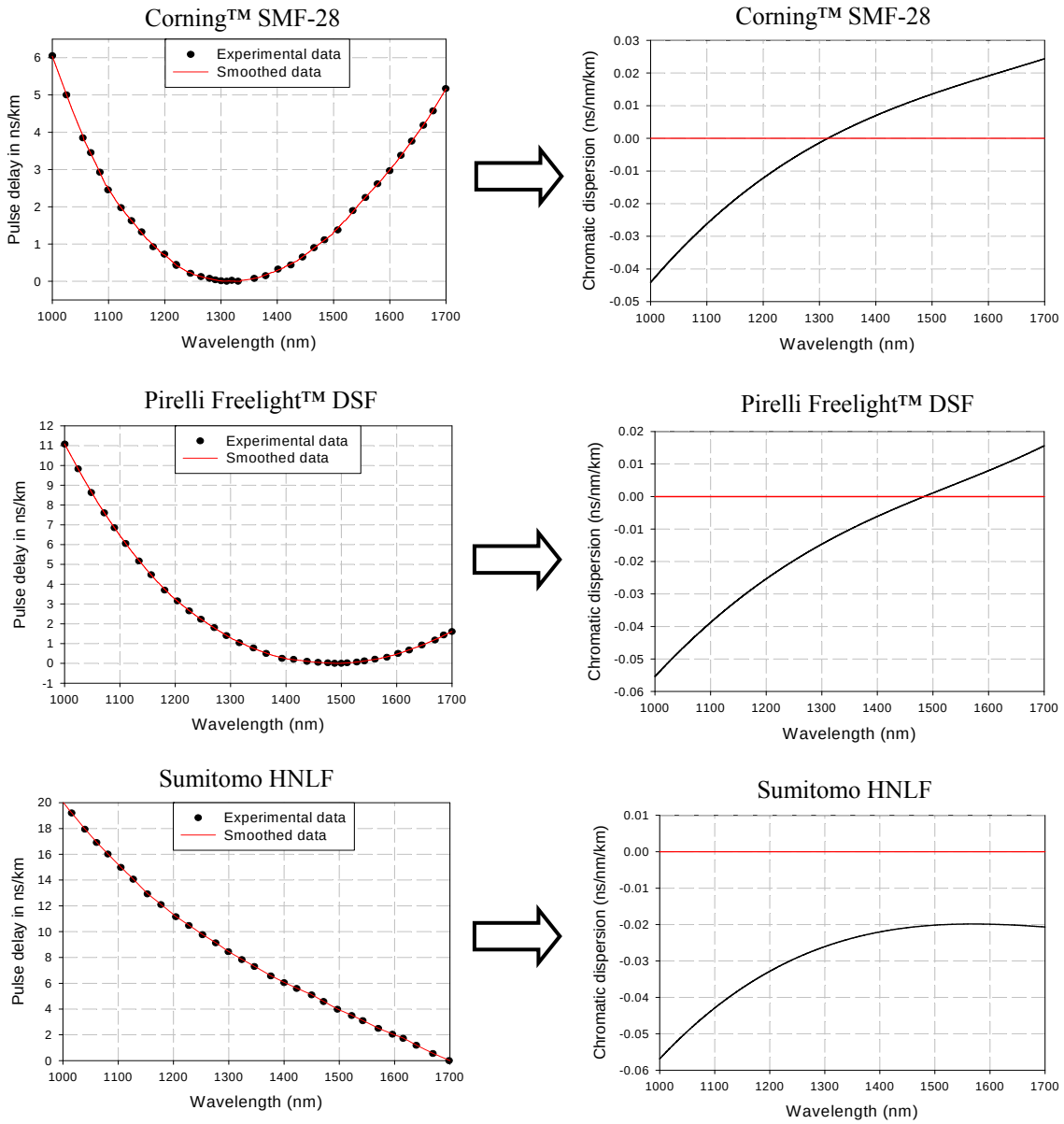

Figure 3.8 Pulse delay measurements and dispersion profiles for the three fibres used for cascaded Raman generation.

As highlighted in the background section the location of the ZDW is important in avoiding FWM effects which can potentially cause the cascaded Raman generation to break down. The Sumitomo HNLF therefore looks promising for constructing an ultra-broadband RFA with its high Raman fibre gain coefficient and normal dispersion.

The cut-off wavelengths for these fibres were also measured experimentally. By illuminating the fibres with a white light source and then bending the fibres, the cut-off wavelengths for the SMF-28, Freelight™ DSF and HNLF were found to be ~1160 nm, ~1370 nm and 1290 nm, respectively. Therefore none of the fibres are actually singlemode at the wavelength of the pump source.

3.2 Experimental results for the pulse-pumped counter-propagating cascaded RFA

One of the most common and simplest ways to measure gain is to use an OSA and note down any increase in the signal power level at its respective wavelength. As in all optical amplifiers, spontaneously generated light is also present in RFAs and it too undergoes amplification along with the signal. If this amplified spontaneously generated light becomes comparable to the signal power level it becomes difficult to distinguish between them. This can occur when the input signal power level is low compared to the vacuum fluctuation level of one photon per unit bandwidth and unit time, in each mode of the amplifier and/or a significant amount of spontaneous light is generated, i.e., if the noise figure is high. The input signal power level from the SC source for a 2 nm bandwidth signal at 1116 nm was ~1 μW. This can be compared to the vacuum fluctuation level, which is similar at 0.172 μW in two polarisation modes in 2 nm at this signal wavelength. Add to this the noise figure, which is at least 3 dB but can be significantly higher, and it is clear that the amplified noise will be comparable to the signal level. This motivates the use of lock-in detection. A lock-in amplifier can be used to detect the magnitude (as well as phase) of a signal modulated at a given frequency, independent of any background light at another frequency (or CW). Since the SC source is based on a MOPA configuration with pulse parameters set by the pulse generator (see figure 3.4), the trigger output from the pulse generator can be directly used for the reference input to the lock-in amplifier. The lock-in amplifier is therefore set up to detect only the seed signal from the SC source and filters out any noise generated from spontaneous light. It can therefore measure low signal power levels irrespective of the

amount of amplified spontaneously generated light. Figure 3.9 shows an example of the signal gain measured from the RFA using the OSA and the lock-in amplifier methods. It can be seen that in this instance, when the average pump power level reaches ~400 mW the signal and noise power levels become comparable. Beyond this it becomes difficult to distinguish between them on the OSA and any subsequent power level measurements can contain large errors. However with the lock-in amplifier it is possible to accurately measure the increase in signal power up to its maximum value and also its subsequent decrease in power due to higher order Raman generation.

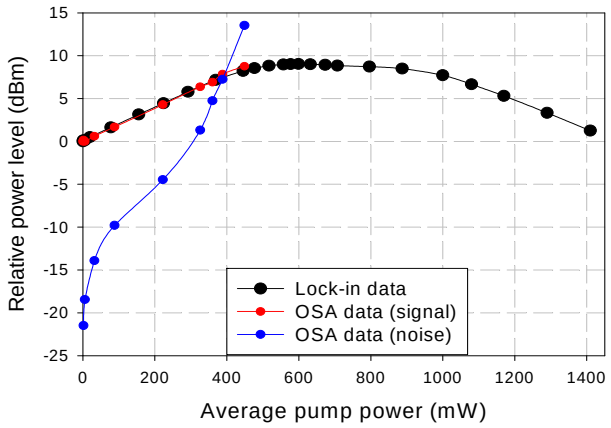

Figure 3.9 Example showing a Raman gain measurement using an OSA and then using a lock-in amplifier.

For the lock-in detection set-up a Stanford SR830 digital lock-in amplifier was employed which had an operating frequency range from 1 mHz to 102 kHz making it suitable for the 100 kHz repetition rate used by the SC source.

3.2.1 Gain results from the HNLF

This measurement technique which was able to measure the full gain profile of a relatively low power signal, is well suited to cascaded Raman gain measurements across the full available transparency window (i.e., 1064 to 1700 nm) of the silica-based Raman generating fibres when pumped by a pulsed Yb MOPA source. To begin with gain measurements were performed on the Sumitomo HNLF since it had the highest Raman fibre gain coefficient and therefore the lowest pump power requirements. The HNLF was supplied at a length of 6 km and due to difficulties in splicing and launching into a fibre with a small core and high Ge content the HNLF had SMF-28 pigtails

spliced onto both ends (using a splicing procedure optimised by Sumitomo). This makes it easy to splice the SMF-28 pigtails to other fibre-pigtailed components such as WDM and tap couplers using standard splice programs since the fibre-pigtails would have similar FRIPs. The splice loss values provided by Sumitomo were 0.9 dB/end around 1100 nm, 0.7 dB/end around 1300 nm and 0.5 dB/end around 1600 nm, although for the purposes of this work, splice losses could be estimated from any background loss measurements. The 6 km HNLF was placed into the RFA set-up shown in figure 3.2 and characterised. The monochromator was tuned to provide a seed signal at the location of the peak Raman gain shift. The cascaded Raman gain measurements were then performed for pump pulses with duty cycles of 20% and 40%. The pulses were approximately high-order super-Gaussian with pulse durations of the order of 150 ns. The most important pulse parameter in this measurement was actually the duty cycle and so primarily the repetition rate was modified albeit with some fine-tuning of the pulse duration to give the desired duty cycle. The duty cycle values given here correspond to the ones measured from the optical pulses on an oscilloscope and not the electrical input pulses.

Figure 3.10 shows the counter-propagating on-off gain measurements for the 6 km HNLF. With a pump wavelength of 1064 nm gain was measured up to the 7th Stokes order, corresponding to a wavelength of 1573.6 nm. The measurement was stopped there since the 8th Stokes order with a wavelength of ~1690 nm was not observable on the OSA to set up the measurement and also the loss of silica-based fibres increases sharply around this wavelength region.

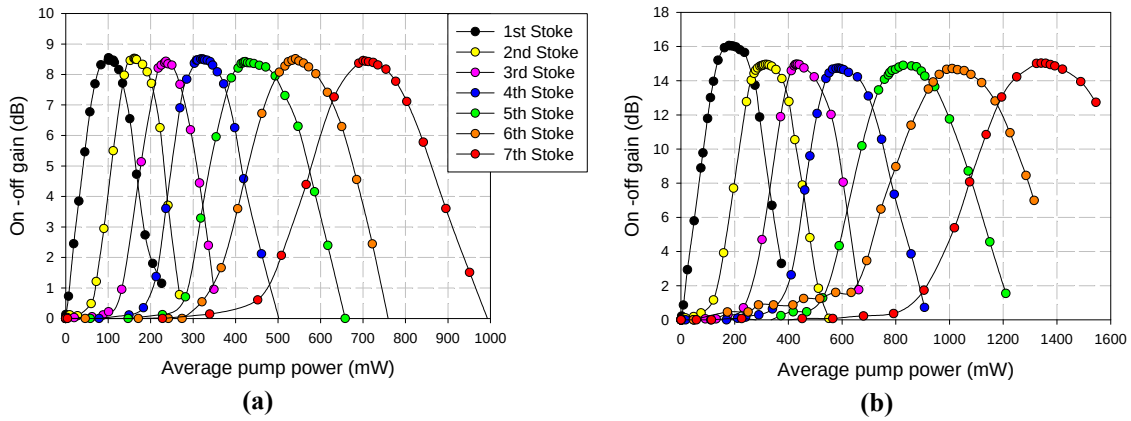

Figure 3.10 Counter-propagating on-off gain over seven Stokes orders for the 6 km HNLF and for high-order super-Gaussian pump pulses, (a) 20% duty cycle and (b) 40% duty cycle. 1st Stoke=1116 nm, 2nd Stoke=1172.4 nm, 3rd Stoke=1235.6 nm, 4th Stoke=1305.8 nm, 5th Stoke=1384.8 nm, 6th Stoke=1473.6 nm, 7th Stoke=1573.6 nm.

However I believe this is the first time a pulse-pumped cascaded Raman gain measurement over seven Stokes orders has been undertaken without the interference of supercontinuum effects (FWM) and for high duty cycles (> 1%) whereby the counter-propagating gain becomes important and a measurable quantity. For pump pulses with a 20% duty cycle, the counter-propagating on-off gain for all Stokes order was ~8.5 dB. With a 40% pump duty cycle the counter-propagating on-off gain across all the Stokes orders had an average value of ~15 dB. The exact values for the highest gain are summarised in table 3.1. It is also necessary to look at the performance of the cascaded RFA in terms of net gain by subtracting the background loss of the amplifier. The background loss of the amplifier includes the attenuation of the HNLF plus any splice losses due to the fibre-pigtails as mentioned earlier. Figure 3.11 shows the counter-propagating net gain measurements for the 6 km HNLF. It can be clearly seen that due to the high background loss of the fibre the net gain is significantly reduced, especially at the low Stokes orders where in some cases the net gain is actually negative. Furthermore, there is also a reduced net gain at the 5th Stokes order wavelength of 1384.8 nm since this coincides with the higher loss region of the OH absorption peak (see figure 2.5).

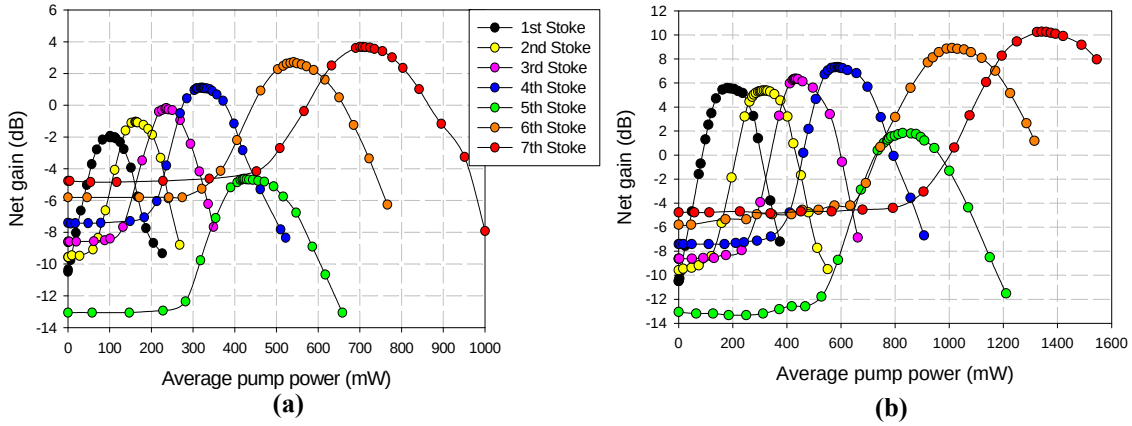

Figure 3.11 Counter-propagating net gain over seven Stokes orders for the 6 km HNLF and for high-order super-Gaussian pump pulses, (a) 20% duty cycle and (b) 40% duty cycle. 1st Stoke=1116 nm, 2nd Stoke=1172.4 nm, 3rd Stoke=1235.6 nm, 4th Stoke=1305.8 nm, 5th Stoke=1384.8 nm, 6th Stoke=1473.6 nm, 7th Stoke=1573.6 nm.

For a discrete RFA, a negative net gain is unsatisfactory, but the data is still useful for comparison purposes. Table 3.1 summarises all the gain measurements for the 6 km HNLF. The average pump power values given here in the tables correspond to the average pump power values launched into the SMF-28 input pigtail.

Stokes order	20% duty cycle			40% duty cycle		
	Average pump power (mW)	On-off gain (dB)	Net gain (dB)	Average pump power (mW)	On-off gain (dB)	Net gain (dB)
1st (1116 nm)	101	8.54	-1.94	179	16.00	5.58
2nd (1172 nm)	161	8.52	-1.05	315	14.94	5.38
3rd (1236 nm)	236	8.43	-0.18	434	14.97	6.35
4th (1306 nm)	318	8.51	1.10	587	14.74	7.32
5th (1384 nm)	423	8.42	-4.64	828	14.89	1.83
6th (1475 nm)	541	8.51	2.71	1010	14.70	8.91
7th (1574 nm)	700	8.45	3.69	1341	15.03	10.26

Table 3.1 Summary of counter-propagating Raman gain measurements for 6 km HNLF.

The attenuation of the HNLF was as expected higher than in a standard singlemode fibre (see figure 2.5 in background section) due to the high Ge concentration with values of 1.66 dB/km around 1064 nm, 0.93 dB/km around 1300 nm, 1.6 dB/km around 1400 nm and 0.62 dB/km around 1500 nm. This is more than double that of SMF-28 with values of ~0.8 dB/km around 1060 nm, ~0.33 dB/km around 1300 nm, ~0.32 dB/km around 1400 nm and ~0.2 dB/km around 1500 nm. However it can also be seen that due to the high Raman fibre gain coefficient, the pump power is still relatively low compared to what is available and so the HNLF length can be reduced and still used for cascaded Raman generation. The length of the HNLF was therefore reduced to 2 km and the gain measurements were repeated for the 20% and 40% pump duty cycles. Figure 3.12 shows the counter-propagating on-off gain measurements for the 2 km HNLF. For pump pulses with a 20% duty cycle the counter-propagating on-off gain across the seven Stokes orders had an average value of ~7.2 dB. With a 40% pump duty cycle the counter-propagating on-off gain across the seven Stokes orders had an average value of ~13.6 dB. The shorter fibre results in a conversion rate that depends more weakly on the pump power in accordance with the effective lengths (cf. equation 2.28). At the pump wavelength of 1064 nm the effective lengths for the 6 km and 2 km HNLFs are 2.345 km and 1.396 km, respectively. Therefore an increase in pump power by a factor of ~1.68 was expected and not too far off what was actually seen in the experiments.

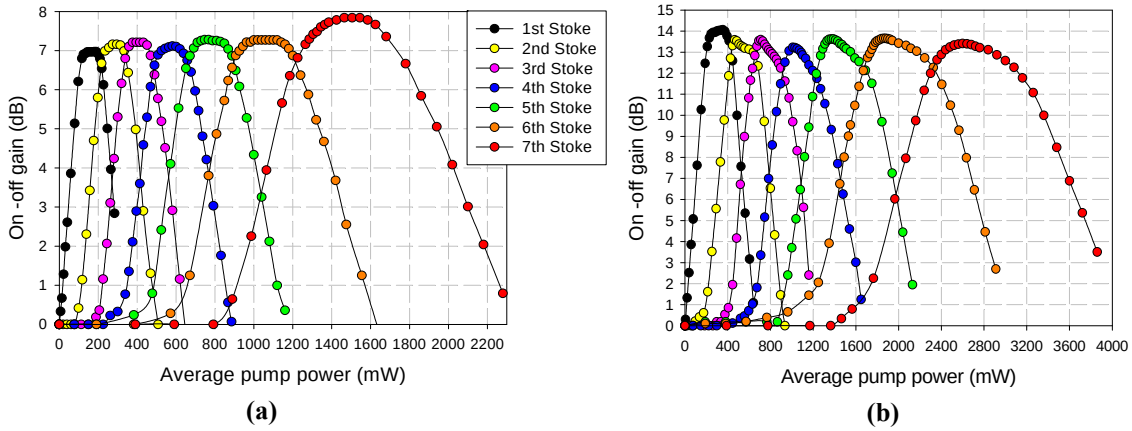

Figure 3.12 Counter-propagating on-off gain over seven Stokes orders for the 2 km HNLF and for high-order super-Gaussian pump pulses, (a) 20% duty cycle and (b) 40% duty cycle. 1st Stoke=1116 nm, 2nd Stoke=1172.4 nm, 3rd Stoke=1235.6 nm, 4th Stoke=1305.8 nm, 5th Stoke=1384.8 nm, 6th Stoke=1473.6 nm, 7th Stoke=1573.6 nm.

Although the 2 km HNLF resulted in a decrease in the on-off gain by ~1.3 dB, it can be seen from figure 3.13 that the net gain is much higher and more suitable for a discrete amplifier.

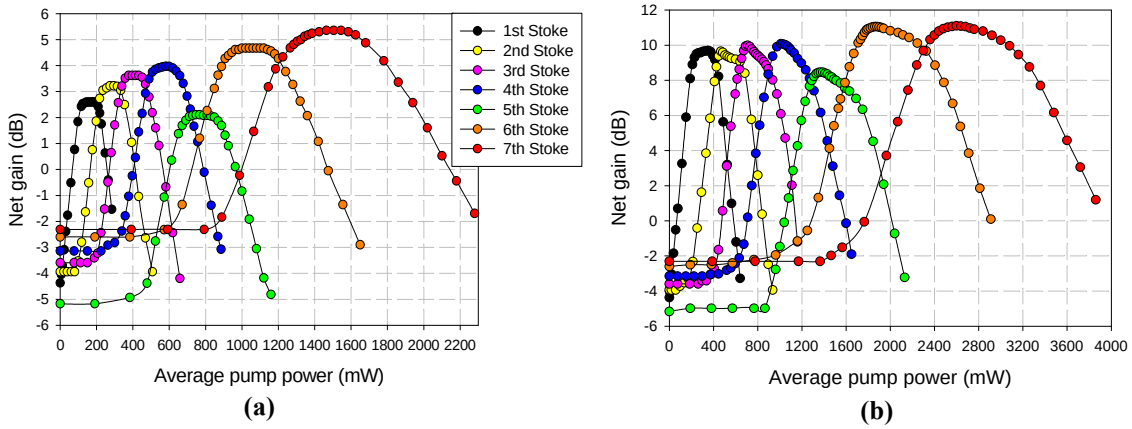

Figure 3.13 Counter-propagating net gain over seven Stokes orders for the 2 km HNLF and for high-order super-Gaussian pump pulses, (a) 20% duty cycle and (b) 40% duty cycle. 1st Stoke=1116 nm, 2nd Stoke=1172.4 nm, 3rd Stoke=1235.6 nm, 4th Stoke=1305.8 nm, 5th Stoke=1384.8 nm, 6th Stoke=1473.6 nm, 7th Stoke=1573.6 nm.

Furthermore, there is still scope to reduce the amplifier length in order to increase the net gain, but this was not pursued, so as not to put too much strain on the free-space launch optics. A summary of all the highest recorded values of measured gain for the 2 km HNLF are shown in table 3.2.

Stokes order	20% duty cycle			40% duty cycle		
	Average pump power (mW)	On-off gain (dB)	Net gain (dB)	Average pump power (mW)	On-off gain (dB)	Net gain (dB)
1st (1116 nm)	167	6.96	2.60	340	14.06	9.70
2nd (1172 nm)	285	7.16	3.22	505	13.60	9.65
3rd (1236 nm)	400	7.21	3.62	750	13.60	9.99
4th (1306 nm)	581	7.11	3.98	1010	13.23	10.08
5th (1384 nm)	750	7.28	2.11	1380	13.63	8.46
6th (1475 nm)	1060	7.27	4.61	1880	13.66	11.05
7th (1574 nm)	1510	7.67	5.36	2600	13.41	11.10

Table 3.2 Summary of counter-propagating Raman gain measurements for 2 km HNLF.

3.2.2 Comparison of gain results between different fibre types

In this section the RFA performance in terms of gain is assessed when the HNLF is replaced with the Freelight™ DSF. Everything else except the fibre is kept the same so that a comparison can be made between the measured values of Raman gain. With its lower Raman fibre gain coefficient, more pump power would be required to reach out to the 7th Stokes order so only the first few Stokes orders are considered for comparison. The first Freelight™ DSF under test had a length of 4 km and therefore an effective length of approximately 2.714 km at the pump wavelength. The same pump pulses were used and SMF-28 pigtails were again used so that the free-space launch set-up could stay the same. At this point I focus on the on-off gain since it is only to be expected that there will be differences in the net gain due to the differing values of background loss. Figure 3.14 shows the counter-propagating on-off gain measurements for the 4 km Freelight™ DSF. For pump pulses with a 20% duty cycle the counter-propagating on-off gain was ~9 dB over the first three Stokes orders. For a 40% duty cycle it was 17.8 dB and 17 dB, for the 1st and 2nd Stokes orders, respectively. These values are higher than those obtained from the HNLF and although the differences may seem small at first glance it is worth pointing out that these are for a counter-propagating system where the gain is reduced in proportion to the pump duty cycle. The difference in on-off gain between the 6 km HNLF and 4 km Freelight™ DSF for the 20% duty cycle pump pulses is ~0.5 dB, with the 4 km Freelight™ DSF having an effective length that is longer by 369 m.

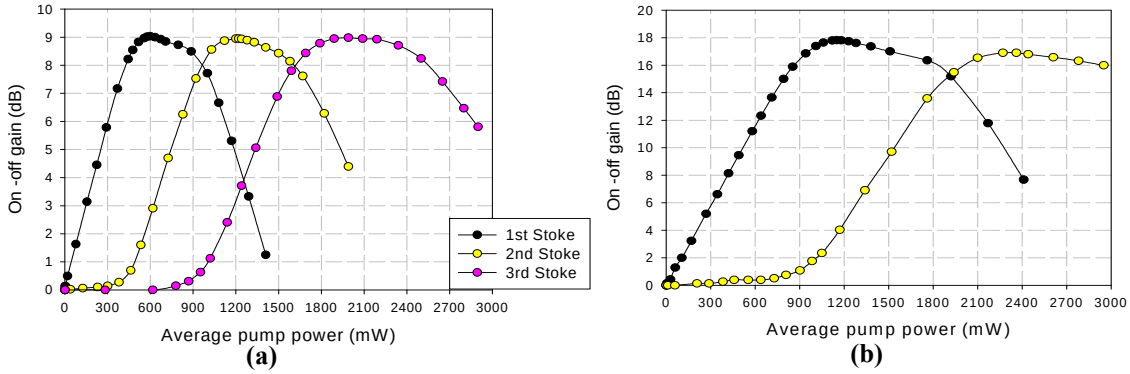

Figure 3.14 Counter-propagating on-off cascaded Raman gain for the 4 km Freelight™ DSF and for high-order super-Gaussian pump pulses, (a) 20% duty cycle and (b) 40% duty cycle. 1st Stoke=1116 nm, 2nd Stoke=1172.4 nm, 3rd Stoke=1235.6 nm.

This would in principle equate to a difference of 2.5 dB for CW pumping. If we now take the 2 dB difference in on-off gain between the 2 km HNLF and 4 km Freelight™ DSF for the 20% duty cycle pump pulse, then this in principle equates to a 10 dB difference for CW pumping. The effective lengths of these fibres are 1.396 km for the 2 km HNLF and 2.714 km for the 4 km Freelight™ DSF, so the effective length for the 2 km HNLF is even shorter.

Freelight™ DSF was developed primarily for long haul optical communication systems, implying a low cost, and there were longer lengths available to test. Therefore, fibre lengths of 6 km and 9.6 km were tested in the RFA set-up. The 6 km length produced very similar results to the 4 km length and so the results are not shown here, but the 9.6 km length produced higher on-off gain values. Figure 3.15 shows the counter-propagating on-off gain measurements for the 9.6 km Freelight™ DSF. For pump pulses with a 20% duty cycle the counter-propagating on-off gain was 11 dB for each of the first 2 Stokes orders. With a 40% pump duty cycle the counter-propagating on-off gain over the 1st Stokes order was 20.3 dB. Once again we see an increase in the maximum on-off gain for the longer Freelight™ DSF although the same pump pulses are used. The effective length for the 9.6 km Freelight™ DSF is 4.484 km and the difference in on-off gain between the 2 km HNLF and 9.6 km Freelight™ DSF is now 3.8 dB for a 20% pump pulse duty cycle which is potentially 19 dB for CW pumping and a significant difference. Furthermore if the HNLF length was reduced further, which is a possibility due to its high Raman fibre gain coefficient, then the on-off gain seems likely to be reduced further.

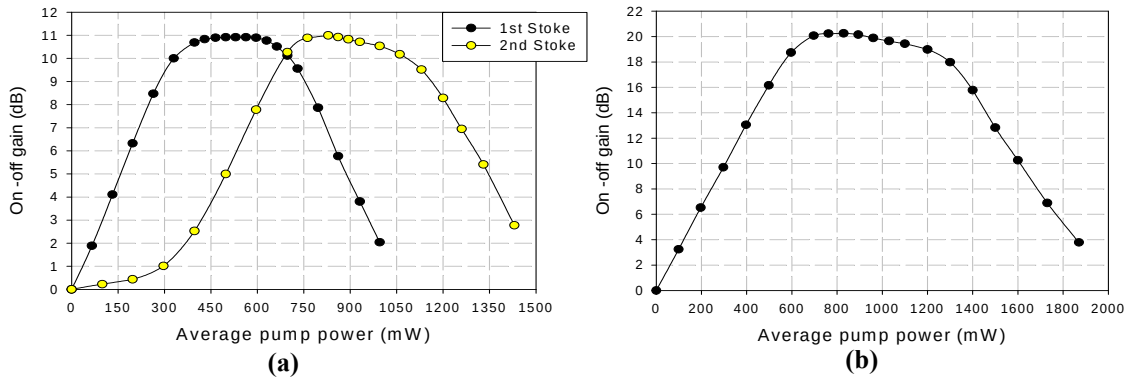

Figure 3.15 Counter-propagating on-off cascaded Raman gain for the 9.6 km Freelight™ DSF and for high-order super-Gaussian pump pulses, (a) 20% duty cycle and (b) 40% duty cycle.

From the background section, in the small-signal regime where pump depletion can be neglected, the on-off counter-propagating gain in decibels for the 1st Stokes order is given by $G^{on-off}(dB) = 4.343 \times C_R \times P_p^{av} \times L_{eff}$. This simply states that for a given effective length the on-off gain in dB is proportional to the Raman fibre gain coefficient of the fibre and the pump power and therefore a fibre with a higher Raman fibre gain coefficient requires less pump power to reach a specified on-off gain. For the two fibres under test here, the HNLF should in theory require 9.44 times less pump power than the Freelight™ DSF for the same effective length. To test this we can extract the pump power requirements for a certain amount of gain from the experimental data for all the RFA tests with different lengths of HNLF and Freelight™ DSF shown earlier in this section. For pump pulses with a 20% duty cycle, the amount of average pump power required to reach an on-off gain of 6 dB was extracted from the experimental data plotted in figures 3.10, 3.12, 3.14 and 3.15. This represents a value where the gain curve is increasing linearly and where pump depletion has yet to occur. The values are shown in table 3.3. The pump power values were then inserted into the equation for calculating the on-off gain, stated above and the expected on-off gain values were calculated. These calculated values are also shown below in table 3.3. In comparing the values, it can be seen that for a given pump power the calculated gain is close to the experimentally measured gain for the Freelight™ DSF, while there appears to be some discrepancies for the HNLF. The input splice loss of ~0.5 dB (for the LP_{01} mode) at the pump wavelength for the HNLF was also taken into account for a more accurate value of the pump power requirement.

Fibre type and length	Effective length (m)	20% duty cycle			
		From experimental data		Theoretical calculation	
		Measured gain (dB)	Pump power required (mW)	Pump power (mW)	Expected gain (dB)
HNLF (6 km)	2345	6	44.5	44.5	6.46
HNLF (2 km)	1396	6	82.8	82.8	7.16
DSF (9.6 km)	4484	6	188	188	6.1
DSF (4 km)	2714	6	304	304	6

Table 3.3 Average pump power requirements to achieve 6 dB on-off gain for a 20% pump duty cycle and theoretical predictions.

Taking into account the different effective lengths, the actual difference in pump power requirement between the 4 km Freelight™ DSF and 6 km HNLF is a factor of ~7.9 and a factor of ~7.14 for the 4 km Freelight™ DSF and 2 km HNLF. Although these factors are still relatively high, they represent a drop from the expected value of 8.55. Similar results are obtained for pump pulses with a 40% duty cycle, where the amount of average pump power required to reach an on-off gain of 12 dB was extracted from the experimental data plotted in figures 3.10, 3.12, 3.14 and 3.15. The values are shown below in table 3.4.

Fibre type and length	Effective length (m)	40% duty cycle			
		From experimental data		Theoretical calculation	
		Measured gain (dB)	Pump power required (mW)	Pump power (mW)	Expected gain (dB)
HNLF (6 km)	2345	12	89.9	89.9	13.1
HNLF (2 km)	1396	12	160.2	160.2	13.9
DSF (9.6 km)	4484	12	365	365	11.9
DSF (4 km)	2714	12	622	622	12.2

Table 3.4 Average pump power requirements to achieve 12 dB on-off gain for a 40% pump duty cycle and theoretical predictions.

Overall, although the higher Raman fibre gain coefficient of the HNLF is clear to see, it appears that the fibre is not being used to its full potential. Furthermore the on-off gain per unit power (dB/mW) is also dropping with fibre length which also suggests the HNLF is not being used to its full potential, even though the net gain is increasing with

shorter fibre lengths. This makes it worthwhile to look into some of the factors which can affect the gain of the RFA.

3.2.3 Factors affecting gain in a pulse-pumped RFA

In considering the factors affecting the gain of the pulse-pumped cascaded RFA, it is worthwhile investigating the maximum achievable gain under ideal conditions using computer simulations. For this a RFA model for co-propagating CW pumping was employed from the commercial software package, VPIphotonics™ and the maximum on-off gain values for the 1st Stokes order were recorded for various fibre lengths using the full Raman fibre gain coefficient profiles shown in figure 3.7. The model is based on the conventional equations for the evolution of the power of the pump and Stokes waves [4]. It is fully spectrally resolved across the whole wavelength range we consider. Note that counter-propagating light is not included. The model also included the attenuation profiles across the full wavelength range of operation and any splice losses where necessary. However no attempt has been made to fully solve for the modes in the HNLF or to accurately calculate the effective area at different wavelengths. Furthermore, we did not include dispersion nor Rayleigh scattering in our simulations. Rayleigh scattering is known to affect the performance of RFAs employing very high pump duty cycles (including CW) and operating with high gains. However with lower pump duty cycles the Rayleigh scattering effects become less prominent since the counter-propagating gain reduces and any double-Rayleigh scattered light is less likely to be overlapping with the pump pulses. The results for the SMF-28, Freelight™ DSF and Sumitomo HNLF are shown below in figure 3.16. It shows that the on-off gain increases for shorter fibre lengths (L< 5 km) where the background loss is lower and the input pump power is higher. Furthermore, it also shows how the on-off gain levels out as the fibre length increases and the effective length approaches its maximum value of $L_{eff} = 1/\alpha_p$. The data indicates that a CW on-off gain of 52-55 dB should be available for the lengths of HNLF that were used in this experiment and for the Freelight™ DSF there should be a CW on-off gain of ~60 dB. The recorded co-propagating CW gain values were then multiplied by the duty cycle of the pump pulses to provide the counter-propagating gain.

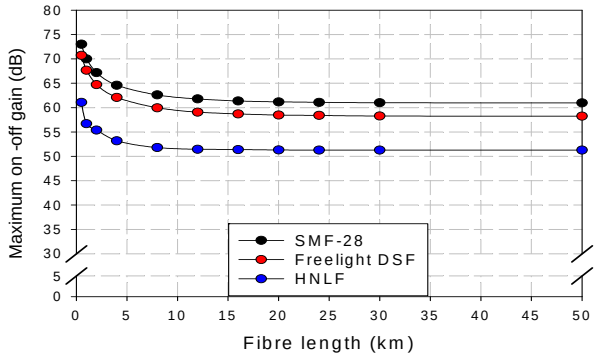

Figure 3.16 Graph showing the simulated results for the maximum on-off gain (for the 1st Stokes order) versus fibre length for three different fibres when pumped by a CW pump source.

Dividing these values by 5 (for a 20% pump duty cycle) and 2.5 (for a 40% pump duty cycle) would therefore indicate to us the maximum achievable on-off gain for a counter-propagating signal with a pump source emitting perfectly rectangular pulses and no walk-off effects exist. Figure 3.17 shows the simulated on-off gain for a 20% pump duty cycle over seven Stokes orders for the 6 km and 2 km lengths of HNLF. The on-off gain for a 40% pump duty cycle would be simply twice that shown in the graphs below. For these simulations a scaling factor was included in the model that takes into account the inverse dependence of g_R on the effective pump wavelength as the gain shifts further away from the initial pump wavelength of 1064 nm in the cascaded process.

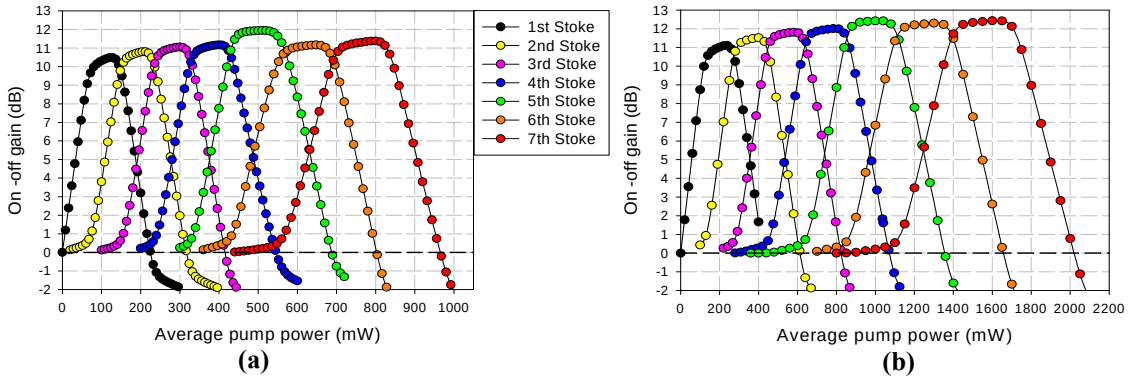

Figure 3.17 Simulated data for on-off gain over seven Stokes orders for a 20% pump duty cycle with (a) 6 km HNLF and (b) 2 km HNLF. 1st Stoke=1116 nm, 2nd Stoke=1172.4 nm, 3rd Stoke=1235.6 nm, 4th Stoke=1305.8 nm, 5th Stoke=1384.8 nm, 6th Stoke=1473.6 nm, 7th Stoke=1573.6 nm.

In comparison to the experimentally measured data, the simulated on-off gain measurements are higher in value. For the 2 km HNLF the difference in on-off gain for a 20% pump duty cycle ranges from 4.1 dB at the 1st Stoke to 4.8 dB at the 7th Stoke. In

fact figure 3.18 shows how on-off gain varies with duty cycle for the 2 km and 6 km HNLFs and how this difference increases to ~25 dB for CW pumping. Similar results were obtained experimentally for both the 1st and 2nd Stokes orders. This is further evidence that the on-off gain being extracted from the amplifiers is below what might be possible.

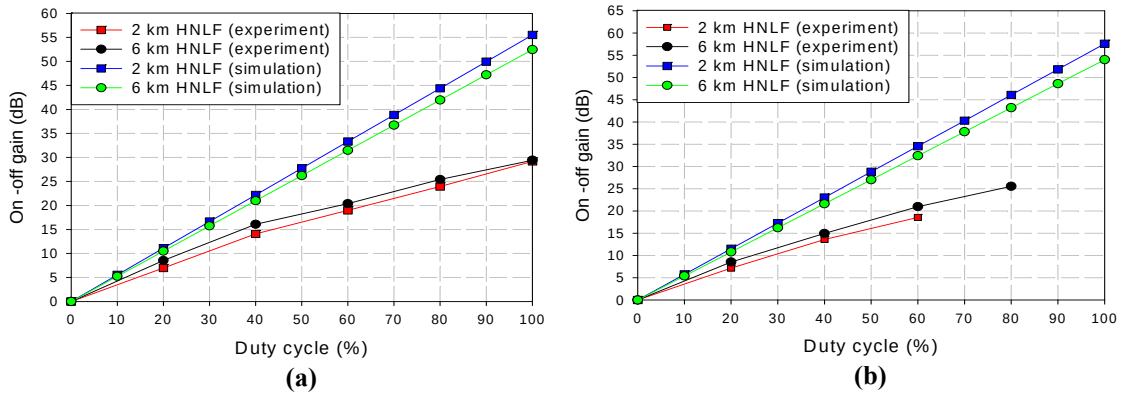

Figure 3.18 Graphs showing on-off gain versus duty cycle for the HNLF using both experimental and simulated data for (a) 1st Stokes order and (b) 2nd Stokes order.

Figure 3.19 shows a direct comparison between the experimental and simulated data over the first few Stokes orders using a 20% pump duty cycle for the 2 km HNLF, 6 km HNLF and the 9.6 km Freelight™ DSF. Only with the longer length of Freelight DSF does the experimental on-off gain come close to matching up with the simulated on-off gain.

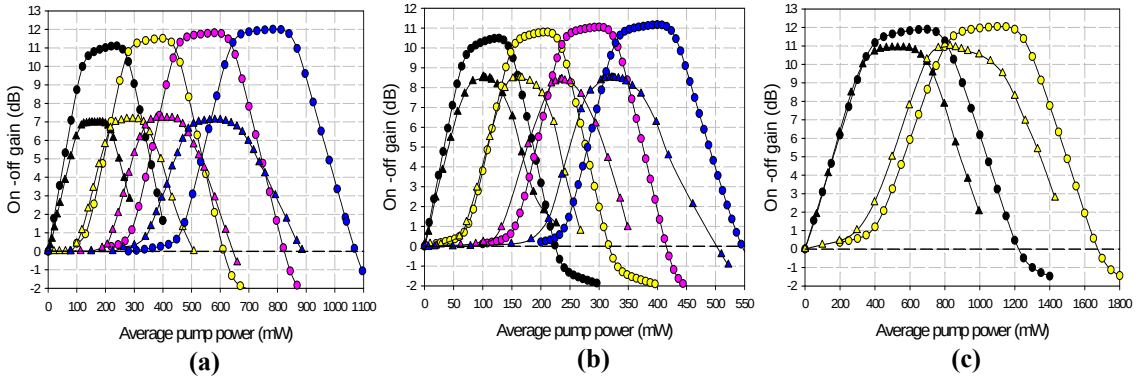

Figure 3.19 Graphs showing direct comparison between experimental data(—▲—) and simulated data (—●—) using a 20% pump duty cycle for (a) 2 km HNLF, (b) 6 km HNLF and (c) 9.6 km Freelight DSF. 1st Stoke (▬)=1116 nm, 2nd Stoke (▬)=1172.4 nm, 3rd Stoke (▬)=1235.6 nm and 4th Stoke (▬)=1305.8 nm.

Next, some of the effects that are not taken into account in the CW model are investigated to see if they could cause the drop in on-off gain values. First of all, an important feature in the maximum achievable gain of a pulse-pumped cascaded RFA is how the pump pulses deplete. In practise square pulses are not really possible so approximate high-order super-Gaussian pulses were used throughout the experiments. Figure 3.20 shows how the pump pulse and the 1st Stokes pulse deplete and also how the 1st Stokes pulse grows during the SRS process for the 6 km HNLF. The pulses were recorded on an oscilloscope after the different wavelengths had been separated by a monochromator. It can be seen that, as expected, the pump pulse does not fully deplete, although it can be seen that a significant part of the pump pulse does deplete, thus participating efficiently in the Raman conversion process. It should be pointed out that the relative amplitudes between the pump pulse and 1st Stoke pulse cannot be directly compared since their different wavelengths result in different amounts of transmission through the monochromator. In terms of the duty cycles, the input pump pulse to the Raman fibre starts with a 20% duty cycle. After propagation through the Raman fibre, at the maximum value of on-off gain for the 1st Stoke (101 mW average pump power) corresponding to the green pulse on plot (b), the duty cycle of the 1st Stokes pulse reduces initially to 17% and then increases to 19% when it reaches its maximum height (133 mW average pump power) corresponding to the pink pulse on plot (b). Although only the pump and 1st Stokes order are shown here, a very similar process repeats itself throughout the cascade. Looking at how the on-off gain grows with the evolution of the pump pulses, it can also be seen from figure 3.20 that the pump pulse for the 1st Stokes order starts to deplete when the on-off gain reaches ~90% of its maximum value (see the black curve on figure 3.20 (a) and the corresponding power of 67 mW on the on-off gain plot). It is also worth pointing out that there is evidence of a small amount of walk-off between the pulses due to the un-depleted part of the pump pulse only being present on one side. Temporal walk-off between pulses at different wavelengths would reduce the on-off gain due to a reduction in overlap but this is not thought to be a major factor in this experiment. We will come back to this later when looking at how the pump pulse depletes in the 2 km HNLF. It is also worth mentioning the occurrence of modulations that can appear on the Stokes pulses when SRS takes place (see for instance figure 3.20 (b)). These modulations with a period of ~20 ns are not present on the original pump pulses and therefore could warrant further investigations.

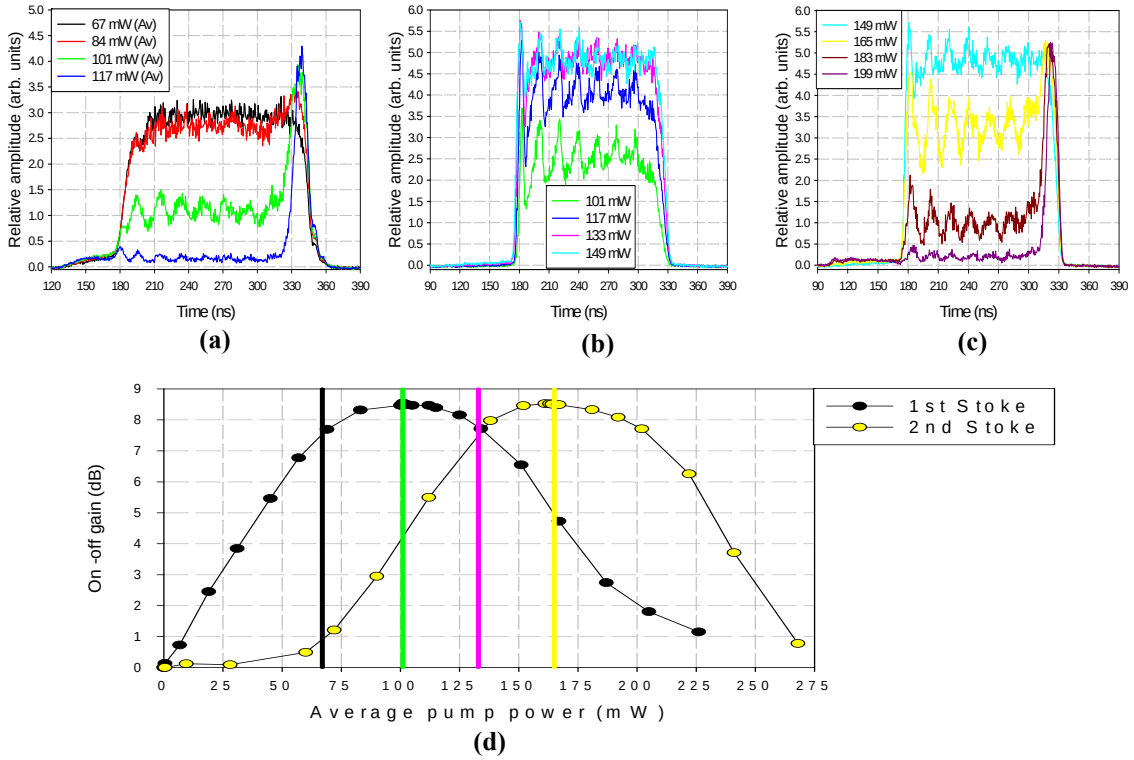

Figure 3.20 Graphs showing the evolution of the pump and 1st Stoke pulses, (a) Depletion of the pump pulse, (b) Growth of the 1st Stokes pulse, (c) Depletion of the 1st Stokes pulse and (d) On-off gain vs. average pump power for the 1st and 2nd Stokes orders for the 6 km HNLF.

Figure 3.21 shows how the pump pulse depletes and how the 1st Stokes pulse first grows and then depletes in the cascaded SRS process for the 9.6 km Freelight™ DSF. The evolution of the pump and the 1st Stokes order pulses in the 9.6 km Freelight™ DSF are very similar to that of the 6 km HNLF, although the on-off gain is higher for the Freelight™ DSF.

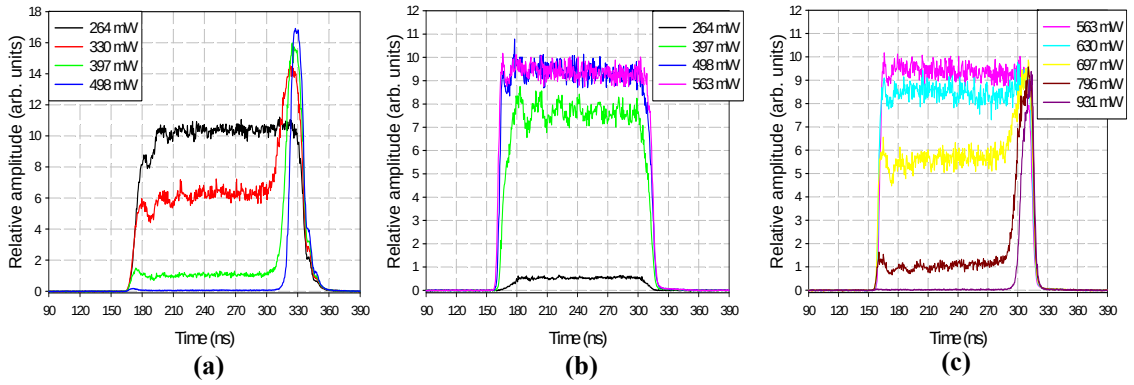

Figure 3.21 Graphs showing the evolution of the pump pulse and the 1st Stoke pulse for the 9.6 km Freelight™ DSF, (a) Depletion of the pump pulse, (b) Growth of the 1st Stokes pulse, (c) Depletion of the 1st Stokes pulse.

Again there appears to be some evidence of walk-off effects. If we now look at the pump pulse depletion for the 2 km HNLF, differences can be seen. Similar to figure 3.21, figure 3.22 shows how the pump pulse depletes and how the 1st Stokes pulse first grows and then depletes cascaded SRS in case of the 2 km HNLF. It can be seen how the depleted pump pulse and the depleted 1st Stokes pulse in figure 3.22 (a) and (c) take on a more symmetrical profile. This is due to a decrease in the walk-off effect due to the shorter length of fibre. The same on-off gain of ~7 dB for the 2 km HNLF was also achieved using 1 μs long pulses as opposed to 150 ns.

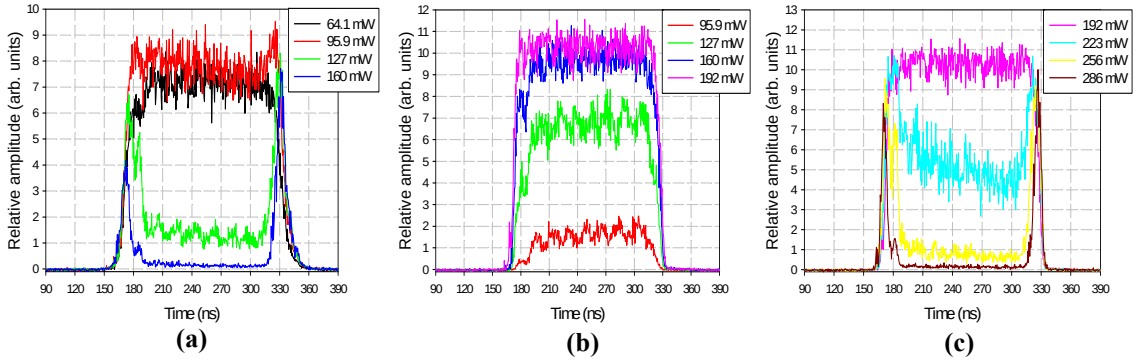

Figure 3.22 Graphs showing the evolution of the pump and 1st Stoke pulses, (a) Depletion of the pump pulse, (b) Growth of the 1st Stokes pulse, (c) Depletion of the 1st Stokes pulse for the 2 km HNLF.

Furthermore if walk-off was having a major effect on the achievable on-off gain then the gain would increase for the shorter fibre length since the walk-off effect is reduced and the overlap between the pulses is increased. For the 6 km HNLF an on-off gain of 8.5 dB was achieved against an on-off gain of 7 dB for the 2 km HNLF. I conclude that there are other factors affecting the amount of on-off gain achievable in these RFAs and also the pump power requirements.

One factor that could lead to a lower on-off gain for shorter fibre lengths is the variation in the number of pump pulses in the RFA. The pump pulses used were approximately high-order super-Gaussian with pulse durations of the order of 150 ns (i.e., spatial pulse length of ~30 m) with duty cycles of 20% and 40%. For a fibre length of 1 km the number of pump pulses would vary between 6 and 7 and between 66 and 67 for a 10 km fibre length. This corresponds to effective pump power variations of 14.3% and 1.5% for the 1 km and 10 km fibre lengths, respectively. The larger variation in the shorter fibre makes the pump power optimisation less effective (i.e., the gain peak becomes less sharp). This would translate into fluctuations in the on-off gain readings

resulting in an average value being recorded. Like the pump power, the on-off gain in dB would fluctuate by 14.3% and 1.5% for the 2 km and 6 km fibre lengths, respectively. An average reading of on-off gain would therefore be 7.15% and 0.75% below the peak value. If the peak on-off gain is 11 dB then the average reading for the on-off gain would be 10.26 dB and 10.92 dB for the 1 km and 10 km fibre lengths, respectively. The large difference in fibre length only results in a difference in on-off gain of 0.66 dB. It would be expected that the difference is even smaller between the 2 km and 6 km HNLF where a difference in on-off gain of ~1.5 dB was measured. Also a difference in on-off gain of ~3.8 dB was measured between the 2 km HNLF and the 9.6 km Freelight™ DSF which is much higher than 0.66 dB.

However, it is also possible that further fluctuations in the on-off gain readings could have occurred due to the relatively slow rate of the polarisation scrambler used in the experiment set-up. The polarisation scrambler operates by actively changing the state of polarisation (SOP) in a random fashion so that over a time average the DOP is close to zero. The frequency at which the SOPs change is given as ~170 kHz which corresponds to a rate of one SOP every 5.88 μs [7]. Therefore, although over a period of time much longer than 5.88 μs the DOP is close to zero, the number of SOPs within the fibre lengths used for the RFA at any given time is limited and reduces with fibre length. For instance the number of SOPs changes between only one and two for a 2 km long fibre. Since the Raman gain is polarisation dependent, the lower number of SOPs means less averaging occurs within the fibre. This could also lead to fluctuations in the on-off gain readings, resulting in an average on-off gain value being recorded instead of the maximum on-off gain value. The issue of fluctuations in the on-off gain readings due to the number of pump pulses within the fibre and the polarisation scrambling technique requires more work and further investigation.

Another possibility for a drop in on-off gain with shorter fibre lengths is a reduced overlap between the pump and signal in the spatial domain due to the modal structure of the fibres, which were not singlemode at the pump wavelength. The highest gain is achieved when the pump and signal are both in the fundamental mode. If the pump is multimode and the signal is singlemode, the Raman gain coefficient assumes two different values depending on whether the pump is in the fundamental mode (LP_{01}) or in the higher order mode (LP_{11}). Figure 3.23 shows the variation in the Raman gain coefficient for a frequency shift of 13 THz between the pump and signal which are in the same polarisation. In the figure, the core radius is varied to describe the singlemode

and multimode operations. In this example the authors report that there could potentially be a 60% reduction in the Raman gain coefficient if the signal is singlemode, but the pump alternates between the fundamental mode and the first higher order mode [8]. To a first order this leads to a reduced Raman efficiency for the RFA (gain per unit power) and would impact the pump power requirements but it does not readily explain the drop in maximum on-off gain.

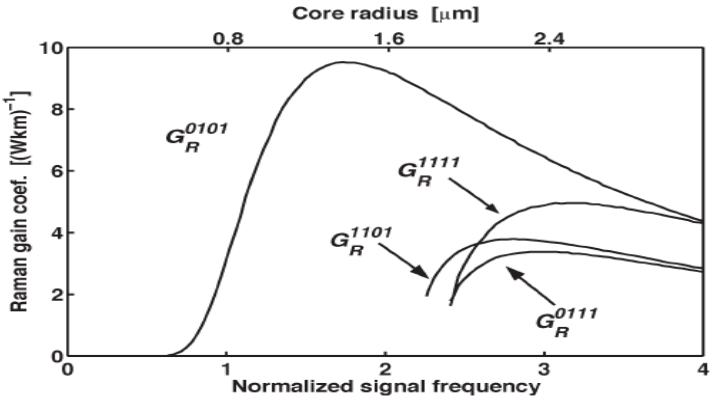

Figure 3.23 Calculated Raman-gain coefficients versus the normalised frequency at the signal wavelength. Each curve is labelled according to the mode of the pump and signal, i.e., G_R^{1101} is the gain coefficient corresponding to the pump being in the LP_{11} mode and the signal in the LP_{01} mode (figure extracted from [8]).

However in the case of a multimode signal, the excitation of different modes can lead to reduced on-off gain values. One example is if we take a fibre that supports both the LP_{01} and the LP_{11} modes at the pump and signal wavelengths and then consider the situation where the pump is launched into just the LP_{01}. If the signal with a total power of 1 mW is launched into just the LP_{01} mode and is amplified to 10 mW, this means the pump has provided 10 dB of gain (assuming no background loss). If the signal is now launched into both modes so that 50% of the power is in the LP_{01} mode and 50% is in the LP_{11} mode, then the pump would still provide 10 dB of gain for the LP_{01} signal but no gain for the LP_{11} mode. In this case the recorded signal power in the off-state (i.e., no pump) is still 1 mW but in the on-state (i.e., pump on) the amplified signal power will be 5.5 mW (corresponding to the amplified LP_{01} signal and the un-amplified LP_{11} signal). The measured on-off gain in this case would be ~7.4 dB, although the pump would still have provided 10 dB of gain for the signal in the LP_{01} mode in the counter-propagating direction. Furthermore, it is the highest gain of any mode in the co-propagating direction that limits the maximum achievable gain in case of pulse-

pumping, and this is not affected by the launch of some signal power into higher-order modes. This example has been greatly simplified since in reality even with their different intensity profiles there would still be some overlap between an LP_{01} and an LP_{11} mode, but it emphasises the point of how overlap between different modes could reduce the on-off gain. It also assumes that the pump power propagates predominantly in the LP_{01} mode. This is a reasonable assumption since the alignment and the mode-matching at splice points are good and since mode-coupling is quite low in high-quality small-core fibres like mine. This also takes into consideration the singlemode nature of the pump. By contrast, the signal seed from the monochromator spatially disperses the light from the SC source.

At the time of writing this report more data is required to confirm or deny the suggestion that overlap plays a role in the reduced on-off gain values that are being seen in the pulse-pumped counter-propagating cascaded RFAs. However during the experimental measurements it was observed that by launching power directly into the LP_{11} mode of the SMF-28 input pigtail fibre at the free-space input, the on-off gain increased from 8.5 dB to ~10.5 dB for the 1st Stokes order when pumping the 6 km HNLF with pulses of a 20% duty cycle. This may well suggest that part of the signal was in the LP_{11} mode, although this cannot be confirmed at the present time. Due to time constraints this was not followed up since at the time the available gain was considered enough to pursue more central experiments such as pumping the RFA with step-shaped pulses.

3.3 Summary

In summary, optical amplification based on cascaded SRS was investigated as a means of providing amplification over an ultra-wide range of wavelengths. A pulse-pumped cascaded RFA was constructed which included building a pulsed MOPA pump source and an ultra-broadband seed signal source for measuring Raman gain across an ultra-wide range of wavelengths. The pulse-pumped cascaded RFA operating in a counter-propagating configuration was then characterised in terms of its gain properties.

Counter-propagating Raman gain measurements were made over seven Stokes orders using different lengths of a HNLF. This spanned a wavelength range of more than 500 nm from the pump wavelength of 1064 nm. For a 20% pump duty cycle, the

peak on-off gain for all Stokes order had an average value of ~8.5 dB and ~7.2 dB for the 6 km and 2 km HNLF, respectively. For a 40% pump duty cycle, the peak on-off gain across all Stokes order had an average value of ~15 dB and ~13.6 dB for the 6 km and 2 km HNLF, respectively. I believe this is the first time such measurements have been made over this wavelength range without the interference of supercontinuum effects (FWM) and for high duty cycles (> 1%) whereby the counter-propagating gain becomes important and a measurable quantity.

Furthermore, the gain results measured from the HNLF were compared with those measured using Freelight™ DSF which is a standard telecommunications fibre and simulated results using a simple CW pumped cascaded Raman amplifier model. Although the pump power requirements were all close to what was expected, it was found that the experimentally measured on-off gain values dropped off as the fibre lengths were reduced. This is not the case for the theoretically predicted gain results. Furthermore, the theoretically predicted gain results were higher than those that were measured experimentally. However, some issues with the experimental set-up have been identified as possible reasons for this but they require further investigations.

3.4 References

[1] J. P. van der Ziel, "Spectral broadening of pulsating $Al_xGa_{1-x}As$ double heterostructure lasers," IEEE J. Quantum Electron. **15**(11), 1277-1281 (1979).

[2] Information available at: http://www.Lumics.com.

[3] Information available at: http://www.analogmodules.com.

[4] G. P. Agrawal, *Nonlinear Fiber Optics, 3rd Ed.* (Academic Press Inc, San Diego CA, 2001).

[5] S. T. Davey, D. L. Williams, B. J. Ainslie, W. J. M. Rothwell, and B. Wakefield, "Optical gain spectrum of GeO_2-SiO_2 Raman fibre amplifiers," IEE Proceedings-J Optoelectronics **136**(6), 301-306 (1989).

[6] L. G. Cohen and C. Lin, "Pulse delay measurements in the zero material dispersion wavelength region for optical fibers," Appl. Opt. **16**(12), 3136-3139 (1977).

[7] Information available at: http://www.fiberpro.com.

[8] K. Rottwitt and J. H. Povlsen, "Analyzing the fundamental properties of Raman amplification in optical fibers," J. Lightwave Technol. **23**(11), 3597-3605 (2005).

Chapter 4 - Raman gain over an ultra-wide range of wavelengths – further characterisation

In this chapter the pulse-pumped cascaded RFA described in chapter 3 is further discussed in terms of temporal gain variations, noise performance and saturation properties. Besides the gain of the cascaded RFA, these properties are also important to measure in the initial assessment of the cascaded RFA performance. Experimental results on these properties are presented and analysed for the single-channel pulse-pumped cascaded RFA, again using different fibre types.

4.1 Temporal gain variations

The use of pulses to pump a RFA can result in a signal experiencing temporal gain variations. As highlighted in chapter 2, this is because the Raman gain becomes time-dependent which then impacts the temporal characteristics of the amplified signal. However, in a counter-pumping configuration, it has been shown that this effect can be minimised by increasing the repetition rate of the pump pulses for a given pump duty cycle [1]. Since it is the relative fluctuation in the number of pump pulses in the Raman fibre that matters, a shorter fibre is expected to be more affected than a longer one.

In this section it is confirmed that the pump repetition rates used throughout the experiments in this thesis are high enough to minimise the effect of temporal gain variations. Therefore the average gain in the counter-propagating direction is still given by the co-propagating gain multiplied by the duty cycle, as stated in equation 2.37 and used throughout chapter 3. The maximum-to-minimum gain variation imposed onto a counter-propagating CW seed-signal at 1116 nm was measured while the repetition rate of the pump pulses was varied. Figure 4.1 shows the maximum-to-minimum on-off gain variation as a function of repetition rate for three different duty cycles, with the 2 km HNLF. This is a worst case, in that it is the shortest fibre length investigated experimentally in this thesis. In all cases, the temporal on-off gain variations were measured when the RFA was operating at maximum gain. The maximum on-off gain was ~3.7 dB for the 10% duty cycle, ~7.1 dB for the 20% duty cycle and ~14 dB for the 40% duty cycle. Indeed it can be seen that the temporal gain variations do reduce as the

repetition rate is increased. Furthermore, at the repetition rates used throughout the work in this thesis, typically 400 kHz to 1.33 MHz, the maximum-to-minimum on-off gain variation at the peak average gain is less than ~1 dB.

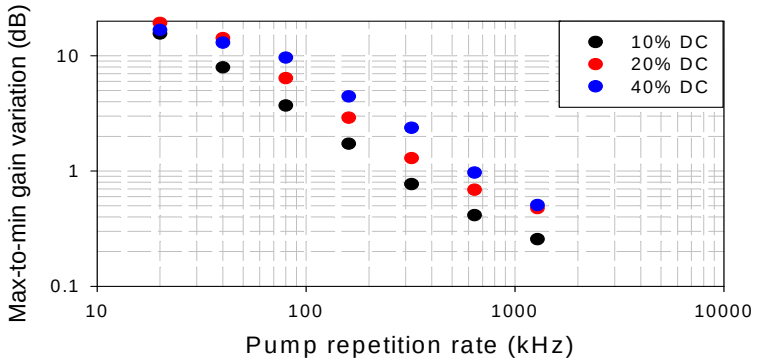

Figure 4.1 Maximum-to-minimum temporal on-off gain variations as a function of pump repetition rate measured experimentally for a pulsed pump source with duty cycles of 10%, 20% and 40% in a 2 km long HNLF.

This is further emphasised in figure 4.2 which shows the temporal gain variations imposed onto the amplified CW signal after propagation through the 2 km HNLF using a constant pump duty cycle of 40% with four different repetition rates. In this example results from using repetition rates of 1.28 MHz, 320 kHz, 80 kHz and 20 kHz are shown. The impact of temporal gain variations on the original CW signal can clearly be seen. The temporal gain variations get progressively worse as the pump repetition rate decreases.

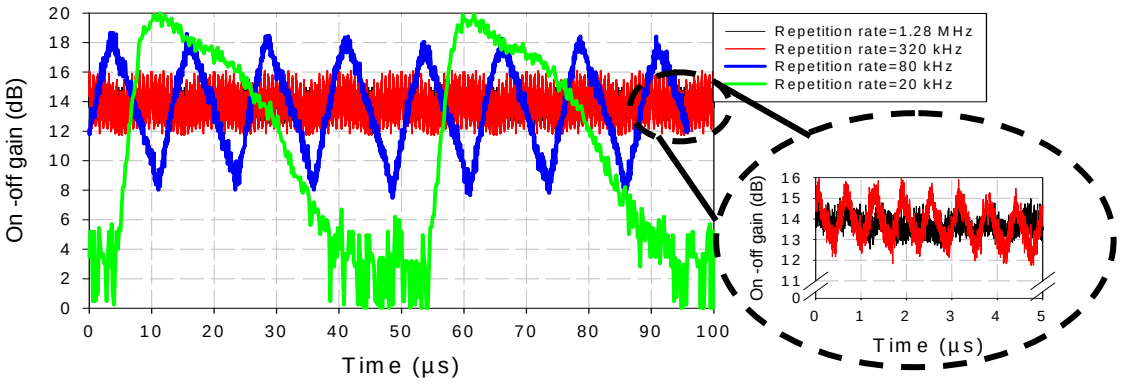

Figure 4.2 Experimentally measured temporal gain variations imposed on to the amplified CW signal after propagation through the RFA for a constant pump duty cycle of 40% with four different repetition rates.

Furthermore, as the pump repetition rate decreases and the gap between the pump pulses starts to approach twice the amplifier length, the CW signal starts to experience periods of no gain in the amplifier and the CW signal becomes pulsed in a similar fashion to a pulse-pumped co-propagating configuration. An example of this is given by the green curve on the graph in figure 4.2 which represents a pump repetition rate of 20 kHz, i.e., pulse length of ~4000 m and a gap between the pump pulses of ~6000 m. At this point equation 2.37 is not suitable for the calculation of the counter-propagating gain.

In terms of a counter-propagating pulse-pumped cascaded RFA, the temporal gain variations for a given pump repetition rate are expected to be similar for amplification at higher Stokes orders. Since the Raman process is essentially instantaneous, the energy at all Stokes orders is largely distributed as it is in the pump pulse pattern. Although the shape of the Stokes pulses can change depending on the pump pulse profile (for instance Gaussian or rectangular), the repetition rate will stay the same. Since it is this factor that determines the impact of temporal gain variations, then little or no difference would be likely for a signal amplified at higher Stokes orders. However this was not confirmed experimentally due to a lack of suitable seed sources at the time of the experiment.

4.2 Noise figure

The principal and inevitable source of noise in optical amplifiers is ASE, which in the case of Raman amplifiers is sometimes known as amplified spontaneous scattering (ASS). Many other sources of noise are also possible in RFAs but these are not inevitable. Their importance depends on the application (see for instance [2]). Therefore a proof-of-principle study on any optical amplifier should include measurements of the amount of spontaneously generated light to assess potential implications on the performance. To assess the performance of an amplifier in terms of its noise generation it is common to use the noise figure (NF) concept. The noise figure quantifies the degradation of the signal-to-noise ratio (SNR) due to the insertion of an amplifier. Here the noise figure of the RFA is estimated by measuring the amount of amplified spontaneous Raman scattering on an OSA and then using the following formula [3]:

$$F = \frac{1}{G}\left(1 + \frac{P_{ASE}(\nu)}{h\nu B_{OSA}(\nu)}\right) = \frac{1}{G}\left(1 + \frac{\lambda^3 P_{ASE}(\lambda)}{hc^2 B_{OSA}(\lambda)}\right) \tag{4.1}$$

A logarithmic dB-scale is normally used for the noise figure, according to:

$$NF = 10\log_{10}(F) \tag{4.2}$$

Here B_{OSA} is the OSA resolution bandwidth and P_{ASE} is the power level of the amplified spontaneous Raman scattering measured within B_{OSA}. This quantity is often called the optical noise figure and can also be expressed in terms of the on-off Raman gain where it is given by the equivalent noise figure, NF_{eq}:

$$NF_{eq} = NF.\exp^{-\alpha_S L} = \frac{1}{G^{on-off}}\left(1 + \frac{\lambda^3 P_{ASE}(\lambda)}{hc^2 B_{OSA}(\lambda)}\right) \tag{4.3}$$

Note that this gives the degradation of SNR only when shot noise dominates the noise of the input signal.

4.2.1 Noise characterisation and noise figure measurements

In this section experimental measurements on the amplified spontaneously scattered power and noise figure of the cascaded RFA are reported. The same pulsed Yb MOPA pump source described in chapter 3 is still used. The measurements were taken by noting the relative increase in average power of the amplified spontaneously scattered light in the counter-propagating direction on the OSA. From here on, the amplified spontaneously scattered light will be referred to as Raman ASE. The relative measurements were then converted to absolute powers by use of a reference signal at the appropriate wavelength and a well-calibrated power meter. The Raman ASE powers and noise figure values shown correspond to the peak of the Raman gain, i.e., the same wavelength at which the gain was measured. The OSA resolution bandwidth was set to 2 nm along with the linewidth (FWHM) of the reference signal.

Figure 4.3 shows the on-off gain and counter-propagating Raman ASE power for the 1st Stokes order plotted against the average pump power for the RFA using the

6 km HNLF. It shows that as expected, the Raman ASE power rises as the pump power and gain increase. However as the pump power if further increased, the gain depletes and reduces but the Raman ASE does not and remains at its highest level.

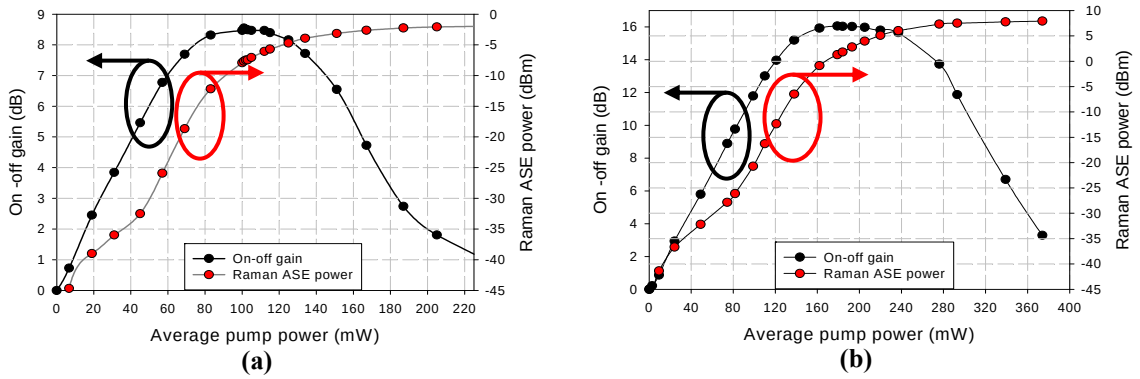

Figure 4.3 Graph showing the on-off gain and growth of Raman ASE power for the 1st Stokes order in the 6 km HNLF, (a) 20% pump duty cycle and (b) 40% pump duty cycle.

At this point it is worthwhile looking at the growth of Raman ASE using a co-propagating CW pumped RFA model in VPIphotonics™ which is based on the following equation [2].

$$\pm \frac{dP_{ASE}^{\pm}}{dz} = -\alpha_{ASE} P_{ASE}^{\pm} + C_R P_P P_{ASE}^{\pm} + C_R [1 + \eta(T)] h \nu_{ASE} B_{ref} P_P \qquad (4.4)$$

where P_{ASE} is the Raman ASE power in one polarisation component and in a bandwidth B_{ref}. Furthermore, $\eta(T)$ is the Bose-Einstein population factor given. The population factor is given by $\eta(T) = \frac{1}{\exp^{(h\Delta\nu/K_B T)} - 1}$, where h is Planck's constant, $\Delta\nu$ is the vibrational frequency, K_B is Boltzmann's constant and T is the fibre temperature in Kelvins. The last term in equation 4.3 represents spontaneous Raman scattering and for SRS that builds up from spontaneous Raman scattering, this is equivalent to using an effective input power of $P_{in}^{eff} \approx h \times \nu_{ASE} \times B_{ref}$ for one polarisation component [4]. At a wavelength of 1116 nm, the effective input power within a bandwidth of 2 nm is approximately equal to 0.086 μW or -40.67 dBm.

Figure 4.4 shows the simulated results from using equation 4.4 to calculate the co-propagating Raman ASE power produced when using the 6 km HNLF in the RFA

set-up. In can be seen from graph (a) that the Raman ASE power closely follows the on-off gain profile, as expected from using equation 4.4. It shows that the Raman ASE starts from the vacuum fluctuation level and is amplified and depleted in accordance with the on-off gain. Graph (b) also shows the corresponding equivalent noise figure profile and how it reaches its minimum value at the maximum gain before turning back on itself.

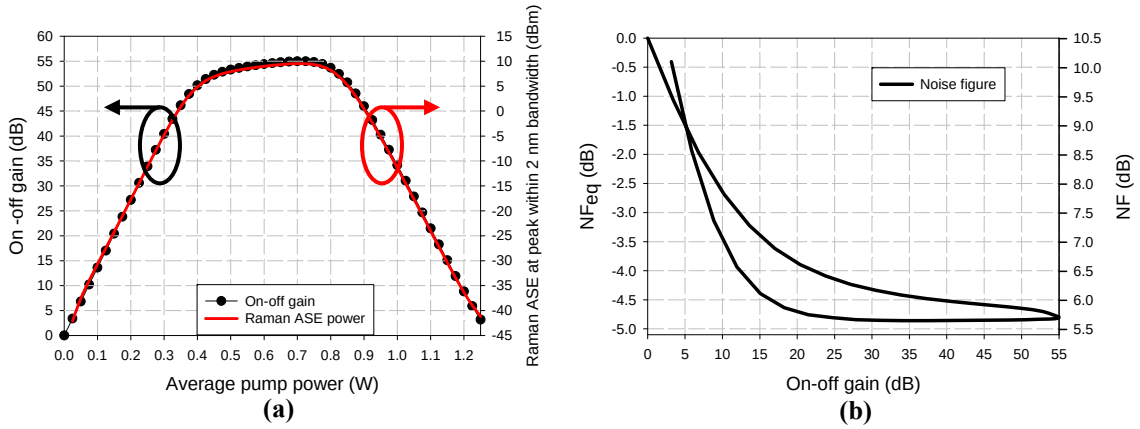

Figure 4.4 Simulated results for the co-propagating Raman ASE produced when CW pumping the 6 km HNLF, (a) On-off gain and Raman ASE power *vs*. the average pump power and (b) Resulting equivalent noise figure *vs*. on-off gain.

Clearly, the experimental counter-propagating Raman ASE behaves quite differently, so in contrast to the gain, the counter-propagating Raman ASE is not straightforwardly related to the co-propagating Raman ASE, and there appear to be several regimes, depending on the pump power. Going back to figure 4.3 it can be seen that for the 1st Stokes order in the counter-propagating direction, in the regime of low pump power, the Raman ASE increases at a much higher rate than the counter-propagating on-off gain. It increases by ~40 dB for the 20% pump duty cycle and ~50 dB for the 40% pump duty cycle, as the counter-propagating on-off gain increases from 0 dB to the maximum value. This is in fact closer to the increase in the co-propagating gain, and indeed the co-propagating Raman ASE, than to the increase in counter-propagating gain, and is an indication that the counter-propagating Raman ASE derives from the co-propagating Raman ASE

One possible mechanism for this is Rayleigh scattering. This can result in light being backscattered within the fibre and specifically that Raman ASE that is co-propagating with the pump pulses to be reflected into the counter-propagating direction, i.e., in the signal direction. It is therefore possible that the measured counter-

propagating Raman ASE originates as co-propagating Raman ASE, initially experiencing a high co-propagating gain before being Rayleigh backscattered and experiencing the counter-propagating gain. The co-propagating Raman gain can be estimated from the measured counter-propagating gain divided by the duty cycle.

To proceed, it is first necessary to assess the Rayleigh backscattering (RBS). The Rayleigh backscattering coefficient κ is given by [2]:

$$\kappa = S\alpha_R \tag{4.5}$$

where S is the fraction of Rayleigh-scattered optical power coupled to the counter-propagating guided mode and α_R is the Rayleigh scattering coefficient. Since Rayleigh scattering typically dominates the propagation loss, these are often similar. The fraction of captured optical power S (for a step-index profile) is given by the ratio of the solid acceptance angle for the fibre to the total solid angle as:

$$S \cong \frac{\pi(NA)^2}{4\pi n_1^2} = \frac{(NA)^2}{4n_1^2} \tag{4.6}$$

In the case of the HNLF, with an NA=0.33 and n_1=1.486, the recapture fraction is equal to 12.33x10^{-3}. This gives an RBS coefficient of κ=3.879x10^{-3} km^{-1} at a wavelength of 1116 nm. This value is high compared to standard transmission fibres (typically ~1x10^{-4} km^{-1} at 1550 nm) due to a high NA and increased Rayleigh scattering losses. These are important consequences of the higher Ge content used to increase the Raman fibre gain efficiency.

For a precise evaluation of the back-scattered Raman ASE at the 1st Stokes it is necessary to know how the forward Raman ASE evolves along the fibre. This requires a numerical solution [5]. For an analytical treatment I will assume that the Raman ASE grows exponentially; i.e., I neglect nonlinear depletion as well as linear attenuation of the pump. This can only give an estimate of the backscattered power, since the decrease in pump power along the fibre is significant in case of 6 dB of loss. Under these conditions it is straightforward to show that the effective length for RBS of the 1st Stokes becomes:

$$L_{eff}^{RBS} = L\frac{\exp\left[G^{on-off}\left(1+\frac{1}{d}\right)-2\alpha_S L\right]-1}{G^{on-off}\left(1+\frac{1}{d}\right)-2\alpha_S L}, \tag{4.7}$$

where L is the fibre length, $G^{on\text{-}off}$ is the on-off gain in nepers for counter-propagating light, and d is the duty cycle. This must then be multiplied by the RBS coefficient as well as the duty cycle to calculate how much power is backscattered. The idea now is to use this formula to calculate the amount of initially forward Raman ASE that gets back-scattered and exits the fibre in the backward direction, and compare it to the backward "intrinsic" Raman ASE that results in the absence of RBS. Both of these quantities are assumed to originate from vacuum fluctuations. For simplicity I neglect the difference in the spontaneous-emission factor n_{sp} for forward and backward ASE. The intrinsic backward Raman ASE is then proportional to $\exp[G^{on\text{-}off} - \alpha_S L]$, and the ratio between the two becomes:

$$\frac{\kappa L d}{\exp\left[G^{on-off}-\alpha_S L\right]}\frac{\exp\left[G^{on-off}\left(1+\frac{1}{d}\right)-2\alpha_S L\right]-1}{G^{on-off}\left(1+\frac{1}{d}\right)-2\alpha_S L} \approx \frac{\kappa L d\exp\left[G^{on-off}/d-\alpha_S L\right]}{G^{on-off}\left(1+\frac{1}{d}\right)-2\alpha_S L}. \tag{4.8}$$

For a 6 km long HNLF, $\kappa L \approx 23.3\text{x}10^{-3}$ or –16.33 dB. It is then clear that already for a relatively low forward net gain of say, 20 dB (4.6 Np); the Rayleigh back-scattered Raman ASE will start to dominate. This corresponds to a forward on-off gain of 28.2 dB and a backward on-off gain of 11.28 dB and 5.64 dB for 40% and 20% duty cycle, respectively. This is in reasonable agreement with the points at which the Raman ASE starts to grow rapidly in figure 4.3, and roughly in proportion to the sum of the forward and backward gain, in agreement with equation 4.7.

It is also possible to assess what the absolute power in 2 nm. For example, we get 32.8 dBm for an on-off gain of 5.64 dB, in good agreement with the experimental results in figure 4.3.

The counter-propagating Raman ASE power follows a similar trend for all Stokes orders with figure 4.5 showing two more examples with the 3rd and 6th Stokes orders for a 20% pump duty cycle and the 6 km HNLF. A drop in the amount of Raman

ASE power can be seen as the Stokes order increases. This can be explained partly due to a drop in power at the vacuum fluctuation level with increasing wavelength (i.e., decreasing photon energy) and also the fixed OSA resolution of 2 nm resulting in a reduced frequency bandwidth, B_{ref} with increasing wavelength. This will lower the effective input power from the 1st to 3rd and 1st to 6th Stokes orders by ~1.2 and 3.6 dB, respectively.

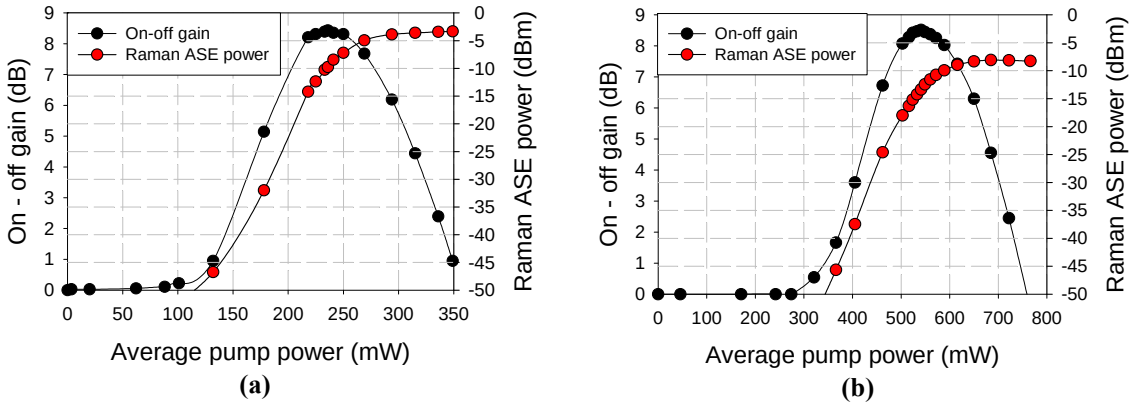

Figure 4.5 Higher-order on-off gain and counter-propagating Raman ASE power for pulse-pumping the 6 km HNLF with a 20% duty cycle, (a) 3rd Stokes order and (b) 6th Stokes order.

To determine the noise figure, equation 4.3 is used to convert the measured Raman ASE powers. Figure 4.6 shows the counter-propagating equivalent noise figure in relation to the on-off gain experienced by an input seed signal for the 6 km HNLF. It shows that the noise figure rises to 20-30 dB at the peak of the on-off gain before it carries on increasing as the on-off gain drops. All seven Stokes orders follow the same trend and are close to each other.

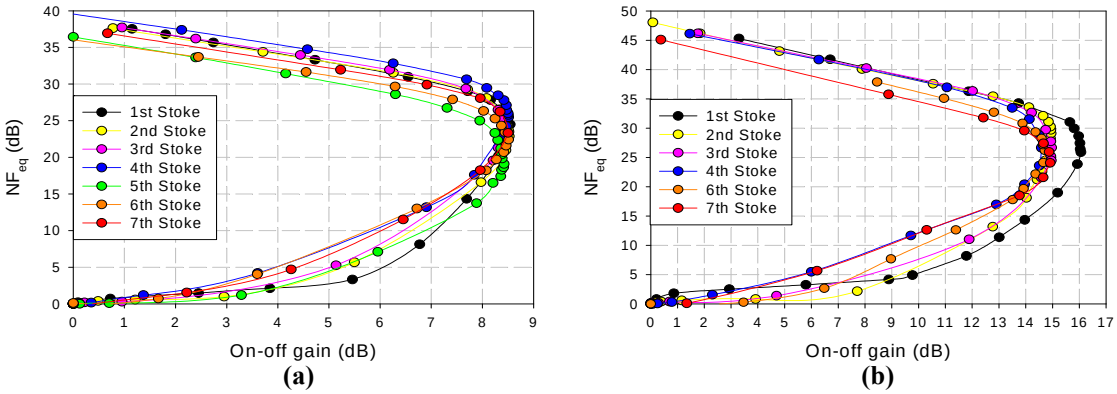

Figure 4.6 Equivalent noise figure vs. on-off gain for the 6 km HNLF with (a) 20% pump duty cycle and (b) 40% pump duty cycle. 1st Stoke=1116 nm, 2nd Stoke=1172.4 nm, 3rd Stoke=1235.6 nm, 4th Stoke=1305.8 nm, 5th Stoke=1384.8 nm, 6th Stoke=1473.6 nm, 7th Stoke=1573.6 nm.

These values of NF_{eq} can be considered fairly high because the noise is dominated by Rayleigh backscattered Raman ASE. The backscattered Raman ASE, first of all experiences the co-propagating gain and then the counter-propagating gain whereas a signal only experiences the counter-propagating gain. In the case of the experiments carried out here, the NF_{eq} always remains high because the on-off gain is reduced due to the generation of the 2nd Stokes order but the counter-propagating Raman ASE remains high.

Although the curves for 20% and 40% duty cycle look similar, it is important to note that for the same gain, the noise figure in the lower branch is lower for the higher duty cycle. Thus, at 40 % duty cycle, the noise figure is 4 – 8 dB for a gain of 8 dB for all Stokes orders, whereas it is 14 – 20 dB for a duty cycle of 20%.

Figure 4.7 shows an example of how different the Raman ASE spectra can potentially be when travelling in different directions relative to the pump. Figure 4.7 (a) shows the co-propagating Raman ASE produced at various power levels using computer simulations for a CW pumped RFA employing a 6 km HNLF. This simulation does not include RBS. As also shown in figure 4.4, the Raman ASE depletes as it drives the Raman cascade process resulting in a decrease of Raman ASE in the wavelength region of the previously generated Stokes orders. This result would also be valid for rectangular pump pulses where the whole pump pulse depletes but not for Gaussian pump pulses [6]. Figure 4.7 (b) shows the counter-propagating Raman ASE spectra experimentally measured on an OSA from the cascaded RFA set-up with a 20% pump duty cycle and the 6 km HNLF. This blue dashed line corresponds to a power level of 270 μW taken from the graph in figure 4.2. This graph shows that even as the gain is pushed out towards the 4th Stokes order the Raman ASE power remains high in the previously generated Stokes orders.

This has implications for chapters 5 and 6 where Raman gain is targeted across multiple Stokes orders at the same time. With the current experimental set-up, if a pump pulse generates gain at the 3rd Stokes order, then there will always be a significant amount of Raman ASE in the wavelength region of the 1st and 2nd Stokes orders. However, it is also possible that these counter-propagating Raman ASE results could be improved with an improved experimental set-up. Further investigations are required as to the impact of non-rectangular pump pulses and possible limitations of the polarisation scrambling technique employed in the current set-up.

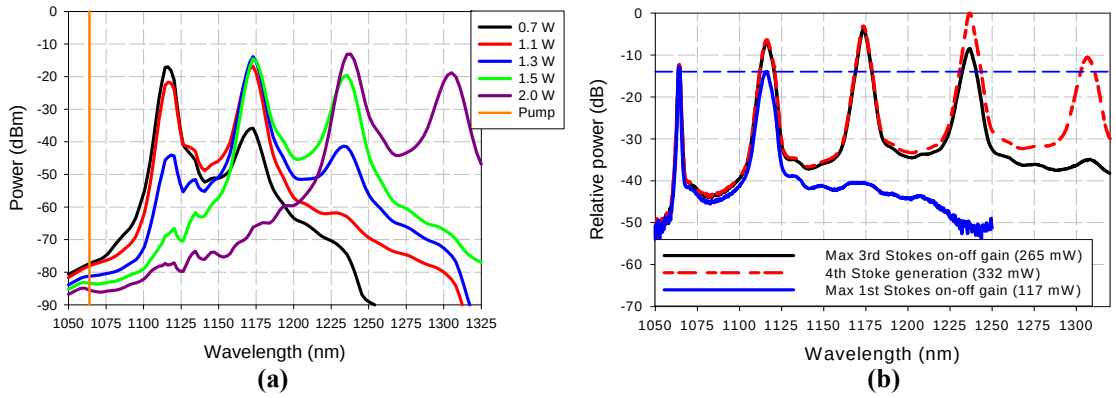

Figure 4.7 Output spectra from a cascaded RFA with the 6 km HNLF at various powers, (a) Modelled output from the RFA CW pumped in the co-propagating direction and (b) Experimental output from the RFA pulse-pumped in the counter-propagating direction.

Further experimental measurements on the amount of Raman ASE generated from the RFA were carried out for the shorter length of HNLF which was reduced from 6 km to 2 km. Figure 4.8 shows the on-off gain and counter-propagating Raman ASE power results for the 1st Stokes order against the average pump power for the RFA using the 2 km HNLF. Again the counter-propagating noise is dominated by the Raman ASE that is Rayleigh backscattered from the co-propagating direction.

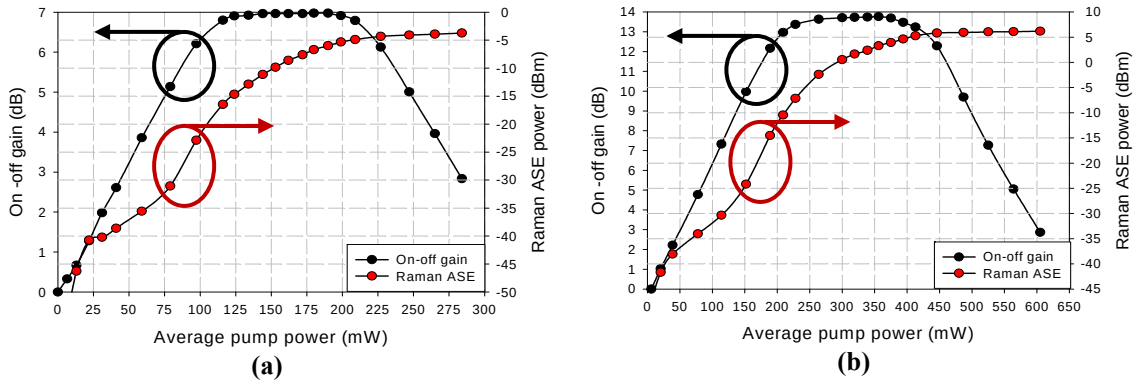

Figure 4.8 Graph showing the on-off gain and growth of Raman ASE power for the 1st Stokes order in the 2 km HNLF, (a) 20% pump duty cycle and (b) 40% pump duty cycle.

In terms of Raman ASE power levels there is actually little difference between the 6 km and 2 km HNLF for the 1st Stokes order (see figure 4.9). At low gains, RBS is not a factor and any differences in backward Raman ASE power are expected to be caused by differences in the ratio of gain to background loss. For higher pump powers, when RBS dominates the difference should be close to the difference in length between

the fibres, according to equation 4.8. This is a factor 3 or 4.8 dB. It is in fact smaller, around 2 dB at high powers and closer to 0 dB at lower ones. This relative increase in the Raman ASE level for the shorter fibre may be due to its higher net gain. Furthermore, using equation 4.7 and comparing the Rayleigh backscattered Raman ASE power to the intrinsic backward Raman ASE it is estimated that for the 2 km HNLF and a 20% duty cycle the backscattered Raman ASE starts to dominate the intrinsic backward Raman ASE at around 4.34 dB. This is in good agreement with the kink in the curve (see figure 4.9 (a)) for the experimental results of the counter-propagating Raman ASE. There is also a good agreement for this point with the 40% duty cycle and the 6 km HNLF.

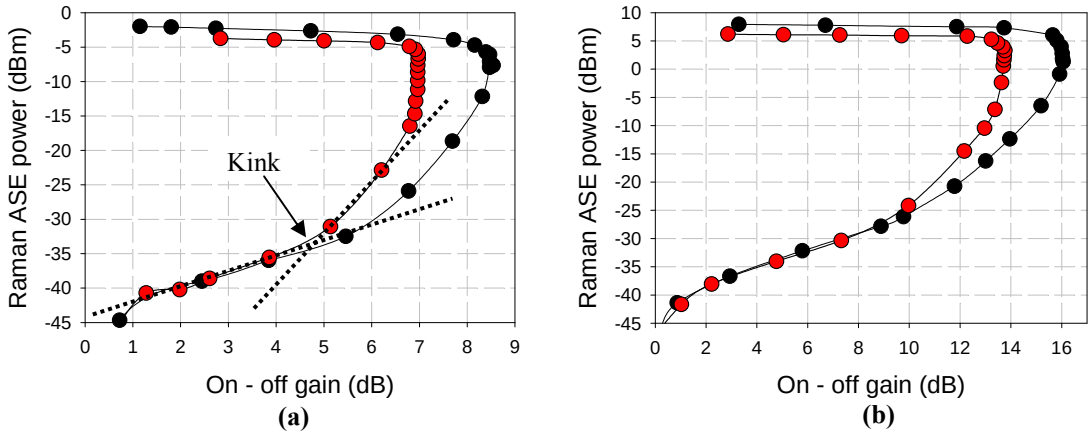

Figure 4.9 Comparison between the Raman ASE powers generated in the 6 km and 2 km HNLFs, (a) 20% pump duty cycle and (b) 40% pump duty cycle. —●— 6 km HNLF and —●— 2 km HNLF.

In terms of the counter-propagating equivalent noise figure, figure 4.10 shows the results in relation to the on-off gain experienced by an input seed signal for the 2 km HNLF. Once again it shows that the noise figure rises to 20-30 dB at the peak of the on-off gain before it carries on increasing as the on-off gain drops. Again all seven Stokes orders follow the same trend and are close together. Since the counter-propagating Raman ASE powers are similar for the 2 km and 6 km HNLFs so are the values of NF_{eq}.

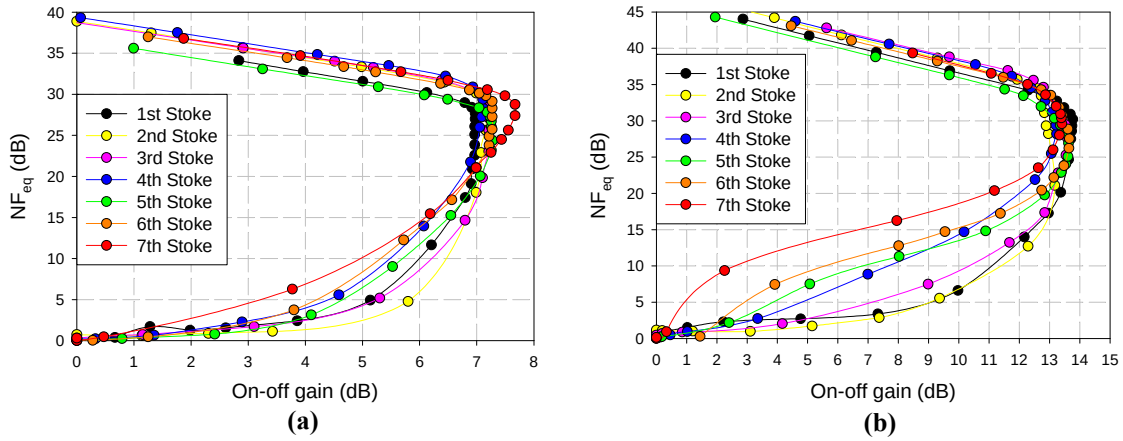

Figure 4.10 Equivalent noise figure *vs*. on-off gain for the 2 km HNLF with (a) 20% pump duty cycle and (b) 40% pump duty cycle. 1st Stoke=1116 nm, 2nd Stoke=1172.4 nm, 3rd Stoke=1235.6 nm, 4th Stoke=1305.8 nm, 5th Stoke=1384.8 nm, 6th Stoke=1473.6 nm, 7th Stoke=1573.6 nm.

This is further emphasised in figure 4.11 which shows a direct comparison between the equivalent noise figure values of the 1st and 2nd Stokes order for the 2 km and 6 km lengths of HNLF.

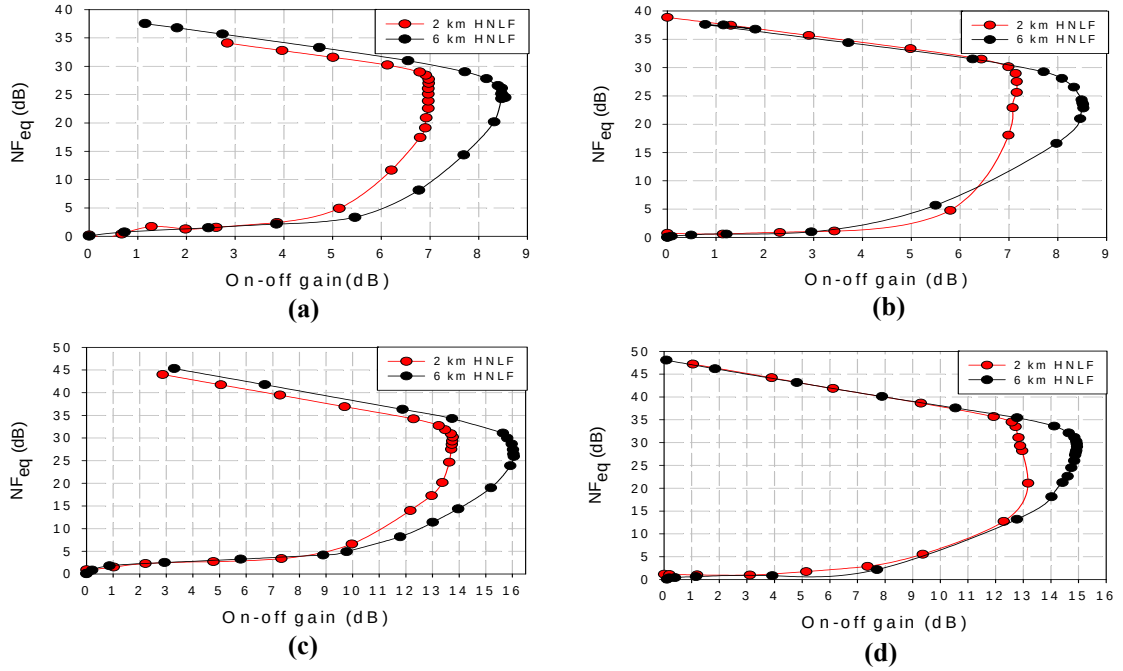

Figure 4.11 Graphs comparing equivalent noise figure measurements between 2 km and 6 km HNLF for (a) 1st Stokes order and 20% pump duty cycle, (b) 2nd Stokes order and 20% pump duty cycle, (c) 1st Stokes order and 40% pump duty cycle and (d) 2nd Stokes order and 40% pump duty cycle.

However due to the different background losses for all the Stokes orders, differences in the intrinsic noise figure, given by equation 4.2, would be expected due to

differences in the net gain. Figure 4.12 shows the intrinsic noise figure results against net gain for both the 6 km and 2 km HNLF. For the 6 km HNLF, differences in NF values are more visible due to the larger differences in the loss and the net gain between the Stokes orders. It can be seen that the 7th Stokes order has the lowest intrinsic noise figure due to the lower background loss and therefore higher net gain. This is the case for both a 20% and 40% pump duty cycle. For the 2 km HNLF, the differences are less visible and the curves become bunched up again with all the Stokes orders having similar noise figure values. This is only to be expected since as the fibre length reduces the net gain approaches that of the on-off gain.

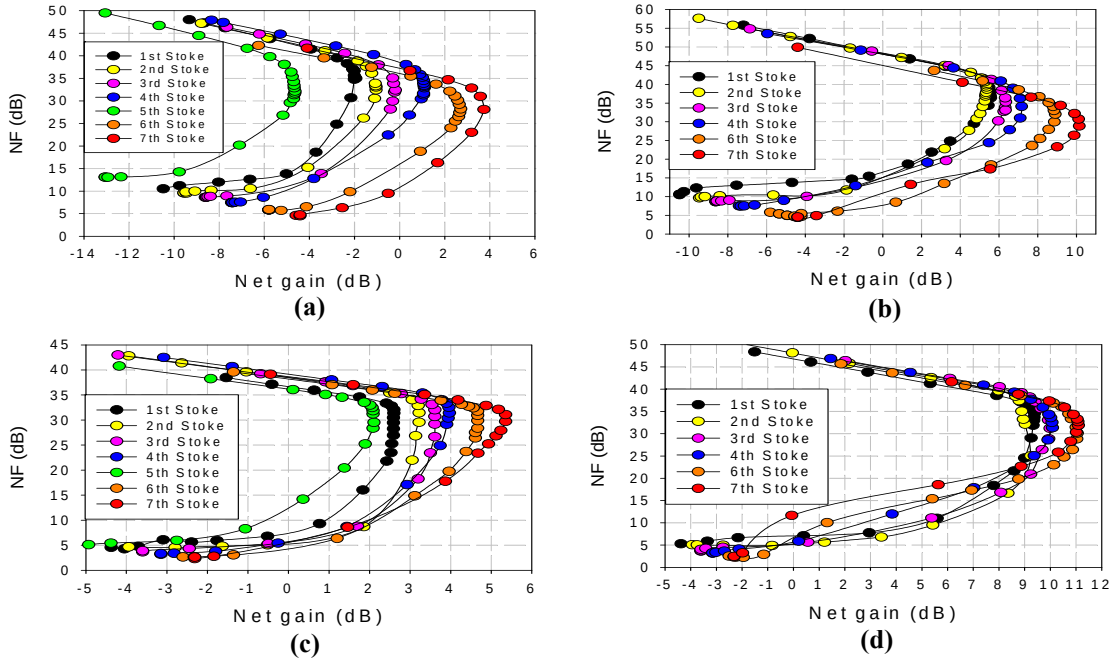

Figure 4.12 Intrinsic NF *vs*. net gain for the HNLF, (a) 6 km and 20% pump duty cycle, (b) 6 km and 40% pump duty cycle, (c) 2 km and 20% pump duty cycle and (d) 2 km and 40% pump duty cycle. 1st Stoke=1116 nm, 2nd Stoke=1172.4 nm, 3rd Stoke=1235.6 nm, 4th Stoke=1305.8 nm, 5th Stoke=1384.8 nm, 6th Stoke=1473.6 nm, 7th Stoke=1573.6 nm.

As well as comparing the different lengths of HNLF, it is also interesting to compare different fibre types such as the HNLF and the Freelight™ DSF. The fibres differ in the amount of germanium added to the core which impacts both the NA and Rayleigh scattering losses which both influence the amount of backscattered power within the fibres. The RBS coefficient for the Freelight™ DSF at a wavelength of 1116 nm is κ=4.038x10^{-4} km^{-1}. This is approximately 9.6 times lower than the RBS coefficient of the HNLF. In some instances this would lead to a lower Rayleigh backscattered power than in the HNLF. However, in a RFA a lower Ge content

typically leads to a lower Raman fibre gain efficiency. This is then met with a higher pump power requirement, a longer fibre length or a trade-off between both. A longer fibre will then result in more Rayleigh backscattered power in accordance with equation 4.7. The Raman fibre gain coefficient of the Freelight™ DSF is approximately 8.6 times lower than that of the HNLF. Therefore, for the same pump power, 8.6 times longer fibre is required. This effectively cancels out the 9.6 times lower RBS coefficient and consequently the counter-propagating Raman ASE powers and noise figure values for the Freelight™ DSF and HNLF are still expected to be similar, if the same pump powers are used.

Figure 4.13 shows the counter-propagating Raman ASE powers for the first three Stokes order generated in a 6 km Freelight™ DSF with a 20% pump duty cycle. Again using equation 4.7, there is a good agreement between the calculated backscattered Raman ASE powers and those from the experimental results for the 1st Stokes order in the Freelight™ DSF. For example, a backscattered Raman ASE power of -17.8 dBm in a 2 nm bandwidth is calculated for an on-off gain of 7 dB.

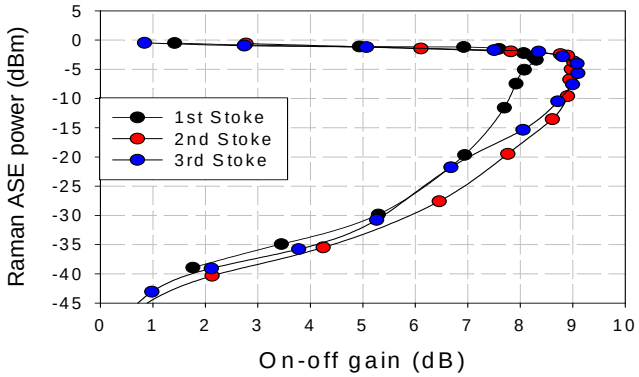

Figure 4.13 Counter-propagating Raman ASE for the first three Stokes orders generated in the 6 km Freelight™ DSF with a 20% pump duty cycle.

Figure 4.14 compares the equivalent noise figure values from the 6 km Freelight™ DSF with the 6 km and 2 km HNLF when a 20% pump duty cycle is used. Plot (a) shows the results for the 1st Stokes order whereas plot (b) shows the results for the 2nd Stokes order. Upon comparison the 6 km Freelight™ DSF and the HNLFs are all similar in value. In the case of the 1st Stokes order the HNLF actually looks better than the 6 km Freelight™ DSF even though it has a much higher RBS coefficient.

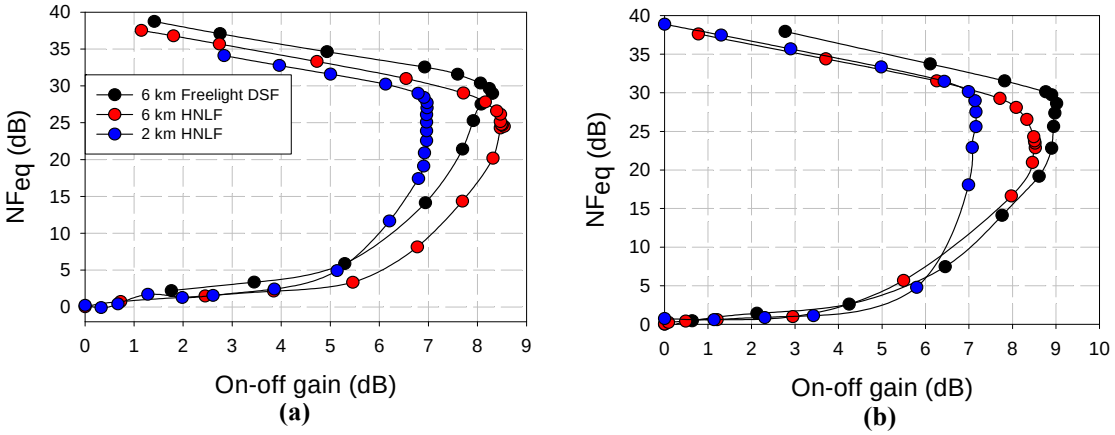

Figure 4.14 Comparison of equivalent noise figure *vs*. on-off gain for the HNLF and Freelight™ DSF of various lengths and a 20% pump duty cycle, (a) 1st Stokes order and (b) 2nd Stokes order.

From the noise measurements for the pulse-pumped cascaded RFA shown so far it appears that there is little or no advantage to using a low-NA fibre to reduce the Rayleigh backscattered power and as a result the overall noise. However this is when the equivalent noise figure is considered, which compares the Raman ASE level to the on-off gain. For a lumped amplifier the actual gain and the corresponding NF are normally more important, and here, the Freelight™ DSF is better than the HNLF, when two fibres of the same length are compared. However this advantage shrinks if two fibres with the same pump power are considered, since the HNLF can then be shorter.

Furthermore, across the seven Stokes orders there is little difference in the equivalent noise figure values for the different lengths of HNLF. The intrinsic noise figure which takes into account the net gain is shown to in some instances be lower for higher Stokes orders. However this is only the case for the longer lengths of HNLF where bigger differences in net gain between the lower and higher Stokes orders are inevitable. Ultimately as the fibre length is reduced and the difference in net gain between the lower and higher Stokes orders becomes smaller, even the intrinsic noise figure values become similar for all Stokes orders.

4.3 Gain saturation

Saturation effects place an upper limit on the maximum achievable gain and power possible in any amplifier [7]. For a contra-directionally pulse-pumped cascaded RFA, the most important saturation effects are forward (cascaded) stimulated Raman conversion (i.e., forward Raman ASE) and signal build-up. Both of these effects deplete the pump and compress the signal gain [8]. The small-signal gain saturation (i.e., limitation on maximum gain) due to generation of higher Stokes orders has already been treated in chapter 3. In this section the gain saturation effect due to an increase in the input signal power is investigated. Gain saturation due to an increase in the input signal power begins when the signal power approaches that of the pump power. This represents the maximum possible output signal power from the RFA. Figure 4.15 (a) shows a simulated example of how the gain saturates as the input signal increases for a CW-pumped RFA using HNLF and operating with a net gain of 16 dB. This was calculated using the CW-pumped RFA model in VPIphotonics^{TM}. It shows how the gain saturates at a lower signal input power for the 6 km HNLF when compared with the 2 km HNLF. This is due to the stronger coupling between the pump and signal in the longer fibre length and also the shorter fibre length of 2 km requires a higher input pump power. It also indicates the differences between a co-propagating and a counter-propagating pump (in the cw regime) due to a difference in the path-average powers along the fibre [8]. Figure 4.15 (b) shows an example of how the pump and signal power evolve along the length of fibre for the 6 km HNLF and for two different input signal powers.

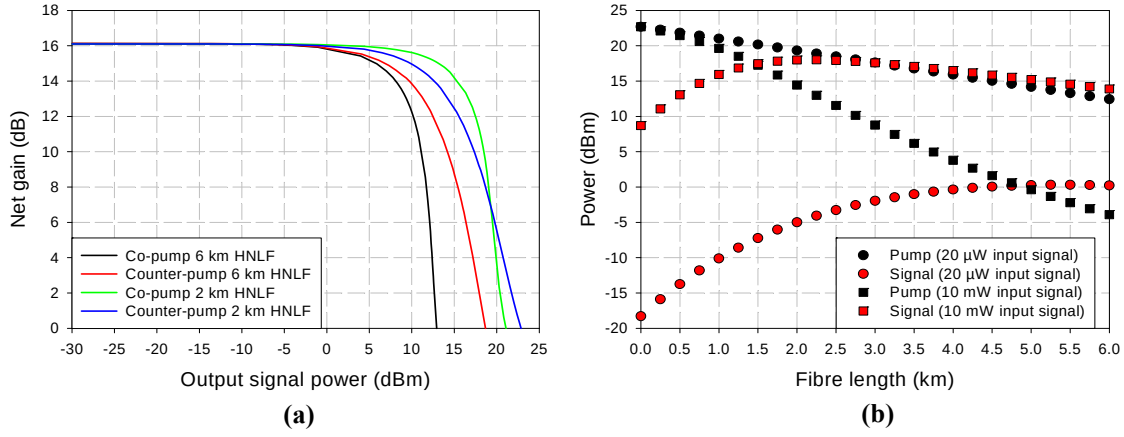

Figure 4.15 Simulated examples showing (a) net gain *vs*. output signal power for co- and counter-pumping of the HNLF with 2 km and 6 km lengths and (b) the power distribution along the 6 km HNLF for different input signal power levels.

It shows how a low power signal at 20 μW operates in the unsaturated regime and is amplified by 16 dB without impacting the decrease of pump power which is dominated by the fibre attenuation. However when the input signal power is increased to 10 mW, the high signal power causes the pump to deplete over a shorter distance than when operating in the small-signal regime. The gain for the signal is subsequently reduced.

4.3.1 Gain saturation measurements

Gain saturation measurements due to an increase in input signal power were performed at the 1st, 2nd and 7th Stokes orders. For these measurements, seed lasers with higher output powers than the SC source had to be used. For the 1st and 2nd Stokes orders an RFL was constructed, while a diode-seeded core-pumped EDFA was used for the 7th Stokes order. These seed lasers were CW rather than pulsed.

The RFL for the 1st Stokes order had an output wavelength of 1116 nm and therefore matched the peak of the Raman gain. The optical output from the RFL was chopped with a 50% duty cycle so that lock-in detection could still be used to accurately measure the gain. I used 1060/1110 WDM couplers at the output to filter out any remaining pump light and 2nd Stokes order light to give a clean signal. The RFL was able to provide a signal at 1116 nm with an average output power up to 200 mW. An attenuator was also used at the RFL output to control the input signal power into the cascaded RFA which added a further minimum insertion loss of ~3 dB. Even so there was more than enough signal power to saturate the RFA constructed using the HNLF since the input pump powers for maximum gain were ~100 mW for the 6 km HNLF and ~160 mW for the 2 km HNLF with a pump duty cycle of 20%.

Figure 4.16 shows the gain saturation plots with a pump duty cycle of 20%, 40% and 60% for the 6 km and 2 km HNLF. The graphs are shown for net gain (dB) versus output power (dBm). The amplifier was set up to operate at the maximum small-signal gain and then the input signal power was increased in stages while the pump power was kept constant. In characterising the saturation properties of an amplifier it is common to use the saturation output power which is defined as the output signal power at which the small-signal gain is reduced by a factor of two (or 3 dB) [9]. The saturated output powers for the 6 km HNLF at pump duty cycles of 20%, 40% and 60% are 10.8 dBm, 9.9 dBm and 9.0 dBm, respectively. For the 2 km HNLF, the saturated output powers at pump duty cycles of 20%, 40% and 60% are 15.2 dBm, 14.9 dBm and 13.0 dBm,

respectively. The difference in saturated output power between the 6 km and 2 km HNLF is approximately 4 - 5 dB. The higher saturated output power is achieved with the 2 km HNLF due to the higher pump power. In an RFA the required pump power increases as the fibre length decreases and so one would also expect the saturation output power to increase as the length decreases. The average input pump power for the 1st Stokes order with a 20% pump duty cycle was 19.5 dBm for the 6 km HNLF and 21.8 dBm for the 2 km HNLF, which goes some way to explaining the difference between the two fibre lengths.

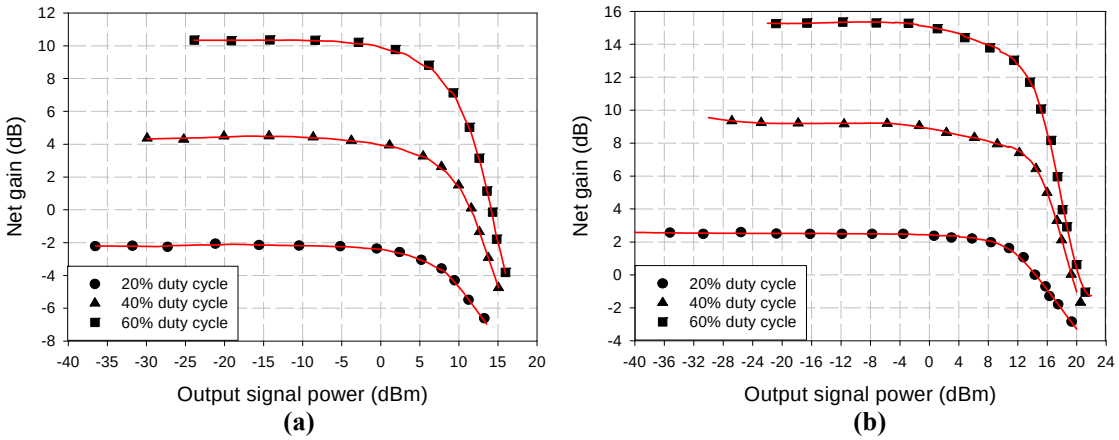

Figure 4.16 Net gain *vs*. output signal power for the 1st Stokes order with pump duty cycles of 20%, 40% and 60% for (a) 6 km HNLF and (b) 2 km HNLF.

Figure 4.17 shows the optical spectra in the counter-propagating direction for various input signal powers from the 2 km HNLF and pump pulses with a 40% duty cycle. These optical spectra correspond to the data shown in figure 4.16 (b) for the 40% pump duty cycle. Figure 4.17 shows four optical spectra for input signal powers of -32.1 dBm, -10.4 dBm, 4.8 dBm and 16 dBm. The first two signal power levels are in the unsaturated regime whereas the last two are in the saturated regime. The 4.8 dBm input signal power correspond to an output signal power of 12.2 dBm and the 16 dBm input signal power corresponds to an output signal power of 18 dBm on figure 4.16 (b). The output spectra stay the same until the signal input power reaches 16 dBm where there is evidence of increased Raman ASE at the 2nd Stokes order and that the signal is generating SRS. This is well into the saturated regime and passed the 3 dB saturated output power. This suggests that the signal is depleting the pump and saturating the gain but has not yet got enough power to generate significant SRS on its own. An output signal power of 18 dBm (i.e., 63 mW) is still relatively low in comparison to the critical

Raman average power of ~375 mW (where the signal is chopped with a 50% duty cycle).

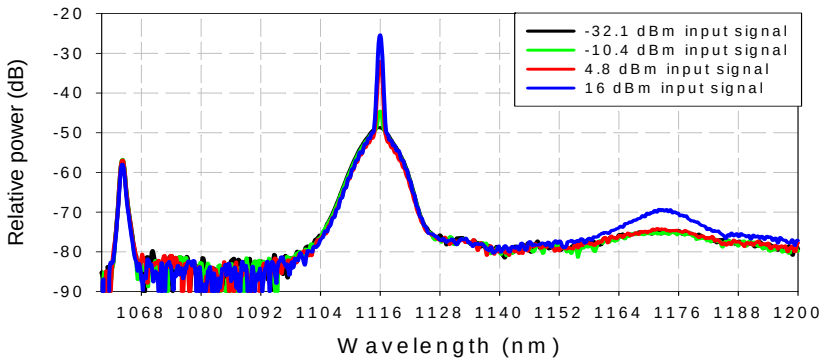

Figure 4.17 Counter-propagating optical spectra taken at various input signal powers at 1116 nm for the 2 km HNLF and a 40% pump duty cycle.

Figure 4.18 shows simulated data for the saturated gain in the counter-propagating direction for a pulse-pumped RFA. The model is based on [10] and gives some insight into the saturation properties of the 1st Stokes order. From figure 4.18 (a) it can be seen that the input signal power saturates earlier for the 40% pump duty cycle than it does for the 20% duty cycle due to the higher gain. For these results 3rd-order super-Gaussian pump pulses were used. Figure 4.18 (b) shows the net gain versus output power and can be compared to the experimental data shown in figure 4.16. The simulated saturated output powers for the 6 km HNLF at pump duty cycles of 20% and 40% are 16.0 dBm and 16.2 dBm, respectively. For the 2 km HNLF, the simulated saturated output powers at pump duty cycles of 20% and 40% are 18.5 dBm and 18.2 dBm, respectively. The difference between the average input pump powers for the two fibre lengths is 2.2 dB. It would also be expected that the saturated output powers be similar for all duty cycles with counter-propagating pump and signal. The reason is that saturation sets in when the signal starts to deplete the pump. Because they are counter-propagating, it is the average signal power that matters, and furthermore the saturation takes place in the signal output, i.e., the pump input, end of the fibre. Consequently, although the signal gain is higher for the higher duty cycle and the signal therefore builds up quicker, the pump is still reduced by the same amount for the same signal output powers in the bulk of the fibre, over a length that is very similar for different duty cycles. However, it is possible that other effects like double Rayleigh backscattering would influence this at high duty cycles. The saturated output power values from the simulations are also

higher than what we obtain in the experiment. The use of a pulsed signal can also affect the saturation characteristics. The simulations use a CW signal whereas it was modulated with 50% duty cycle in the experiments. Nevertheless, it is clear that a significant fraction of the pump can be converted into signal. If the duty cycle of the signal is lower than that of the pump then the signal peak power can exceed that of the pump. This opens up for SRS of the signal, and that reduces the (average) saturation output power for low signal duty cycles. The model is simplified in many ways and does not take into account the generation of the 2nd Stokes order or higher. Therefore it cannot be expected to reproduce the experimental saturation powers in case of SRS from the signal.

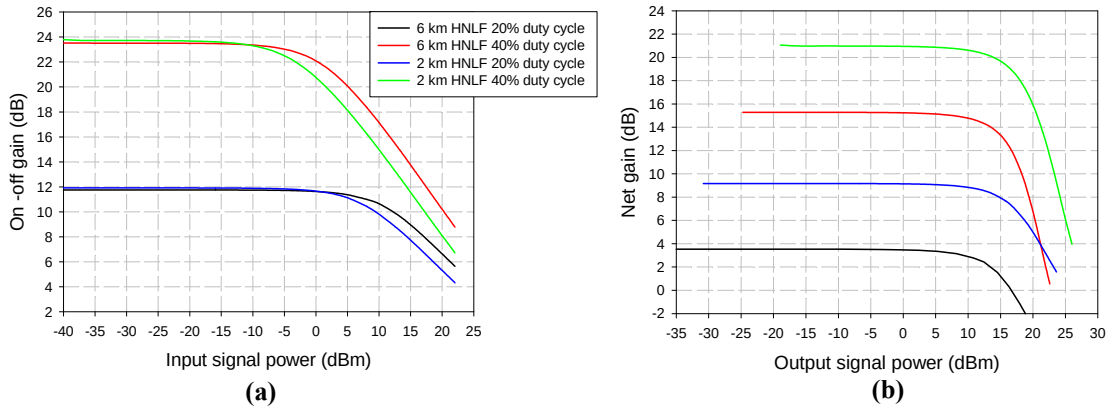

Figure 4.18 Modelled plots showing the saturation properties for the 1st Stokes order in a pulse-pumped counter-propagating RFA using 3rd-order super-Gaussian pulses. (a) On-off gain *vs*. input signal power and (b) Net gain *vs*. output signal power.

For the 2nd Stokes order gain saturation measurements, a cascaded RFL was constructed with an output wavelength of 1172 nm. Again the optical output was chopped with a 50% duty cycle so that lock-in detection could be used and WDM couplers were used to clean up the signal from any residual pump and 1st Stokes order light. The cascaded RFL had an output power of ~450 mW after the chopper. For the 7th Stokes order, a TLS tuned to a wavelength of 1575 nm was used to seed a core-pumped EDFA. The TLS output was also pulsed with a 50% duty cycle so that lock-in detection could be used. The output power from the 1575 nm MOPA source was 300 mW. Figure 4.19 shows the gain saturation plots for the 2nd and 7th Stokes orders with the 6 km and 2 km HNLF for different pump duty cycles. The 2nd Stokes order appears to be saturating earlier than the 1st and 7th Stokes orders, especially for the 40% and 60% pump duty cycles. This was not investigated further, so the reason remains unclear at the present

time. The experimentally measured saturation output powers for all three Stokes orders are summarised in table 4.1.

While no pulse-pumped counter-propagating cascaded RFA model was available to investigate the saturation properties in conditions similar to the experimental ones, some insights can be gained by using the CW co-pumped cascaded RFA model in VPIphotonics™.

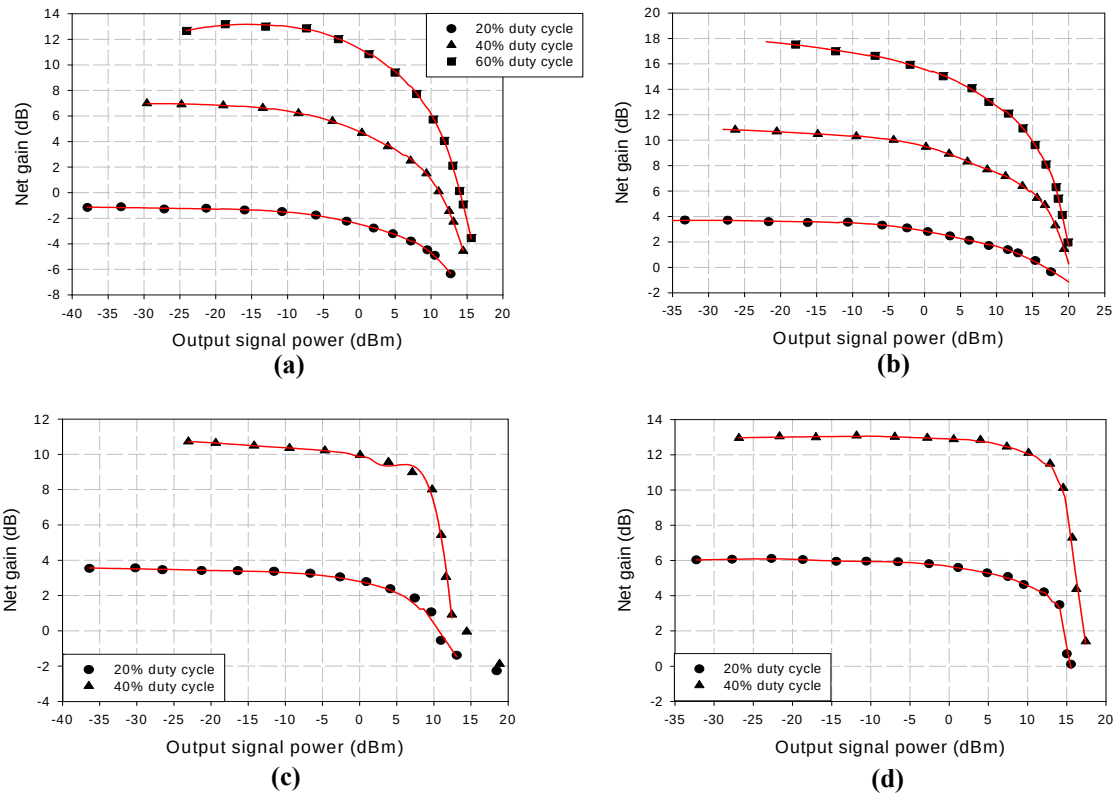

Figure 4.19 Net gain *vs.* output signal power with various pump duty cycles for (a) 2nd Stokes order and 6 km HNLF, (b) 2nd Stokes order and 2 km HNLF, (c) 7th Stokes order and 6 km HNLF and (d) 7th Stokes order and 2 km HNLF.

	2 km HNLF			6 km HNLF		
Duty cycle (%)	20%	40%	60%	20%	40%	60%
1st Stokes order	**15.2 dBm**	**14.9 dBm**	**13.0 dBm**	**10.8 dBm**	**9.9 dBm**	**9.0 dBm**
2nd Stokes order	**14.4dBm**	**8.2 dBm**	**5.0 dBm**	**8.6 dBm**	**2.8 dBm**	**3.8 dBm**
7th Stokes order	**14.1 dBm**	**14.3 dBm**	**N/A**	**9.8 dBm**	**9.7 dBm**	**N/A**

Table 4.1 Summary of saturation output powers experimentally measured for the 1st, 2nd and 7th Stokes orders from the HNLF.

Figure 4.20 shows two simulated examples of how the gain saturates in a CW co-pumped cascaded RFA as a consequence of increasing the power of the signal located at the wavelength of the peak Raman gain. Plot (a) shows the gain saturation data for seven Stokes orders (i.e., 1st to the 7th) taken individually while operating the RFA at the maximum small-signal gain for each respective Stokes order. The Raman gain saturates and due to the high gain, eventually turns in on itself as the signal power becomes strong enough to pump the next Stokes order. Plot (b) further shows the gain saturation data for four Stokes orders (i.e., 1st to the 4th) taken individually while operating the RFA at a net gain of ~16 dB for each respective Stokes order. It can be seen on both plots that the saturated output power increases as the Stokes order increases.

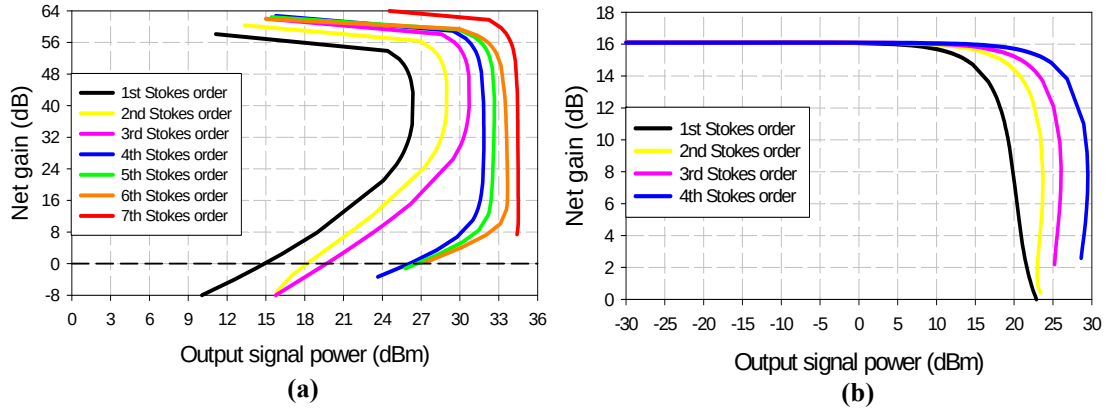

Figure 4.20 Simulation examples showing the saturation properties of a co-pumped cascaded RFA using the 2 km HNLF (a) net gain (maximum) *vs.* output signal power for seven Stokes orders and maximum gain, (b) net gain *vs.* output signal power for four Stokes orders and a net gain of ~16 dB.

This can be explained by looking at the power distribution along the fibre length as maximum power is generated at each Stokes order. Figure 4.21 shows two examples of the power distributions for each Stokes order along the 2 km HNLF when the target is to generate maximum gain at the 1st and 4th Stokes orders. It can be seen in plot (b), where maximum gain is generated at the 4th Stokes order, the effective length over which the power is distributed is much shorter than the effective length used to generate maximum gain at the 1st Stokes order (see plot (a)). This is because most of the fibre length is used to generate earlier Stokes orders in the Raman cascade [11]. The continually shortening of the effective length for increasing Stokes orders would then result in a higher critical power for generating the next Stokes order which would result in a higher signal power being possible.

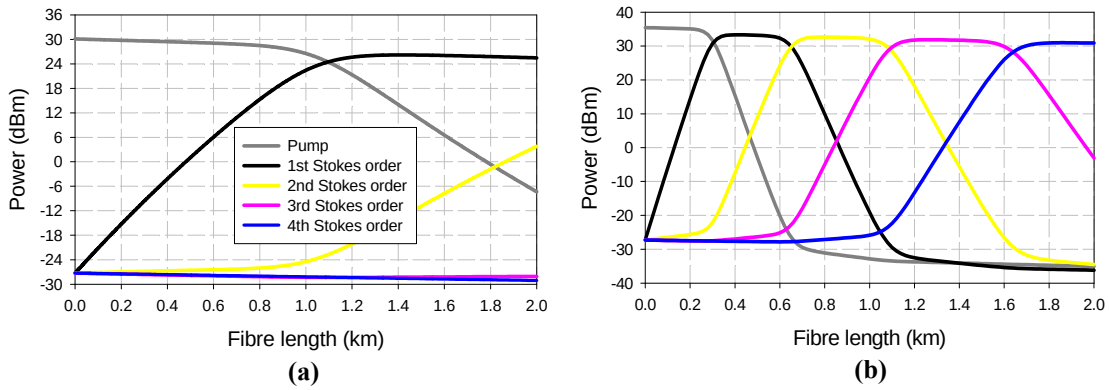

Figure 4.21 Simulation examples showing the power distribution along the 2 km HNLF when the gain is shifted to different Stokes orders, (a) Maximum gain at the 1st Stokes order and (b) maximum gain at the 4th Stokes order.

However, differences in the saturation characteristics of a pulse-pumped counter-propagating cascaded RFA and a CW co-pumped cascaded RFA would be expected. In the pulse-pumped RFA the rate of Raman conversion is determined by the peak power of the pump pulses. The average power of the pump pulses will always be lower than the peak power. For instance, pump pulses with a 20% duty cycle will have an average power five times lower than the peak power. In a counter-pumped configuration the pump power is exhausted in the amplifier as the signal power approaches the average power of the pulsed pump source and not the peak power. Therefore, even though the gain has saturated due to a lack of pump photons, the average power of the amplified signal can still be well below the peak power of the pump pulses. This means the counter-propagating signal power (at the 1st Stokes order) will not be strong enough to reach the critical power for generating the 2nd Stokes order as it will still be well below the pump power (i.e., the peak power of the pulses) required for generating the 1st Stokes order. This was indeed highlighted earlier in the experimental measurements for the pulse-pumped counter-propagating RFA (see figure 4.17).

For all the results shown so far the saturation measurements were taken at constant pump powers, corresponding to that which achieved the maximum small-signal gain from the RFA. However it is also possible in some instances to increase the saturation output power by increasing the input pump power when operating in the saturated regime. This can be seen in figure 4.22 which shows two examples. A 40% pump duty cycle is used for both HNLF lengths of 6 km and 2 km. The red line

represents the original data where the pump power is kept constant while the blue line represents the new data whereby the pump power was increased until the new maximum gain is reached. For the 1st Stokes order the saturation output powers with increased pump powers for the 6 km HNLF at pump duty cycles of 20%, 40% and 60% are 15.0 dBm, 13.4 dBm and 10.2 dBm, respectively. For the 2 km HNLF, the saturated output powers with increased pump power at pump duty cycles of 20%, 40% and 60% are 19.8 dBm, 19.0 dBm and 17.5 dBm, respectively.

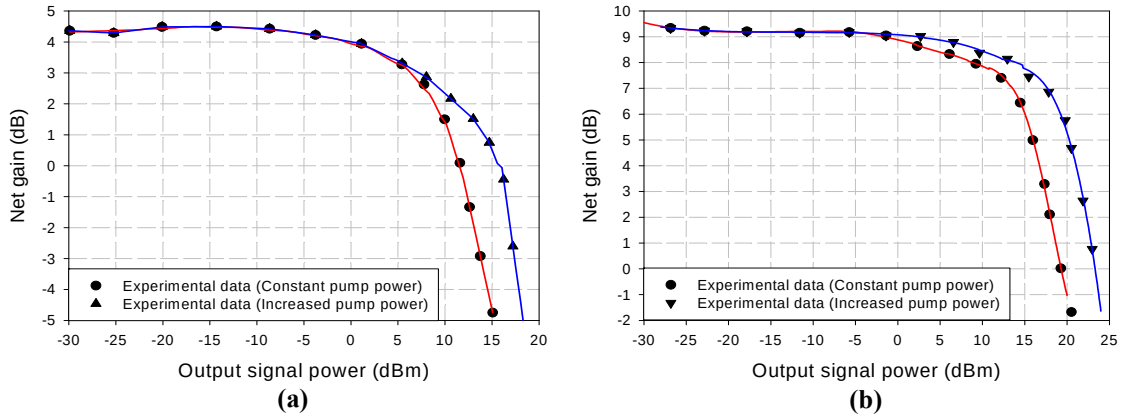

Figure 4.22 Net gain *vs.* output signal power for the 1st Stokes order and a 40% pump duty cycle with both constant and increasing pump power for (a) 6 km HNLF and (b) 2 km HNLF.

Looking at how the pump pulses deplete for the case in figure 4.22 (b), differences can clearly be seen when the signal power is in the small-signal and saturated regimes. Figure 4.23 (a) shows the pump pulse depletion in the small-signal regime for an input signal power of 90.5 µW. Here the pump pulse depletion is initiated by the amplified spontaneously scattered light. In the case of the 40 mW input signal, the high signal power causes the pump pulse to deplete earlier than in the small-signal regime as shown previously with the CW model in figure 4.15.

At an average pump power of 285 mW where the maximum small signal gain occurs, the pump pulse has still not fully depleted. It is therefore possible to increase the pump power and the gain before significant transfer to the next Stokes orders. Furthermore, the depletion is more uniform since it is partly caused by the signal. This avoids the patterning affects that result with co-propagating Stokes powers with a small walk-off.

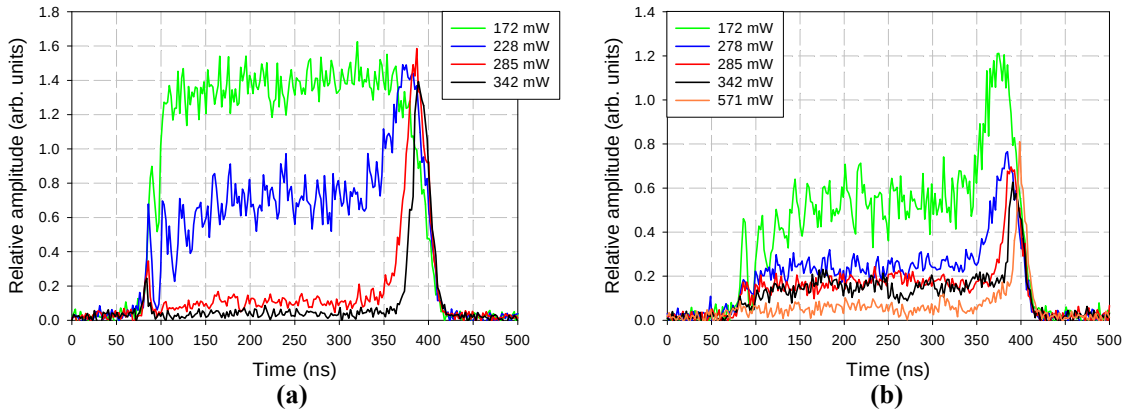

Figure 4.23 Pump pulse depletion plots for the 1st Stokes order at various pump powers (average) for a 40% pump duty and 2 km HNLF with different input signal power levels, (a) 90.5 µW signal power and (b) 40 mW input signal power. Power values in the graph legend correspond to the average pump power levels.

So far, however the increase in gain and saturated output power was only significant for the 1st Stokes order. There was some increase in gain in the saturated regime for the 2nd Stokes order but this occurred at higher input signal powers and did not affect the saturated output power. For the 7th Stokes order an increase in pump power in the saturated regime had little effect on the gain. (This effect therefore seems limited for a cascaded RFA). It is not yet understood but may be related to a smaller relative change in effective length for SRS of a certain order as the cascade is extended. In illustrative terms one could say that as the cascade extends from 1st to 2nd order, the effective length is halved so the pump power can be doubled, thus allowing for higher saturation output power. However, when the cascade is extended from 7th to 8th order, the effective length is only reduced by 14%.

In any case, for the saturation output powers, the pump power is the most important parameter. In the case of an RFA the pump power requirement is dependent on the fibre length and the Raman fibre gain coefficient and therefore so is the saturated output power. Therefore using a shorter fibre length for the RFA increased the saturated output powers.

4.4 Summary

In this chapter, cascaded RFAs have been assessed in terms of temporal gain variations, the noise performance and gain saturation properties. First of all, it was confirmed that the impact of temporal gain variations on an amplified signal that can result as a consequence of pulse-pumping can indeed be limited by using pump pulses at high repetition rates. At the repetition rates used throughout the work in this thesis, typically 400 kHz to 1.33 MHz, the maximum-to-minimum on-off gain variation at the peak average gain was less than ~1 dB.

Next the noise performance of the pulse-pumped cascaded RFA was investigated in terms of the amount of counter-propagating Raman ASE that was generated. These were then converted into noise figure values. As with the gain data, measurements were taken for pump duty cycles of 20% and 40% and for 6 km and 2 km fibre lengths. It was found that the counter-propagating noise figure in the RFA was dominated by Raman ASE that was initially co-propagating with the pump pulses being Rayleigh backscattered into the counter-propagating direction, i.e., in the signal direction. Therefore the measured counter-propagating Raman ASE initially experienced the co-propagating gain before being backscattered and experiencing the counter-propagating gain. This resulted in noise figure values between 20 and 30 dB at the maximum gain for all fibre lengths and pump duty cycles. For the HNLF, it was shown that there was little difference in the equivalent noise figure values across all seven Stokes orders for the different lengths.

It was also concluded that there was little effect in shortening the fibre length to reduce the Rayleigh backscattered power as any reduction in fibre length resulted in an increase in the required pump power by the same factor. Therefore the only difference in the counter-propagating Raman ASE powers was a result of different counter-propagating on-off gain values between the different fibre lengths. Also from the noise measurements available it appears that the advantage in using a low-NA fibre to reduce the Rayleigh backscattered power and overall noise power is limited. This was verified by repeating the counter-propagating Raman ASE power measurements for different lengths of Freelight™ DSF. The Freelight™ DSF with a lower NA has a lower recapture fraction of the Rayleigh backscattered light which for a given input pump power would result in a lower amount of backscattered power than in the HNLF. However, the lower NA is a result of a lower doping concentration of germanium which

in a RFA typically leads to a lower Raman fibre gain efficiency. This is then met with a higher pump power requirement, a longer fibre length or a trade-off between both. This trade-off results in more Rayleigh backscattered power. The Raman fibre gain coefficient of the Freelight™ DSF is approximately 8.6 times lower than that of the HNLF. Therefore, for the same effective length, 8.6 times more pump power is required and vice-versa. This effectively cancelled out the 9.6 times lower RBS coefficient and consequently the counter-propagating Raman ASE powers and noise figure values for the Freelight™ DSF and HNLF were similar, if the fibre lengths are chosen to yield the maximum length for the same pump power. However, for a given gain level, the noise level can be decreased substantially by using a higher duty cycle.

Finally, an initial assessment of the pulse-pumped single-channel cascaded RFA was carried out in terms of the gain saturation properties. Measurements of the gain saturation due to an increase in the input signal power at the 1^{st}, 2^{nd} and 7^{th} Stokes orders were taken at various pump duty cycles and fibre lengths for the HNLF. It is still possible that limitations in the high power signal lasers and the measurement set-up affected the results in some instances. However, some interesting observations were possible. In the counter-pumped pulsed cascaded RFA, the amplified signal grows enough to deplete the pump and saturate the gain but does not reach a high enough power to generate further SRS on its own. As mentioned earlier, in the pulse-pumped RFA the rate of Raman conversion is determined by the peak power of the pump pulses. The average power of the pump pulses is therefore always lower than the peak power. In a counter-pumping configuration the pump power is exhausted in the amplifier as the signal power approaches the average power of the pulsed pump source and not the peak power. Therefore, even though the gain has saturated due to a lack of pump photons, the average power of the amplified signal can still be well below the peak power that is required for further SRS. However this depends on the duty cycle of the signal and pump.

For the saturation output powers, the pump power is the most important parameter. With the counter-pumping configuration used here, it is the average pump power that is important as opposed to the peak power in a co-pumping configuration. Moreover, since the pump power requirement in an RFA is dependent on the fibre length and the Raman fibre gain coefficient so is the saturated output power. It was shown that when using a shorter length of the HNLF for the cascaded RFA which required more pump power, the saturated output powers also increased. Counter-

propagating saturation output power measurements were given for 20%, 40% and 60% pump duty cycles and HNLF lengths of 2 and 6 km. In terms of the absolute maximum values for the saturated output powers, a pulse-pumped counter-propagating cascaded RFA computer model is required to investigate this. Unfortunately, only a CW pumped co-propagating cascaded RFA was available during the time this work was carried out. Some simulated data from the CW pumped cascaded RFA model were reported which showed that the saturated output powers increased as the Stokes order increased. This was explained by a shortening of the effective interaction length for higher Stokes orders. As the Raman cascade moves to higher Stokes orders, increasing amounts of the fibre are used to generate earlier Stokes orders. However, as already mentioned, different mechanisms can affect the way the gain saturates for a co-pumped and counter-pumped RFA and further investigations are required.

4.5 References

[1] P. J. Winzer, J. Bromage, L. E. Nelson, M. D. Mermelstein, C. Horn, and C. H. Headley, "Repetition rate requirements for time-division multiplexed Raman pumping," J. Lightwave Technol. **22**(2), 401-408 (2004).

[2] J. Bromage, "Raman amplification for fiber communications systems," J. Lightwave Technol. **22**(1), 79-93 (2004).

[3] D. M. Baney, P. Gallion, and R. S. Tucker, "Theory and measurement techniques for the noise figure of optical amplifiers," Opt. Fiber Technol. **6**, 122-154 (2000).

[4] R. G. Smith, "Optical power handling capacity of low loss optical fibers as determined by stimulated Raman and Brillouin scattering," Appl. Opt. **11**(11), 2489-2494 (1972).

[5] C. Headley and G. P. Agrawal, *Raman amplification in fiber optical communications systems, Ch. 5.3.1.1* (Elsevier Academic Press, 2005).

[6] K. K. Chen, S. U. Alam, P. Horak, C. A. Codemard, A. Malinowski, and D. J. Richardson, "Excitation of individual Raman Stokes lines in the visible regime using rectangular-shaped nanosecond optical pulses at 530 nm," Opt. Lett. **35**(14), 2433-2435 (2010).

[7] G. P. Agrawal, *Fiber-Optic Communications Systems, 3rd Ed. Ch. 6* (John Wiley & Sons, Inc., New York, 2002).

[8] Y. Aoki, "Properties of fiber Raman amplifiers and their applicability to digital optical communication systems," J. Lightwave Technol. **6**(7), 1225-1239 (1988).

[9] C. Headley and G. P. Agrawal, *Raman amplification in fiber optical communications systems, Ch. 4* (Elsevier Academic Press, 2005).

[10] P. C. Becker, N. A. Olsson, and J. R. Simpson, *Erbium-Doped Fiber Amplifiers: Fundamentals and Technology* (Academic Press, San Diego, CA, 1999).

[11] H. Wei, Z. Tong, M. Wang, and S. Jian, "Analysis of Raman amplifiers' transient effects and TDM-pumped Raman amplifiers using the finite-difference method," Micro. Opt. Technol. Lett. **41**(5), 407-410 (2004).

[12] C. Yijiang and A. W. Snyder, "Saturation and depletion effect of Raman scattering in optical fibers," J. Lightwave Technol. **7**(7), 1109-1117 (1989).

Chapter 5 – Spectral gain control using shaped pump pulses

The previous chapter showed it is possible to get Raman gain over a wide range of wavelengths through pulse-pumping a cascaded RFA. However, the gain was restricted to a relatively narrow wavelength range at any one time. Some applications call for gain that extends over a wide wavelength range at any given time. Thus, in this chapter the focus shifts to pulse-shaping and a pulse-pumped cascaded RFA targeting gain across multiple Stokes orders by way of shaped pump pulses. Pulse shaping offers a way of extending the Raman gain bandwidth, albeit at the expense of the maximum gain. Experimental results using a single pump wavelength are presented and discussed for the cascaded RFA, again using different fibre types, along with some first results on the saturation characteristics.

5.1 Introduction

The Raman gain spectrum produced from pumping a Raman fibre with step-shaped optical pulses consisting of multiple levels is experimentally investigated. Such a pulse profile contains sections with different instantaneous powers. By adjusting the height (i.e., instantaneous power) of each step appropriately, different parts of the pulse transfer their power to different Stokes orders leading to a controllable gain spectrum covering multiple Stokes orders. It is believed this could open up opportunities for an ultra-broadband RFA.

From chapter 3 and figure 5.1, which shows how the gain at different Stokes orders depends on pump power, it can be seen that it is already possible to generate equal gain at two Stokes orders with a single pump source, either CW or pulsed by simply balancing the amount of power that is launched into the amplifier. In fact it is also possible to generate gain across three Stokes orders, although the distribution of gain across the three Stokes orders is uneven. However this pumping scheme offers limited control and it is only possible to generate equal gain at more than two Stokes orders with this scheme if two or more pump wavelengths are used.

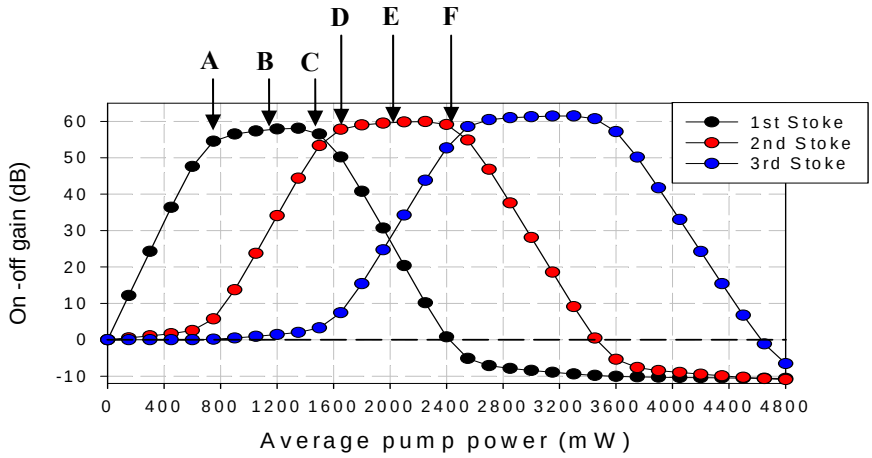

Figure 5.1 Example showing the on-off gain across three Stokes orders.

A more controlled pumping scheme uses pulse shaping to control the instantaneous power across the profile of the pulse. The instantaneous power ultimately determines the number of conversion steps in the cascade and therefore the spectral location of the gain. The Raman gain can be tailored by creating pulse trains with varying instantaneous powers. Figure 5.2 (a), (b) and (c) shows three examples of pump pulses with varying instantaneous powers that could be used for generating gain across multiple Stokes orders in a controlled fashion. The instantaneous powers in these examples are set for generating gain across two Stokes orders using the 2 km HNLF, although they could be set to generate gain across more Stokes orders. Figure 5.2 (d), (e) and (f) shows the pulse profiles at the pump, 1st Stokes and 2nd Stokes wavelengths after propagation through the 2 km HNLF. Following the same principle as the rectangular pulse used in chapter 3, the step-shaped pulse (figure 5.2 (a)) is the most flexible format for converting power into multiple Stokes orders, and most efficient when gain at non-adjacent Stokes orders is required [1]. Due to the flat-top regions within the step-shaped pulse, different segments of the pump pulse can be cleanly transferred to the targeted Stokes orders by appropriately setting the heights of each step. This is not possible with the triangle pulse shown in figure 5.2 (b) where part of the pulse is left at the pump wavelength due to its low instantaneous power. In principle the pulse shape shown in 5.2 (c), which also uses an increasing gradient profile like the triangle pulse, could also be used to increase the transfer efficiency. Here the minimum instantaneous power has been raised from zero to the height needed for conversion to the 1st Stokes order. This results in very little power being left at the pump wavelength. Such a pulse may be easier to generate than the stepped pulse, but it is less flexible. In

terms of gain, there may be subtle difference when walk-off is significant, and the noise properties are likely to be different. However the details have yet to be investigated. Furthermore, this pulse profile is less efficient for transferring power to non-neighbouring Stokes orders, i.e., 1st and 3rd order.

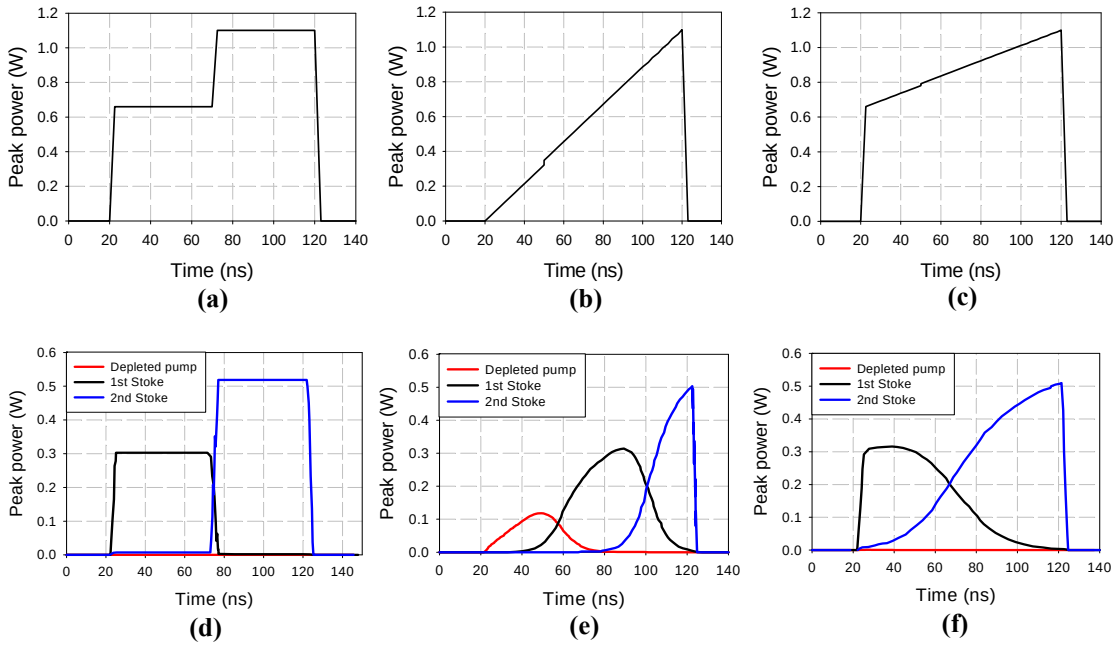

Figure 5.2 Example showing three pump pulse shapes ((a), (b) and (c)) for generating gain across two Stokes orders and using simulations, the resulting pulse shapes of the 1st and 2nd Stokes after propagation through the 2 km HNLF ((d), (e) and (f)).

In the case of targeting gain across multiple Stokes orders, there are many contributions to the overall gain spectrum. An accurate prediction of the overall gain spectrum generally requires computer simulations taking into account the full Raman gain spectrum but an intuitive idea of the amount of gain can still be obtained by looking further at figure 5.1. This can be done by taking the step-shape pump pulse in figure 5.2 (a) as an example. Although this is a single pulse with a single pump wavelength, the two steps can be considered as two separate pump sources. The first pump, which consists of the step with the lower-level, targets gain directly at the 1st Stokes order while the second pump, which consists of the step with the higher-level, targets gain directly at the 2nd Stokes order. However, in a cascaded RFA each of these pumps can also provide further gain to the neighbouring Stokes orders of the one it is targeting directly. The amount of this secondary contribution to the gain at neighbouring Stokes orders varies depending on power, which can be seen by looking at figures 5.1 and 5.3.

Figure 5.3 shows the simulated Raman gain spectra, using the CW pumped cascaded RFA model, of the 2 km HNLF at different pump powers which are also highlighted A, B and C in figure 5.1. The black curve in figure 5.3 represents a pump power of 0.7 W and corresponds to point A in figure 5.1. At this point the gain at the 1st Stokes order is close to maximum whereas the gain at the 2nd Stokes order is relatively small. This point roughly marks the onset of pump depletion. Beyond this, the red and blue curves which correspond to points B and C show that over the region from 0.7 – 1.5 W the gain at the 1st Stokes order remains relatively similar but the gain at the 2nd Stokes order increases rapidly. For these pump powers, i.e., across the plateau of high 1st-Stokes gain, the contribution to the 2nd Stokes order can lie anywhere in the range of ~10-90% of the gain generated directly at 1st Stokes order. In a cascaded RFA targeting gain across multiple Stokes order the amount of secondary gain generated at the 2nd Stokes order is an important consideration in obtaining a flat Raman gain spectrum.

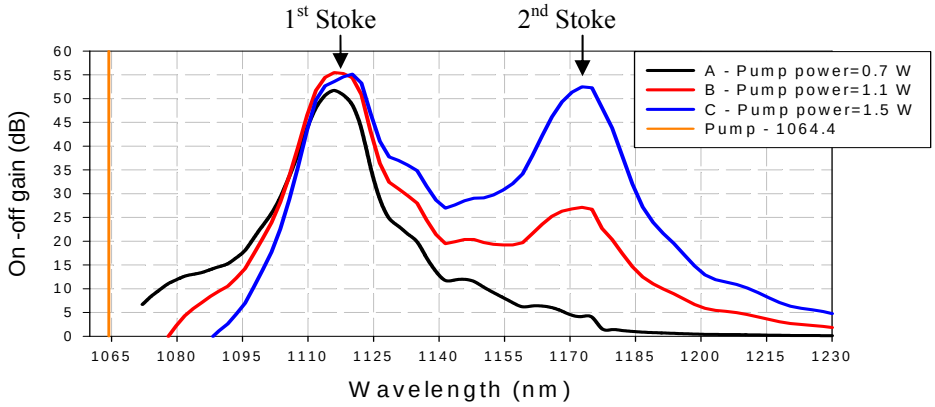

Figure 5.3 Raman gain spectra across the 1st and 2nd Stokes orders for different input pump powers into the 2 km HNLF.

We now look at the second pump, i.e., the section of the pulse with the higher level which is targeting gain primarily at the 2nd Stokes order. Figure 5.4 shows the Raman gain spectra of the 2 km HNLF at various pump powers which are also highlighted D, E and F in figure 5.1. It can be seen that across the range of powers from 1.65 – 2.45 W, the gain at the 2nd Stokes is much the same. However, there is also gain generated for the neighbouring Stokes orders which varies significantly depending on the pump power. The amount of gain in the neighbouring Stokes orders can vary (in a

"see-saw effect") between ~10-90% of the gain generated at the 2nd Stokes order for pump powers across the plateau of high 2nd-Stokes gain.

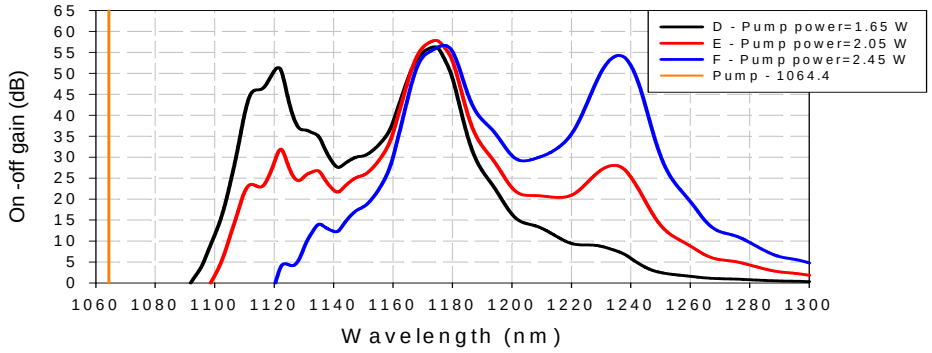

Figure 5.4 Raman gain spectrum across the 1st, 2nd and 3rd Stokes orders for different input pump powers into the 2 km HNLF.

While the shape of the gain spectrum and the level of gain at individual Stokes orders clearly can be controlled by the parameters of the pump pulse, there are still important restrictions on the possible gain spectra. If we look at the Raman gain spectra as the pump power is increased and higher Stokes orders are generated then it can be seen that the spectral gain integral (i.e., the area under the Raman gain profile) remains relatively constant. This can be seen in figure 5.5 which displays the Raman gain spectra generated with seven different pump power levels using a pump wavelength of 1064 nm and the 2 km HNLF.

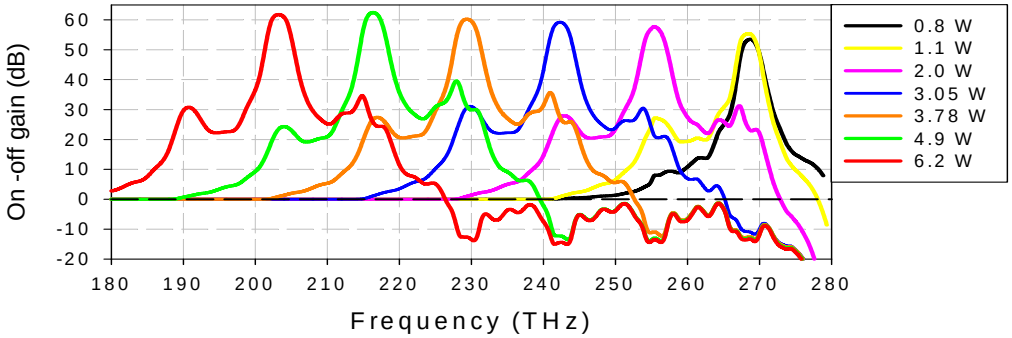

Figure 5.5 Simulated Raman gain spectra generated with seven different CW pump power levels in a 2 km long HNLF. Note that the 1st Stokes order is to the right, since a frequency scale is used.

Figure 5.6 shows the results for the spectral integration of the Raman gain spectra generated at various input pump powers. Integrating the Raman gain spectra shows that the spectral integral initially rises with pump power since the Raman gain at

the 1st Stokes order increases with pump power. Once the pump power becomes high enough to generate higher Stokes orders (i.e., between 1 W and 2 W), the spectral integral curve starts to level off as the gain is then shifted between Stokes orders rather than constantly increasing. Integrating over the full bandwidth from 180 to 280 THz (i.e., 1070 to 1700 nm) the spectral integral then starts to fall off with increasing pump power. This is due to the residual gain at lower Stokes orders becoming negative as the high pump power shifts the gain to higher Stokes orders (see figure 5.1 and the red curve in figure 5.5.) However, figure 5.6 also shows that by just integrating over the regions of positive gain, the spectral integral levels off. Therefore, for pump powers sufficiently high for cascaded Raman generation, simulations show that the spectral integral over the region with positive gain is approximately equal to 1.1×10^{15} dB Hz for a CW pump, over the parameter range I studied. Thus, in this regime, a continued increase of the pump power shifts the Raman gain rather than increasing it, insofar as the spectral bandwidth remains the same, and the spectral integral is limited to $\sim1.1\times10^{15}$ dB Hz $\times$ d. Here, we take the pump duty cycle d into account, since the Raman gain scales by this in case of counter-propagating pulse-pumping.

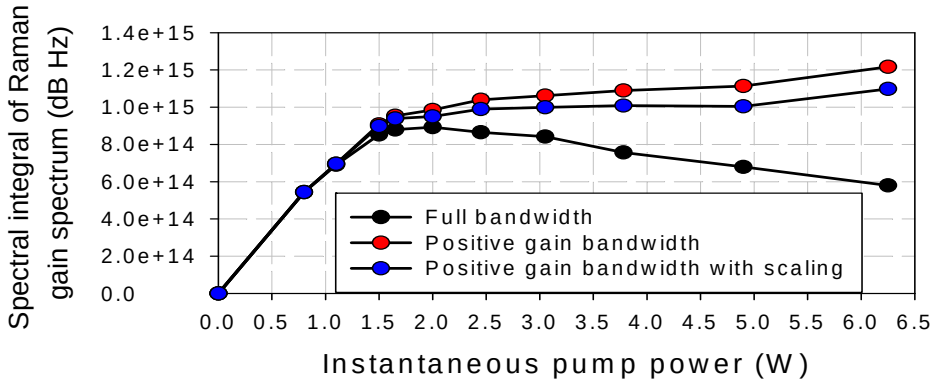

Figure 5.6 Spectral integrals of Raman gain spectrums *vs*. instantaneous pump power for CW pumped cascaded SRS in the 2 km HNLF.

In fact, if the differences in maximum on-off gain between the Stokes orders are taken into account, the spectral integral turns out to be even flatter over the region of higher pump powers. Using the CW pumped cascaded RFA model, the on-off gain increases from ~55.5 dB at the 1st Stokes order up to ~62 dB at the 6th Stokes order. The higher maximum on-off gain at higher Stokes orders will produce a greater area underneath the Raman gain spectra, thus increasing the spectral integrals. The blue data points in figure 5.6 represent the spectral integrals over the region with positive gain

whereby the maximum on-off gain for all Stokes orders has been scaled down to equal that of the 1st Stokes order.

The spectral integral value of ~1.1×10^{15} dB Hz × d offers a way of estimating the gain – bandwidth product of a multi-level pulse-pumped cascaded RFA. For instance, the spectral integral suggests that a maximum gain of ~11 dB could be possible over a bandwidth of 100 THz (i.e., 180 to 280 THz or 1070 to 1700 nm.) It should be noted that this excludes the smaller negative gain contributions that can occur at lower Stokes orders. Furthermore, it assumes that the full 100% pump duty cycle is employed and a reasonably flat Raman gain spectrum spanning 100 THz is possible.

The effect on the gain spectrum of different power levels for each step is illustrated in figure 5.7. Even though the gain spectra in figure 5.3 and 5.4 are for a CW pumped co-propagating pulse-pumped cascaded RFA, the counter-propagating gain can again be calculated by multiplying the CW gain spectra by the duty cycles of their respective pump pulse sections. Then for the dual-level pump pulse the Raman gain spectra in figures 5.3 and 5.4 can be added together to obtain the composite Raman gain spectrum. It should be noted that even when the direct (i.e., primary) contribution to the gain is the same the secondary contribution can result in quite different gain spectra.

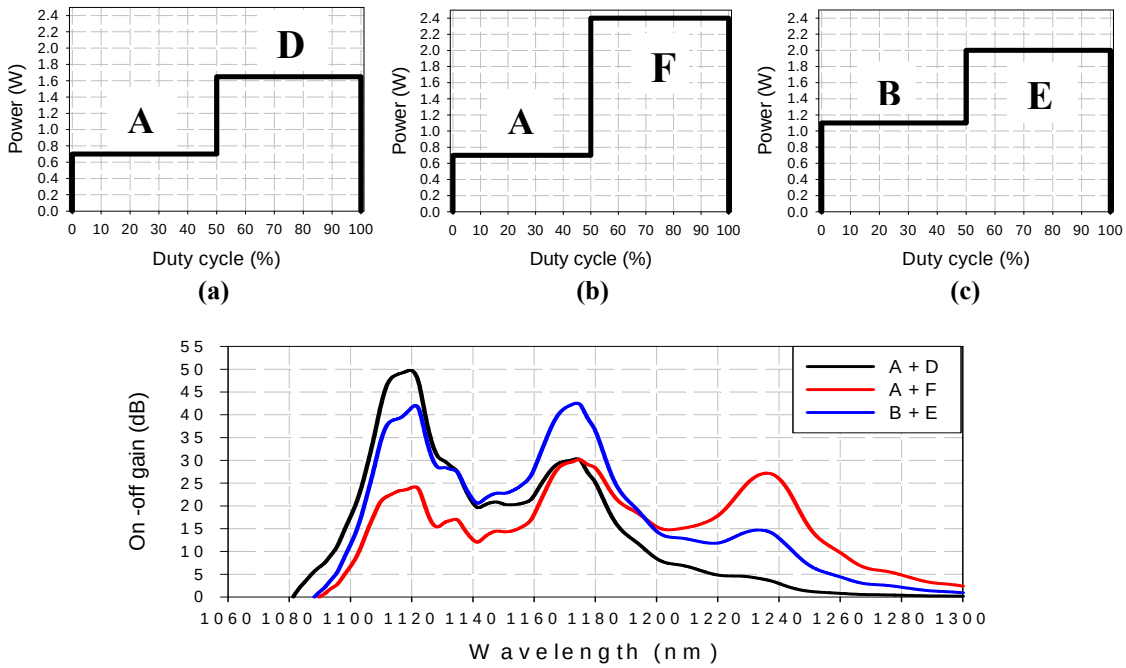

Figure 5.7 Pump pulse profiles and simulated resultant Raman gain spectra after propagation through the 2 km HNLF, (a) Dual-level pulse with height ratio 0.42:1, (b) Dual-level pulse with height ratio 0.29:1 and (c) Dual-level pulse with height ratio 0.55:1.

Further modifications to the overall gain spectrum are also possible by increasing the number of steps in the pump pulse. It is worth noting that there is also a negative contribution to the total gain spectrum which only impacts the outcome when targeting gain across three or more Stokes orders (see figure 5.1). Any section of the pulse which targets gain at the 3rd Stokes order will also generate some nonlinear absorption at the 1st Stokes orders and if the 4th Stokes order is targeted there will be some absorption at the 1st and 2nd Stokes order and so on.

Finally it is worth pointing out that there is a small contribution that is always present, even in the un-depleted pump regime due to the broad bandwidth nature of the Raman gain coefficient spectra. As shown in figure 5.8 the section of the pump pulse which generates gain for the 1st Stokes order will also generate a small amount of gain for the 2nd Stokes order since the tail of the Raman gain coefficient spectrum extends into its wavelength range. This would then be added to the gain generated by the section of the pump pulse which targets gain directly at the 2nd Stokes order. This extra component of gain depends on the Raman gain spectrum but is always present and can range from 4-7% of the maximum gain for the silica-based fibres under test in this report. This is shown in terms of gain by the black curve in figure 5.3 (i.e., pump power = 0.7 W). However, beyond this pump power level and into the pump depletion regime the 1st Stokes order starts to pump the 2nd Stokes order and the gain spectra change as shown by the red and blue curves in figure 5.3.

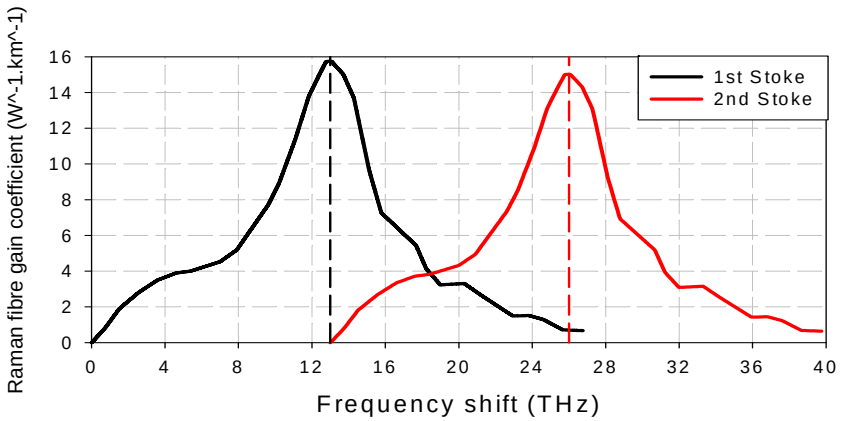

Figure 5.8 Graph showing the overlap of the Raman fibre gain coefficient spectra between neighbouring Stokes orders for the HNLF.

It can be seen that there are many contributions to the overall gain spectrum in a cascaded RFA generating gain over multiple Stokes orders but control and optimization over this gain spectrum can be achieved by modifying the instantaneous power and duty

cycle of each section of the step-shaped pump pulse, as well as managing the number of steps in the pump pulse. Furthermore, by treating each section of the pump pulse as a separate pump source, a co-propagating CW model can be used to calculate the resulting overall counter-propagating Raman gain spectrum.

5.2 Experimental measurements

This section details my experimental measurements on the Raman gain spectra produced from pumping a Raman fibre with step-shaped optical pulses consisting of multiple levels. The same pulsed Yb MOPA source described in chapter 3 is still used here. Figure 5.9 shows the Raman gain spectra produced from the 2 km HNLF using dual-level pumping with various duty cycles. With dual-level pumping, gain across two Stokes orders is targeted. Curve A corresponds to a pump pulse with a total duty cycle of 20% (so 10% for each level). Curve B corresponds to a pump pulse with a total duty cycle of 50% (25% for each level). Curve C corresponds to a pump pulse with a total duty cycle of 100%, i.e., 50% for each level.

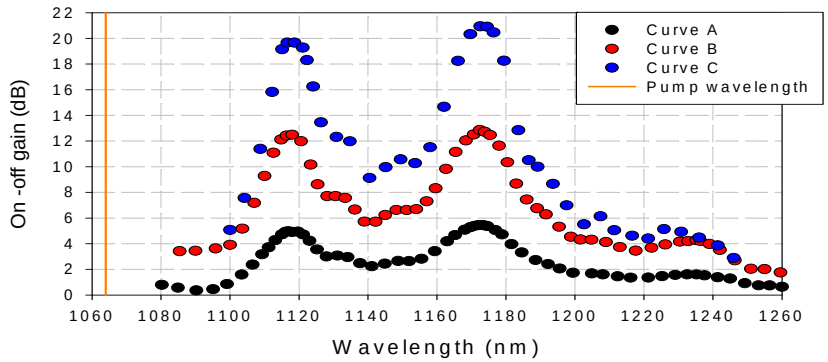

Figure 5.9 Raman gain spectra across two Stokes orders produced from dual-level pumping the 2 km HNLF. Curve A: 20% total duty cycle, 10% for each level. Curve B: 50% total duty cycle, 25% for each level. Curve C: 100% total duty cycle, 50% for each level.

The pump pulse profiles are shown in figure 5.10. For all the pulses each section corresponds to a different instantaneous power, resulting in different amounts of Raman conversion. The levels are adjusted so that the power of the lower-level section of the pulse is enough to supply gain at the 1st Stokes order and the power of the higher-level section is enough to supply gain at the 2nd Stokes order. The power levels of the pump pulses were adjusted so that all sections operated in the pump depletion regime similar

to curve B+E in figure 5.7 and were therefore close to being fully converted to their targeted Stokes orders.

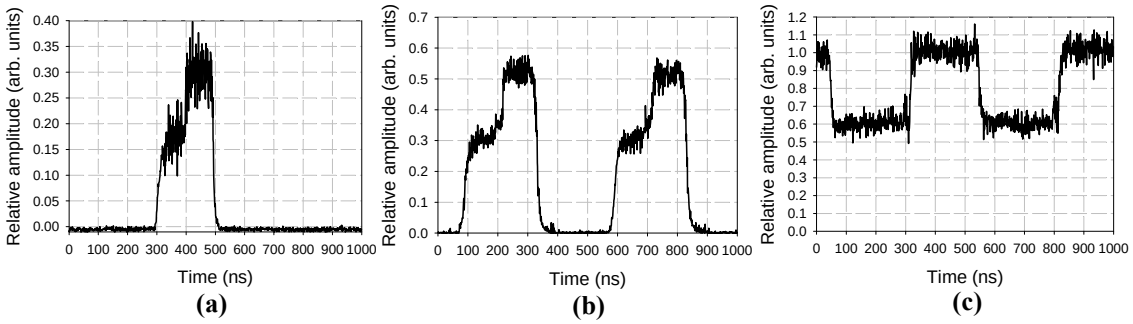

Figure 5.10 Pump pulse profiles, (a) total duty cycle of 20% and 10% for each level, (b) total duty cycle of 50% and 25% for each level, (c) total duty cycle of 100% and 50% for each level.

Figure 5.11 shows an example of this using the step-shaped pump pulses with a total duty cycle of 50%, i.e., 25% for each step. Plot (a) shows the initial pump pulse, whereas plots (b) and (c) show the resultant pulse profiles after Raman conversion at the 1st and 2nd Stokes orders, respectively. With this amount of conversion it can be seen from curve B in figure 5.7 that the resultant peak gain at the 1st and 2nd Stokes orders is 12.5 dB and 12.9 dB. The total average input power for this gain was 502 mW. From figure 3.18 in chapter 3, the direct contribution to the 1st and 2nd Stokes order gain for a 25% duty cycle pulse and the 2 km HNLF is ~8.7 dB. Therefore in this instance there is also a ~4 dB secondary contribution to the gain of each Stokes order as explained earlier. This was also confirmed by measuring the on-off gain in the 2 km long HNLF for approximately 3rd-order super-Gaussian pump pulses (i.e., single-step) with a 25% duty cycle and the same instantaneous powers as each step of the dual-level pump pulses.

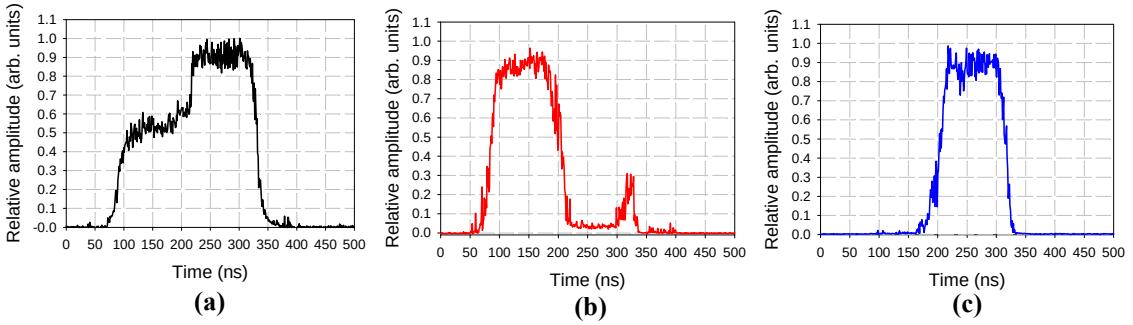

Figure 5.11 Pulse profiles (a) Initial temporal profile of pump pulse, (b) Temporal profile of co-propagating 1st-Stokes power after propagation through 2 km of HNLF (c) Same as (b) but for 2nd Stokes order.

Figure 5.12 shows the resulting on-off gain for the 1st and 2nd Stokes orders. The height ratio of the dual-level pump pulse in figure 5.11 (a) is approximately 0.55:1. Therefore from the total input pump power of 502 mW, the average input pump power for first and second section of the pump pulse is estimated to be 178 mW and 324 mW. These power levels have been highlighted on figure 5.12. The single-step super-Gaussian pump pulse with a 25% duty cycle and peak power of 178 mW generates 8.6 dB of on-off gain at the 1st Stokes order and 4.1 dB of on-off gain at the 2nd Stokes orders. Likewise, the same pump pulse with a 25% duty cycle and peak power of 324 mW generates 8.83 dB of on-off gain at the 2nd Stokes order and 4.3 dB of on-off gain at the 1st Stokes orders. This gives a total on-off gain of 12.9 dB at the 1st Stokes order and 12.93 dB at the 2nd Stokes order. These results are in good agreement with those shown by curve B in figure 5.9. Also the net gain can be calculated by simply subtracting the background loss from the on-off gain.

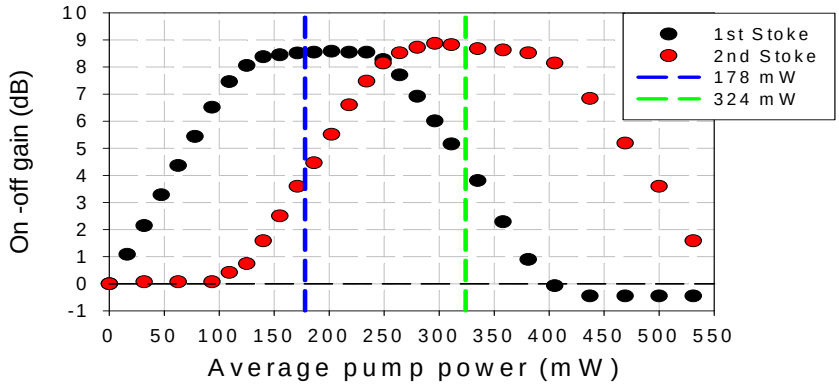

Figure 5.12 On-off gain *vs*. average pump power for the 2 km HNLF using approximately 3rd-order super-Gaussian pump pulses with a 25% duty cycle.

Furthermore, the gain can also be pushed out to the 2nd and 3rd Stokes orders by increasing the average pump power and slightly modifying the relative step height of the 1st level. Figure 5.13 shows the gain spectrum produced from the 2 km HNLF using the step-shaped pump pulse with a total duty cycle of 50% with 25% for each step. The total average pump power to push the gain out to the 2nd and 3rd Stokes order was 797 mW. The pump powers values are all in agreement with the expected values based on the results for the single-step super-Gaussian pulses used in chapter 3. The peak on-off gain at the 2nd and 3rd Stokes orders was 11.5 dB and 12.3 dB, respectively.

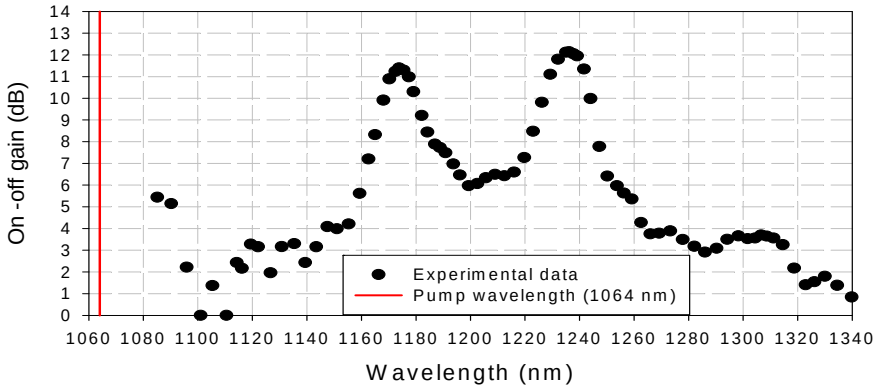

Figure 5.13 Raman gain spectrum across two Stokes orders (2nd and 3rd order) produced from dual-level pumping the 2 km HNLF with a total duty cycle of 50% with 25% for each level.

Another interesting aspect of these gain spectra is how the bandwidth compares between different fibre types and in particular different Ge concentrations. Figure 5.14 shows the normalised Raman gain coefficient spectra for the HNLF, Freelight™ DSF and the SMF-28. As discussed in chapter 3 the increasing amount of Ge results in the double peak structure of pure silica disappearing into a single peak at a slightly lower frequency shift. Furthermore, it also results in a narrowing of the main peak in the Raman gain coefficient spectra [2]. Therefore it may be expected that a lower Ge content fibre like SMF-28 would perform better than the HNLF in terms of gain bandwidth.

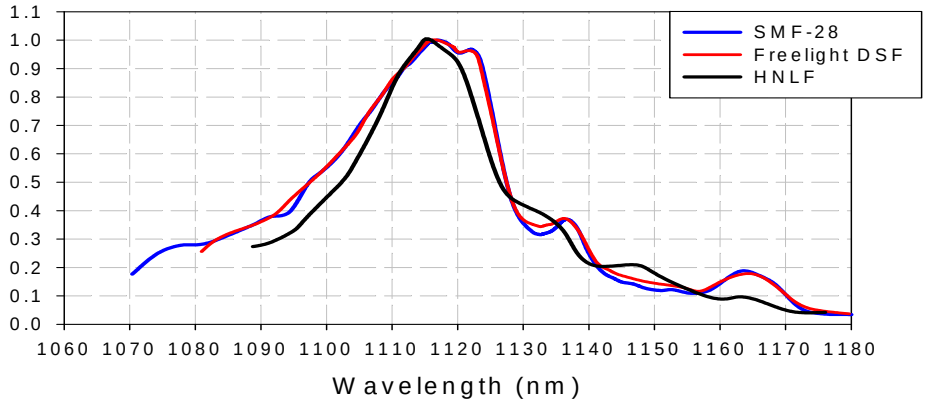

Figure 5.14 Scaled Raman gain coefficient spectra for SMF-28, Freelight™ DSF and HNLF at a pump wavelength of 1064 nm.

This was put to the test by comparing all three fibre types when dual-level pumping was employed to provide similar on-off gain values for both the 1st and 2nd Stokes orders for all fibres. Figure 5.15 shows the resulting experimentally measured

gain spectra. It can be seen that the bandwidth is indeed wider for the 2nd Stokes order with the lower Ge content fibres. However this is not the case at the 1st Stokes order where in fact the SMF-28 bandwidth is narrower.

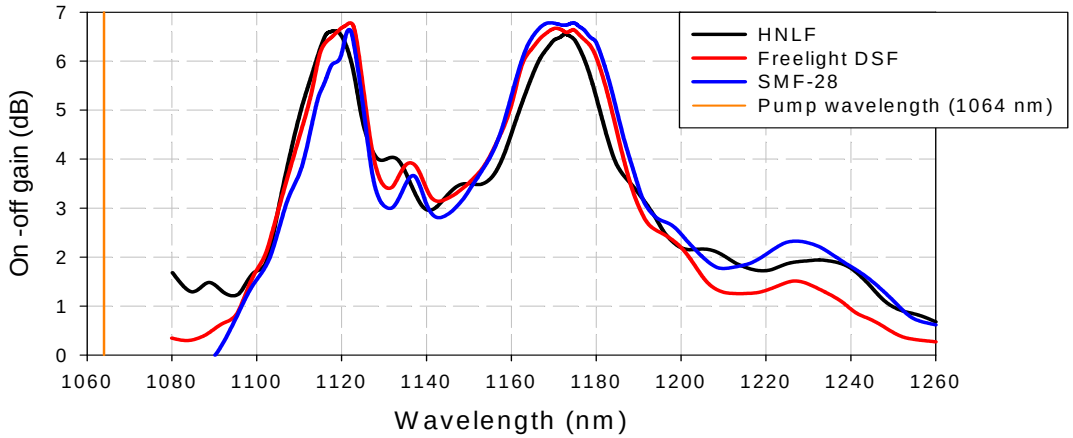

Figure 5.15 Bandwidth comparison between the Raman gain spectra produced with three different types of Raman fibres using dual-level pulse-pumping.

This is due to the double peak structure in the Raman gain spectrum of pure silica. This can be seen in figure 2.9 of chapter 2 where is was also shown that the second peak disappears as the Ge content increases until the Raman gain spectrum becomes a single peak structure for high Ge content fibres such as the HNLF. With the double peak structure, as the pump power increases the peak on the short wavelength side starts to pump the peak on the long wavelength side [3]. This is shown in figure 5.16 using computer simulations. At low pump power levels the Raman gain spectrum increases without any interactions within the Raman gain spectrum. However once the pump depletion regime is reached, internal pumping within the Raman gain spectrum occurs resulting in a narrower gain bandwidth and the peak on the long wavelength side becoming stronger. This effect is worst for pure-silica fibres but reduces for fibres with increasing Ge concentration. This is why the effect is worse in SMF-28 than in Freelight™ DSF and HNLF. Although the normalised Raman gain spectra look similar for the SMF-28 and Freelight™ DSF, this is probably due to limitations in resolution of the measurement technique. In terms of the experimental result it may be possible to reduce the instantaneous power of the section of the pump pulse generating gain directly at the 1st Stokes order. Although this was not attempted in the experimental work, operating this section of the pump pulse in the un-depleted regime could increase the gain bandwidth, albeit with a reduction in maximum gain by

at least ~10%. However a larger duty cycle can compensate for this. It is also worth noting that the secondary contribution of gain to the 1st Stokes order from the section of pump pulse targeting gain at the 2nd Stokes order may well narrow the 1st-order gain bandwidth.

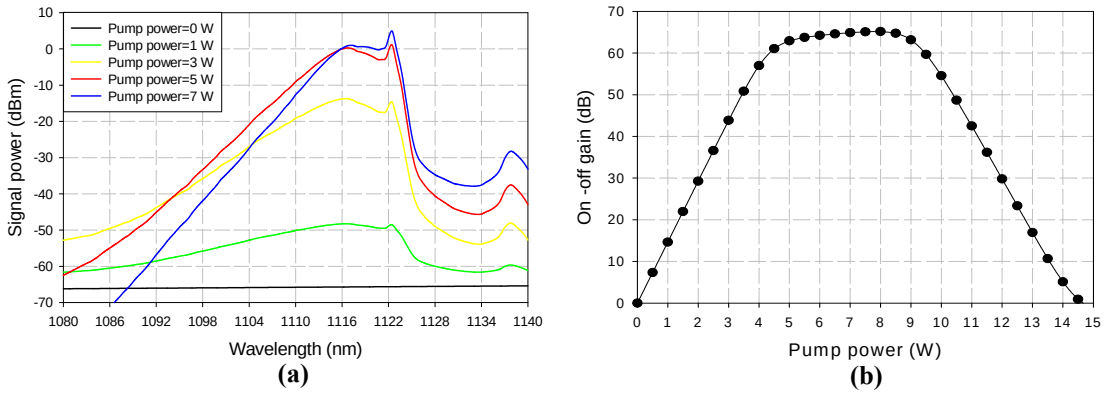

Figure 5.16 (a) Dependence of the 1st Stokes order Raman gain spectrum with pump power and (b) corresponding on-off gain *vs*. pump power curve.

As well as generating gain across two Stokes orders, gain across three Stokes orders with multi-level pumping was also investigated. In this case a negative contribution to the gain and further additional secondary contributions also need to be taken into consideration. Figure 5.17 shows a three-level step-shaped pump pulse and the resulting Raman gain spectrum. The pump pulse has a total duty cycle of 75% with each step having a ~25% duty cycle. The average pump power and the instantaneous power of each level were set so that each section of the pump pulse was close to being completely converted to its targeted Stokes order. For close to full conversion to each Stokes order the total average pump power was 990 mW and the ratio of each level was 0.34:0.65:1. The resulting Raman gain spectrum is unbalanced in terms of the on-off gain across the three Stokes orders with the 1st Stoke approximately 4 dB down on the 2nd and 3rd Stokes. As mentioned earlier, to get a more even gain distribution across all three Stokes orders the individual duty cycles of each level can be modified to compensate against the secondary contributions to the overall gain spectrum. Since the 2nd Stoke order gain now receives secondary contributions from both sections of the pump pulse directly targeting gain at the 1st and 3rd Stokes orders, the duty cycle of the 2nd level was reduced to counteract this. The gain spectrum could also be modified by

changing the heights of the individual levels and operating some sections of the pump pulse in the un-depleted regime.

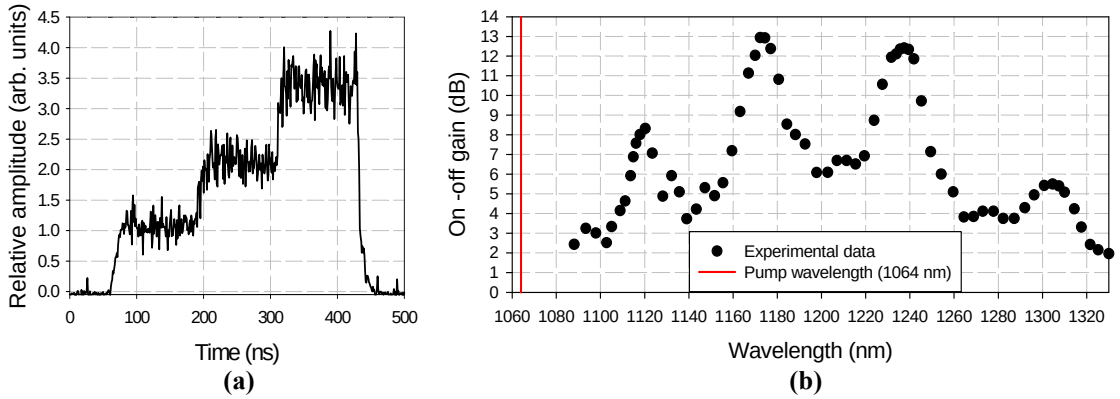

Figure 5.17 Multi-level pulse pumping of the 2 km HNLF, (a) Input pump pulse with three levels, each having a 25% duty cycle and (b) Resulting Raman gain spectrum.

Figure 5.18 shows the multi-level pump pulse with three steps used to generate a gain spectrum with an approximately equal maximum on-off gain across all three Stokes orders. Furthermore it also shows the sections of the pump pulse which are transferred to the three Stokes orders. In this example the pump pulse has a total duty cycle of 47% (see figure 5.18 (a) but the individual duty cycles of each level are no longer equal. The first level has a duty cycle of ~22%, the second level has a duty cycle of ~7% and the third level has a duty cycle of ~18%. The height ratio of the individual steps was kept the same as before at 0.34:0.65:1 so that the instantaneous power of each section corresponded to that require for close to full conversion to its respective Stokes order. The total average power required was 590 mW. Figures 5.18 (b), (c) and (d) show the sections of the pump pulse which were transferred to the 1st, 2nd and 3rd Stokes orders, respectively. This was done by separating the different wavelengths of the Stokes orders using a monochromator. The different duty cycles of each Stokes order and therefore the different primary contribution to the gain spectrum can be clearly seen. The average peak on-off gain across all three Stokes orders is approximately 7.9 dB. This could be increased by simply doubling the individual duty cycles to double the gain.

These results show that it is possible to use shaped pump pulses with multiple levels to generate gain simultaneously across multiple Stokes orders with a high degree of control. The gain spectrum can be modified and adjusted by changing the duty cycle

or the instantaneous power through either changing the height of each level or the average pump power.

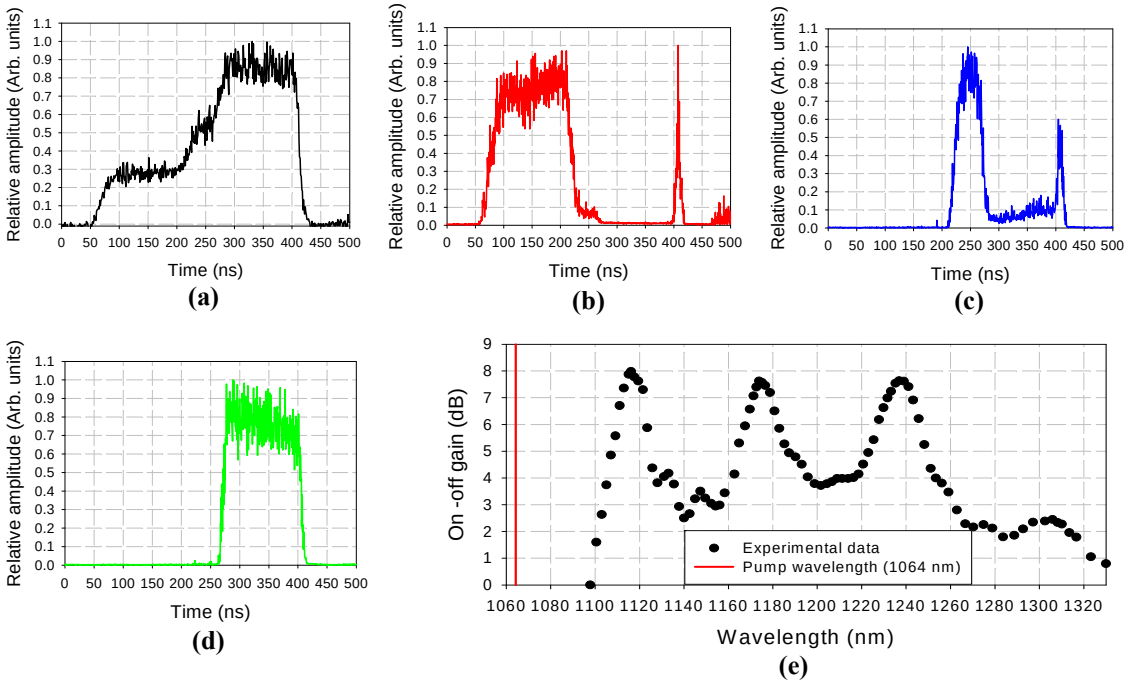

Figure 5.18 Multi-level pulse pumping of the 2 km HNLF showing temporal traces and gain spectrum, (a) Input pump pulse with three levels with a total duty cycle of 47%, (b) Output pulse at the 1st Stokes order, (c) Output pulse at the 2nd Stokes order, (d) Output pulse at the 3rd Stokes order and (e) Resulting Raman gain spectrum.

However it is not possible to realise a continuous gain spectrum across multiple Stokes orders with a single pump wavelength. There will always be gaps between neighbouring Stokes orders due to the intrinsic characteristics of the silica Raman gain. The spectral location of gain for each Stokes order is determined from the location of the peak gain at the previous Stokes order, which is ultimately determined from the wavelength of the initial pump source. However, shifting the pump wavelength can change the spectral location of the Raman gain and so the use of multiple pump wavelengths could be employed to fill in the gaps of lower gain between the peaks of neighbouring Stokes orders.

5.3 Gain saturation and Raman ASE properties

When targeting gain across multiple Stokes orders through the use of shaped pump pulses, a high signal power at one of the Stokes orders can also influence the gain

at the other Stokes orders since the process is initiated from the same pump source. Furthermore, SRS can transfer power directly between the signal wavelengths [4]. An example using a high-power 1116 nm signal at the 1st Stokes order and two low power signals (i.e., 1 μW) at 1172 nm and 1235 nm corresponding to the 2nd and 3rd Stokes order is shown in figure 5.19. In this example, the measurements were taken for dual-level pumping of the 2 km HNLF. The pump pulse is the same as that shown in figure 5.11, while the unsaturated gain spectrum is shown in figure 5.9 as curve B. Note here that this amplifier did not target gain at 1235 nm, but the secondary gain at this wavelength was still characterised. Figure 5.19 (a) shows how the gain for the low-power signals at 1172 nm and 1235 nm stays the same as the 1116 nm signal power is increased up to a input power level of ~5 dBm. At this point as the 1116 nm input signal power is further increased, the gain at 1116 nm also starts to increase while at 1172 nm and 1235 nm it starts to drop. This can be explained by looking at the pulse profiles after propagation through the fibre at each signal wavelength. Figure 5.19 (b) shows the pulse profiles after propagation through the fibre when the input signal power at 1116 nm was 2.5 mW (4 dBm). Here the sections of the input pump pulse are still cleanly converted to their targeted Stokes orders. However when the input signal power is increased beyond this, the gain starts to change. Figure 5.19 (c) shows the pulse profiles after propagation through the fibre when the input signal power at 1116 nm was 16.6 mW (12.2 dBm). Here the high power signal which propagates in the opposite direction to the pump takes most of the power from the pump which reduces the Raman ASE power which is driving the Raman cascade. The cascade is slowed down so that less power is transferred to the 2nd Stokes order and therefore there is less gain for the 1172 nm signal. This can be seen by noting that the section of the pump pulse that would normally be converted to the 2nd Stokes order (as in figure 5.19 (b)) now resides in the 1st Stokes order, even though the average input pump power remains the same. This results in an increase in gain at the 1st Stokes order and a decrease in gain at the 2nd and 3rd Stokes orders. The drop in gain at the 2nd and 3rd Stokes orders is due to a lower pump power as opposed to self saturation but is influenced by the saturation effect imposed by the high signal power at the 1st Stokes order.

In reality this process is quite complicated with many interactions and primary and secondary contributions to the overall gain at the individual Stokes orders. However this does highlight differences in the saturation effects between the single-level pump pulse (as in chapter 4) and the multi-level pump pulse.

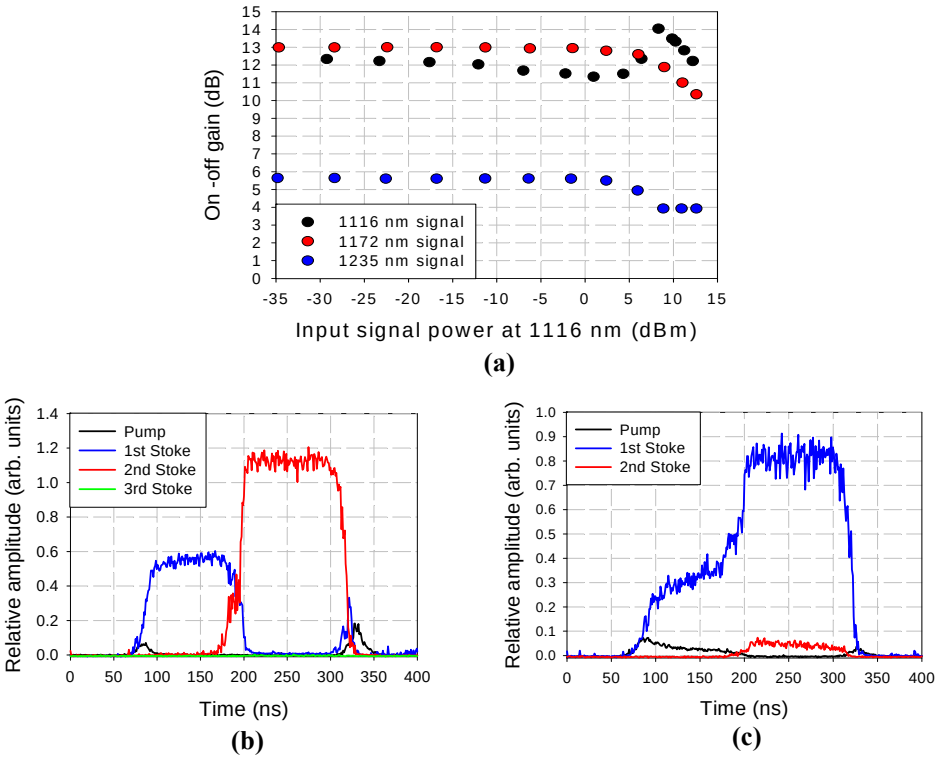

Figure 5.19 Example showing the result of an increasing input signal power at the 1st Stokes order when dual-level pumping the 2 km HNLF, (a) On-off gain for three signal wavelengths versus input signal power at 1116 nm, (b) Temporal pulse profiles after propagation through the fibre with an input signal power of 2.5 mW at 1116 nm and (c) Temporal pulse profiles after propagation through the fibre with an input signal power of 16.6 mW at 1116 nm.

In these measurements direct SRS between signals is small due to the low signal powers. However this can change at higher signal powers, in particular for low signal duty cycles.

As in chapter 4 there is scope for increasing the pump power to replenish the gain at the 2nd Stokes order, which was lost due to the high signal power at the 1st Stokes order. This is shown in figure 5.20 whereby the total average pump power is increased from ~550 mW to ~650 mW for the scenario described previously and presented in figure 5.19 (a) and (c). By increasing the average pump power, the section of the pump pulse with the highest instantaneous power is converted back into the 2nd Stokes order. Beyond this the gain at the 1st Stokes order becomes depleted and higher Stokes orders are generated. Note however that I did not investigate the full parameter space. An interesting question that is beyond the scope of my work is to what extent targeted gains at different Stokes orders can be obtained with different signal power.

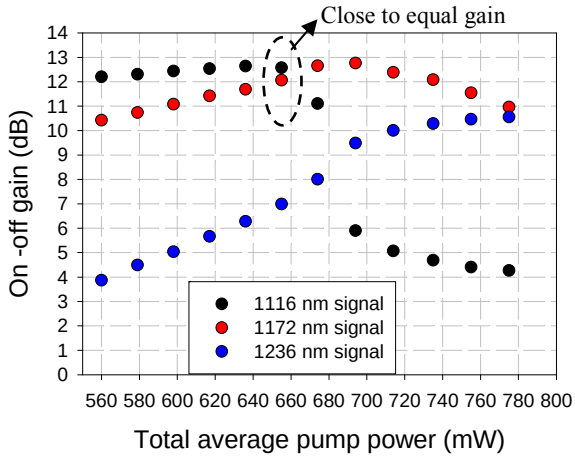

Figure 5.20 On-off gain *vs.* total average pump power for three signal wavelengths at different Stokes orders when pumping the 2 km HNLF with dual-level pulses.

Noise properties with multi-level pumping are very important but a thorough investigation is outside the scope of this thesis. One would expect the noise properties of such a multi-level pulse-pumped cascaded RFA to change depending on the details of the pump pulses. The fact that similar gain spectra can be obtained with different pulse shapes leads to the question how this influences the noise. It was shown in the experimental measurements in chapter 4 how the Raman ASE increased as the instantaneous pump power increased. Furthermore it was shown that with the current experimental set-up the counter-propagating Raman ASE does not deplete when the gain is pushed out towards higher Stokes orders. This means that if a section of a step-shaped pump pulse generates gain at the 3rd Stokes order, then there will always be a significant amount of Raman ASE left behind in the region of the 1st and 2nd Stokes orders. Therefore if a second section of the pump pulse then targets gain at a lower Stokes order than the original pulse, the Raman ASE and therefore the noise figure will be high even if the power level of the second section of the pump pulse is operated in the un-depleted regime (i.e., lower power than that required to reach maximum gain). However it is worth pointing out that even with the current experimental set-up, the section of the pump pulse targeting gain at the final Stokes order can be operated without influence from higher order Stokes and therefore does exhibit some control over the noise properties in terms of the total amount of Raman ASE. Furthermore, it is still possible that the noise properties could be improved with an improved experimental set-up but this requires further investigations. Nevertheless, it seems clear that some

noise penalty will result when the amplifier is operating on several Stokes orders simultaneously.

5.4 Summary

In summary, the Raman gain spectra generated from pumping the HNLF with pulses of varying instantaneous powers (i.e., step-shaped) has been investigated as a means of providing gain over multiple Stokes orders simultaneously. This has been done with a view to extending the gain bandwidth of a standard RFA which typically only targets gain across one Stokes order at any one time. Using simulations, it was shown how the Raman gain spectrum and the spectral integral (i.e., the area under the Raman gain spectrum) changed with instantaneous pump power. The spectral integral offers a way of estimating the gain – bandwidth product of a multi-level pulse-pumped cascaded RFA. For pump powers sufficiently high for cascaded SRS, the spectral integral over the region with positive gain was calculated to be approximately equal to 1.1×10^{15} dB Hz × d, where d is the pump duty cycle. Therefore the spectral integral is limited to 1.1×10^{15} dB Hz for a duty cycle of 100%, which suggests that a maximum gain of ~11 dB could be possible over a bandwidth of 100 THz (i.e., 180 to 280 THz or 1070 to 1700 nm.)

Control over the shape of the pump pulses is achieved by utilising the advantages of the pump source being in a MOPA configuration. Using a single wavelength MOPA pump source, equal gain across two and three Stokes orders was demonstrated experimentally by pumping with two and three step pulses, respectively. Furthermore, comparisons were made between the Raman gain spectra generated from pumping the HNLF and two different fibre types with dual-level pulses. The other two fibres used for comparison had lower amounts of germanium which results in a broader Raman gain coefficient spectrum. However, it was concluded that the lower germanium content fibres did not result in a significantly broader bandwidth for the overall Raman gain profile. Thus, the advantage of a higher Raman fibre gain coefficient for the HNLF outweighed any reduction in the overall bandwidth of the gain spectrum. Therefore the HNLF is an attractive gain medium for generating cascaded Raman gain over multiple Stokes orders. Furthermore, some initial results are also presented into the saturation of a multi-level pulse-pumped cascaded RFA. Noise properties were considered as well,

and some noise penalty is expected relative to the single-level case discussed in chapter 4. However both of these areas are in need of further work.

5.5 References

[1] K. K. Chen, S. U. Alam, P. Horak, C. A. Codemard, A. Malinowski, and D. J. Richardson, "Excitation of individual Raman Stokes lines in the visible regime using rectangular-shaped nanosecond optical pulses at 530 nm," Opt. Lett. **35**(14), 2433-2435 (2010).

[2] S. T. Davey, D. L. Williams, B. J. Ainslie, W. J. M. Rothwell, and B. Wakefield, "Optical gain spectrum of GeO_2-SiO_2 Raman fibre amplifiers," IEE Proceedings-J Optoelectronics **136**(6), 301-306 (1989).

[3] R. H. Stolen, C. Lee, and R. K. Jain, "Development of the stimulated Raman spectrum in single-mode silica fibers," J. Opt. Soc. Am. B **1**(4), 652-657 (1984).

[4] A. R. Chraplyvy and P. S. Henry, "Performance degradation due to stimulated Raman scattering in wavelength-division-multiplexed optical-fibre systems," Electron. Lett. **19**(16), 641-643 (1983).

Chapter 6 – Spectral gain control using shaped pump pulses and multiple pump wavelengths

In this chapter the work on pulse-shaping and gain across multiple Stokes orders is further investigated. In chapter 5, a single pump wavelength was employed and the Raman gain bandwidth was extended by use of multi-level pump pulses. Here the gain bandwidth is further increased by using multiple pump wavelengths in a TDM pumping scheme, as well as multi-level pump pulses. This extends the useable bandwidth of the Raman gain spectrum by filling in the gaps between neighbouring Stokes orders. Experimental results using two pump wavelengths and multi-level pump pulses are presented and discussed for the cascaded RFA, again using different fibre types. Some first results on the saturation characteristics are also presented, as are simulated gain spectra produced from using three pump wavelengths and multi-level pump pulses.

6.1 Introduction

By using a TDM pumping scheme, pump-to-pump Raman interactions between the multiple pump sources (i.e., pump wavelengths) are avoided and the resulting Raman gain spectrum is a superposition of the individual Raman gain spectra from the individual pump sources [1, 2]. In this case the same principles outlined in chapter 5.1 are applied to the process of obtaining the total Raman gain and overall gain spectrum along with an extra secondary contribution.

The TDM pumping scheme (see figure 6.1) restricts the duty cycle available for each pump wavelength in order to avoid pump-to-pump Raman interactions. With an even split between two pump wavelengths, there is a maximum of 50% of the total duty cycle available for each pump. Any increase in the duty cycle at one pump wavelength must be met with a decrease at the other pump wavelength. This reduction in the duty cycle would affect the primary contribution of gain from each individual pump wavelength to the total gain. However following on from the introduction in chapter 5, there are further secondary contributions to the total gain and overall gain spectrum due to the broadband nature of the Raman gain coefficient spectrum.

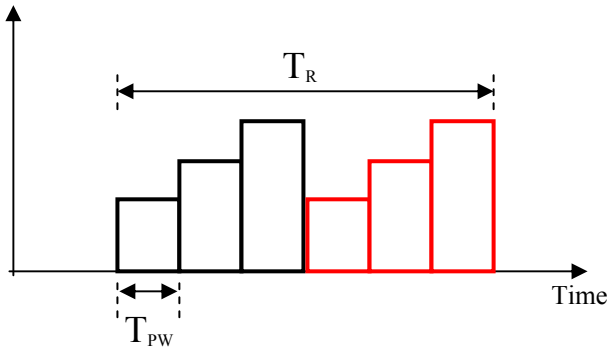

Figure 6.1 TDM pumping with two pump wavelengths and multi-level pulses.

This can be seen by looking at the overlapping Raman fibre gain coefficient spectra for two pump sources with wavelengths located at 1064 and 1090 nm shown in figure 6.2. With a frequency shift of 52 nm in the HNLF, the 1090 nm pump wavelength represents a wavelength located in the middle of the 1064 nm pump source and the peak of the 1st Stokes order that the 1064 nm pump generates. It can be seen that as well as increasing the gain between the neighbouring Stokes orders of the 1064 nm pump, the 1090 nm pump also provides further contributions to the 1st and 2nd Stokes orders of the 1064 nm pump. As in chapter 5, the exact amounts of gain would vary depending on the input pump power. In the un-depleted pump regime, i.e., before significant SRS has occurred, figure 6.2 shows that the amount added to the peak of the 1st Stokes order of the 1064 nm pump is ~25% of the peak gain (i.e., primary or direct contribution) generated by the 1090 nm pump. Likewise, the amount added to the peak of the 2nd Stokes order of the 1064 nm pump is ~20% of the peak gain (i.e., primary contribution) generated by the 1090 nm pump.

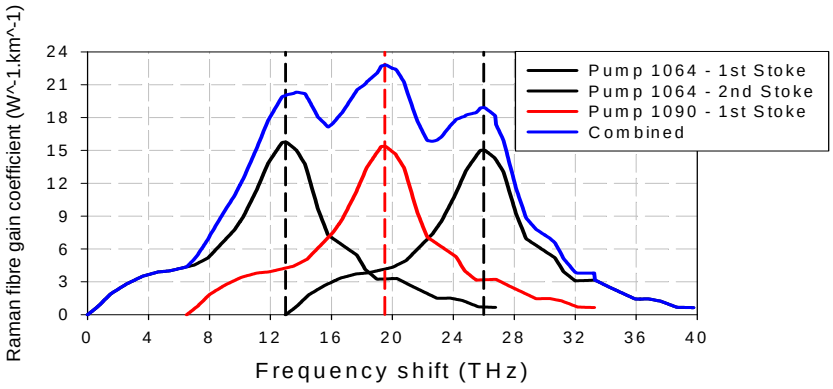

Figure 6.2 Graph showing the overlap between the Raman fibre gain coefficient spectra from the HNLF at the 1st and 2nd Stokes orders from a pump source at 1064 nm and the 1st Stokes order from a pump source at 1090 nm.

In the pump depletion regime the distribution of gain becomes more complicated as the 1st Stokes order pumps the 2nd Stokes order as shown in chapter 5. However there will be significant overlap between the individual gain spectra from each pump source which will affect the overall gain spectrum. It should also be noted that these secondary contributions to the overall gain spectrum would shift in wavelength if the wavelength of the 2nd pump source was changed from 1090 nm. The location of any other pump wavelengths used in a TDM pumping scheme would also be an important parameter to optimizing the ultra-broadband Raman gain spectrum.

6.2 Experimental measurements

6.2.1 Experimental set-up

In this section, experimental measurements on the Raman gain spectra produced from pumping a Raman fibre with step-shaped pulses from two pump sources of different wavelengths are reported. For the use of two pump wavelengths in a TDM pumping scheme, the MOPA source had to be modified. The new MOPA set-up is shown in figure 6.3. The 1064 nm pulsed laser remains the same as described previously in chapter 3. However the 1090 nm pulsed laser source consists of a Yb fibre laser that uses FBGs for feedback and wavelength selection. This output is then modulated by an AOM to give the desired pulse shapes. Both seed sources are combined into a single fibre using a 1064/1090 WDM coupler before entering the GTWave pre-amplifier (same as in chapter 3) to boost the power up to ~400 mW before entering the power-amplifier stage. The power-amplifier stage is the main difference applied to the updated MOPA source. At this stage the two signals at 1064 and 1090 are split into separate amplifiers using a 1064/1090 WDM coupler. The reason for this is that if only a single amplifier is used, then the 1064 nm signal can end up "pumping" the 1090 nm signal resulting in a transfer of power from the short wavelength to the longer wavelength signal. Note that because a Yb-doped fibre amplifier stores energy in an excited state rather than transferring it immediately, the fact the 1064 nm and 1090 nm signals are temporally separated does not prevent energy transfer between them. Thus, in this case the 1090 nm signal power becomes much higher than the 1064 nm signal power, when in fact close to equal powers in the two signals is required.

To counteract this, the power at the power-amplifier input can be adjusted, either by introducing a loss element at 1090 nm or by adjusting the power output of the initial pulsed seed lasers. However, thermal effects cause the power between the two signals to become unbalanced as the amplifier heats up and the result is a MOPA output that quickly becomes difficult to control. When this power drift in the MOPA source is transferred to the Raman amplifier, the gain measurements become difficult and unsteady over time.

It was therefore chosen to use two separate power amplifiers and then recombine the outputs into one delivery fibre, again using a 1064/1090 WDM coupler. The 1064 amplifier was a 12 m long cladding pumped Yb-doped phosphosilicate fibre with a 7/140 µm core/cladding diameter and a core-NA of 0.15. A TFB was used to combine the pump and signal in a co-pumping configuration. The 1090 amplifier used a 12 m long cladding pumped Yb-doped aluminosilicate fibre in a GTWave™ configuration. The signal fibre pigtails have 6/125 µm core/cladding diameters and an NA of 0.14. The GTWave bundle also contained two multimode pump fibres with 105/125 µm core/cladding diameters and an NA of 0.22. Using separate amplifiers meant that the output powers could be controlled independently of each other by simply adjusting the pump power to the amplifiers. The set-up for the RFA remained the same as described in chapter 3.

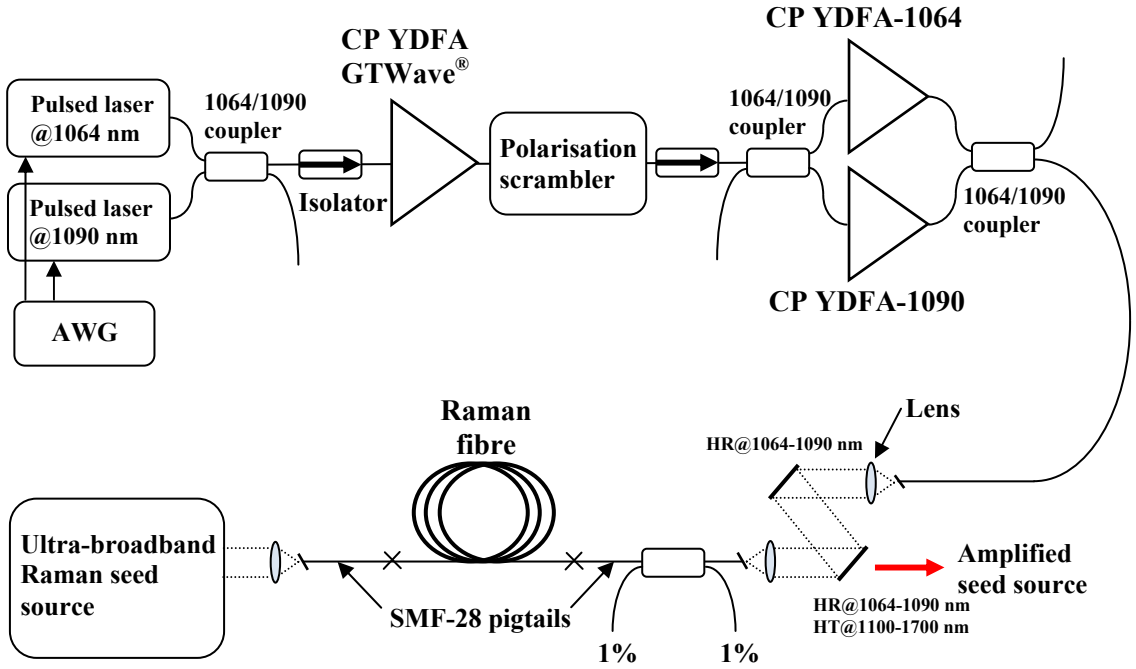

Figure 6.3 Schematic of the dual wavelength MOPA pump source and Raman amplifier test-bed. AWG: Arbitrary waveform generator; CP: Cladding pumped; YDFA: Ytterbium-doped fibre amplifier; HR: High reflectivity; HT: High transmission.

6.2.2 Experimental results

First of all, the use of the superposition principle for attaining the overall gain spectrum generated from two pump wavelengths with dual-level pump pulses was investigated experimentally. In the context of a RFA employing a TDM pumping scheme, the superposition principle proposes that the overall gain spectrum generated from multiple pump sources can be obtained as the summation of the individual gain spectra produced from each individual pump source. If proven, this can simplify the analysis of investigating the overall gain profile generated from multiple pump sources. This is because the CW model employed in chapter 3 can be used to calculate the gain spectra from each individual pump source, rather than a more complex pulse-pumped RFA model taking into account the pump-to-pump Raman interactions. Using the dual wavelength MOPA pump source according to figure 6.3, the application of the superposition principle to the TDM pumped cascaded RFA was tested and ultimately verified. Figure 6.4 shows five gain spectra for the 2 km HNLF. Curves A and B show the individual Raman gain spectra measured when operating the two pump wavelengths on their own with dual-level pump pulses. These were configured to give approximately equal gain (at the peaks) across both Stokes orders. The individual gain spectrum produced from the 1064.25 nm pump source is the same as that shown in figure 5.9 in chapter 5. Curve C shows the resulting gain spectrum from simply adding together curves A and B. Following on from this, curve D shows the Raman gain spectrum measured experimentally when both pump wavelengths were operated together in a TDM pumping scheme. It can be seen that there is a good correlation between curves C and D. Furthermore, curve E shows the Raman gain spectrum from simply taking the experimental data produced from the 1064.25 nm pump source, shifting it in frequency as though it came from a 1090.81 nm pump source and then adding the two sets of data together. This also shows good agreement to the experimental data in curve D, even though only the experimental data taken with the 1064.25 nm pump source was used.

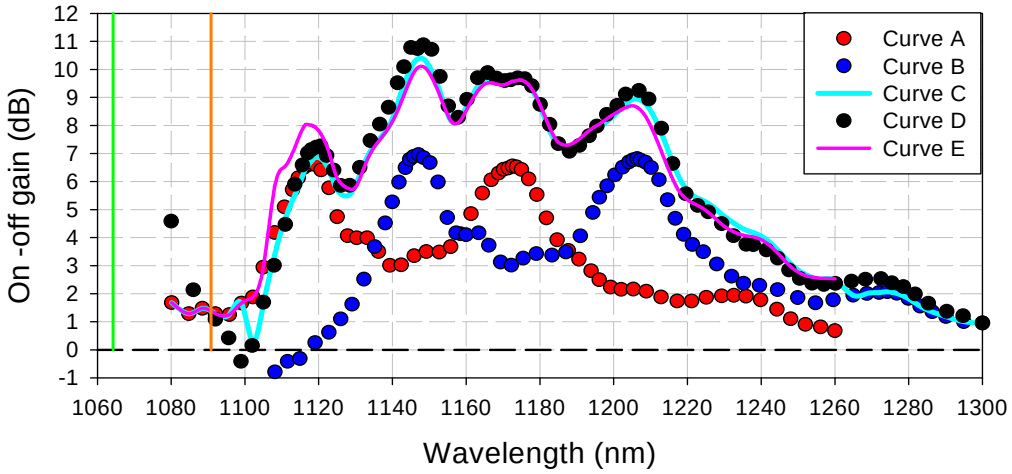

Figure 6.4 Raman gain spectra produced when pumping the 2 km HNLF with dual-level pulses from two pump wavelengths at 1064.25 nm and 1090.81 nm. Curve A: Raman gain spectrum from the 1064.25 nm pump source. Curve B: Raman gain spectrum from the 1090.81 nm pump source. Curve C: Raman gain spectrum from adding together curves A and B. Curve D: Raman gain spectrum from both pump wavelengths used together in a TDM pumping scheme. Curve E: Predicted Raman gain spectrum from taking Curve A, shifting it in frequency as though it came from a 1090.81 nm pump source and then adding the two sets of data together.

The temporal pump pulse profiles used to obtain the results shown in figure 6.4 are shown in figure 6.5 (a) along with (b) and (c) which show the resulting pulse profiles after Raman conversion to the 1st and 2nd Stokes orders when the TDM pumping scheme was used to produce curve D. Again the average pump power and the peak power of each level was set so that each section of the pump pulse was close to being completely converted to its targeted Stokes order.

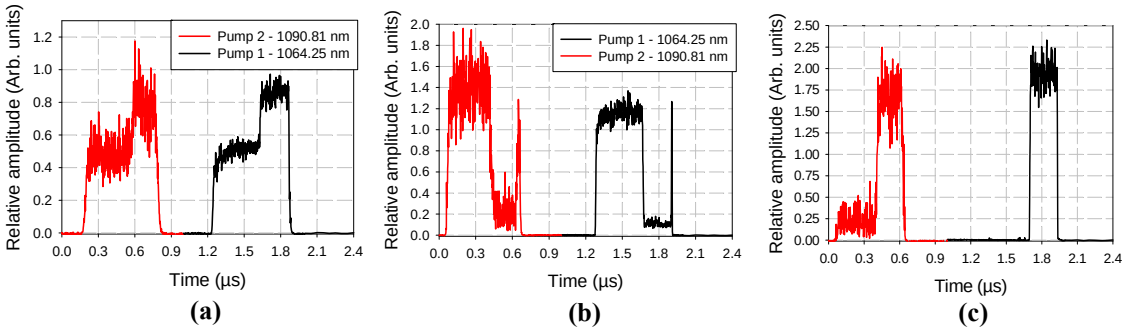

Figure 6.5 Temporal pulse profiles used for dual wavelength pumping the 2 km HNLF, (a) Initial pump pulses, (b) Co-propagating 1st-Stokes power after propagation through HNLF and (c) Same as (b) but for 2nd Stokes order.

The graphs show that the superposition principle applies to the final, overall Raman gain spectrum when a TDM pumping scheme is used and that multiple pump wavelengths can be used to fill in the gaps in gain between neighbouring Stokes orders. Important restrictions here are that the signal power and the counter-propagating gain are sufficiently low to keep the counter-propagating power low, since this otherwise couples the pump power in different time slots. However it can also be seen that further manipulation of the pulse parameters is required in order to obtain a more even distribution of gain across the combined Raman gain bandwidth. Looking at figure 6.4 it can be seen that the gain is lower in the region of ~1120 nm which is the 1st Stokes order produced from the lower pump wavelength at 1064.25 nm. This is due to lower secondary contributions to the gain spectrum in this wavelength region, whereas the 1st Stokes order from the longer wavelength pump receives higher indirect contributions in gain as shown in figure 6.2. To counteract this, the primary contribution to the 1st Stokes order gain from the shortest wavelength pump can be increased by increasing its duty cycle.

Accordingly, figure 6.6 shows two examples of a TDM pumped cascaded RFA with dual-level pump pulses whereby the gain distribution is flatter across the Raman gain spectrum. The Raman gain spectrum in curve A was produced when the total duty cycle of both pump wavelengths was ~41% whereas the Raman gain spectrum in curve B was produced when the total duty cycle of both pump sources was ~75%. This is reflected in the peak gain values.

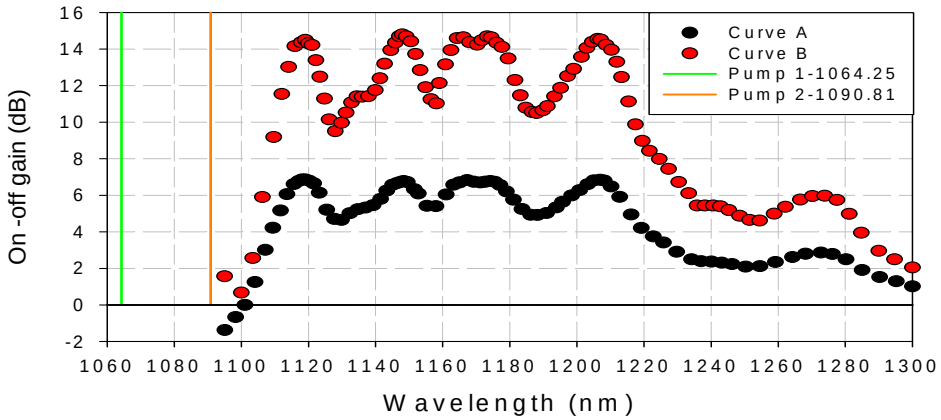

Figure 6.6 Raman gain spectra across two Stokes orders produced from dual-level pumping the 2 km HNLF with two pump wavelengths at 1064.25 nm and 1090.81 nm in a TDM pumping scheme. Curve A: 41% total duty cycle. Curve B: 75% total duty cycle.

The dual-level pump pulses used to obtain these Raman gain spectra are shown in figure 6.7. For all the pump pulses the height ratio between the two levels is 0.6:1. The total average input power used to produce the Raman gain spectra in figure 6.6 with the pump pulses in figure 6.7 was 452 mW and 944 mW, respectively. The ratio of average pump power between the two pump wavelengths would closely follow that of their respective duty cycles. In both cases the ratio was approximately 0.74:1 with the 1064 nm pump having the higher average pump power. It can also be seen that the individual duty cycles of each level are heavily weighted at the lower level of the short wavelength pump and the higher level of the longer wavelength pump. These two sections of the pump pulses correspond to the beginning and end of the resulting Raman gain spectrum. These are the sections of the Raman gain spectrum that can receive the lowest secondary gain contributions and this has to be compensated for by increasing the primary contributions (i.e., the duty cycle) to the total gain. This is reflected in the pump pulse profiles. Again the peak power of each level was set so that each section of the pump pulse was close to being fully converted to its targeted Stokes order.

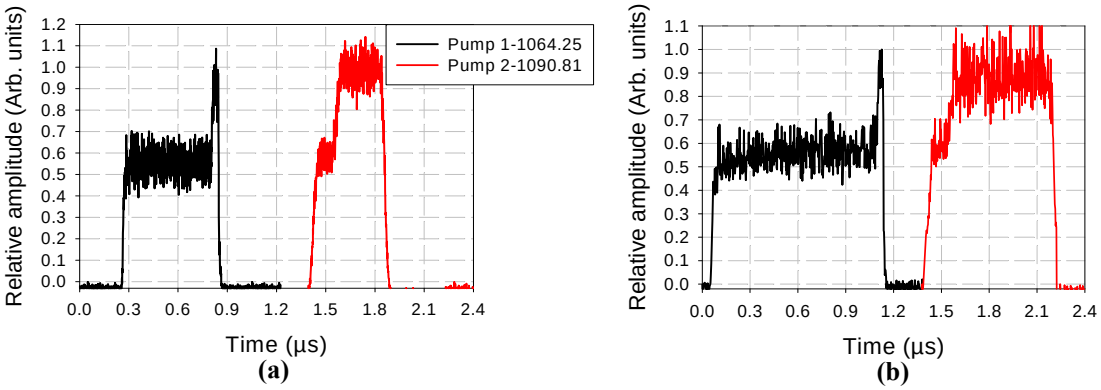

Figure 6.7 Temporal pump pulse profiles, (a) total duty cycle of 41% and (b) total duty cycle of 75%.

Using the pump pulses in figure 6.7 (b) as an example, figure 6.8 shows the temporal traces of power Raman-scattered to the 1st and 2nd Stokes orders after propagation through the 2 km HNLF. Plot (a) shows the depleted pump pulses, where it can be seen that only small section on the edges of the pulses are un-depleted and remain at the pump wavelength. Plots (b) and (c) show the pulse shapes as Raman-scattered to the 1st and 2nd Stokes orders, respectively. This further highlights the differences needed in the individual duty cycles to produce a flatter Raman gain spectrum.

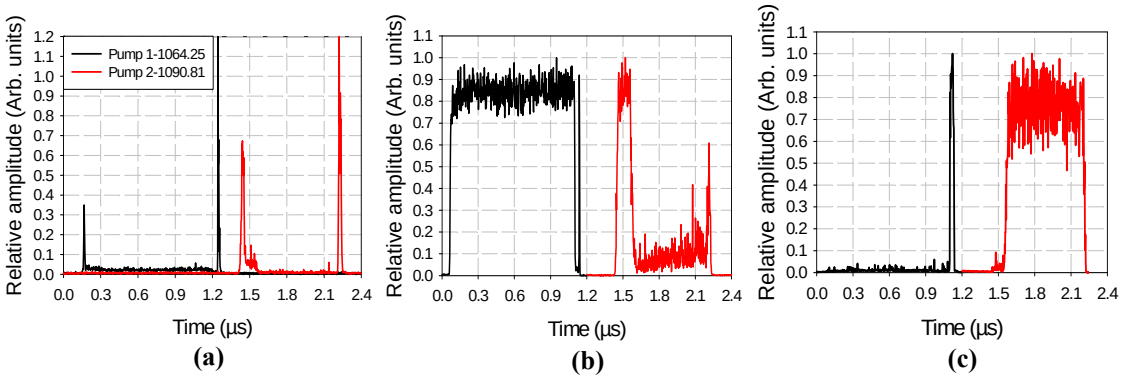

Figure 6.8 Temporal profiles after propagation through the 2 km HNLF (a) Depleted pump pulses, (b) Co-propagating 1st-Stokes power after propagation through HNLF (c) Same as (b) but for 2nd Stokes order.

In addition, figure 6.9 shows the Raman gain spectrum produced when the gain is pushed out to the 2nd and 3rd Stokes orders with the dual wavelength pump and dual-level pump pulses. The overall gain spectrum is still very similar to the one where the gain covered the 1st and 2nd Stokes orders. The total average pump power required to push the gain out to the 2nd and 3rd Stokes order in this case was 708 mW with 437 mW in the 1064 nm pump and 271 mW in the 1090 nm pump. Also shown in figure 6.9 are the pump pulses used to obtain this Raman gain spectrum. The pump pulses take up approximately 33% of the available 100% duty cycle, so it is still possible to increase the maximum gain across the Raman gain profile in figure 6.9 (b).

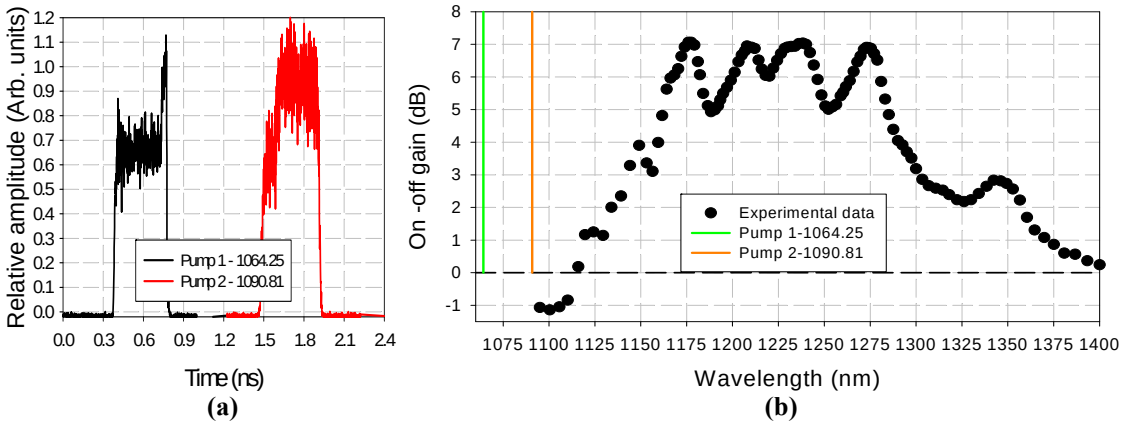

Figure 6.9 Dual-level pulse pumping of the 2 km HNLF with two pump sources at different wavelengths, (a) Input pump pulses and (b) Resulting Raman gain spectrum covering the 2nd and 3rd Stokes orders.

Next the dual wavelength pumping with dual-level pump pulses is applied to the Freelight™ DSF and the SMF-28. Figure 6.10 shows the resulting experimentally

measured gain spectra which are overlapping for comparison purposes. Due to the different Raman fibre gain efficiencies of the fibres under test, different fibre lengths and different pump duty cycles were used in order to obtain the Raman gain spectra. Even so, the pump pulse shapes were not too dissimilar to those used for the HNLF and shown in figure 6.7 (a). For the Freelight™ DSF the dual-level 1064 nm pump pulse had individual duty cycles for the 1st and 2nd section of 14.5% and 1.3%. The 1090 nm pump used a single level pump pulse with a duty cycle of 11.8% and which targeted gain primarily at the 2nd Stokes order. For the SMF-28 the dual-level 1064 nm pump pulse had individual duty cycles for the 1st and 2nd section of 7.55% and 1.1%. The 1090 nm pump used a single level pump pulse with a duty cycle of 6.3% and which targeted gain primarily at the 2nd Stokes order. This resulted in different maximum gain values so the graphs have been normalised. It can be seen that the Raman gain spectra are quite similar and there does not appear to be any major advantage to using a lower Ge content fibre whose Raman gain coefficient spectra have wider bandwidths. The SMF-28 and Freelight DSF still show evidence of internal-pumping within the 1st Stokes order of the resulting Raman gain spectra as previously shown in chapter 5. Even so, the overall Raman gain spectra still span approximately 110 nm, with a highest max-to-min variation in gain (dB) of ~40% for the SMF-28 and ~30% for the Freelight™ DSF and HNLF.

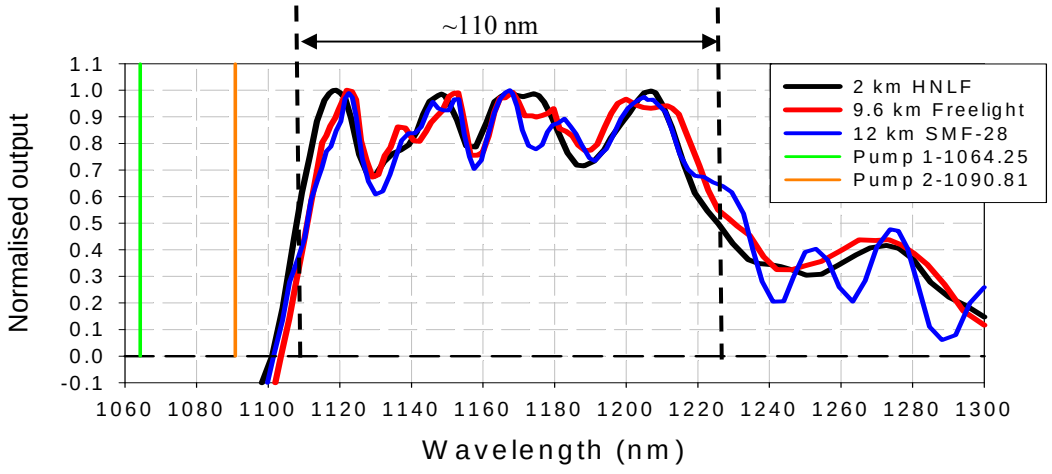

Figure 6.10 Bandwidth comparison between the Raman gain spectra produced from three different types of Raman fibres using dual-level pulse pumping and two pump wavelengths.

However it is probable that in this instance it could be improved slightly by reducing the wavelength spacing between the longer wavelength pump and the shorter wavelength pump. It could definitely be improved by use of three or more pump wavelengths.

Following on from this the Raman gain was again pushed out to the 2nd and 3rd Stokes orders for further comparison. In this case, only the experimental data from the Freelight DSF and the HNLF could be compared due to the occurrence of SC effects in the SMF-28. This can be seen in figure 6.11 which shows counter-propagating ASE spectra resulting from cascaded Raman generation in the 12 km SMF-28 with the 1090.81 nm pump source as the average input pump power is increased. As the Raman cascade is pushed out to the 3rd Stokes order at ~1275 nm, other competing nonlinear effects occur due to the location of the ZDW at ~1290-1310 nm [3]. This severely affected the gain at the 3rd Stokes order and consequently there was no point in comparing the result of this Raman gain spectrum from the SMF-28 with the other fibre types.

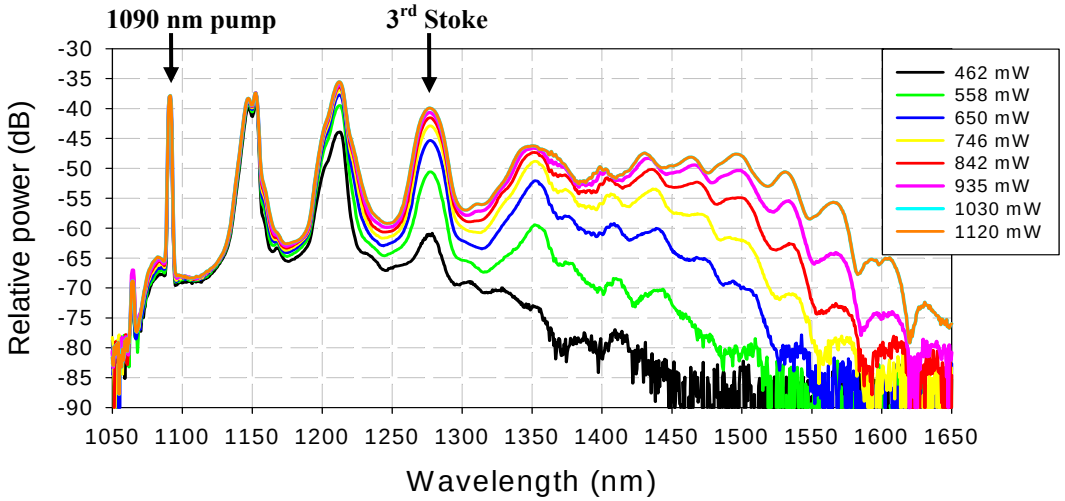

Figure 6.11 Counter-propagating ASE spectra from cascaded Raman generation with the 1090.81 nm pulsed pump source in the 12 km SMF-28 fibre. Super-continuum effects occur as the average input pump power is increased.

However it was still possible in the Freelight™ DSF and the HNLF as shown in figure 6.12. The overall Raman gain spectra span approximately 130 nm, with a highest max-to-min variation in gain (dB) of ~20% for the Freelight DSF and ~30% for the HNLF. The overall gain spectrum for the HNLF remains very similar to that produced over the 1st and 2nd Stokes orders in figure 6.10, while there are improvements in the flatness of the overall Freelight DSF gain spectrum.

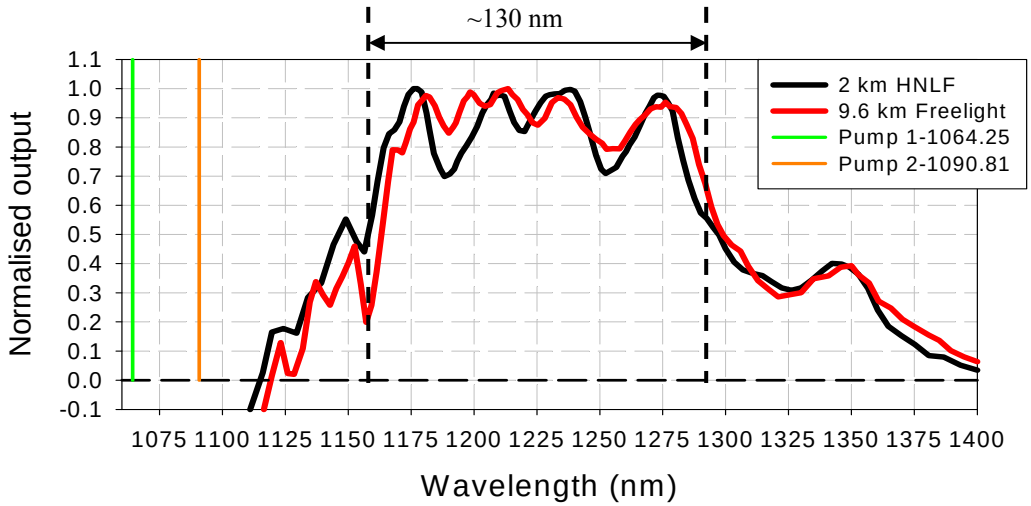

Figure 6.12 Bandwidth comparison between the Raman gain spectra across the 2nd and 3rd Stokes orders produced from two Raman fibres (HNLF & Freelight™) using dual-level pulse pumping and two pump wavelengths.

These experimental results have shown the capabilities of generating ultra-broadband gain by using shaped pulses and two pump wavelengths to pump a cascaded RFA. The experimental set-up as it is, is only suited to two pump wavelengths due to the use of 1064/1090 WDM couplers. Even so, ultra-broadband gain covering two Stokes orders simultaneously, including the 1st and 2nd orders and the 2nd and 3rd orders has been experimentally demonstrated. Furthermore the experiments were repeated with three different silica-based fibres, all of which had different Ge content. It is concluded that there is little advantage in terms of bandwidth to using a low Ge content fibre. This is also further emphasised by the fact that the lower Ge content fibres typically require much higher pump powers.

The use of three pump wavelengths and further extending the Raman gain bandwidth through use of multi-level pump pulses was done with computer simulations due to time constraints on experimental work.

6.3 Simulated results

In this section we look at the simulated Raman gain spectra produced from pumping the 2 km HNLF with multiple pump wavelengths and multi-level pulses. Experimental results using two pump wavelengths (i.e., 1064.25 and 1090.81 nm) were

presented in the last section and so simulated results will be presented that can be compared to this set-up, along with some variations in the pump wavelength spacing. In addition, simulations using three pump wavelengths are also carried out to show how this can improve the flatness of the overall Raman gain spectrum.

As mentioned in chapter 5, a co-propagating CW model is employed which is based on equation 2.35 in chapter 2. This is valid with a TDM pumping scheme since none of the pump wavelengths used to produce the step-shaped pulses are overlapping in time. Therefore they can all effectively be treated as separate pump sources whose resulting gain spectra can be simply added together, in the absence of signal-induced gain saturation and gain saturation from counter-propagating Raman ASE. The counter-propagating gain for a pulse pattern with a certain duty cycle is obtained by taking the individual Raman gain profiles from each effective pump source and multiplying it by the relevant duty cycles. Adding these individual gain spectra together gives a good representation of the overall Raman gain spectrum produced in a TDM pulse-pumped counter-propagating cascaded RFA.

For all the simulated gain spectra shown in this section only the individual duty cycles of each pulse section were varied in order to optimize the overall Raman gain spectrum and obtain a flat gain distribution. It is also possible to modify the gain by altering the level of each step and thus altering the instantaneous power of each section of the pulse. However this is considerably more time consuming since a gain spectrum would have to be taken at every power level used. It was therefore chosen to fix the instantaneous power levels of each section of the pulse to the centre of the flat-top regions on the gain profiles, i.e., points A, B and C in figure 6.13.

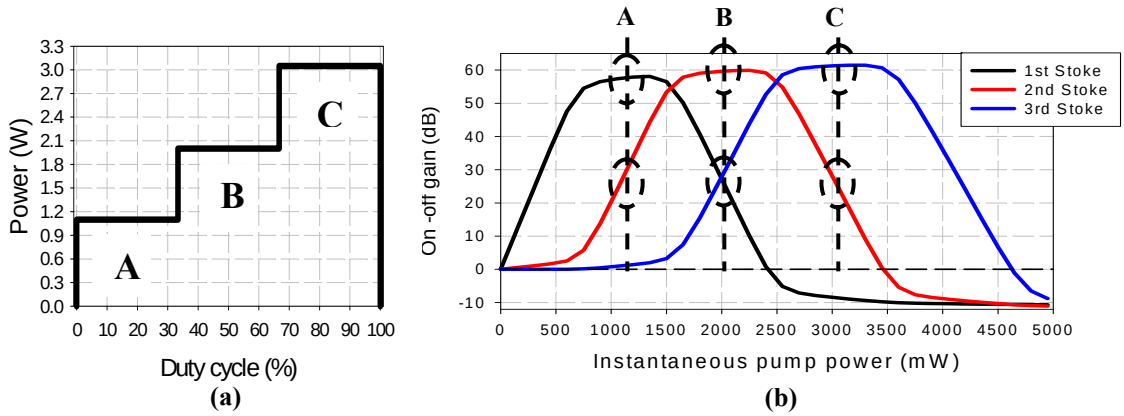

Figure 6.13 (a) Three-level pump-pulse with set instantaneous power levels and (b) On-off gain *vs*. pump power across three Stokes orders for the 2 km HNLF.

This is in line with the operating regime used in the previously reported experimental results. The height ratio of each level of the pump pulse was therefore 0.367:0.667:1. The individual duty cycles of the pump pulse shown in figure 6.13 are then modified to accommodate more pump wavelengths and provide a certain amount of gain at a specific Stokes order. It can also be seen on figure 6.13 (b) that the power levels are set-up so that for each primary contribution of gain to a Stokes order, there will always be a further secondary contribution of ~45-50% to the neighbouring Stokes orders which modifies the overall gain spectrum.

The first simulated gain spectra are shown in figure 6.14 (a) for pumping the 2 km HNLF with two pump wavelengths and dual-level pulses. For curves A and B the two pump wavelengths are the same as those used in the experimental work, i.e., 1064.25 and 1090.81 nm. Curve A shows the gain spectrum produced if each individual section of the pump pulses all had a 25% duty cycle, whereas curve B shows a gain spectrum optimised for flatness. This was done by adding all the individual gain spectra together and then looking at the overall gain spectrum while the individual duty cycles were modified. For curve B, the individual duty cycles for the 1st and 2nd section of the pump pulses were adjusted to 48% and 5% for the 1064.25 nm pump and 10% and 35% for the 1090.81 nm pump, respectively. The pump pulses used to produce curve B are shown in figure 6.14 (b). A good correlation in the shape of the gain spectra can be seen between the simulated data of curve B and the experimental data in figure 6.6.

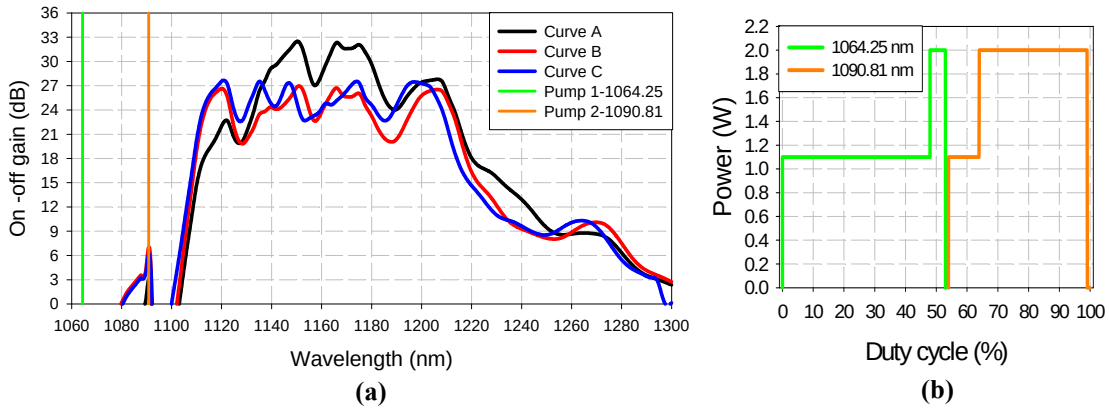

Figure 6.14 (a) Simulated Raman gain spectra over two Stokes orders from pumping the 2 km HNLF with two pump wavelengths (1064.25 and 1090.81 nm) and dual-level pulses. Curve A: Raman gain spectrum when each section of the pump pulses has an equal duty cycle of 25%. Curve B: Flattened Raman gain spectrum from pump pulses with unequal duty cycles. Curve C: Flattened Raman gain spectrum from pump pulses with unequal duty cycles and the longer pump shifted to 1087 nm. (b) Pump pulses used to produce curve B.

Differences in the total amount of gain were to be expected due to the differences between the simulated and experimentally measured on-off gain values as highlighted in chapter 3. Curve C shows the Raman gain spectrum produced when the longer pump wavelength is shifted from 1090.81 nm to 1087 nm. In this case the individual duty cycles for the 1st and 2nd section of the pump pulses were adjusted to 46% and 7% for the 1064.25 nm pump and 10% and 35% for the 1087 nm pump, respectively. Improvements in the flatness of the Raman gain spectrum can be seen albeit at the expense of a slight reduction in the overall bandwidth.

Figure 6.15 shows the Raman gain spectra produced when the bandwidth is extended by targeting gain across three Stokes orders with two pump wavelengths at 1064.25 and 1090.81 nm. Curve A shows the gain spectrum produced if each individual section of the pump pulses all had a 16.4% duty cycle. Curve B shows a flattened gain spectrum obtained by modifying the duty cycles. However, when producing curve B, even though gain across three Stokes orders was targeted only dual-level pump pulses with a height ratio set at 0.367:1 were used. This means the instantaneous powers were set for the 1st and 3rd Stokes orders only, i.e., points A and C on figure 6.13. In this case the individual duty cycles for the pump pulse sections were adjusted to 39% and 18% for the 1064.25 nm pump and 21% and 23% for the 1090.81 nm pump, respectively. With this set-up there was little advantage to changing the pump wavelength separation.

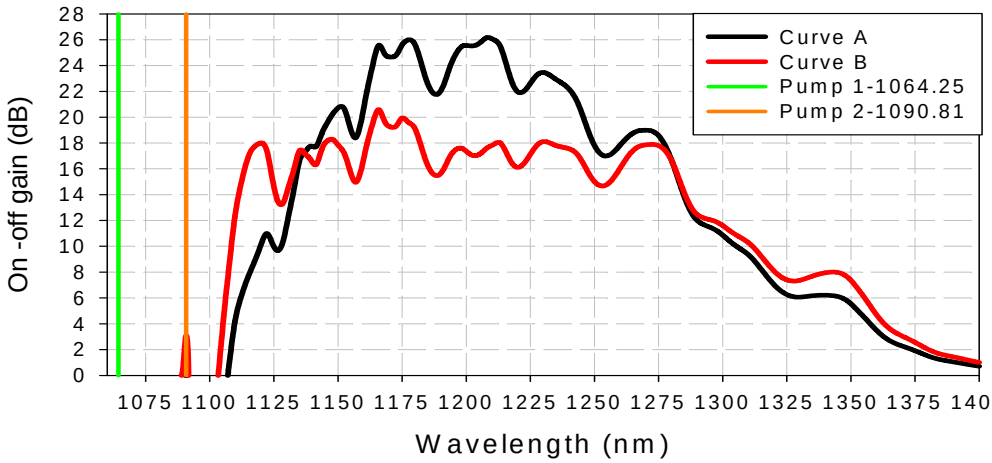

Figure 6.15 Simulated Raman gain spectra over three Stokes orders from pumping the 2 km HNLF with two pump wavelengths (1064.25 and 1090.81 nm) and three-level pulses. Curve A: Raman gain spectrum when each section of the pump pulses has an equal duty cycle of 16.4%. Curve B: Flattened Raman gain spectrum from pump pulses with unequal duty cycles.

In fact the gain distribution across the Raman gain spectrum could be improved in terms of flatness by optimizing the instantaneous power of the 1st section of the pulse for each pump wavelength. Even when the section of the pump pulse which is targeting gain directly at the 2nd Stokes order is set to zero, there is still a high amount of gain supplied to this wavelength region through the secondary contributions from the pulse sections generating gain directly at the 1st and 3rd Stokes orders. This can be seen in figure 6.13 (b) by noting the amount of gain for the 2nd Stokes order at points A and C on the red curve. Furthermore there are also more secondary contributions to the gain in the 2nd Stokes wavelength region from using two pump wavelengths as highlighted in figure 6.2. With the instantaneous power levels set as they are, the numerous secondary contributions of gain to the 2nd Stokes wavelength region can make it impossible to obtain the flattest possible Raman gain distribution by simply modifying the individual duty cycles of the pump pulses. However looking at figure 6.13 (b), if the instantaneous power at point A is reduced this would reduce the secondary contribution of gain to the 2nd Stokes order, while the primary contribution to the gain at the 1st Stokes order remains relatively similar. In this case, a flatter gain distribution than that shown on curve B in figure 6.15 should be obtained. Following the same principle, the instantaneous power of point C on figure 6.13 (b) could also be increased to obtain a flatter gain distribution. Even so, the gain bandwidth in figure 6.15 has been extended by ~60 nm (i.e., approximately one Stokes shift) from that in figure 6.14 by targeting gain across three Stokes orders as opposed to two.

While experimental measurements were only taken using two pump wavelengths, the outcome of using three pump wavelengths could be investigated using computer simulations. The use of multiple pump wavelengths for the cascaded RFA were tested and it was concluded that three pump wavelengths was enough to achieve good flatness for a Raman gain spectrum covering multiple Stokes orders. The use of more pump wavelengths offered only marginal improvements in gain flatness and would increase the complexity of the MOPA pump source. Figure 6.16 shows four flattened Raman gain spectra covering three Stokes orders (i.e., 1st, 2nd and 3rd) pumped by 2, 3, 4 and 5 pump wavelengths. The maximum gain for all plots was very similar but here they have been normalised to make comparisons. It can be seen that there is a big improvement moving from two to three pump wavelengths but then not much improvement in using four or five pump wavelengths.

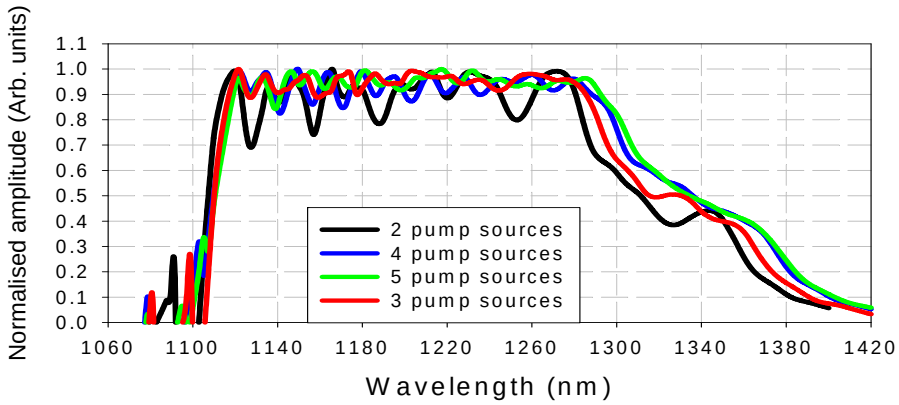

Figure 6.16 Comparison of flattened simulated Raman gain spectra covering three Stokes orders pumped with different numbers of pump wavelengths; Black curve: 2 pump wavelengths of 1064 and 1090 nm; Red curve: 3 pump wavelengths of 1064, 1081 and 1098 nm; Blue curve: 4 pump wavelengths of 1064, 1077, 1090 and 1103 nm; Green curve: 5 pump wavelengths of 1064, 1074.4, 1084.8, 1095.2 and 1105.6 nm.

However, it should be noted that more pump wavelengths may be able to achieve more complex gain shapes with a higher resolution, although the scope for this is limited by the bandwidth of the Raman gain coefficient. Note also that the optimisation was manual and therefore somewhat limited.

The three pump wavelengths used were 1064 nm, 1081 nm and 1098 nm, whereby the wavelength spacing was approximately one Stokes shift in the HNLF of 52 nm divided by 3. Figure 6.17 (a) shows the Raman gain spectra produced from pumping the 2 km HNLF with the three pump wavelengths and dual-level pump pulses targeting gain across the first two Stokes orders. Again curve A shows the gain spectrum when all sections of the pump pulses carry the same duty cycle, i.e., 16.4%. Curve B shows the gain spectrum when the pump pulse duty cycles have been optimised for a flat Raman gain spectrum. With three pump wavelengths, a much flatter gain spectrum than when using two pump wavelengths (see figure 6.14) can be obtained. The pump pulses used to produce curve B are shown in figure 6.17 (b). In the case of three pump wavelengths the individual duty cycles for the pump pulse sections were adjusted to 40% for the 1064 nm pump, 17% and 12% for the 1081 nm pump and 2% and 28% for the 1098 nm pump. Indeed for the 1064 nm pump pulse, only a single-step pulse was used which targeted gain directly at the 1st Stokes order, i.e., a peak power corresponding to point A on figure 6.13 (b).

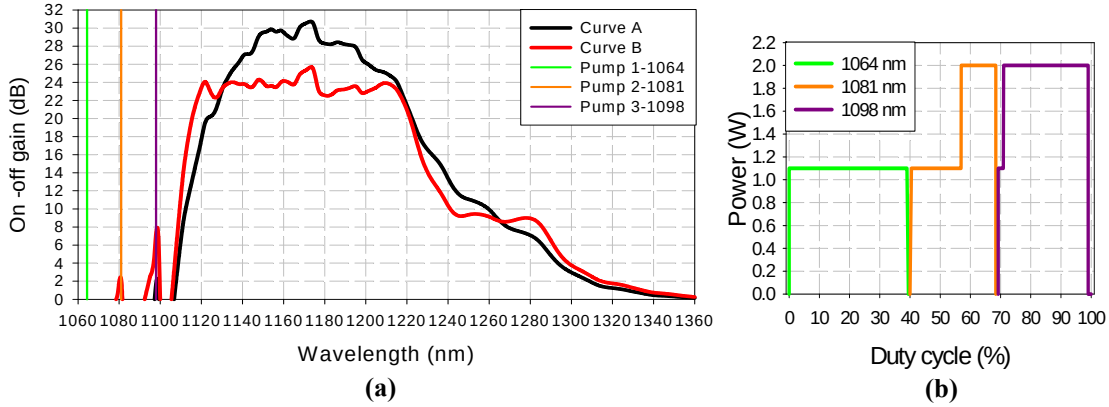

Figure 6.17 (a) Simulated Raman gain spectra over two Stokes orders from pumping the 2 km HNLF with three pump wavelengths (1064, 1081 and 1098 nm) and dual-level pulses. Curve A: Raman gain spectrum when each section of the pump pulses has an equal duty cycle of 16.4%. Curve B: Flattened Raman gain spectrum from pump pulses with unequal duty cycles. (b) Pump pulses used to produce curve B.

Again it is also probable that an even flatter gain spectrum could be obtained with some slight modifications of the instantaneous power levels of the pump pulses. It is also worth noting that the average maximum gain is only 1-2 dB lower (see figure 6.14 and 6.17) when using three pump wavelengths to target gain across two Stokes orders as opposed to two pump wavelengths.

Following on from this, three pump wavelengths were used to generate gain across three Stokes orders. In figure 6.18 (a), curve A shows the gain spectrum when all pulse sections carry the same duty cycle, i.e., 11%, whereas curve B shows the best outcome in gain flatness when varying the individual duty cycles of the pump pulses. For this a combination of two-level and three-level pump pulses was used as shown in figure 6.17 (b). The 1064 and 1081 nm pumps used dual-level pump pulses, the instantaneous powers of which were set to target gain directly at the 1st and 3rd Stokes orders, i.e., points A and C in figure 6.13 (b). The individual duty cycles for the pump pulse sections were adjusted to 34% and 10% for the 1064 nm pump and 16% and 14% for the 1081 nm pump, respectively. The 1098 nm pump used a three-level pulse whose individual duty cycles were adjusted to 9%, 2% and 15%. Again further improvements could be achieved by modifying the instantaneous power levels of the pump pulse profile. The average maximum gain is ~17 dB which is similar to that when using only two pump wavelength, but in this case the gain spectrum is flatter.

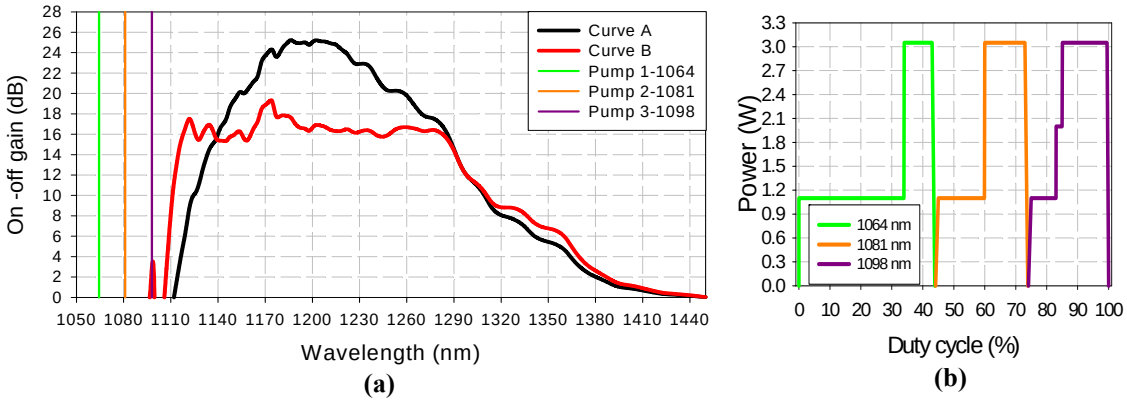

Figure 6.18 (a) Simulated Raman gain spectra over three Stokes orders from pumping the 2 km HNLF with three pump wavelengths (1064, 1081 and 1098 nm) and multi-level pulses. Curve A: Raman gain spectrum when each section of the pump pulses has an equal duty cycle of 11%. Curve B: Flattened Raman gain spectrum from pump pulses with unequal duty cycles. (b) Pump pulses used to produce curve B.

Simulations were also performed for shifting the gain to longer wavelengths by using higher Stokes orders. First of all, gain was targeted over the 5th, 6th and 7th Stokes orders. This shifts the gain to the wavelength region ~1350-1700 nm, further highlighting the flexibility of the pulse-pumped cascaded RFA. Figure 6.19 shows the gain spectra that have been optimized for flatness produced from using two pump wavelengths at 1064.25 and 1090.81 nm. Curve A generates gain over the 6th and 7th Stokes orders, whereas curve B generates gain over the 5th, 6th and 7th Stokes orders. In both cases, dual-level pump pulses were employed, although the instantaneous powers were set to different levels. In a similar fashion to that shown in figure 6.13, the power levels of the sections of the pulse targeting gain at the 5th, 6th and 7th Stokes orders were set to 5.5 W, 7 W and 8.65 W, respectively. Again for each primary contribution of gain to a Stokes order, there will always be a further secondary contribution of ~45-50% to the neighbouring Stokes orders and the overall gain spectrum. For curve A, the individual duty cycles for the pump pulse sections were set to 37% and 10% for the 1064.25 nm pump and 15% and 36% for the 1090.81 nm pump, respectively. The power levels were set to 7 W and 8.65 W which targeted gain directly at the 6th and 7th Stokes orders. For curve B, the individual duty cycles for the pump pulse sections were set to 29% and 19% for the 1064.25 nm pump and 26% and 26% for the 1090.81 nm pump, respectively. In this case the power levels were set to 5.5 W and 8.65 W which targeted gain directly at the 5th and 7th Stokes orders. Due to the wavelength dependence of the Raman shift the Raman gain bandwidth is broader for

higher Stokes orders and extends over ~200 nm for curve A and ~300 nm for curve B. The average maximum gain is also slightly higher, although this can be explained by noting that the on-off gain increases for increasing Stokes orders (see figure 3.17 in chapter 3).

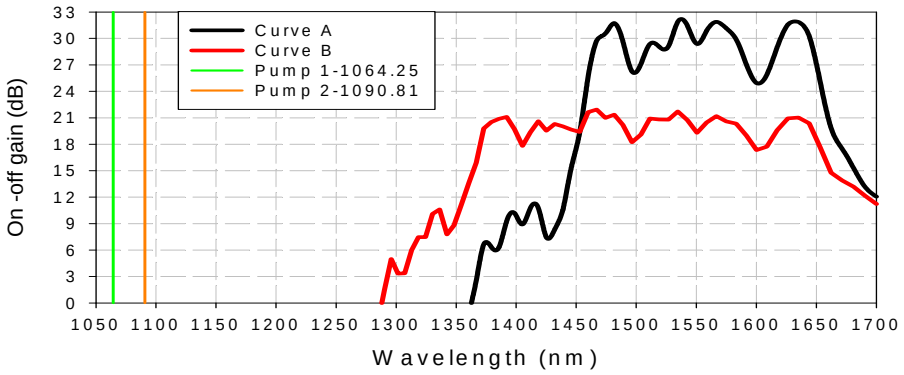

Figure 6.19 Simulated Raman gain spectra from pumping the 2 km HNLF with two pump wavelengths (1064.25 and 1090.81 nm) and dual-level pulses. Curve A: Flattened Raman gain spectrum across the 6th and 7th Stokes order. Curve B: Flattened Raman gain spectrum across the 5th, 6th and 7th Stokes orders.

Again it looks like the flatness of the gain spectrum could be improved by reducing the spacing between the two pump wavelengths. However, using three pump wavelengths would provide better results.

Figure 6.20 shows the resulting gain spectra when the three pump wavelengths of 1064, 1081 and 1098 nm are used. Curve A shows the gain spectrum when gain was targeted over the wavelength region covered by the 6th and 7th Stokes orders. To produce the flattened gain spectrum in curve A, a combination a single-step and dual-level pump pulses were used. The 1064 nm pump used a single step pulse with a duty cycle of 32% and a peak power that targeted gain at the 6th Stokes order, i.e., 7 W. For the 1081 and 1098 nm pumps, dual-level pulses were used. The individual duty cycles for the pump pulse sections were set to 15% and 18% for the 1081 nm pump and 5% and 30% for the 1098 nm pump, respectively. The power levels were set to 7 W and 8.65 W which targeted gain directly at the 6th and 7th Stokes orders. To produce the flattened gain spectrum in curve B, dual-level pump pulses were used with the power levels set to 5.5 W and 8.65 W which targeted gain directly at the 5th and 7th Stokes orders. The individual duty cycles for the pump pulse sections were set to 21% and 11% for the 1064 nm pump, 15% and 13% for the 1081 nm pump and 19% and 21% for the 1098 nm pump, respectively. The resulting simulated gain spectrum has an average on-

off gain of ~20 dB across a gain bandwidth of ~290 nm and covers the wavelength region from 1370 to 1670 nm. Again it can be seen that the flatness of the Raman gain spectrum can be improved without any major effect on the average maximum gain.

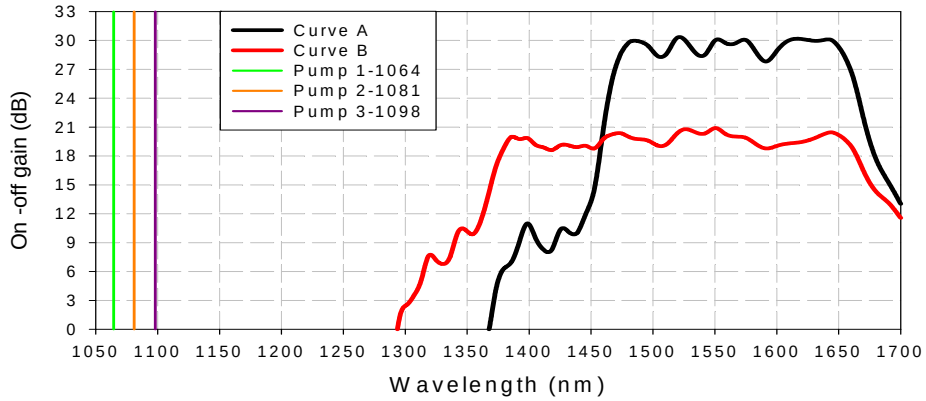

Figure 6.20 Simulated Raman gain spectra from pumping the 2 km HNLF with three pump wavelengths (1064, 1081 and 1098 nm) and dual-level pulses. Curve A: Flattened Raman gain spectrum across the 6th and 7th Stokes order. Curve B: Flattened Raman gain spectrum across the 5th, 6th and 7th Stokes orders.

Last of all, multi-level pump pulses with up to seven levels were used to generate a Raman gain spectrum targeting gain across all seven Stokes orders from the 1st to the 7th. In figure 6.21, curve A shows the gain spectrum when all pulse sections carry the same duty cycle, i.e., 4.67%, whereas curve B shows the best outcome in gain flatness when varying the individual duty cycles of the pump pulses. The resulting simulated flattened gain spectrum has an average on-off gain of ~9 dB across a gain bandwidth of ~500 nm.

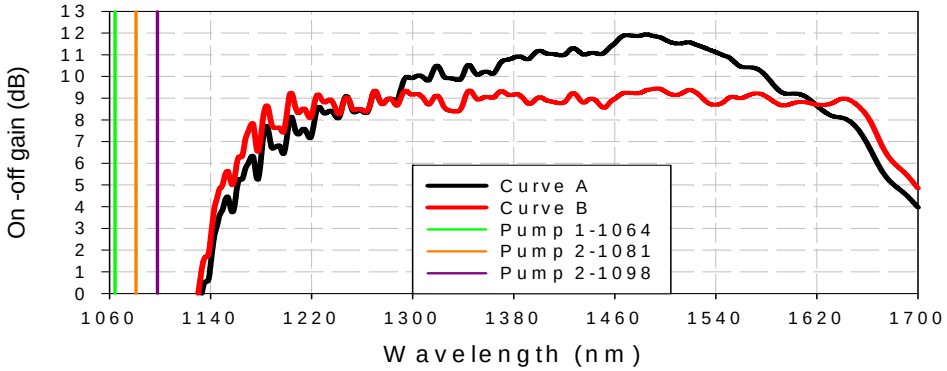

Figure 6.21 Simulated Raman gain spectra covering seven Stokes orders from pumping the 2 km HNLF with three pump wavelengths (1064, 1081 and 1098 nm) and multi-level pulses with up to seven levels. Curve A: Raman gain spectrum when each section of the pump pulses has an equal duty cycle of 4.67%. Curve B: Flattened Raman gain spectrum across seven Stokes orders.

As mentioned in chapter 5, the absolute maximum one could expect for gain covering the wavelength range from the 1st to the 7th Stokes orders would be ~11 dB. However this value did not include the smaller negative gain contributions that occur at the lower Stokes orders. The individual gain spectra generated from each section of the multi-level pump pulses that make up the flattened Raman gain spectrum in figure 6.21 are shown in figure 6.22. The negative gain contributions at the lower Stokes orders can clearly be seen making, 9 dB a reasonable figure.

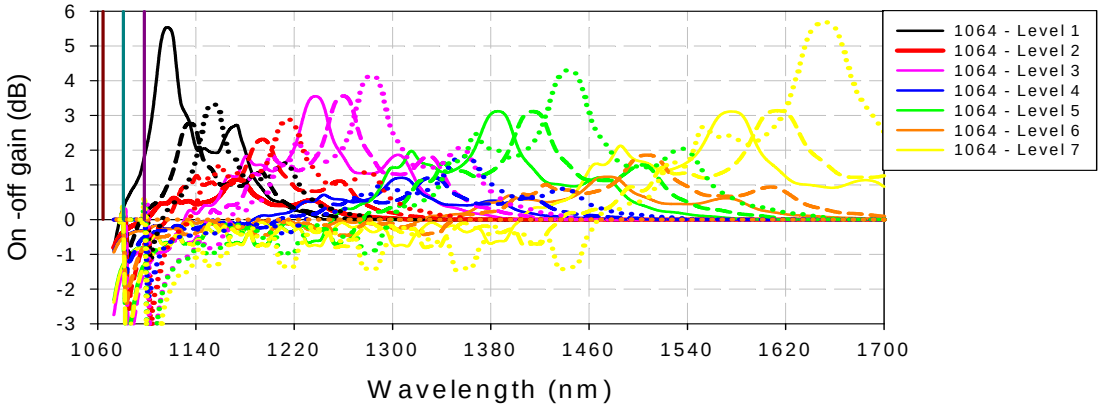

Figure 6.22 Individual gain spectra from each section of the multi-level pump pulses that generate the flattened Raman gain spectrum in figure 6.21 targeting gain across seven Stokes orders. (▬) 1064 nm pump source; (– – –) 1081 nm pump source; (••••••) 1098 nm pump source.

6.4 Gain saturation and Raman ASE properties

In this section some first investigations are presented into the saturation characteristics of a cascaded RFA pumped at two wavelengths with dual-level pulses. It was shown in chapter 5 how a high power signal at one Stokes order can influence the gain at the other when using dual-level pump pulses to target gain across two Stokes orders. In that case only a single pump wavelength was employed and the gain at the two Stokes orders were linked in that they originated from the same pump source/wavelength.

Following on from this, in a multi-wavelength pumped cascaded RFA the signal saturation of a Stokes order originating from one pump wavelength can also influence the gain at the Stokes orders originating from the other pump wavelength. However this is a very complicated process due to the many different overlapping contributions to the overall Raman gain spectrum. As shown in figure 6.2, the Raman fibre gain coefficient

spectra from the two pump wavelengths at 1064 and 1090 nm overlap due to their broadband nature. This is further highlighted in figure 6.23 (a) and (b) which again shows the ultra-broadband gain spectrum represented by curve B in figure 6.14 but also shows the individual gain spectra from each section of the pump pulses. It shows that the 1064 nm pump can still contribute gain in the same wavelength region as the Stokes orders from the 1090 nm pump. Indeed, this is what results in the varying pulse duty cycles necessary to produce the flat ultra-broadband gain spectra shown in the previous sections. Moreover, this does also mean that the total gain at any given wavelength is not solely generated by one section of a multi-level pump pulse or from one single pump wavelength. Therefore the gain saturation induced by a high power signal at one Stokes order can influence the gain at other Stokes orders that overlap with it and which are generated from other pump wavelengths.

However, the individual gain spectra making up the overall Raman gain spectrum can vary a lot depending on the operating regime, i.e., the power level of each step of the pump pulses. This was shown in figures 5.3 and 5.4 whereby the distribution of gain changes depending on whether the power level operates in the un-depleted or depleted regimes and how far into the depleted region it extends. This requires modification of the individual duty cycles of the pump pulses which would result in the individual gain spectra contributing different amounts of gain to the overall Raman gain spectrum. An example of this is also shown in figure 6.23 where the dual-level pump pulses in plot (c) are also used to generate a flat gain spectrum over the 1st and 2nd Stokes orders (plot (d)). For this the power levels of the 1064 nm pump pulse were modified so that they differ from the pump pulse in figure 6.23 (a). However both sets of pump pulses can be configured in terms of duty cycles to give a flat gain distribution across the 1st and 2nd Stokes orders. This would then result in different saturation characteristics for the cascaded RFA. It is also worth noting how the different instantaneous powers result in differences in the maximum gain between the two gain spectra even though the full 100% duty cycles were used.

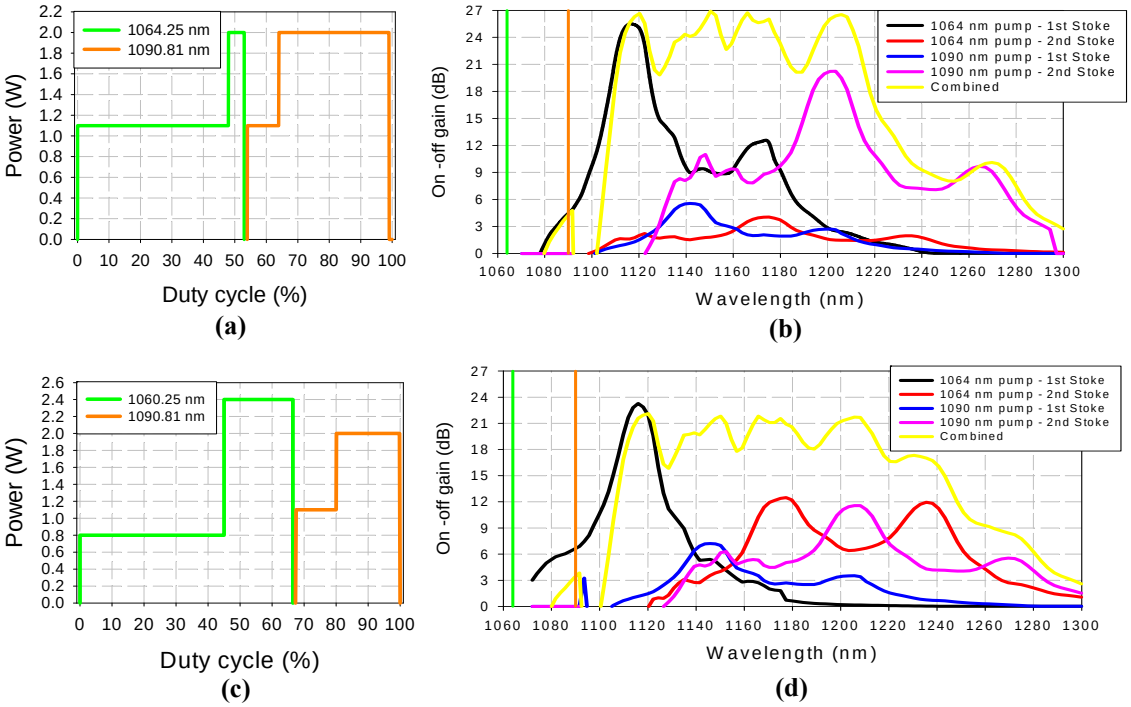

Figure 6.23 Two examples of dual-level pump pulses and corresponding total Raman gain spectra optimized for flatness, including individual gain spectra from each section of the pump pulses.

Investigating the saturation characteristics of a multi-level TDM pumped RFA using computer simulations would require a complex model and would not be possible with the CW model used previously to investigate the gain spectra. Even so, some first experimental results with a high power signal at 1116 nm were taken. The unsaturated Raman gain spectrum corresponds to the one represented by curve B in figure 6.6 where the four main peaks all had an on-off gain of ~14.4 dB. The input signal power at 1116 nm was then increased while a low power signal was used to measure the gain at the wavelengths of the other three gain peaks, i.e., 1148 nm, 1174 nm and 1206 nm. Figure 6.24 shows the results. As the 1116 nm signal power is increased, its gain saturates and it eventually has an effect on the gain at the other signal wavelengths at an input power level of ~6 dBm. The gain at 1174 nm drops quickly at this point along with the gain at 1206 nm although at a slower rate, while the gain at 1148.5 nm increases slightly and then starts to decrease. The drop in gain at 1174 nm is similar to the scenario described in chapter 5 whereby the Raman cascade is slowed down due to a reduction in co-propagating SRS power which is driving the Raman cascade.

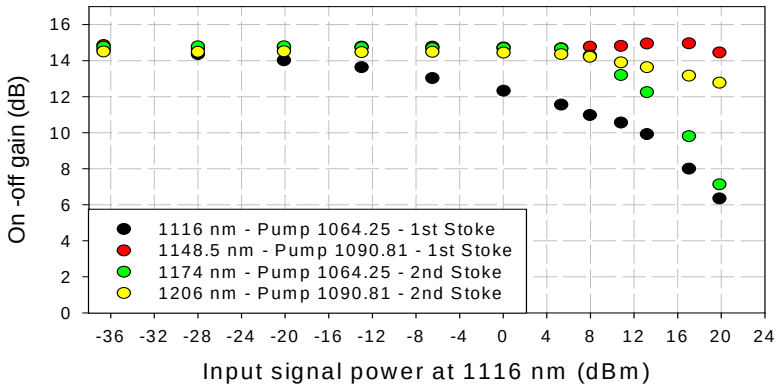

Figure 6.24 Example showing the result of an increasing input signal power at the 1st Stokes order when pumping the 2 km HNLF with dual-level pulses and two pump wavelengths. The graph shows the on-off gain for four signal wavelengths *vs*. input signal power at 1116 nm.

This can be seen in figure 6.25 which shows the counter-propagating Raman ASE spectra as the 1116 nm signal power is increased. The high power 1116 nm signal takes most of the power from the pump resulting in less ASE at the first Stokes order and ultimately at the 2nd Stokes order of the 1064 nm pump.

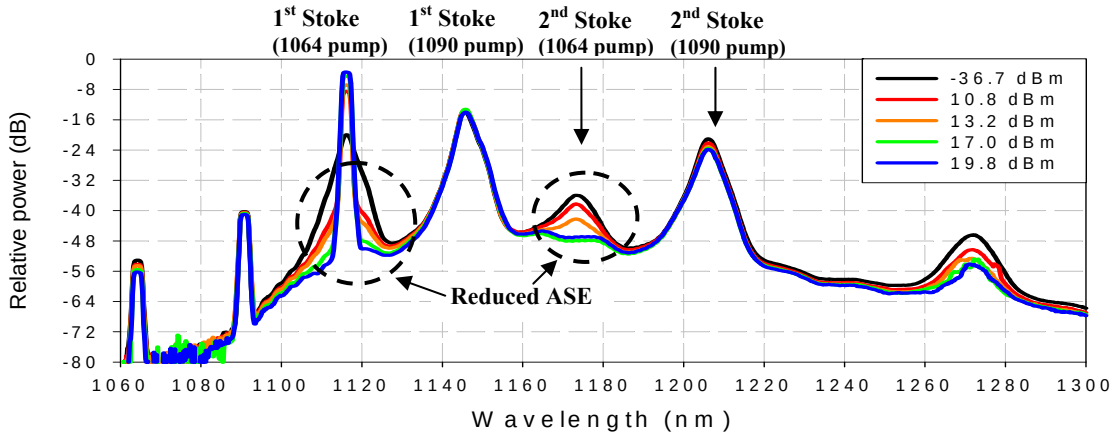

Figure 6.25 Example showing the effect on the Raman ASE spectrum when increasing the power of an 1116 nm signal. The signal powers are shown in the graph legend. The unsaturated Raman ASE spectrum represented by the black curve corresponds to that produced with the gain spectrum of curve B in figure 6.6.

As shown in chapter 5 this results in the section of the pump pulse that is normally converted to the 2nd Stokes order residing in the 1st Stokes order. In this example the duty cycle of this 2nd Stokes section of the pump pulse is only ~2-3% (see figure 6.7 (b)) and therefore the primary contribution is relatively small. However as shown in figure 6.23 (a) and (c) the pump pulse profiles can vary significantly and

subsequently the duty cycle and gain from this section of the pump pulse can increase. The duty cycle of this second section of the pump pulse is set depending on how much gain is provided in this wavelength region by the first section of the pump pulse which is targeting gain at the 1st Stokes order. This is highlighted by the black curves on the gain spectra shown in figure 6.23 (b) and (d). One would expect these different pumping situations to result in different saturation characteristics.

Furthermore, the individual duty cycles of the dual-level 1064 nm pump pulse also affect the required individual duty cycles of the dual-level 1090 nm pump pulse. This means that the gain provided by the 1064 nm pump to the wavelength regions of the 1st and 2nd Stokes orders of the 1090 nm pump can also vary. Therefore with the saturated gain at 1116 nm (i.e., the peak of the 1st Stoke by the 1064 nm pump) induced by a high power signal, a drop in gain would also be expected at 1148.5 nm and 1206 nm which corresponds to the peaks of the 1st and 2nd Stokes shifts from the 1090 nm pump. One can expect that the drop in gain would depend on the make-up and individual duty cycles of the pump pulses which result in different overlapping gain contributions. This would probably result in the gain changing (i.e., dropping in most cases) at different rates. Indeed this is the case for the signal gain at 1206 nm which as mentioned earlier, starts to drop off at the same time as the 1172 nm gain but at a slower rate.

However, at the point when the 1172 nm and 1206 nm gain starts to drop the gain at 1148.5 nm increases slightly and then drops off slightly. It possible that the gain could continue to drop after this but more signal power than that available in this set-up would be required to test this. The reason for this may well be answered by looking at the pulse profiles at each signal wavelength after propagation through the fibre for different input signal powers at 1116 nm. These are shown in figure 6.26, with (a), (b) and (c) generated from the 1064 nm pump and (d), (e) and (f) generated from the 1090 nm pump. Plots (a) and (d) show the pulse profiles with an input signal power at 1116 nm of -36 dBm, i.e., in the unsaturated regime. Plots (b) and (e) show the pulse profiles with an input signal power at 1116 nm of 8.9 dBm, i.e., just as the gain at 1172 nm and 1206 nm starts to drop. Plots (c) and (f) show the pulse profiles with an input signal power at 1116 nm of 14.15 dBm, i.e., operating well into the saturated regime. While the effect of the high power 1116 nm signal on the 1064 nm pump has been explained, it also appears to have a further effect on the conversion of the 1090 nm pump pulse even though the 1090 nm seems to provide little gain in this wavelength

region. The second section of the 1090 nm pump pulse is not as cleanly converted to the 2nd Stokes order in comparison to the unsaturated regime which may go some way to explaining the increase in gain. However, the full reason behind this is not clear at the present time and requires further investigation, such as taking the individual gain spectra from each section of the pump pulses as well as more signal power and high power signals at other wavelengths.

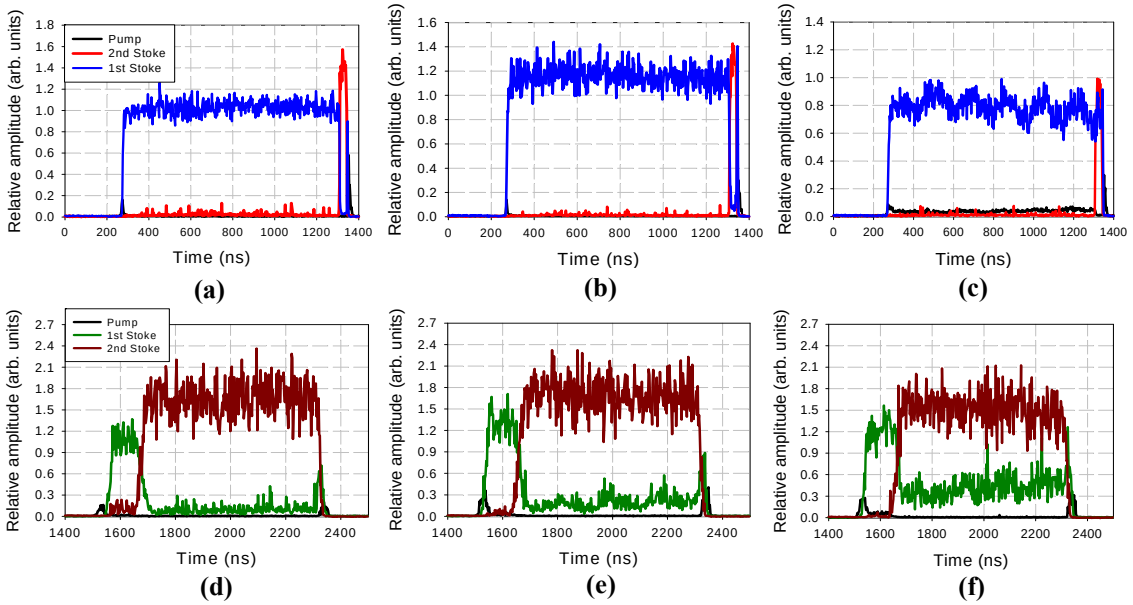

Figure 6.26 Temporal pulse profiles after propagation through the 2 km HNLF with three different input signal powers at 1116 nm. Plots (a), (b) and (c) are generated from the 1064 nm pump when the input signal power at 1116 nm was -36 dBm, 8.9 dBm and 14.15 dBm, respectively. Likewise plots (d), (e) and (f) are generated from the 1090 nm pump when the input signal power at 1116 nm was -36 dBm, 8.9 dBm and 14.15 dBm, respectively.

Figure 6.27 shows the results when changing the high power signal from 1116 nm to 1172 nm. Again a low power signal was used to measure the gain at the wavelengths of the other three gain peaks, i.e., 1116 nm, 1148 nm and 1206 nm. The gain can be seen to change at different rates and also the 1148 nm gain still increases. A high power signal in the region of 1148 nm or 1206 nm (i.e., the peaks of the Stokes shifts from the 1090 nm pump) would be expected to produce different saturated gain data.

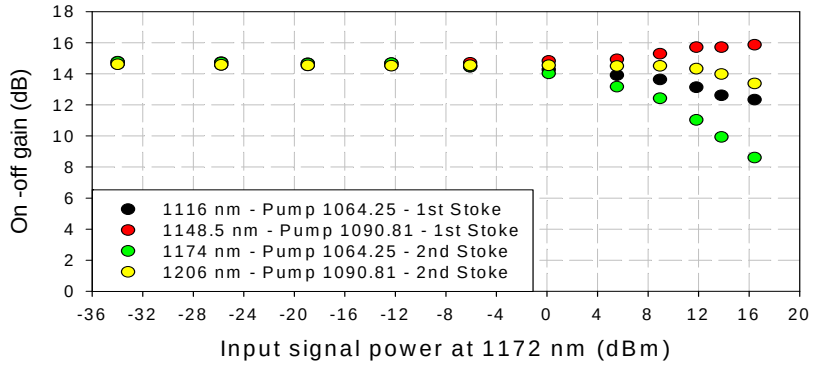

Figure 6.27 Example showing the result of an increasing input signal power at the 2nd Stokes order when pumping the 2 km HNLF with dual-level pulses and two pump wavelengths. The graph shows the on-off gain for four signal wavelengths *vs*. input signal power at 1172 nm.

Even though a larger study could be dedicated to the saturation properties of multi-wavelength, multi-level pulse-pumped cascaded RFA, some first results have been shown here which show how a high power signal can influence the gain across the whole ultra-broadband Raman gain spectrum and not just the Stokes order in which the high power signal is located. Overall, this makes for a quite complex nonlinear system, which is difficult to control. While I here only considered a static pump scenario, it would be attractive to make the most of the MOPA pump source by adjusting the pump parameters according to the signal powers to control the characteristics of the RFA also in the saturated regime.

It was highlighted in chapter 5 that the noise properties of such a pulse-pumped cascaded RFA would change depending on what pump pulses are used and at what instantaneous power level each section is operated at. Although little attention was paid to this at the time of these experimental measurements a few points can be made using the results in chapter 4 and using figure 6.25. Furthermore, it was shown in figure 6.23 how a flattened Raman gain spectrum across multiple Stokes orders could be obtained with different step-shaped pump pulses. This was obtained by operating at different power levels and modifying the individual duty cycles of the 1064 nm pump pulse accordingly. It would also be expected that this would further modify the noise properties as well as the saturation characteristics. It was also pointed out chapter 5 that the section of the pump pulse targeting gain at the final Stokes order (of any pump wavelength) could potentially be operated without influence from higher Stokes orders even with the current experimental set-up. Although more emphasis was placed on obtaining a flat Raman gain spectrum, an example of this can be seen in the ASE

spectrum shown by the black curve in figure 6.25. The 2nd Stokes orders of the 1064 nm and 1090 nm pumps have different amounts of Raman ASE. This is because the 1064 nm pump was operating in the early stages of depletion whereas the 1090 nm pump was operating heavily into the depleted regime. This is backed up by looking at the amount of Raman ASE generated at the 3rd Stokes orders.

Again a larger study could be dedicated to the noise properties of multi-wavelength, multi-level pulse-pumped cascaded RFA but some important points have been highlighted here.

6.5 Summary

In summary we have demonstrated an ultra-broadband RFA with a controllable gain spectrum by pumping with shaped pulses from an Yb-doped fibre MOPA source and by using multiple pump wavelengths in a TDM pumping scheme. This has demonstrated the flexibility and the substantial scope for generating controllable broadband gain. Experimental results for the Raman gain spectra generated from pumping the HNLF with dual-level pulses and two pump wavelengths have been presented. Raman gain spectra spanning over 100 nm covering the wavelength regions from ~1110 to 1220 nm and ~1160 to 1290 nm were experimentally demonstrated. Furthermore, as with the single pump wavelength cascaded RFA in chapter 5, comparisons were also made between the Raman gain spectra generated from pumping the HNLF and two lower Ge content fibres with dual-level pulses and two pump wavelengths. Again it was concluded that the HNLF is an attractive gain medium for generating cascaded Raman gain over multiple Stokes orders.

Further investigations of the potential Raman gain spectra were also carried out using computer simulations. The theoretical predictions were first of all used to corroborate the experimental results for the dual-wavelength pumped ultra-broadband Raman gain spectra covering multiple Stokes orders. Then the use of more than two pump wavelengths to improve the flatness of the gain spectra was investigated. It was concluded that three pump wavelengths was sufficient for good flatness and that the use of more pump wavelengths did not offer any major improvement in gain flatness and would also increase the complexity of any MOPA pump source. However, although not considered here, it is also possible to generate other spectral gain shapes and it should

be noted that more pump wavelengths should be able to achieve more complex gain shapes. Theoretical predictions were also given for pushing the gain out to the 1.5 μm spectral region as well as extending the ultra-broadband gain bandwidth across seven Stokes orders (i.e., 1st to the 7th Stokes order) which resulted in an average on-off gain of ~9 dB spanning across a gain bandwidth of ~500 nm. Again, some initial results and discussions are also offered into the saturation and Raman ASE properties of a multi-level and multi-wavelength pulse-pumped cascaded RFA.

While this chapter used TDM to avoid interaction between different pump wavelengths, it may still be possible to have several pump wavelengths at the same time, and then perhaps achieve greater gain over a greater bandwidth. This requires greater control as it creates a more complicated nonlinear system, but one can envisage some cases in which this is a relatively minor complication. However this remains to be investigated.

6.6 References

[1] L. F. Mollenauer, A. R. Grant, and P. V. Mamyshev, "Time-division multiplexing of pump wavelengths to achieve ultrabroadband, flat, backward-pumped Raman gain," Opt. Lett. **27**(8), 592 (2002).

[2] Y. Emori, S. Kado, and S. Namiki, "Broadband flat-gain and low-noise Raman amplifiers pumped by wavelength-multiplexed high-power laser diodes," Opt. Fiber Technol. **8**, 107-122 (2002).

[3] Information available at: http://www.corning.com/opticalfiber/.

Chapter 7 – Summary and future work

7.1 Summary

The primary objective of the work carried out in this thesis was to construct and investigate the potential for an electronically controllable ultra-broadband RFA based on cascaded SRS. Recent advances in RE doped high-power fibre MOPA pump sources are utilised to achieve the electronic control of the cascaded RFA. The MOPA configuration allows for excellent control of the pump pulse parameters which have not been readily available in the past. The use of a MOPA pump source allows the generation of well-controlled pump pulses (i.e., shape and power) which in turn allows for controlling the Raman gain spectra that are generated in cascaded RFAs. A MOPA source was built using Yb doped fibres allowing for output wavelengths ranging from ~1050 to 1100 nm. This allows the potential for generating Raman gain at any signal wavelength from 1100 to 2000 nm in a silica-based fibre.

In chapter 3, cascaded Raman wavelength shifting across a wide range of wavelengths using single-level pump pulses (i.e., approximate super-Gaussian pulses) was demonstrated. The cascaded RFA had a counter-propagating pump and signal and used a single MOPA pump source with a fixed output wavelength of 1064 nm. This RFA only targeted gain at a single Stokes order at any one time (i.e., single-channel amplification) but had the flexibility of controlling the pulse parameters to increase the conversion efficiency and shift the Raman gain to any desired Stokes order within the transparency window of the Raman generating fibre. A silica-based HNLF was used to demonstrate cascaded Raman wavelength shifting up to seven Stokes orders with counter-propagating gain measurements made across all seven Stokes orders. Counter-propagating gain measurements were made for pump duty cycles of 20% and 40% and for 6 km and 2 km fibre lengths. From a pump wavelength of 1064 nm, the location of the peak gain of the 7th Stokes order was ~1575 nm which demonstrated the potential for gain covering more than 500 nm. Comparisons were also made between the gain results from the HNLF and two telecommunication fibres (SMF-28 and Freelight™ DSF), along with gain results from computer simulations. This highlighted some possible issues with the amount of achievable gain from the cascaded RFA in the experimental characterisation. Although the pump power requirements were all close to

what was expected, it was found that for all the fibres under test, the experimentally measured on-off gain values dropped off as the fibre lengths were reduced. This is not the case for the theoretically predicted gain results which also suggest that a higher on-off gain should be possible. Some issues with the experimental set-up were identified as possible reasons for this and were outlined at the end of chapter 3. However as mentioned earlier, I believe this is the first time counter-propagating Raman gain has been measured over the wavelength range of seven Stokes orders without the interference of supercontinuum effects (FWM) and for high duty cycles (> 1%) whereby the counter-propagating gain becomes important and a measurable quantity.

In chapter 4, the pulse-pumped cascaded RFA reported in chapter 3 was further assessed in terms of temporal gain variations, noise and saturation properties. It was confirmed that the temporal gain variations that can result as a consequence of pulse-pumping reduced as the repetition rate was increased. For the work carried out in this thesis the repetition rates were typically in the range of 400 kHz to 1.33 MHz. In this case the maximum-to-minimum on-off gain variation at the peak average gain was shown to be less than ~1 dB.

In terms of the noise performance, measurements were made on the amount of Raman ASE generated in the cascaded RFA which were then converted into noise figure values. Measurements were again taken for pump duty cycles of 20% and 40% and for 6 km and 2 km fibre lengths. It was found that the counter-propagating noise figure in the cascaded RFA was dominated by Raman ASE that was initially co-propagating with the pump pulses before being Rayleigh backscattered into the counter-propagating direction, i.e., in the signal direction. Therefore the measured counter-propagating Raman ASE initially experiences the co-propagating gain before being backscattered and experiencing the counter-propagating gain. This resulted in noise figure values between 20 and 30 dB at the maximum gain for all fibre lengths and pump duty cycles which can be considered high compared to standard RFAs operating in the un-depleted pump regime. For the HNLF, it was shown that there was little difference in the equivalent noise figure values across all seven Stokes orders for the different lengths. The intrinsic noise figure which takes into account the net gain is shown to be lower for higher Stokes orders in some instances. However this is only the case for the longer lengths of HNLF where bigger differences in net gain between the lower and higher Stokes orders are inevitable. As the fibre length is reduced and the difference in

net gain between the lower and higher Stokes orders becomes smaller, even the intrinsic noise figure values become similar for all Stokes orders.

It was also concluded that there was little effect in shortening the fibre length to reduce the Rayleigh backscattered power as any reduction in fibre length resulted in an increase in the required pump power by the same factor. Therefore the only difference in the counter-propagating Raman ASE powers was a result of different gain values between the different fibre lengths. Also from the noise measurements available it appears the advantage in using a low-NA fibre to reduce the Rayleigh backscattered power and overall noise power is limited. This was verified by repeating the counter-propagating Raman ASE power measurements for the Freelight™ DSF. The lower NA of the Freelight™ DSF results in a RBS coefficient which for a given input pump power would result in a lower amount of backscattered power than the HNLF. However, the lower NA is a result of a lower doping concentration of germanium which in a RFA typically leads to a lower Raman fibre gain coefficient. This is then met with a higher pump power requirement, a longer fibre length or a trade-off between both. This trade-off results in more Rayleigh backscattered power. The Raman fibre gain coefficient of the Freelight™ DSF is approximately 8.6 times lower than that of the HNLF. Therefore, for the same effective length, 8.6 times more pump power is required and vice-versa. This effectively cancelled out the 9.6 times lower RBS coefficient and consequently the counter-propagating Raman ASE powers and noise figure values for the Freelight™ DSF and HNLF were similar, if the fibre lengths are chosen to yield the maximum length for the same pump power. However, for a given gain level, the noise level can be decreased substantially by using a higher duty cycle.

Next, signal-induced gain saturation in the pulse-pumped counter-propagating cascaded RFA was investigated. Measurements were carried out at the 1^{st}, 2^{nd} and 7^{th} Stokes orders with various pump duty cycles and fibre lengths for the HNLF. It was shown that the amplified signal grows enough to deplete the pump and saturate the gain but does not reach a high enough power to generate further SRS on its own. In the pulse-pumped counter-propagating cascaded RFA, it is the average power of the pump pulses that is the important parameter. In a counter-pumping configuration the pump power is exhausted in the amplifier as the signal power approaches the average power of the pulsed pump source and not the peak power. Since the rate of Raman conversion is determined by the peak power of the pump pulses, the average power of the pump pulses is always lower than the peak power. Therefore, as the amplified signal power

approaches that of the average pump power, the gain starts to saturate due to a lack of pump photons. At this point, the average power of the amplified signal is still well below the peak power of the pump pulses and therefore that required for further SRS. However this depends on the duty cycle of the signal and pump.

For the saturation output powers, given by the output signal power at which the small-signal gain reduces by a factor of two, the pump power is the most important parameter. This can be either the average power or peak power depending on the relative direction of the pump and signal waves. Since the pump power requirement in an RFA is dependent on the fibre length and the Raman fibre gain coefficient so is the saturated output power. It was shown that when using a shorter length of the HNLF for the cascaded RFA which required more pump power, the saturated output powers also increased. Counter-propagating saturation output power measurements has been reported for pump pulses with 20%, 40% and 60% duty cycles and HNLF lengths of 2 and 6 km. In terms of the absolute maximum values for the saturated output powers, a pulse-pumped counter-propagating cascaded RFA computer model is required to investigate this. Unfortunately, only a CW pumped co-propagating cascaded RFA was available during the time this work was carried out. Some simulated data from the CW pumped cascaded RFA model were reported which showed that the saturated output powers increased as the Stokes order increased. This was explained by a shortening of the effective interaction length for higher Stokes orders. As the Raman cascade moves to higher Stokes orders, increasing amounts of the fibre are used to generate earlier Stokes orders. However, as discussed in this thesis, different mechanisms can affect the way the gain saturates for a co-pumped and counter-pumped RFA and more in-depth investigations are required.

Chapters 5 and 6, report further experiments on the Raman gain spectra produced from pumping the HNLF with step-shaped pump pulses. The step-shaped pump pulses consist of multiple levels with different instantaneous powers. It was shown that the instantaneous powers could be set so that different parts of the pump pulses transferred their energy to different Stokes orders leading to a controllable gain spectrum covering multiple Stokes orders at the same time. This was seen as a way to extend the gain bandwidth of the pulse-pumped cascaded RFA. In chapter 5, this was investigated using a single wavelength MOPA pump source. First of all, computer simulations were used to give an insight into how the different sections of the step-shaped pump pulses would contribute to the resulting composite Raman gain spectra. It

was shown how the Raman gain spectrum and the spectral integral (i.e., the area under the Raman gain spectrum) changed with instantaneous pump power, with the spectral integral value offering a way of estimating the gain – bandwidth product of a multi-level pulse-pumped cascaded RFA. For pump powers sufficiently high for cascaded SRS, the spectral integral over the region with positive gain was calculated to be approximately equal to 1.1×10^{15} dB Hz × d, where d is the pump duty cycle. This calculated spectral integral value suggested that a maximum gain of ~11 dB could be possible over a bandwidth of 100 THz (i.e., 180 to 280 THz or 1070 to 1700 nm) when a 100% pump duty cycle was employed.

Then using a single wavelength MOPA pump source, equal gain across two and three Stokes orders was demonstrated experimentally by pumping with two and three-step pulses, respectively. Comparisons were also made between the Raman gain spectra generated from pumping the HNLF and two different fibre types with dual-level pulses. The other two fibres used for comparison had lower amounts of germanium which results in a broader Raman gain coefficient spectrum. However, it was concluded that the lower germanium content fibres did not result in a significantly broader bandwidth for the composite Raman gain profile. Thus, the advantage of a higher Raman fibre gain coefficient for the HNLF outweighed any reduction in the overall bandwidth of the gain spectra. Therefore, the HNLF was still considered an attractive gain medium for generating cascaded Raman gain over multiple Stokes orders. Some initial results into the saturation and noise properties of the multi-level pulse-pumped cascaded RFA were also presented but both these areas are in need of further work.

In chapter 6, the work carried out on pumping the cascaded RFA with step-shaped pulses was progressed by using multiple pump wavelengths in a TDM pumping scheme. This extended the useable bandwidth of the composite Raman gain spectra by filling in the gaps between the neighbouring Stokes orders generated from a single pump wavelength. With the use of two pump wavelengths and more manipulation of the individual duty cycles of each section of the step-shaped pump pulses, a flatter composite Raman gain profile could be obtained. Experimental results for the Raman gain spectra generated from pumping the HNLF with dual-level pulses and two pump wavelengths were presented. Raman gain spectra spanning over 100 nm covering the wavelength regions from ~1110 to 1220 nm and ~1160 to 1290 nm were demonstrated. Furthermore, comparisons were also made between the Raman gain spectra generated from pumping the HNLF and the two lower Ge content fibres with dual-level pulses and

two pump wavelengths. Again it was concluded that the HNLF was an attractive gain medium for generating cascaded Raman gain over multiple Stokes orders.

Further results for the potential Raman gain spectra that would be possible were presented using computer simulations. The theoretical predictions were used to back up the experimental results from the dual-wavelength pumped Raman gain spectra covering two and three Stokes orders. Then the use of more than two pump wavelengths to improve the flatness of the gain spectra was investigated. It was concluded that three pump wavelengths would be sufficient for good flatness and that the use of more pump wavelengths did not offer any major improvement in gain flatness. Theoretical predictions were also given for pushing the gain out to the 1.5 μm spectral region. The ultra-broadband gain bandwidth was also extended across seven Stokes orders (i.e., 1st to the 7th Stokes order) with an average on-off gain of ~9 dB spanning across a gain bandwidth of ~500 nm. Again, some brief results and discussions were also provided into the saturation and Raman ASE properties of the multi-level and multi-wavelength pulse-pumped cascaded RFA.

Overall the work carried out so far has presented a good proof of principle study with most of the measurements reported in this thesis being carried out for the first time. All in all, this work has demonstrated the flexibility and the substantial scope for generating controllable ultra-broadband gain using cascaded Raman generation.

7.2 Future work

The immediate focus on the future work for this project can remain on the fundamental aspects of the pulsed cascaded RFA. As mentioned previously, most of the measurements reported so far have been carried out for the first time along with the building of the experimental set-ups used to take these measurements. Therefore there is still a significant amount of work, such as polarisation properties, that could be carried out to help with the understanding of what is undoubtedly a complex amplifier set-up.

Even so, there are still potential limiting factors with the current experimental set-up that can be investigated using the existing available experimental equipment.

Polarisation and modal overlap issues were identified as two possible factors which could be reducing the gain values below the maximum that might be possible. These issues could be investigated further with any improvements also impacting the

noise and saturation characteristics and thus leading to potential improvements in these areas as well. Polarisation and in particular the scrambling technique, looks like it could be an important issue in achieving the highest possible gain and best noise performance. Further investigations and measurements here would be useful for a better understanding of how the pump, signal and co- and counter-propagating Raman ASE interact. Measurements on the co-propagating gain would also be beneficial.

Furthermore, from the experimental measurements it was observed that by launching the pump power directly into the LP_{11} mode of the SMF-28 input pigtail fibre at the free-space input of the RFA, the on-off gain increased from 8.5 dB to ~10.5 dB for the 1st Stokes order when pumping the 6 km HNLF with pulses of a 20% duty cycle. Finding the reasons behind this may also be informative, although the HNLF only supports the LP_{11} mode for the first three Stokes orders.

Clean rectangular pump pulses with flat-top profiles would make perfect pump pulses for the cascaded RFA but are in practice difficult to achieve. However, the use of pump pulses with a profile as close as possible to that of a clean rectangular pulse would be ideal and worth pursuing in the future.

These investigations would also be useful for the cascaded RFA pumped with shaped pulses as they could also potentially improve the gain, noise and saturation properties for this type of RFA. Also the possibility of generating other spectral gain shapes rather than those with flat-top profiles could be investigated. More complex gain shapes may be possible with the availability of more pump wavelengths and adaptively shaped pump pulses.

Noise appears likely to be the most significant concern of this approach for many applications. Whereas the PRF was sufficient to reduce temporal variations in the counter-propagating gain, it seems likely that a higher PRF will reduce the noise.

Publications

- C. Farrell, C. Codemard, and J. Nilsson, "Spectral gain control using shaped pump pulses in a counter-pumped cascaded fiber Raman amplifier," Opt. Express **18**(23), 24126-24139 (2010).
- C. Farrell, C. Codemard, and J. Nilsson, "A counter-propagating cascaded Raman fiber amplifier pulsed pumped with a 1.06 μm source," *Frontier in Optics*, (16-20 Sept 2007, San Jose, CA, 2007), paper FWB2.
- C. Farrell, C. Codemard, and J. Nilsson, "A Raman fibre amplifier generating simultaneous gain across multiple Stokes orders by using step shaped optical pulses," *3rd EPS/QEOD Europhoton Conference*, (31 Aug - 05 Sep 2008, Paris, France, 2008), paper THoC5.
- P. Dupriez, C. Farrell, M. Ibsen, J. K. Sahu, J. Kim, C. Codemard, Y. Jeong, D. J. Richardson, and J. Nilsson, "1 W average power at 589 nm from a frequency doubled pulsed Raman fiber MOPA system," Proc. SPIE **6102,** (2006).
- J. Nilsson, S. Yoo, P. Dupriez, C. Farrell, M. S. Z. Abidin, J. Ji, J.-N. Maran, C. Codemard, Y. Jeong, J. K. Sahu, D. J. Richardson, and D. N. Payne, "Fiber MOPAs with high control and high power," *AOE*, (30 Oct - 2 Nov 2008, Shanghai, 2008), paper SaB2.
- C. Codemard, C. Farrell, V. Philippov, P. Dupriez, J. K. Sahu, and J. Nilsson, "1 mJ narrow-linewidth pulsed fiber MOPA source at 1535 nm," *CLEO/Europe*, (12 - 17 Jun 2005, Munich, Germany, 2005).
- C. Codemard, C. Farrell, P. Dupriez, V. Philippov, J. K. Sahu, and J. Nilsson, "Millijoule high-peak power narrow-linewidth sub-hundred nanosecond pulsed fibre MOPA at 1.55 microns," Comptes Rendus Physique **7**(2), 170-176 (2006).
- P. Dupriez, A. Piper, C. Farrell, A. Malinowski, J. K. Sahu, Y. Jeong, B. C. Thomsen, J. Nilsson, D. J. Richardson, L. M. B. Hickey, and M. N. Zervas, "High average power picosecond pulses from a fiber amplified diode at 1060 nm," *CLEO/Europe - EQEC*, (12 - 17 Jun 2005, Munich, Germany, 2005), CJ3-1.